This electronic thesis or dissertation has been downloaded from the King's Research Portal at https://kclpure.kcl.ac.uk/portal/



The potential of inhaled albumin nanoparticles as a delivery strategy to improve the therapeutic profile of PDE4 inhibitors

Stolfa, Ivana

Awarding institution: King's College London

The copyright of this thesis rests with the author and no quotation from it or information derived from it may be published without proper acknowledgement.

END USER LICENCE AGREEMENT



Unless another licence is stated on the immediately following page this work is licensed

under a Creative Commons Attribution-NonCommercial-NoDerivatives 4.0 International

licence. https://creativecommons.org/licenses/by-nc-nd/4.0/

You are free to copy, distribute and transmit the work

Under the following conditions:

- Attribution: You must attribute the work in the manner specified by the author (but not in any way that suggests that they endorse you or your use of the work).
- Non Commercial: You may not use this work for commercial purposes.
- No Derivative Works You may not alter, transform, or build upon this work.

Any of these conditions can be waived if you receive permission from the author. Your fair dealings and other rights are in no way affected by the above.

Take down policy

If you believe that this document breaches copyright please contact <u>librarypure@kcl.ac.uk</u> providing details, and we will remove access to the work immediately and investigate your claim.

Download date: 08. Oct. 2023

The potential of inhaled albumin nanoparticles as a delivery strategy to improve the therapeutic profile of PDE4 inhibitors

Ivana Stolfa

A thesis submitted in partial fulfilment of the requirement for the degree of Doctor of Philosophy (PhD)



Institute of Pharmaceutical Science
King's College London
November 2022

Abstract

Background: Selective phosphodiesterase (PDE) 4 inhibitors have been developed as novel anti-inflammatory drugs. Despite the licensing of roflumilast (RFM) tablets for reducing exacerbations in patients with severe COPD associated with chronic bronchitis and a history of exacerbations, RFM use has been severely hindered by the dose-limiting side effects. It was hypothesised that delivery via the lungs may provide an improved therapy if the challenges of formulating a poorly soluble drug and retaining it in the lungs after inhalation can be overcome. Hence this work aimed to develop albumin nanoparticles encapsulating RFM as a delivery strategy for a prototype PDE4 inhibitor. This body of work focused on (i) fabrication and characterisation of RFM in albumin nanoparticles (HSA-NPs); (ii) formulation of the NPs within respirable microparticles; (iii) design and application of *in vitro* and *in vivo* models of acute lung inflammation.

Methods: To investigate the potential of HSA-NPs to deliver RFM effectively to the lungs, reducing exposure to the gastrointestinal tract, formulation approaches, *in vitro* assays and an *in vivo* guinea pig models were developed. NPs were formulated using a desolvation method and physiochemical characterisation performed using dynamic light scattering and nanoparticle tracking analysis. *In vitro* assays were used to determine the NP degradation and the drug release in the presence of lung fluid-levels of proteases. Spray-drying was adopted to convert NPs suspension into a respirable mannitol-based microparticles. *In vitro* and *in vivo* models were designed using lung epithelial cells and guinea pigs, respectively. Lipopolysaccharide (LPS) from *E. Coli* was used to trigger inflammation and RFM and dexamethasone (as a positive control) were used in an anti-inflammatory treatment protocol. For *in vivo* studies, a RFM suspension was developed for nebulisation to guinea pigs.

Results: HSA-NPs were manufactured successfully and shown to undergo degradation and drug release in a simulated lung environment. The use of LPS *in vitro* and *in vivo* resulted in robust acute lung inflammation models. *In vivo* the inflammation was shown to be suppressed by orally administered RFM, but not significantly via nebulisation, indicating that either an increase in the delivered dose or longer exposure to the drug may be required for anti-inflammatory activity. An alternative hypothesis is that PDE4 inhibitors need to be administered systemically to be effective as anti-inflammatory

agents. Promisingly, the nebulisation of NPs did not change particle size, polydispersity index (PDI) or zeta potential.

Conclusion: This study confirmed that HSA-NPs can be formulated into respirable microparticles and undergo degradation in a lung simulated environment, therefore representing a potential strategy to provide retained release in the lung. Despite lung delivery of RFM not resulting in a robust anti-inflammatory effect, hence preventing studies on the efficacy of nebulised drug-loaded NPs, this work highlights the potential value of pursuing HSA-NPs as a drug delivery strategy.

Declaration

The work in this thesis is based on research performed within the Institute of Pharmaceutical Science, Faculty of Life Sciences and Medicine, King's College London, UK and Vectura Group LTD, Chippenham, UK.

I hereby declare all the experimental work presented in this thesis (Chapter 2-6) was entirely carried out by myself. For some of the *in vivo* experiments described in this thesis, the surgical procedure only was carried out by Dr Sandra Rudman as stated in paragraph 5.3.3.2.

The Covid-19 pandemic partially affected my PhD project, as it reduced the amount of allocated time that I was supposed to spend at the industrial partner, Vectura Ltd. As a result, some experiments had to be carried out only once.

I hereby declare that no part of this thesis has previously been submitted in substance for any other degree or qualification, and it is the result of my own work unless otherwise stated in the text.

The copyright of this thesis rests with the author and no quotation from it or information derived from it may be published without proper acknowledgment.

Conference Presentations

- 1. <u>Ivana Stolfa</u>, Ayasha Patel, Nick Childerhouse, Gemma Keegan, Clive Page & Ben Forbes, 2019. "Roflumilast-loaded albumin nanoparticles for pulmonary drug delivery". Poster presentation. *Drug Delivery to the Lungs (DDL)*, *Edinburgh*, *UK*.
- 2. <u>Ivana Stolfa</u>, Ayasha Patel, Arcadia Woods, Nick Childerhouse, Gemma Keegan and Ben Forbes, 2019. "Albumin nanoparticles for pulmonary drug delivery". Poster presentation. *European Aerosol Conference (EAC), Gothenburg, SWE*.
- 3. <u>Ivana Stolfa</u>, Clive Page & Ben Forbes, 2020. "Development of an in vivo preclinical model of COPD in guinea pigs to study the anti-inflammatory effects of inhalaed roflumilast". Poster presentation. *Drug Delivery to the Lungs (DDL)*, *Edinburgh*, *UK*.
- 4. <u>Ivana Stolfa</u>, Clive Page & Ben Forbes, 2021. "Development of an in vivo preclinical model of COPD in guinea pigs to study the anti-inflammatory effects of inhaled roflumilast". Oral presentation. *School of Cancer and Pharmaceutical Sciences PGR Symposium at King's College London, London, UK.*
- 5. <u>Ivana Stolfa</u>, Clive Page & Ben Forbes, 2021. "Development of a drug delivery system to the lungs: manufacture, *in vitro* and *in vivo* characterization of roflumilast albumin nanoparticles", 2021. LIDo iCASE Presentation Day, London, UK.
- 6. <u>Ivana Stolfa</u>, Clive Page & Ben Forbes, 2022. "Investigation of the potential of inhaled roflumilast albumin NPs for COPD treatment". Oral presentation. *School of Cancer and Pharmaceutical Sciences PGR Symposium at King's College London, London, UK*.

7. <u>Ivana Stolfa</u>, Clive Page & Ben Forbes, 2022. "Inhaled albumin nanoparticles as delivery strategy to improve the risk/benefit ratio of PDE-4 inhibitors". Poster presentation. *American Association Pharmaceutical Scientists (AAPS)* 2022 *PHARMSCI 360, Boston, MA*.

Acknowledgements

This PhD has been a 4-years long journey which could not have been the same without the people I met – supervisors, friends, and family.

I would like to thank my two supervisors, Prof. Ben Forbes and Prof. Clive Page. In a number of ways each of them made an impact on this work and on myself, allowing me to evolve, thrive, fail and improve during these past four years.

I would like to thank my supervisors from Vectura, Dr Gemma Keegan, Dr Nick Childerhouse and Dr Mireia Puig for their support and expertise.

Emigrating allowed me to make this journey possible. Leaving behind my 'safe heaven' - my family, my friends, and my country- was not easy four years ago as it is not nowadays. But I just know this was the only way. I therefore would like to thank the people that made my daily life in London better.

My parents - which no matter how far away they are - are always with me.

My sisters without whom I could not imagine my life.

Giulio ed Elena, the birth of which signified a new way of being happy, being loved and love.

Roberto for the joy he brings to me, for his care and for just being with me in the last years.

I would like to thank Stefania which weekly helped me navigating the unknown.

I would like to thank the friends I made in London. Carla, Nadia, Laura, for being my first family here and with which I spent endless days on the 5th floor of FWB. Abhi, Ziru and Ola which have been good colleagues and friends.

Ringraziamenti

Questo PhD e' stato un viaggio lungo 4 anni che non sarebbe stato possibile senza le persone che ho incontrato – supervisors, amici e famiglia.

Vorrei ringraziare i miei due supervisors, Prof. Ben Forbes e Prof. Clive Page. In molteplici modi, ognuno di loro ha avuto un impatto su questo lavoro e sulla mia persona, permettendomi in questi anni di evolvere, crescere, fallire e migliorarmi.

Vorrei ringraziare i miei Vectura supervisors, Dr Gemma Keegan, Dr Nick Childerhouse e Dr Mireia Puig per il loro supporto e per le loro competenze.

E' stato emigrare che mi ha permesso di intraprendere questo viaggio. Lasciare quattro anni fa il mio porto sicuro – la mia famiglia, i miei amici e la mia terra – non e' stato semplice e non lo e' ancora oggi. Ma so che cosi' doveva essere. Vorrei quindi ringraziare le persone che hanno reso migliore la mia vita qui a Londra.

I miei genitori che sono sempre con me, indipendentemente da quanto fisicamente distanti siano.

Le mie sorelle senza le quali non riesco a immaginare la mia vita.

Giulio ed Elena, la cui nascita ha semplicemente portato con se' un nuovo modo di essere felice, di essere amati e amare.

Roberto, per la gioia che mi dona, per la cura che ha di me e semplicemente per essere stato con me negli ultimi anni.

Vorrei ringraziare Stefania che settimanalmente mi ha aiutato a navigare l'ignoto.

Vorrei ringraziare i miei amici qui a Londra. Carla, Nadia e Laura, con le quali ho speso infinite giornate al 5º piano del nostro dipartimento e per essere state la prima famiglia qui a Londra. Abhi, Ziru e Ola, per essere stati dei buoni colleghi e amici.

Table of Content

| Abstrac | t | 2 |
|----------|--|----|
| Declara | tion | 4 |
| Confere | ence Presentations | 5 |
| Acknow | vledgements | 7 |
| Ringraz | ziamenti | 8 |
| Table of | f Content | 9 |
| | Γables | |
| | Figures | |
| | | |
| | Equations | |
| | Abbreviations | |
| СНАРТ | TER 1: General Introduction | 28 |
| 1.1 | General introduction | 28 |
| 1.2 | Drug management and inhaled drug treatment of COPD | 30 |
| 1.2.1 | Diagnosis and initial assessment | 30 |
| 1.2.2 | COPD clinical phenotypes | 31 |
| 1.2.3 | Pharmacological therapy for stable COPD patients | 32 |
| 1.2.4 | Pharmacology of PDE inhibitors | 35 |
| 1.3 | Nanocarriers-mediated drug delivery systems: an overview | 43 |
| 1.3.1 | Polymeric nanoparticles (PNPs) | 44 |
| 1.3.1 | Polymeric micelles | 45 |
| 1.3.2 | Dendrimers | 46 |
| 1.3.3 | Exosomes | 48 |
| 1.3.4 | Albumin-based nanocarriers | 48 |
| 1.3.5 | Lipid-based nanoparticles | 52 |
| 1.4 | Design considerations for albumin nanocarriers for pulmonary delivery: | |
| | improving lung deposition | 54 |
| 1.4.1 | Appropriate particle size for lung delivery: design of nanoparticle embedded | in |
| | microparticles (NEMs) | 54 |

| | 1.4.2 | pulmonary delivery | 56 |
|----|--------|---|-----|
|] | 1.5 | Fate of inhaled NPs and microparticles: what happens to pulmonary | |
| | | delivered carriers? | 51 |
|] | 1.6 | Aims and scope of the thesis | 4 |
|] | 1.7 | Research questions and objectives | 4 |
| ~T | I A DT | ER 2: Manufacture and characterisation of roflumilast album | |
| | | rticles (RFM-HSA-NPs) | |
| | 2.1 | Introduction | |
| | | Preparation techniques for albumin nanoparticles manufacture | |
| | | Crosslinking techniques | |
| | | Determinants for a controlled size, PDI and zeta potential NPs population | |
| | | Degradation of albumin nanoparticles | |
| | | Drug loading into albumin nanoparticles | |
| | 2.1.6 | Drug release from albumin nanoparticles | 3 |
| 2 | 2.2 | Aims and objectives | 0 |
| | | Methods | |
| | 2.3 | Manufacture of blank and drug-loaded albumin NPs via desolvation method. | |
| | | Calculation of degree of cross-linking of HSA NPs | |
| | | Physiochemical characterisation of nanoparticles suspension: Dynamic Light | ' 1 |
| | 2.3.3 | Scattering and Nanoparticle Tracking Analysis (NTA) |)2 |
| | 2.3.4 | Quantification of encapsulated albumin | |
| | | 2.3.4.1 Yield and albumin quantification via bicinchoninic acid (BCA) protein | |
| | | issay9 | |
| | | Bicinchoninic acid (BCA) protein assay validation | |
| | | <i>In vitro</i> model of lung protease to investigate the stability of albumin NPs9 | |
| | | Quantification of encapsulated roflumilast | |
| | 2 | 2.3.7.1 Roflumilast quantification using a high-performance liquid | |
| | C | chromatography (HPLC) detection method | 16 |
| | 2.3.8 | Validation of High-Performance Liquid Chromatography (HPLC) detection | |
| | | method |)7 |
| | 2.3.9 | Optimisation of a dialysis bag release method for RFM | 9 |

| 2.4 Results | 100 |
|--|---|
| 2.4.1 Physiochemical characterisation | on of NPs via Dynamic Light Scattering (DLS) |
| and Nanoparticles Tracking A | nalysis (NTA)100 |
| 2.4.2 Evaluation of albumin yield ar | nd roflumilast encapsulation into NPs102 |
| 2.4.2.1 NPs albumin yield an | d validation of a BCA assay102 |
| 2.4.2.2 Roflumilast encapsula | ation into HSA-NPs and validation of an HPLC |
| quantification method | |
| 2.4.3 In vitro model of lung protease | e to investigate the stability of albumin NPs 105 |
| 2.4.4 Roflumilast release over time | from albumin NPs110 |
| 2.5 Discussion | 117 |
| 2.5.1 Investigating the degradation of | of albumin NPs via the use of trypsin118 |
| 2.5.2 HSA-NPs provided a sustained | d release of the encapsulated RFM compared to |
| the release of free RFM | 119 |
| 2.5.3 NPs degradation rate is affected | ed by the pH of trypsin solution120 |
| 2.6 Conclusion | 123 |
| CHAPTER 3: RFM-HSA-NPs in | mannitol-based microparticles powder for |
| | 125 |
| 3.1 Introduction | 125 |
| | 125 |
| | s (NEMs)126 |
| 3.2 Aims and objectives | 131 |
| · | |
| | |
| | nufacture |
| • | nic characterisation of microparticles |
| | g on size and polydispersity index (PDI) of |
| | |
| | on |
| | tion (DVS) and differential scanning calorimetry |
| • • • | |
| | |
| | |
| 3.4.1 Physiochemical and aerodynai | nic characterisation of microparticles 134 |

| Particles size distribution (PSD) | 35 |
|---|---|
| Differential scanning calorimetry (DSC) and dynamic vapour sorption (DVS) |) |
| | 36 |
| Discussion1 | 39 |
| Conclusion1 | 45 |
| FFR 4· Anti-inflammatory activity of roflumilast in an in vit | ro |
| | |
| | |
| Introduction14 | 46 |
| Aims and objectives14 | 49 |
| Methods1 | 50 |
| Cell culture conditions | 50 |
| Experimental design | 50 |
| Effect of fetal bovine serum concentration on cytokine release | 50 |
| Optimisation of LPS- induced inflammation model | 53 |
| Exposure of LPS-exposed BEAS-2B cells to roflumilast | 53 |
| Statistical analysis | 55 |
| Results1 | 56 |
| Effect of fetal bovine serum concentration on IL-8 and IL-6 basal release from | n |
| BEAS-2B cells | 56 |
| Effect of LPS on IL-8 and IL-6 production in BEAS-2B1 | 57 |
| Anti-inflammatory activity of dexamethasone in an LPS-challenged BEAS-21 | В |
| model1 | 62 |
| Investigating the anti-inflammatory activity of roflumilast pre-treatment in an | l |
| LPS-challenged BEAS-2B model | 63 |
| Discussion1 | 65 |
| Conclusion1 | 71 |
| ΓΕR 5: A guinea pig model of lung inflammation for evaluation | of |
| ilast anti-inflammatory activity1 | |
| Introduction1 | 73 |
| Aims and objectives1 | 85 |
| | Differential scanning calorimetry (DSC) and dynamic vapour sorption (DVS) 15 |

| 5.3 | Metho | ds | 185 |
|------------|-----------|--|-------|
| 5.3. | 1 Prelimi | nary and qualitative assessment of LPS exposure: intratracheal | |
| | adminis | stration | 185 |
| 5.3. | 2 Design | of a whole-body chamber LPS-induced inflammation model in gui | nea |
| | pigs | | 186 |
| | 5.3.2.1 | Preparation of Lipopolysaccharide stock solution | 186 |
| | 5.3.2.2 | Nebuliser setting | 186 |
| | 5.3.2.3 | LPS dose-response in guinea pigs using a whole-body chamber m | odel |
| | | | |
| 5.3. | 3 Oral ad | ministration of roflumilast in LPS-exposed guinea pigs | |
| | 5.3.3.1 | Preparation of roflumilast suspension for oral administration | 188 |
| | 5.3.3.2 | Oral administration of roflumilast suspension in an LPS-inflamma | ıtion |
| | model | | 188 |
| | 5.3.3.3 | Statistical analysis | 189 |
| 5.4 | Results | S | 189 |
| 5.4. | 1 Lung d | istribution of a dye after intratracheal administration | 189 |
| 5.4. | 2 LPS-in | duced lung inflammation in guinea pigs | 191 |
| 5.4. | 3 Anti-in | flammatory activity of orally administered roflumilast in LPS-expo | sed |
| | guinea | pigs | 193 |
| 5.5 | Discus | sion | 195 |
| | | | |
| 5.6 | Conclu | ısion | 203 |
| CHAP | TER 6: | In vivo anti-inflammatory activity of nebulised roflumilast | 205 |
| 6.1 | Introd | uction | 205 |
| 6.2 | Aims a | nd objectives | 214 |
| 6.3 | Metho | ds | 214 |
| 6.3. | 1 Manufa | acture and characterisation of roflumilast suspension prior to in vivo |) |
| | | stration | |
| | 6.3.1.1 | Manufacture of roflumilast suspension | 214 |
| | 6.3.1.2 | Ensuring dose homogeneity, investigating particle shape and | |
| | geometri | ic size distribution using Malvern Morphologi 4 system and drug | |
| | Č | ation | 215 |

| | 6.3.1.3 | Aerodynamic characterisation of nebulised rollumilast using the | Next |
|------|------------|--|--------|
| | Generati | on Impactor (NGI) | 216 |
| | 6.3.1. | 3.1 NGI settings | 216 |
| | 6.3.1. | 3.2 Evaluation of the respirability of nebulised roflumilast | |
| | suspe | nsion | 217 |
| 6.3. | 2 Exposu | are of LPS-challenged guinea pigs to a pre-treatment of roflumilast | via |
| | nebulis | ation using a whole-body chamber model | 219 |
| | 6.3.2.1 | Calculation of in vivo delivered dose (DD) of roflumilast | 219 |
| | 6.3.2.2 | Nebulised roflumilast administered to LPS-challenged guinea pig | gs 219 |
| 6.3. | 3 Physio | chemical characterisation of nebulised NPs using the Dynamic Lig | ;ht |
| | Scatter | ing | 220 |
| 6.4 | Result | S | 220 |
| 6.4. | | sation of roflumilast suspension prior to in vivo administration: pa | |
| | size, ge | eometric diameter, and aerodynamic assessment | 220 |
| | 6.4.1.1 | Particle shape and geometric size distribution of roflumilast | |
| | suspensi | on | 220 |
| | 6.4.1.2 | Aerodynamic assessment of roflumilast suspension using the Ne | xt |
| | Generati | on Impactor (NGI) | 222 |
| 6.4. | 2 Pulmoi | nary administration of roflumilast to LPS-challenged guinea pigs u | sing a |
| | whole- | body chamber model | 227 |
| | 6.4.2.1 | Calculation of in vivo delivered dose (DD) | 227 |
| | 6.4.2.2 | Pulmonary delivery of roflumilast in LPS-challenged guinea pigs | s229 |
| 6.4. | 3 Impact | of nebulisation on the HSA-NPs physiochemical characteristics | 231 |
| 6.5 | Discus | sion | 232 |
| 6.5. | 1 In vitro | nebulisation of blank and RFM-HSA-NPs | 232 |
| 6.5. | 2 Effect | of inhaled RFM on lung inflammation in vivo | 234 |
| 6.6 | Conclu | ısion | 239 |
| СНАР | PTER 7: | General Discussion | |
| | | | |
| 7.1 | | al premise | |
| 7.2 | Drug-l | oaded albumin NPs for lung delivery | 242 |
| 7.3 | Contri | bution to knowledge | 246 |

| 7.4 | Experimental limitations | 246 |
|--------|--------------------------|-----|
| 7.5 | Future work | 248 |
| 7.6 | Conclusion | 249 |
| Refere | nces | 252 |
| Appen | dix | 292 |

List of Tables

| Table 1.1 Classification of airflow limitation severity in COPD patientis with |
|--|
| FEV ₁ /FVC < 0.7030 |
| Table 1.2 COPD patients classification according to symptoms and severity risk.31 |
| Table 1.3 Maintenance medications in COPD patients35 |
| Table 1.4 Inhaled PDE4 and dual PDE3 - PDE4 inhibitors for the treatment of |
| COPD and asthma and corresponding current development stage41 |
| Table 1.5 Nanocarriers for drug delivery for respiratory therapy47 |
| Table 1.6 Albumin-based formulations approved for clinical use51 |
| Table 1.7 Advantages and disadvanategs of different type of inhaler devices59 |
| Table 2.1 Advantages and disadvantages of albumin nanoparticles manufacture |
| methods available in the literature69 |
| Table 2.2 Factors affecting size and zeta potential of albumin nanoparticles75 |
| Table 2.3 Examples of drugs that can be encapsulated in albumin NPs described in |
| the literature80 |
| Table 2.4 Evaluation of correlation between drug loading methods in albumin NPs |
| and resulting drug release profiles |
| Table 2.5 Summary of HPLC method for roflumilast detection and quantification. |
| 98 |
| Table 2.6 Schematic representation of the different combination of stirring rate |
| (rpm) and ethanol addition rate (mL/min) tested in the optimisation of the NPs |
| manufacture process101 |
| Table 2.7 Size, polydispersity index (PDI) and zeta potential of blank and drug |
| loaded albumin nanoparticles101 |
| Table 2.8 Validation of BCA assay as method for albumin yield over three |
| concentrations (low, medium and high)104 |
| Table 2.9 Stability of roflumilast in water-acetonitrile solution over 7 days105 |
| Table 2.10 Calculated mass balance in the dialysis bag at time 0 and after 24 h112 |
| Table 2.11 Size, PDI and derived count rate of NPs at time 0 (- trypsin) and at time |
| 24 h of incubation (NPs left in the dialysis bag) |

| Table 2.12 Variation of size, PDI and derived count rate after 24 h of incubation |
|--|
| with trypsin activated and not activated were recorded using dynamic light |
| scattering116 |
| Table 2.13 Variation of size, PDI and derived count rate after 7 h of incubation with |
| trypsin were recorded using dynamic light scattering117 |
| Table 3.1 Features of nanoparticles (NPs), large porous particles (LPPs), large |
| porous nanoparticles (LPNPs) and nano-embedded microparticles (NEMs)127 |
| Table 3.2 (A) Spray dried feedstock (FS) solution and solvent composition. (B) List |
| of parameters adopted in the spray-drying process132 |
| Table 3.3 Properties and aerodynamic performance of spray-dried powders |
| composed of 40% (w/w) RFM-HSA-NPs embedded in a mannitol matrix135 |
| Table 3.4 Particle size distribution (D_{10} , D_{50} and D_{90}) expressed as equivalent volume |
| diameters of the spray died powder measured with using the Hydro MV on the |
| Malvern Mastersizer136 |
| Table 3.5 Melting points of mannitol polymorphic forms reported in the literature. |
| 137 |
| Table 5.1 Rodent models reflecting COPD and related respiratory disorders/ |
| fibrosis described in the literature with their advantages, disadvantages, and |
| corresponding pathophysiological features176 |
| Table 5.2 Advantages and disadvantages of different exposure methods that can be |
| adopted in the pulmonary exposure of the disease inducing substance in pre-clinical |
| animal models184 |
| Table 6.1 Definitions of the most used parameters for aerosol characterisation218 |
| Table 6.2 Volume distribution statistics over 9 measurements for the RFM |
| suspensions (500 μg/mL) calculated using Morphologi 4 Malvern Instrument221 |
| Table 6.3 Mass distribution across NGI stages recovered after the nebulisation of a |
| volume of 4 mL of RFM suspension (500 μg/mL)225 |
| Table 6.4 Aerosol performance parameters of two different concentrations of RFM |
| suspensions in 0.9% saline/ 0.2% Tween $80 + 0.05\%$ DMSO when nebulised with |
| Aerogen Pro226 |
| Table 6.5 Evaluation of calculated masses available over different stages of the NGI |
| after nebulisation227 |
| Table 6.6 Dataset of values used to calculate the delivered dose (DD)229 |

| Table 6.7 Summary of details of the in vivo administration of RFM suspe | nsion using |
|---|-------------|
| the nebulisation as route of administration | 229 |
| Table 6.8 Size, polydispersity index (PDI) and zeta potential of blank | c and drug |
| loaded nanoparticles (NPs) prior and after nebulisation with Aerogen P | ro®232 |

List of Figures

| Figure 1.1 General overview of factors that may contribute to the active |
|---|
| pharmaceutical ingredient (API) therapeutic activity after its delivery through the |
| pulmonary route28 |
| Figure 1.2 Non-proportional Venn diagram of chronic obstructive pulmonary |
| disease32 |
| Figure 1.3 Intracellular signalling of phosphodiesterase enzymes36 |
| Figure 1.4 PDE inhibitors: from the ophylline to $2^{ m nd}$ generation38 |
| Figure 1.5 Schematic representation of the most common nanocarriers for drug |
| delivery44 |
| Figure 1.6 Site of deposition of inhaled particles based on the aerodinamic diameter |
| and mechanims of NPs delivery through aerosol of nanoparticles embedded in |
| microparticles55 |
| Figure 2.1 Structure of humna serum albumin (HSA)66 |
| Figure 2.2 Illustration of the main steps in the desolvation (A) and emulsification (B) |
| manufacturing methods71 |
| Figure 2.3 Schematic correlation between albumin nanoparticles conformations and |
| drug release profiles89 |
| Figure 2.4 Schematic representation of the manufacture process of blank and |
| roflumilast (RFM)-loaded human serum albumin nanoparticles (HSA-NPs)91 |
| Figure 2.5 Schematic diagram of the indirect method of roflumilast quantification: |
| (1) Separation of free drug and encapsulated roflumilast; (2) processing of non- |
| encapsulated drug; (3) analysis of non-encapsulated drug using an HPLC method. |
| 97 |
| Figure 2.6 In vitro drug release model. Schematic representation of the in vitro drug |
| release study experimental set up100 |
| Figure 2.7 Size distribution from NTA and DLS measurements of monodisperse |
| roflumilast albumin NPs (left panel) with an illustrative NTA video frame of one of |
| the samples analysed (right panel)102 |
| Figure 2.8 Intra-day validation of linearity of human serum albumin (HSA) in the |
| concentration range 200 – 2000 μg/mL103 |
| Figure 2.9 Linear relationship between RFM concentration and area under the |
| curve in the range 0.5 – 150 µg/mL, |

| Figure 2.10 Characterisation of HSA NPs for degradation studies106 |
|---|
| Figure 2.11 Degradation profile of RFM-HSA-NPs following exposure to 0.1 (A), |
| 0.25~(B) and $0.5~mg/mL~(C)$ of trypsin compared to phosphate buffered saline at |
| $37^{\circ}\mathrm{C}$ (control); (D) Degradation profile of RFM-HSA-NPs following exposure to 0.1 |
| mg/mL of trypsin over 40 minutes only107 |
| Figure 2.12 Degradation, aggregation and increase in polydispersity index of the |
| RFM-HSA-NPs following exposure to different concentrations of trypsin (0.1, 0.25 |
| and 0.5 mg/mL) at 37° C for up to 4 hours |
| Figure 2.13 Representative chromatogram of RFM (20 $\mu\text{g/mL}$) in phosphate saline |
| buffer (PBS) 0.01 M/ 0.8% Tween 80110 |
| Figure 2.14 In vitro drug release of roflumilast solution in DMSO (100%) 111 |
| Figure 2.15 Impact of different volumes of dialysis bag content on the free drug |
| release |
| Figure 2.16 Drug release of free RFM and human serum albumin (HSA) solution in |
| presence and absence of trypsin (0.0325 mg) (trypsin:albumin ratio = $1:100$) 113 |
| Figure 2.17 Drug release of free RFM incubated with human serum albumin (HSA) |
| NPs in presence and absence of trypsin (0.0325 mg) (trypsin:albumin ratio = 1:100). |
| |
| Figure 2.18 Drug release of RFM-HSA-NPs in presence of trypsin activated or not |
| activated. Trypsin activation was performed changing the pH to 7 - 9 via the |
| addition of 1 N NaOH115 |
| Figure 2.19 Drug release of RFM-HSA-NPs in presence of activated trypsin116 |
| Figure 3.2 Schematic representation of critical phases of spray drying process which |
| regulate the final particle morphology: constant drying phase and falling drying |
| phase129 |
| Figure 3.3 Dynamic scanning calorimetry (DSC) thermogram of RF-HSA-NPs (40%) and the scanning calorimetry (DSC) thermogram of RF-HSA-NPs (40%) and the scanning calorimetry (DSC) thermogram of RF-HSA-NPs (40%) and the scanning calorimetry (DSC) thermogram of RF-HSA-NPs (40%) and the scanning calorimetry (DSC) thermogram of RF-HSA-NPs (40%) and the scanning calorimetry (DSC) thermogram of RF-HSA-NPs (40%) and the scanning calorimetry (DSC) thermogram of RF-HSA-NPs (40%) and the scanning calorimetry (DSC) and the scanning calorimetry (DSC) thermogram of RF-HSA-NPs (40%) and the scanning calorimetry (DSC) and the scanning calorimetry (DSC) thermogram of RF-HSA-NPs (40%) and the scanning calorimetry (DSC) and t |
| w/w) embedded in mannitol microparticles (60% w/w) (NEMs)137 |
| Figure 3.4 Dynamic vapour sorption isotherm of roflumilast albumin nanoparticles |
| embedded in mannitol (NEMs) (blue reference)139 |
| Figure 3.5 Dynamic vapour sorption isotherm (hysteresis) of RFM-HSA-NPs |
| embedded in mannitol (NEMs). |
| Figure 4.1 Schematic representation of the experimental design adopted in the |
| evaluation of the effect of serum on cytokine secretion152 |

| Figure 4.2 Schematic representation of 'treatment protocol' and 'modified |
|---|
| treatment protocol' adopted155 |
| Figure 4.3 (a) Effect of fetal bovine serum (2% or 10%) in cell culture medium on |
| secretion level of TNF- α , IL-8 and IL-6. (b) The different regimes for exposing cells |
| to fetal bovine serum |
| Figure 4.4 Effect of lipopolysaccharide exposure (24 h) on IL-8 and IL-6 production |
| in BEAS-2B |
| Figure 4.5 (a) Effect of lipopolysaccharide (800 and 1000 ng/mL) on TNF- $lpha$ and IL- |
| 8 production in BEAS-2B when cells are incubated with different percentages of |
| fetal bovine serum (2 % or 10%) on day 1 and 2. (b) The different regimes for |
| exposing cells to fetal bovine serum160 |
| Figure 4.6 Effect of different exposure times to lipopolysaccharide (800 ng/mL) on |
| IL-6 production from BEAS-2B cells. Cells were seeded on day $\boldsymbol{0}$ in culture medium |
| which was replaced with fresh medium on day 1; on day 2 cells were exposed to LPS |
| $(800 \ ng/mL)$ or culture medium (control) for the allocated exposure times161 |
| Figure 4.7 Effect of dexamethasone pre-treatment on IL-6 production from LPS- |
| challenged BEAS-2B cells |
| Figure 4.8 IL-8 level released by LPS-stimulated BEAS-2B cells in presence or |
| absence of roflumilast treatment |
| Figure 4.9 Effect of roflumilast pre-treatment (1.5 - 3 - 24 h) on IL-6 production |
| from LPS-challenged BEAS-2B |
| Figure 5.1 Experimental set up used in the design of a whole-body chamber model: |
| an Aerogen Pro® nebuliser is fitted on the top of a plexiglass chamber187 |
| Figure 5.2 Schematic representation of the designed inflammation whole-body |
| chamber model in male Dunkin-Hartley guinea pigs188 |
| Figure 5.3 Representative pictures (dorsal and ventral views) of guinea pig lungs |
| showing how the specific technique of intratracheal administration used can impact |
| the distribution of an instilled solution |
| Figure 5.4 Representative morphology of cells recoverable from the BAL of guinea |
| pigs191 |
| Figure 5.5 Total and differential cell count from bronchoalveolar lavage fluid |
| (BALF) of guinea pigs exposed to increasing concentration of lipopolysaccharide |
| from F. Coli |

| Figure 5.6 Levels of human tumour necrosis factor alfa (TNF-α) in bronchoalveolar |
|--|
| lavage fluid (BALF) from guinea pigs four hours after the exposure to increasing |
| doses of Lipopolysaccharide (LPS)193 |
| Figure 5.7 Representative guinea pig BAL cytospin preparations194 |
| Figure 5.8 Oral administration of free RFM. Total and differential count of cells |
| recovered from bronchoalveolar lavage fluid of guinea pigs195 |
| Figure 6.1 Schematic representation of relationship between particle deposition |
| mechanisms in the lungs and particle aerodynamic diameter206 |
| Figure 6.2 Schematic representation of three main mechanisms of particles |
| deposition in the lungs based on the particle aerodynamic diameter: impaction, |
| sedimentation and diffusion206 |
| Figure 6.3 Schematic representation of manufacture, characterisation, and |
| aerodynamic assessment of nebulised aerosols of roflumilast suspension prior to in |
| vivo administration215 |
| Figure 6.4 Experimental set-up for Next Generation Impactor (NGI) testing217 |
| Figure 6.5 Representative particles images of 500 μg/mL RFM suspensions using |
| Malvern Instrument (50x)221 |
| Figure 6.6 Evaluation of streaking phenomena223 |
| Figure 6.7 A) Roflumilast mass (%) stage deposition from NGI when 100 µg/mL |
| (red) and 500 μ g/mL (blue) suspensions are nebulised at 15 L/min using an Aerogen |
| Pro; (B) Cut-off sizes of Next Generation Impactor system at 15 L/min224 |
| Figure 6.8 Estimation of the delivered dose (DD). Schematic representation of the |
| calculation of the concentration of substance in the air (C)228 |
| Figure 6.9 Nebulisation of RFM suspension (saline \pm 0.2% Tween 80 \pm 0.05% |
| DMSO) in LPS-challenged guinea pigs. Total and differential count of cells |
| recovered from bronchoalveolar lavage fluid (BALF) of guinea pigs230 |
| Figure 6.10 Levels of human tumour necrosis factor alfa (TNF-alfa) in |
| bronchoalveolar lavage fluid (BALF) of RFM treated LPS-challenged guinea pigs. |
| 231 |
| Figure 7.1General abstract showing main outcomes of each experimental chapter |
| 251 |
| Figure 0.1 Schematic representation of the method (method 1) adopted for the direct |
| quantification of the roflumilast encapsulated in HSA- |
| NPs 292 |

| quantification NPs | of | the r | oflumilast | encapsul | ated in | HSA- |
|-----------------------|---|---------------|---|---------------|-------------|--------------|
| Figure 0.3 Re | epresentativ | e chromate | ograms of F | RFM in wat | er:acetonit | rile (30:70) |
| (samples | obtained | via | method | l 1 | and | method |
| 2) | • | ••••• | • | ••••• | ••••• | 293 |
| | | | | | | |
| | | | | L | ist of E | quations |
| Equation 2.1 (| Calculation | of number | of HSA mole | ecules availa | ble | 92 |
| Equation 2.2 N | Number of (| GLU molec | ules | ••••• | ••••• | 92 |
| Equation 2.3 (| Calculation | of working | reagent req | uired | •••••• | 93 |
| Equation 2.4 (| Calculation | of NPs yield | d | ••••• | ••••• | 94 |
| Equation 2.5 I | Limit of det | ection/quar | tification fo | rmula | ••••• | 94 |
| Equation 2.6 (| Calculatin o | of accuracy | expressed as | error | ••••• | 95 |
| Equation 2.7 (| Calculation | of sampling | g accuracy e | xpressed as | % relative | error95 |
| Equation 2.8 I | Relative sta | ndard devia | ation (%) | ••••• | •••••• | 95 |
| Equation 2.9 I | Encapsulati | on efficienc | y (%) | ••••• | ••••• | 96 |
| Equation 3.1 I | Peclet numb | er | ••••• | ••••• | ••••• | 128 |
| Equation 5.1 (| Calculation | of the deliv | ered dose ac | hievable via | inhalation | 202 |
| Equation 5.2 (| Calculation | of respirate | ory minute v | olume | ••••• | 202 |
| Equation 6.1 S | Stokes' num | ıber equatio | on | ••••• | ••••• | 207 |
| Equation 6.2 S | Settling velo | city | ••••• | ••••• | ••••• | 207 |
| Equation 6.3 A | Aerodynam | ic particle d | liameter (dae | e) | •••••••••• | 208 |

List of Abbreviations

99mTc Sodium Pertechnetate

ACN Acetonitrile

API Active Pharmaceutical Ingredient

BALF Bronchoalveolar lavage fluid

BBB Brain blood barrier
BCA Bicinchoninic acid

BEAS-2B Bronchial epithelial cells

BLM Bleomycin

BSA Bovine serum albumin

BW Body weight

cAMP Cyclic adenosine phosphate

cGMP Cyclic guanosine monophosphate
CMC Critical micellar concentration

COPD Chronic obstructive pulmonary disease

CS Cigarette-smoke

CSE Cigarette smoke extract

CXCL8 Chemokine ligand 8
CYPs Cytochromes P450

dae Aerodynamic particle diameter

DD Delivered dose

DLS Dynamic Light Scattering

DMPE Dimyristoylphosphatidylethanolamine

DMSO Dimethyl sulfoxide
DPI Dry powder inhaler

DPPC Dipalmitoylphosphatidylcholine

DSC Differential Scanning Calorimetry

DSPE-PEG 1,2-distearoyl-sn-glycero-3-phosphoethanolamine-Poly(ethylene glycol)

DTX Docetaxel

DVS Dynamic Vapour Sorption

ECOPD Exacerbation of chronic obstructive pulmonary disease

ED₅₀ Effective dose

EE Encapsulation efficiency

ELISA Enzyme-linked immunosorbent assay

EMA European Medicines Agency

FBS Fetal bovine serum

FDA U.S. Food and Drug Administration

FEV₁ Forced Expiratory Volume in one second

FITC Fluorescin isothiocyanate

FPD Fine particle dose
FPF Fine particle fraction
FVC Forced vital capacity

GLU Glutaraldehyde

GOLD Global Initiative for Chronic Obstructive Lung Disease

GSD Geometric standard deviation

GSK GlaxoSmithKline

HARBS High affinity rolipram-binding site

HCPT 10 – Hydroxycamptothecin

HPLC High performance liquid chromatography

HSA Human serum albumin

IC₅₀ Half maximal inhibitory concentration

ICS Inhaled corticosteroid
IF Inhalable fraction

IL-6 Interleukin-6 IL-8 Interleukin-8

Kcps Kilo counts per second LABA Long-acting β_2 agonist

LAMA Long-acting muscarinic antagonist

LARBS Low affinity rolipram-binding site

LBP Lipopolysaccharide binding protein

LHC-9 Laveck medium

LOD Limit of detection

LOQ Limit of quantification

LPNPs Large porous nanoparticles

LPNs Lipid nanoparticles

LPPs Large porous particles

LPS Lipopolysaccharide

mCD14 Membrane CD14

Methocel Methyl cellulose

MMAD Mass median aerodynamic diameter

MW Molecular weight
NA Avogadro number

NabTM Nanoparticle-albumin bound
NCLs Nanostructured lipid carriers
NEMs Nanoparticles in microparticles

NGI Next Generation Impactor

NOAEL No observed adverse effect level

NPs Nanoparticles

NTA Nanoparticle tracking analysis

OVA Ovalbumin

p.o. Oral administration
PAMAM Poly (amidoamine)

PBS Phosphate buffered saline

PDE Phosphodiesterase

PDI Polydispersity index

PEG Poly (ethylene glycol)- dimethyl ether

PEG₄₀₀ Polyethylene glycol 400

PGA Polyglycolide
pI Isolectric point
PLA Polylactic acid
PLC Polycaprolactone

PLGA Poly lactic-co-glycolic acid

pMDI Pressurised metered dose inhaler

PNPs Polymeric nanoparticles

PO Phosphodiester oligonucleotides

PSD Particle Size Distribution
PVP Poly N-vinyl pyrrolidone

QT Quercetin
RFM Roflumilast

RFM-HSA-NPs Roflumilast albumin nanoparticles

RH Relative Humidity

RMV Respiratory minute volume RSD Relative standard deviation SABA Short acting β_2 agonist

SAMA Short acting

SD Standard deviation

SLNs Solid lipid nanoparticles

SMIs Soft-mist inhalers

SS Stock solution

TFA Trifluoroacetic acid

TiO₂ Titanium dioxide

TLR Toll-like receptor

TNF- α Tumour necrosis factor- α

UV Ultraviolet

WR Working reagent

1.1 General introduction

Pulmonary delivery represents an extremely useful but challenging way of administering therapeutics for both local and systemic activity. Successful aerosol particle delivery to the lungs is complex as there are many factors that will dictate the effective deposition of an aerosol into the lungs, including aerodynamic particle diameter, density, shape, pathological conditions that may have altered the physiology of the lungs as well as the clearance mechanisms (**Figure** 1.1). The use of pulmonary delivery represents an advantageous way to obtaining high dose exposure at the target site and reduction of side effects associated with systemic exposure. It also allows for drugs to avoid first pass metabolism which may lead to a reduction of the free fraction of the drug available to reach its target.

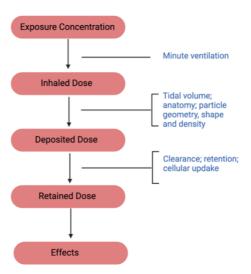


Figure 1.1 General overview of factors that may contribute to the active pharmaceutical ingredient (API) therapeutic activity after its delivery through the pulmonary route. Adapted from Oberdörster, 1993.

Roflumilast (RFM) is a phosphodiesterase (PDE) 4 inhibitor drug approved for the treatment of the exacerbations of chronic obstructive pulmonary disease (COPD) in patients with a chronic bronchitic phenotype. Prescribed as a once daily oral tablet, RFM

is characterised by anti-inflammatory activity, but has an unfavourable therapeutic index due to gastrointestinal side effects and weight loss. The latter is greatest in patients with most severe COPD that may be already experiencing reduction of weight due to the respiratory conditions and the metabolic drive/energy to control the breathing (Jolley & Moxham, 2009). Strategies to overcome the downsides of this drug class developed in the past decade include screening and design of i) new molecules targeting only the enzyme isoform responsible for the therapeutic activity rather than the side effects and ii) new molecules exclusively for the inhalation route. However, those strategies have not been completely successful so far, hence the need for pursuing new formulation strategies.

Nanocarriers have shown great potential compared to 'conventional formulations' for the delivery of hydrophobic drugs which can be otherwise very difficult to deliver. Nanocarriers can protect their payload from unwanted degradation, they possess a high surface area, and they allow modulation of the drug release rate. Human serum albumin (HSA) based nanoparticles (NPs) represent one of these non-conventional formulation approaches which has gained attention in the past years, especially after the approval of Abraxane (paclitaxel loaded-HSA-NPs) as intravenous treatment for different types of

cancer.

The opportunity to combine nanotechnology with the advantages of pulmonary delivery has been demonstrated by the success of the Arikayce®, Insmed Inc., an inhaled (delivered via nebulisation) liposome amikacin formulation for the treatment of Mycobacterium avium complex infections (Arikayce Liposomal; Khan & Chaudary, 2020). Therefore, the rationale behind this experimental work was to investigate the use of HSA-NPs loaded with RFM via the pulmonary route as an alternative and new drug delivery strategy to try and reduce the side effects associated with RFM, but also to investigate the fate of HSA-NPs in the lungs and their potential as a drug carrier.

This thesis outlines the relevant background material in **Chapter 1**, focusing on the pharmacology of PDEs inhibitors, the successes, and drawbacks of different type of nanocarriers intended for pulmonary delivery, the challenges to overcome when designing a carrier for pulmonary drug delivery, as well as their fate after inhalation. The

following chapters, **Chapters 2-6**, explore the potential of RFM-HSA-NPs for pulmonary delivery using a variety of *in vitro* and *in vivo* experimental approaches.

54

1.2 Drug management and inhaled drug treatment of COPD

5556

1.2.1 Diagnosis and initial assessment

5758

59

60

61

62

63

64

65

66 67

68

69

70

71

72

73

74

75

76

COPD is a multifactorial clinical condition related mainly to the exposure to smoking and characterised by persistent respiratory symptoms and airflow limitation due to airways and alveolar abnormalities. The Global Initiative for Chronic Obstructive Lung Disease (GOLD) reports are a useful tool used by clinicians for the diagnosis, management, and prevention of COPD. The aims of the COPD assessment are to determine the degree of airflow limitation, the disease severity, and the risk of future events as exacerbations, hospital admission or death to guide therapy. The severity of airflow limitations is evaluated via a spirometric assessment. Spirometry is performed after the administration of a dose of at least one short-acting bronchodilator to minimise any variability of the measurement. Spirometry allows to measure the volume of air exhaled from the point of maximal inspiration (forced vital capacity, FVC) and the volume of air exhaled during the first second of this test (forced expiratory volume in one second, FEV₁). A ratio between FEV₁ and FVC < 0.70 corresponds to the presence of airflow limitation in the patient. Based on this ratio, the severity of the airflow limitation is described by four categories (GOLD 1, GOLD 2, GOLD 3 and GOLD 4): mild, moderate, severe and very severe (**Table** 1.1) (Gold Initiative for Chronic Obstructive Lung Disease, Global Strategy for the Diagnosis, Managment, and Prevention of Chronic Obstructive Pulmonary Disease, 2022).

77

Table 1.1 Classification of airflow limitation severity in COPD patientis with $FEV_1/FVC < 0.70$.

| GOLD 1 | Mild |
|--------|-------------|
| GOLD 2 | Moderate |
| GOLD 3 | Severe |
| GOLD 4 | Very Severe |

The assessment of symptoms in COPD patients also requires the use of disease specific health status questionnaires followed by the analysis of the patient's exacerbation history. An exacerbation is defined as an acute worsening of respiratory symptoms, from the stable state and beyond normal day-to-day variations that is acute in onset which results in additional therapy (Rodriguez-Roisin, 2000; Vogelmeier et al., 2020). A low risk of exacerbation is defined as one or less exacerbation in a year not resulting in hospitalisation, whereas in presence of a minimum of two exacerbations in a year resulting in hospital admission there is a high risk of exacerbation (Vogelmeier et al.,

87 2020).

The last step in the COPD assessment is the evaluation of the obtained values with the "ABCD" assessment tool to achieve a classification of the patient. Four categories can be defined based on the symptoms assessment score, the exacerbation history, and the spirometry results (**Table** 1.2) (A. R. Patel et al., 2019).

Table 1.2 COPD patients classification according to symptoms and severity risk.

| Group A | Less symptoms, low risk |
|---------|--------------------------|
| Group B | More symptoms, low risk |
| Group C | Less symptoms, high risk |
| Group D | More symptoms, high risk |

1.2.2 COPD clinical phenotypes

The concept of phenotype is referred to "those attributes of the disease alone or in combination that describe the differences between individuals with COPD in relation to parameters that have clinical significance" (MeiLan K. et al., 2010). Although there is still no consensus on the exact number and definition of COPD phenotypes, those should be used to classify patients in subgroups allowing a better diagnosis and determination of the most appropriate therapy that results in meaningful outcomes. In 1989 Snider (Snider, 1989) represented the COPD phenotypes using a non-proportional Venn diagram in which three subgroups of COPD were introduced: chronic bronchitis, asthma and emphysema, with a common chronic airflow limitation (**Figure** 1.2) (Corlateanu et al., 2020; Marsh et al., 2008).

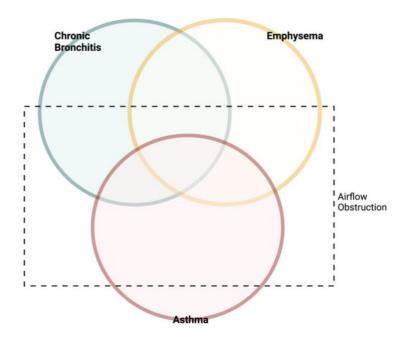


Figure 1.2 Non-proportional Venn diagram of chronic obstructive pulmonary disease.
 Adapted from Marsh et al., 2008

Chronic bronchitis is associated with excess FEV₁, and it is defined as the presence of a productive cough for three months in each of two successive years (V. Kim & Criner, 2015). Emphysema is the destruction of alveolar walls and the permanent loss of the anatomical structure of the air spaces distal to terminal bronchioles. This condition led to airflow limitation, progressive dyspnea and cough. Asthma is likely to be considered a condition on its own and it is characterised by the narrowing of the airway lumen, with a reduced expiratory airflow that results in symptoms such as wheeze and cough (Mannino D., 2003). The use of a phenotypical approach in the nonpharmacological and pharmacological management of COPD is a key aspect in a more personalised treatment (Corlateanu et al., 2020) as very often those phenotypes overlap, representing a challenge for clinicians.

1.2.3 Pharmacological therapy for stable COPD patients

The pharmacological therapy for COPD is aimed to treat symptoms, reduce the frequency and severity of exacerbations, and improve health status of patients. Most of the drugs are administered through the pulmonary route and therefore a proper technique in using the inhalers is required by the patients. The classes of drugs commonly used in the management of COPD patients are listed in **Table** 1.3.

The β₂ agonists bind the β₂ adrenergic receptors increasing the level of cyclic adenosine

The β_2 agonists bind the β_2 adrenergic receptors increasing the level of cyclic adenosine monophosphate (cAMP) and leading to the relaxation of the airway smooth muscle. There are short-acting (SABA) and long-acting (LABA) β_2 agonists, whereas those differ for the duration of action (4-6 hours and 12 hours or more for SABAs and LABAs respectively). Formoterol and salmeterol are LABAs and are administered twice daily. Those significantly improve lung volumes, dyspnoea, exacerbation rate and number of hospitalisations. In contrast, indacaterol is a LABA administered once daily that improves

breathlessness and exacerbations rate.

Antimuscarinic drugs block the M_3 muscarinic receptor expressed in airway smooth muscle which activation induces a bronchoconstrictor effect. Short acting muscarinic antagonists (SAMAs) (ipratropium bromide) can also block the M_2 muscarinic receptor which can potentially cause vagally induced bronchoconstriction. Long-acting muscarinic antagonists (LAMAs) as glycopyrronium bromide have prolonged binding to M_3 , but faster dissociation from the M_2 with a consequent prolonged bronchodilator effect.

In the COPD management the degree of bronchodilation can be improved with combinations of bronchodilators with different mechanism and duration of actions. A pharmacological therapy with inhaled bronchodilators is key for the management of symptoms (both prevention and reduction). Symptom reduction and FEV₁ improvement are achieved with a regular and as-needed use of SABA and SAMA, with a combination of those resulting in improved outcomes. Lung function, dyspnoea and exacerbation are consistently reduced by a treatment with LABAs and LAMAs, with an improved therapeutic effect provided by the combination therapy rather than the monotherapy. Usually, SABAs are prescribed for immediate symptom relief and their use on a regular basis is not recommended. In the case of patients with severe breathlessness a combination therapy with LAMA/LABA can be offered as initial treatment or LABA/ICS for patients with high risk of exacerbations and higher blood eosinophil counts. Although regular treatment with only ICS does not modify the decline of FEV₁, a therapy based on ICS in combination with LABA is more effective than the two compounds alone in the

160 improvement of lung function and exacerbations. ICS can also be included in a triple inhaled therapy with LABA and LAMA with improved benefits compared to LABA/ICS, 161 162 LABA/LAMA or LAMA monotherapy. The anti-inflammatory therapy in stable COPD patients is based on the use of inhaled 163 164 corticosteroids, oral glucocorticoids, PDE4 inhibitors, antibiotics and mucoregulators. A 165 regular treatment with inhaled corticosteroids has no effect on the long-term decline of FEV₁, whereas a combination of this class of drugs with LABA is more effective than 166 167 either drug alone in the improvement of lung function and exacerbations in patients with 168 moderate to severe COPD. 169 Oral glucocorticoids are usually not adopted in the chronic daily treatment of COPD 170 because of their systemic effects but they play a role in the management of exacerbations. Mucolytic are in some cases used in patients not receiving ICS to reduce the exacerbations 171 172 and slightly improve the health status. 173 Theophylline, the most used methylxanthine, is known to be a non-selective PDE 174 inhibitor. Its use in the COPD therapy management is not recommended unless other 175 long-term bronchodilators are not available. An additional PDE inhibitor with a selective 176 activity towards the isoform 4 of the enzyme is roflumilast. A more detailed description 177 of this drug is shown in paragraph 1.2.4. 178

Table 1.3 Maintenance medications in COPD patients.

| Drug category | | Generic Drug Name | |
|--------------------------|---------------------|----------------------------|--|
| β ₂ agonists | | | |
| | Short-acting (SABA) | Fenoterol, Salbutamol | |
| | Long-acting (LABA) | Formoterol, Indacaterol | |
| Anticholinergics | | | |
| | Short-acting (SAMA) | Ipratropium bromide | |
| | Long-acting (LAMA) | Glycopyrronium bromide | |
| Methylxanthines | | | |
| | - | Theophylline | |
| Phosphodiesterase 4 Inhi | bitor | | |
| | - | Roflumilast | |
| Mucolitic agents | | | |
| | - | Carbocysteine, N- | |
| | | acetylcysteine | |
| | Combination therapy | | |
| SABA/SAMA | - | Fenoterol/ipratropium | |
| | | Salbutamol/ipratropium | |
| LABA/LAMA | - | Formoterol/glycopyrronium | |
| | | Indacaterol/glycopyrronium | |
| LABA/Inhaled | - | Formoterol/beclomethasone | |
| corticosteroids (ICS) | | Formoterol/budesonide | |

1.2.4 Pharmacology of PDE inhibitors

COPD is an airway disease characterised by progressive airflow obstruction associated with an underling degree of chronic airways inflammation (Barnes et al., 2015). The use of the PDE4 inhibitor RFM can be considered in patients with severe to very severe airflow limitation, chronic bronchitis and exacerbations as addition to a treatment with long-acting bronchodilators with or without ICS (Gold Initiative for Chronic Obstructive Lung Disease, Global Strategy for the Diagnosis, Managment, and Prevention of Chronic Obstructive Pulmonary Disease, 2022).

PDEs are a class of intracellular enzymes responsible for the degradation of cAMP and cyclic guanosine monophosphate (cGMP) into the inactive 5' AMP and 5' GMP respectively. cAMP and cGMP usually bind and activate protein kinase (A and G respectively) which phosphorylate substrates that control different physiological processes such as the release of inflammatory mediators and the airway smooth muscle relaxation (**Figure** 1.3) (Beavo & Brunton, 2002). The inhibition of this degradation pathway mediated by PDE inhibitors results in a wide range of cellular processes, signalling and transcription of genes involved in both regulating the activation of inflammatory cells and airway smooth muscle relaxation of relevance to COPD. The resulting increased level of cAMP and cGMP and the following downstream activation of phosphorylation cascades results in airway muscle relaxation and inhibition of inflammatory pathways, depending on which PDEs are present in relevant cell types (Conti et al., 2003).

The PDE family of enzymes has 11 isoforms (PDE1 to PDE11) which are differently distributed in the body, and which possess different sensitivities for cAMP and cGMP. The isoforms 4, 7 and 8 are highly selective towards cAMP only, whereas PDE 5, PDE 6 and PDE 9 for cGMP only. The remaining isoforms have activity for both cyclin nucleotides (Houslay & Adams, 2003; Keravis & Lugnier, 2012) (Figure 1.3).

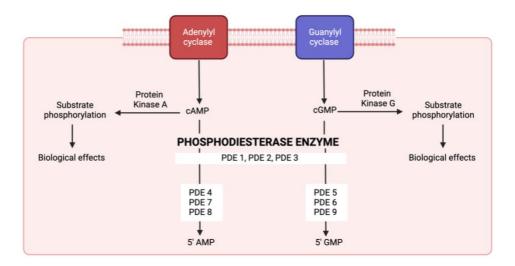


Figure 1.3 Intracellular signalling of phosphodiesterase enzymes.

The PDE4 family is comprised of four genes (A, B, C, D) whereas the enzymes distribution is broad in the body with isoforms located in the brain, spleen, gastrointestinal tract, hearth, testis, kidneys and lungs. Importantly, PDE4 is also expressed in many

inflammatory cells (T-cells, eosinophils, neutrophils, monocytes) involved in the pathogenesis of COPD (Beavo et al., 2011).

Theophylline was the first PDE inhibitor discovered and has long been recognised for its use in the treatment of airways diseases in part due to its non-selective inhibition of the PDE enzymes (Figure 1.4). Theophylline is effective in the treatment of COPD but is characterised by a weak and non-selective inhibitory activity on PDE enzymes. With the recognition that airway smooth muscle relaxation mainly comes from PDE3 inhibition, and that anti-inflammatory activity is a result of PDE4 inhibition, there was a major drive to discover and develop more selective PDE inhibitors to improve the efficacy and safety of theophylline (Boswell-Smith, Cazzola and Page, 2006). Theophylline has been reported to reduce the proportion of neutrophils and interleukin-8 (IL-8 or chemokine (C-X-C motif) ligand 8, CXCL8) levels in the sputum obtained from patients with COPD (Culpitt et al., 2002). However, the absence of a PDE selectivity accounts in part for the very narrow therapeutic window for theophylline as adverse effects usually occur when the drug plasma concentration is > 20 mg/mL, although side effects may also develop at lower plasma concentration levels (Barnes, 2013). The most frequent are nausea, headache, and increased acid secretion. Higher concentrations can induce convulsions, cardiac arrhythmias, and diuresis due to the additional adenosine receptor antagonist activity of theophylline (Barnes, 2013). Hence, the use of theophylline is limited by the unfavourable therapeutic window of this drug which necessitates careful titration and plasma monitoring. In addition, due to the metabolism of theophylline mainly driven by the cytochromes (CYP) (1A2 with a smaller contribution of 2E1 and 3A4) there are a range of possible interactions with other drugs metabolised by the same CYP isoforms.

The wide range of side effects induced by theophylline highlighted the need for new drugs with greater selectivity towards PDE3 and 4 (Figure 1.4). Rolipram is considered a first generation PDE4 inhibitor and was characterised by a significant increase of the selectivity towards the isoform 4, but this drug still had many gastrointestinal side effects such as nausea and diarrhoea. An improved safety profile was subsequently obtained with the second generation of PDE4 inhibitors. This new class was designed following the discovery of two specific binding sites of PDE4. The high affinity rolipram-binding site (HARBS) mainly located in the central nervous system and parietal glands and the low affinity rolipram-binding site (LARBS) in immunocompetent cells. Indeed, rolipram

interacts with high potency with the HARBS ($K_D \sim 2$ nM) and lower with the LARBS ($K_D \sim 200$ nm -2000 nM) (Souness & Rao, 1997). Therefore the 2^{nd} generation molecules, RFM and cilomilast were designed to have an increased specificity for the LARBS, to hopefully result in an improved therapeutic index compared to the ophylline (Boswell-Smith, Cazzola and Page, 2006).

However, despite the intention that the therapeutic index of the second generation of PDE4 inhibitors would have an improved therapeutic window by reducing the affinity towards the HARBS of PDE4, this has turned out to not be the case and it was subsequently confirmed that the HARBS coincides with the holoenzyme responsible for the enzyme catalysis (Laliberté et al., 2000). The catalytic machinery of PDE4 uses Mg²⁺ as cation cofactor. The binding of this cofactor to the enzyme results in two coexisting conformers that can bind inhibitors in a different way: the holoenzyme exists when the enzyme binds the cation, whereas the apoenzyme is represented by the free enzyme (Laliberté et al., 2000).

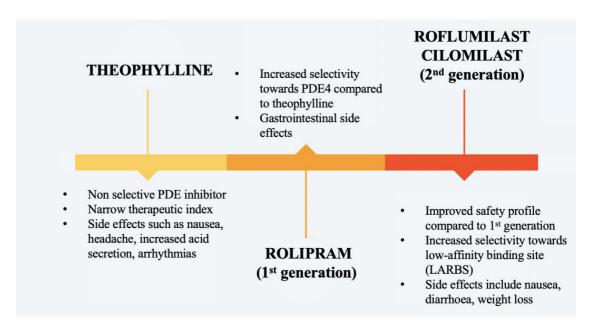


Figure 1.4 PDE inhibitors: from the ophylline to 2^{nd} generation.

Robichaud (Robichaud et al., 2002) suggested that the emesis caused by PDE4 inhibitors is rather a result of the inhibition of the PDE4D subtypes of the enzyme. This finding highlighted a new potential strategy to overcome the unfavourable therapeutic index by designing a PDE4 subtype-selective activity inhibitor. However, considering that rodents – usually used as species in preclinical models – are non-vomiting species, the potential

of those new selective PDE4 subtype inhibitors was investigated in a new model looking at the effect of the drugs on the duration of anaesthesia induced by the xylazine/ketamine combination as PDE4 plays a key role in the anaesthesia induced by α_2 -adrenoreceptor activation in mice. Interestingly, a positive correlation was found between the potency in reducing the anaesthesia and the propensity of the molecule to induce emesis in ferrets. This correlation was related to the proportion of the compound present in the brain compared to plasma (Robichaud et al., 2002). RFM - as non-subtype selective PDE4 inhibitor - was demonstrated to have an improved therapeutic index compared to cilomilast which in contrast has a PDE4D selectivity. Some suggested there was a need to develop selective PDE4B inhibitors to improve the therapeutic window further, but to date, no selective PDE4B inhibitors have been developed or approved (Ariga et al., 2004; Phillips, 2020).

Considering this background discussed above, an improvement of the therapeutic index of the PDE4 inhibitors could be perhaps achieved via following three different strategies: i) identify new molecules that can bind the LARBS preferentially over the HARBS; ii) target the isoform PDE4B rather than the isoform PDE4D which is considered to be correlated with the onset of emesis; iii) identify new molecules that have a low penetration of the blood brain barrier (BBB). However, considering that the postrema (which acts as chemoreceptor trigger zone for emesis) is not protected by the BBB, this strategy, as well as the others has been flawed and unsuccessful and has not resulted in any therapeutic improvements.

RFM was developed as the most selective new PDE4 inhibitor with an improved therapeutic window compared to the previous PDE inhibitors generations and as a oncedaily oral treatment therapy (500 μ g) for a subset of COPD patients with severe and recurrent exacerbations. RFM is a lipophilic and highly permeable molecule that is rapidly absorbed after oral administration. It is metabolised in the liver to the metabolite N-oxide by CYP3A4 and CYP1A2. Interestingly, the N-oxide metabolite also accounts for the total therapeutic activity, and both metabolite and parent molecule are extensively metabolised. The effective half-life for RFM is in the range of 8 – 31 h, whether the terminal half-life for the metabolite is in the range of 11 – 47 h. Due to the long half-life, the systemic exposure, and the potency of the metabolite, only one administration per day is recommended for its clinical use. Although the metabolite is threefold less active than

303 RFM with respect to the PDE4 inhibition, it has a 10- to 12- fold higher plasma 304 concentration compared to RFM (Baye, 2012; European Medicines Agency, 2010). 305 306 Both RFM and its N-oxide possess selective inhibitory activity towards the PDE4 307 (Hatzelmann & Schudt, 2001). In vivo, orally delivered RFM has been demonstrated to 308 improve the inflammatory responses and the lung parenchymal destruction when 309 administered to mice exposed to cigarette smoke, as well as providing improvements of 310 the lung fibrotic damage induce by bleomycin (Hatzelmann et al., 2010). 311 312 In clinical studies, RFM – administered at the clinical dose of 500 µg once daily for 4 313 weeks - reduced by 39% the LPS-induced neutrophilia in patients compared to placebo 314 (Hohlfeld et al., 2008). Furthermore, RFM reduced the increased number of neutrophils 315 in the induced sputum of COPD patients by approximately 35% (Grootendorst et al., 316 2007). Overall, the drug showed an improved safety profile compared to cilomilast, but 317 a variety of adverse effects were still reported. Compared to cilomilast, vomiting is rare 318 (Rabe et al., 2005) but other frequently reported side effects included diarrhoea, weight 319 decrease, nausea and headache (Calverley et al., 2009). Hence, despite the expectations 320 of an improved therapeutic index for this drug originally showed compared to previous 321 PDE4 inhibitors, there is still a low compliance and the risk/benefit ratio is highly 322 unfavourable which ultimately hinders the wider use of this drug (Mokry et al., 2021; 323 Singh et al., 2021). 324 325 Considering that these strategies to overcome the disadvantageous therapeutic index of 326 PDE4 inhibitors have failed, two new strategies, both based on the use of the inhalation 327 route have been developed: i) design of new molecules with a sub-type specificity that 328 are suitable for pulmonary delivery; ii) encapsulation of molecule with a less favourable 329 profile in 'non-conventional' formulation i.e. nanoparticles, microparticles, liposomes to 330 be administered via the pulmonary route. 331 332 So far, the investigation of new inhaled PDE4 inhibitors has not been successful (Phillips, 333 2020b; Singh et al., 2021)(**Table** 1.4). Throughout the last 20 years many molecules were 334 designed, and preclinical and clinical studies performed which, in most of the cases, was

followed by withdrawal from the companies' pipelines (Phillips, 2020a). This was the

case of the moderately potent AWD-12-281, (Elbion/GlaxoSmithKline (GSK) (half

335

maximal inhibitory concentration (IC₅₀) = 9.7 nM), to fimilast from Pfizer (IC₅₀ = 140 nM), UK-500,001 from Pfizer (IC₅₀ = 1 nM) and GSK256066 from Glaxo SmithKline (IC₅₀ = 0.003 nM), which was designed as a very promising molecule having a HARBs ratio (HARBs IC₅₀/LARBS IC₅₀) of at least 17, compared to 4.4 for RFM (Nials et al., 2011; Tralau-Stewart et al., 2011).

In a wider study aimed to design new and improved PDE4 molecules, Astra Zeneca (de Savi et al., 2014) attempted to rationalise the lack of success of UK-500,001 and GSK256066 while conducting a bigger study screening new PDE inhibitor molecule (de Savi et al., 2014). They suggested that in order to obtain a better drug, GSK designed one with low aqueous solubility and oral bioavailability, whereas Pfizer's API was characterised by high metabolic clearance and high plasma protein binding to achieve a minimal systemic exposure, hence minimal side effects.

Table 1.4 Inhaled PDE4 and dual PDE3 – PDE4 inhibitors for the treatment of COPD and asthma and corresponding current development stage.

| Molecule name | Company | Development stage |
|---------------|------------------------|-------------------|
| AWD-12-281 | Elbion/GlaxoSmithKline | Discontinued |
| Tofimilast | Pfizer | Discontinued |
| UK-500,001 | Pfizer | Discontinued |
| GSK256066 | GlaxoSmithKline | Discontinued |
| Ensifentrine | Verona Pharma | Clinical stage |
| Tanimilast | Chiesi | Clinical stage |

Results obtained from De Savi (de Savi et al., 2014) showed that AstraZeneca molecule had a high plasma protein binding but that the exposure of LPS-challenged rats to a dry powder aerosol of UK-500,001 resulted in inconsistent inhibition of LPS-induced

neutrophilia, despite the significant dose delivered to the lungs. The lack of antiinflammatory activity in this rat model may be explained by insufficient potency of the molecule which was not compensated by the high doses deposited or as suggested above it may be necessary to have systemic exposure of a PDE4 inhibitor to have an antiinflammatory activity. Likewise, the administration of GSK266066 did not result in significant inhibition of the lung inflammation when tested in a pre-treatment regime (drug administered 12 h before the challenge). The lack of activity was suggested to be due to the unsuitable window time adopted in the *in vivo* model and with an insufficient availability of the free fraction of the molecule in the target range. However, studies carried out by GSK (Nials et al., 2011) showed that the lipophilic nature of the GSK266066 allowed its retention in the lung tissue up to 40 h, even after the conclusion of the inflammatory event. However, De Savi (de Savi et al., 2014) suggested that it is very likely that the drug is in the lung tissue but not in an 'available' form, perhaps as solid form or in lipid compartments and that the concentration of the free compound which is required for the therapeutic activity in the intracellular cytoplasm -which is where PDE4 is located- was not high enough to exert a pharmacological activity.

371

372

373

374

375

376

377

355

356

357

358

359

360

361

362

363

364

365

366

367

368

369

370

Another novel inhaled PDE inhibitor is ensifentrine/RPL554 which has dual inhibitory activity against PDE3 and PDE4 (Abbott-Banner & Page, 2014) that induces both a bronchodilator and an anti-inflammatory activity (Franciosi et al, 2013). Results from a Phase 3 ENHANCE-2 ("Ensifentrine as a Novel Nebulized COPD thErapy") recently carried out showed that an improvement in lung function and a reduction in COPD exacerbation were achieved (www.veronapharma.com).

- 379 A second molecule that has produced some promising results was designed by Chiesi.
- They identified a new PDE4 inhibitor called tanimilast (CHF6001), available as a powder
- 381 for inhalation administered via NEXThaler® (Chiesi proprietary multi-dose inhaler)
- which has so far gained positive outcomes in preclinical and clinical studies. It is 10-fold
- more potent than RFM ($IC_{50} = 0.026$ nM), with a HARBs ratio of 40.6 (Moretto et al.,
- 384 2015) and able to equally inhibit both isoforms A and D of the enzyme (Armani et al.,
- 385 2014).
- 386 In vitro assays have showed that CHF6001 is able to induce more potent inhibition of
- tumour necrosis factor-alfa (TNF- α) production from alveolar macrophages and lung
- 388 tissue isolated from COPD patients compared to RFM (Lea et al., 2019). In addition, in

vitro it significantly reduced the adhesion of neutrophils to the endothelium and their degranulation, in combination with a reduction of cytokine secretion (Schioppa et al., 2022). In vivo, CHF6001 was extremely effective when administered intratracheally to ovalbumin sensitised-rats and intranasally to mice using a cigarette smoke model in both preventive and interventional applications. In the context of the side effects, which is one of the main driving reasons of this investigation, any emesis correlated effect (using ketamine/xylaxine-induced anaesthesia as measures) were recorded at doses 50- to 150fold higher than the anti-inflammatory ED₅₀ in rats. The lack of systemic side effects was confirmed in a ferret model. CHF6001 did not induce emesis up to 10-20 mmol/kg, a dose considerably higher to the dose of GSK256066 that induced emesis (1 mmol/kg) (Villetti et al., 2015). The positive outcomes were corroborated in a randomised, double-blind, placebo-controlled study where CHF6001 was administered via single-dose or multidose dry-powder inhaler. Results confirmed that this molecule has a good safety profile also in vivo with no relationship between dose and adverse effects (Mariotti et al., 2018). Overall, the positive outcomes for this molecule appeared to be related to its high potency, prolonged half-life, low permeability and high protein plasma binding which are key in limiting the free fraction of the drug in the systemic circulation hence the occurrence of the systemic side effects (Facchinetti et al., 2021).

Considering the background provided above, it is now evident that multiple strategies aimed to improve the therapeutic index of this class of drugs have failed. Here the need to pursue the investigation of a different strategy based on the use of a nanoplatform able to encapsulate the only PDE4 inhibitor approved so far, RFM. The well-known anti-inflammatory potency of RFM will be combined with the proven potential of the HSA-NPs. The success and the drawbacks of the HSA-NPs as well as the use of the pulmonary delivery as a lung-selective route of administration will be illustrated in the following paragraphs.

1.3 Nanocarriers-mediated drug delivery systems: an overview

There are many nanostructures used for drug delivery purposes, each of them differing for shape, size, type of payload and interactions with the biological environment (**Figure** 1.5). Those features overall dictate the characteristics, advantages, and disadvantages of each nanocarrier, with specific use in different clinical areas. Detailed classifications of

the most used nanostructures are reported in several reviews in the literature (Cheng et al., 2021; Edis et al., 2021; Hossen et al., 2019; Mazdaei & Asare-Addo, 2022; Shan et al., 2022) and in book chapters (Pathak & Thassu, 2016) with a specific focus on those used in inhalation (Ibarra-Sánchez et al., 2022; Paranjpe & Müller-Goymann, 2014).

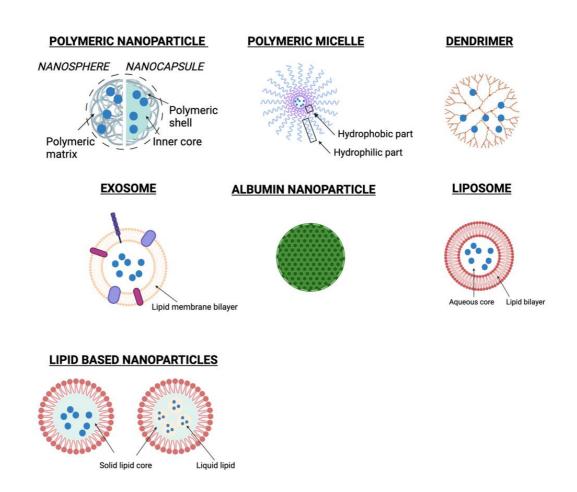


Figure 1.5 Schematic representation of the most common nanocarriers for drug delivery.

1.3.1 Polymeric nanoparticles (PNPs)

Polymeric nanoparticles (PNPs) are colloidal systems made up by natural or synthetic polymers. The PNPs include both i) nanospheres, which are nanostructures characterised by dense polymeric matrix containing the drug and ii) nanocapsules, hollow structures with the drug contained within the polymeric matrix (**Figure** 1.5) (Mora-Huertas et al., 2010). The PNPs are characterised by high encapsulation efficiency, biocompatibility, and efficient delivery of macromolecules (Gagliardi et al., 2021; Ibarra-Sánchez et al., 2022). The polymers commonly used for the manufacture of these nanostructures are

- chitosan, poly lactic-co-glycolic acid (PLGA), polyglycolide or poly glycolic acid (PGA),
- polylactic acid (PLA) or polyethylene glycol (PEG).
- 440 PNPs are widely used as nanocarriers for the delivery of therapeutics via inhalation
- 441 (Ibarra-Sánchez et al., 2022) (Table 1.5). Studies reported the use of PNPs for the
- delivery of linezolid for the treatment of tuberculosis (Shah et al., 2020) and
- budesonide/theophylline for the treatment of asthma (Buhecha et al., 2019). The use of
- PNPs loaded with chemotherapy agents for the treatment of pulmonary cancer is widely
- reported (Cheng et al., 2021; Gagliardi et al., 2021; Hossen et al., 2019). Nan (Nan, 2019)
- investigated the co-delivery of cisplatin and doxorubicin in 1,2-distearoyl-sn-glycero-3-
- phosphoethanolamine-Poly (ethylene glycol) (DSPE-PEG) NPs for lung cancer therapy.

448449

1.3.1 Polymeric micelles

450

- Polymeric micelles are characterised by a bilayer structure made of a hydrophobic inner
- core and a hydrophilic outside layer also called 'corona' (Figure 1.5). Due to this bi-
- 453 functional structure, the encapsulation of poorly soluble water drugs into polymeric
- 454 micelles can improve the drug's solubility, also protecting the drug from degradation and
- increasing the time of circulation in the blood stream (Ibarra-Sánchez et al., 2022). Poly
- N-vinyl pyrrolidone (PVP) and PEG are often used for the corona layer, whereas PLA
- and polycaprolactone (PLC) are adopted for the hydrophobic core.

458

- Polymeric micelles have been used for the combined delivery of genes and drugs for the
- 460 treatment of acute pulmonary inflammation (G. Kim et al., 2018). Moazeni and co-
- workers (Moazeni et al., 2012) reported the preparation and evaluation of inhalable
- 462 itraconazole chitosan micelles for the treatment of pulmonary fungal infections.
- Moreover, the potential of polymeric micelles for the treatment of lung cancer has been
- 464 investigated by Gill and colleagues (Gill et al., 2011). Paclitaxel-loaded polymeric
- 465 micelles were fabricated from PEG₅₀₀₀-DSPE and tested over the conventional paclitaxel
- 466 formulation (Taxol) using a *in vivo* mouse model. Results showed that PNPs provided a
- better release profile over Taxol as well as increased drug localisation in the lung tissue
- 468 (Table 1.5).

469

1.3.2 Dendrimers

Dendrimers are small synthetic macromolecules with a size from 2 to 10 nm (Sherje et al., 2018). Those tree-like structures are characterised by 3D shape, globular structure, and high branching points. The structure consists of a core of a single atom or molecule from which one or more branches depart from. The branches are formed from repeated units connected by branch connections. The final structure is characterised by radial concentric layers which are key for the properties of this nanocarrier (Figure 1.5). The polymers used in the manufacture of these nanostructures are poly(amidoamine) (PAMAM), poly-L-lysine or polyglycerol.

The use of dendrimers as drug delivery systems for inhalation is not very common due to the potential cytotoxicity and reactivity deriving from the presence of different charges on the dendrimers' surface. However, some successful studies are reported in the literature. Nasr (Nasr et al., 2014) investigated the potential of beclomethasone dipropionate dendrimers as aerosol nanocarriers for pulmonary delivery via nebulisation. Zhong and colleagues (Zhong et al., 2016) investigated the pulmonary delivery of doxorubicin-conjugated PAMAM dendrimers as delivery strategy to reduce cardiac accumulation and improve antitumor activity of doxorubicin in lung metastasis showing successful results (Table 1.5).

Table 1.5 Nanocarriers for drug delivery for respiratory therapy.

| Type of nanocarrier | Drug | Clinical applications | Ref |
|---|-----------------------------------|-------------------------------|------------------------|
| Polymeric NPs (PLGA) | Linezolid | Tuberculosis | (Shah et al., 2020) |
| Polymeric NPs (PLA) | Budesonide/Theophylline | Asthma/COPD | (Buhecha et al., 2019) |
| Polymeric NPs (DSPE-PEG/Miglyol® 812) | Cisplatin, doxorubicin | Lung cancer | (Nan, 2019) |
| Polymeric micelle (Chitosan) | Itraconazole | Pulmonary fungal infections | (Moazeni et al., 2012) |
| Polymeric micelle (Cholesterol-conjugated polyamidoamine) | Resveratrol/heme oxygenase-1 gene | Acute lung injury | (G. Kim et al., 2018) |
| Polymeric micelle (PEG ₅₀₀₀ -DSPE) | Paclitaxel | Lung cancer | (Gill et al., 2011) |
| Dendrimer (PAMAM) | Beclomethasone dipropionate | Asthma | (Nasr et al., 2014) |
| Dendrimer (PAMAM) | Doxorubicin | Lung cancer | (Zhong et al., 2016) |
| Exosome | - | Idiopathic pulmonary fibrosis | (Dinh et al., 2020) |
| Exosome | microRNA molecules | Lung cancer | (Nie et al., 2020) |

1.3.3 Exosomes

2

1

- 3 Exosomes are small extracellular vesicles with a size of 40 to 120 nm (Elsharkasy et al.,
- 4 2020) (Figure 1.5). Cells form exosomes to carry nucleic acids, proteins, lipids, and other
- 5 metabolites, therefore playing a key role in the cell communication. Due to their origin
- 6 from cell membranes, they possess a low to non-toxicity and a low clearance rate. An
- 7 additional advantage is the presence of endogen biomarkers on their surface which
- 8 increases the interactions of exosomes with the receptor cells membrane.

9

- 10 Exosomes have been used as delivery systems for the treatment of idiopathic pulmonary
- fibrosis (Dinh et al., 2020) and non-small cell lung cancer (Nie et al., 2020) (Table 1.5).

12

1.3.4 Albumin-based nanocarriers

redisperse in water prior to infusion.

1314

15

16

17

18

19

20

21

22

23

24

25

26

27

28

29

30

31

32

When investigating the potential of a nanoplatform for therapeutic administration, it is fundamental to identify the properties that the nanoplatform possess as well as the improvements that it provides compared to 'non-conventional' formulations. HSA-NPs represent an interesting formulation that reached the market in 2005 with the U.S. Food and Drug Administration (FDA) approval of Abraxane[®], which is currently used for the treatment of metastatic breast cancer, nonsmall cell lung cancer, metastatic adenocarcinoma of the pancreas, bladder cancer and gastric cancer (Table 1.6). Abraxane[®] is the trade name of nanoparticle albumin-bound (nab[™]) paclitaxel (nabpaclitaxel). The manufacture of nab-paclitaxel is called nab-technology and is based on an emulsion-evaporation cross-link method (Fu et al., 2009). The first step of this method is based on the dropwise addition of the oil phase (paclitaxel dissolved in chloroform) to the aqueous phase (HSA solution 1% w/v presaturated with 1% chloroform). The final emulsion is then obtained by homogenisation of the crude emulsion at high pressure and by recycling the emulsion through homogenizer. The nanosuspension obtained with this manufacture method possessed a size of ~ 130 nm and a zeta potential of -31 mV which allowed stability in aqueous phase. After manufacture, the NPs suspension is filtered to provide sterility and to remove particles with an unsuitable size. In order to improve the stability of the product, lyophilisation is utilised obtaining a powder which can be easily

Abraxane[®] replaced the former clinical formulation (Taxol) in which paclitaxel was dissolved in cremophor and ethanol. The use of those cosolvents was fundamental to enable the administration of the drug due to its hydrophobic nature. However, the use of those cosolvents was associated with severe adverse effects which limited its use. Patients experienced acute adverse effects, neutrophilia and hypersensitivity reactions which required preventive treatment with corticosteroids.

The first advantage provided using Abraxane over Taxol was represented by the reduced ratio of side effects. Indeed, in the newer formulation the drug is present in a non-crystallised amorphous state, and it is noncovalently bound to the albumin molecules. In this form, the drug can easily access the target site in contrast to the former formulation where the cremophor micelles hinder the release of the compound resulting in a lower free drug amount in the blood and a following reduced therapeutic activity. In addition, those micelles also slow the elimination rate from the blood resulting in an increased systemic exposure and higher risk of cosolvents correlated side effects (van Zuylen et al., 2001).

In addition, Abraxane showed rapid tissue distribution, increased biodistribution volume and higher rate of clearance. The tumour concentration of paclixatel increased when administered encapsulated in HSA-NPs, explained by the increased transcytosis of Abraxane across the endothelial cells compared to Taxol as demonstrated in a mice model of bearing human breast tumour xenograft (Desai et al., 2006). Indeed, albumin is a key element for tumours as they require it for proliferation and sustainment. In addition, the use of Abraxane increased the tolerability of the drug in terms of concentration. Taxol was injected at 0.3 -1.2 mg/mL with an infusion time of 3 -24 h, whereas Abraxane can be injected over 30 min at 2 -10 mg/mL (Chen et al., 2015; Ibrahim et al., 2002, 2005; Spada et al., 2021).

Besides Abraxane, there are other two albumin NPs-based formulations that have been approved as radiopharmaceuticals for clinical use (Table 1.6). Nanocoll is an albumin colloidal NPs formulation used as a diagnostic as an alternative to sulfur colloid NPs. The injectable formulation is obtained via reconstitution with sodium Pertechnetate (99m Tc) (GE Healthcare, 2015). Nanocoll has a small particle size (mean diameter of 30 nm, with most particles with a size < 80 nm) which allows a quicker migration through the

69 lymphatic system with a consistent and suitable retention within the sentinel lymph nodes. 70 Moreover, due to the higher rate of localisation in the bone marrow after intravenous injection, those NPs are more likely usable for bone marrow imagining compared to the 71 72 sulfur NPs (Thakor et al., 2016). Another albumin-based formulation is Optison which is 73 in the form of albumin microsphere (Table 1.6). It is an injectable suspension of HSA 74 microspheres with perflutren gas as contrast agent. The albumin microspheres have a 75 mean diameter between 3.0 and 4.5 µm with 95% of the microspheres having a size less 76 than 10 µm. This formulation is indicated for use in patients with suboptimal 77 echocardiograms to improve the delineation of the left ventricular endocardial borders 78 (FDA, 2012).

- 80 Extensive reviews about the *in vitro* and *in vivo* investigation of albumin NPs besides the 81 clinical outcomes of various albumin NPs encapsulating a wide range of therapeutic
- 82 agents are reported in the literature (Elzoghby et al., 2012; Hornok, 2021; Karimi et al.,
- 83 2016; Sleep, 2015; Spada et al., 2021).

Table 1.6 Albumin-based formulations approved for clinical use.

| Trade name | Drug | Type of formulation | Physiochemical properties | Therapeutic indication | Advantages |
|---------------|------------------------------|--|--|--|--|
| Abraxane® | Paclitaxel | Nanoparticle albumin- bound (nab [™]) paclitaxel (nab- paclitaxel) | Size: ca 130 nm Zeta potential: -31 mV | Metastatic carcinoma Nonsmall cell lung cancer Metastatic adenocarcinoma of the pancreas Bladder cancer Gastric cancer | Reduced ration of side effects compared to Taxol (paclitaxel in cremophor and ethanol Rapid tissue distribution Increased biodistribution volume Higher rate of clearance Increase concentration of paclitaxel in the tumour Reduced time and frequency of infusion |
| Nanocoll | Sodium Pertechnetate (99mTc) | Technetium- 99m albumin nanocolloid | Size: mean diameter of 30 nm, with most particles with a size < 80 nm | Radiopharmaceutical (diagnostic use only) | Small size allows good retention within the sentil lymph nodes Suitable for bone marrow imaging due to high rate of localisation in the bone marrow |
| Optison | Perflutren | Albumin microspheres with perflutren | Size: mean diameter between $3-4.5 \mu m$ | Diagnostic use only | |

1.3.5 Lipid-based nanoparticles

Despite the positive results obtained, the investigation of the albumin NPs as an inhalable carrier for pulmonary diseases is less explored than other routes of administration as highlighted in the previous paragraph. To our knowledge, the research of inhaled albumin NPs has not yet reached clinical stages and appears to be still preliminary. However, the use of a wide range of other types of nanocarriers has been demonstrated to have potential for pulmonary delivery with advantages compared to 'conventional therapies' (Table 1.5). For example, the lipid nanoparticles (LPNs) have been used in inhaled medicines as described in a comprehensive review highlighting the current trends for drug delivery in respiratory diseases therapeutics which has recently been published (Ibarra-Sánchez et al., 2022).

Indeed, LPNs represent the most successful type of nanocarrier for lung delivery so far developed considering the formulations that have been approved and reached the clinical use. LPNs are characterised by a lipid coating of phospholipids, cholesterol, or surface modified lipids with a therapeutic agent inside the vesicle. Over the decades, studies have been performed to improve their profile and two new categories have been created: solid lipid nanoparticles (SLNs) and nanostructured lipid carriers (NCLs) (Figure 1.5). Compared to liposome which are characterised by a lipid bilayer with an aqueous core, SLNs and NCLs have a hydrophobic core which allows the encapsulation of hydrophobic therapeutics. The aerodynamic diameter of LPNs can vary from 100 nm to larger NPs (up to 2.5 μ m in the case of liposomes). Due to their main component being represented by physiological lipids, they are considered highly biocompatible. This drug delivery system has been demonstrated to be safe in a murine inhalation model when administered as repeated inhalation exposure at concentration lower than 200 μ g deposited dose (Nassimi et al., 2010).

The progress achieved by researchers in the field of LPNs is indeed represented by the first liposomal-based formulation approved by FDA. In 1995 Doxil®, a PEGylated liposome-encapsulated doxorubicin formulation, was approved for the treatment of a wide range of cancers. However, this was for intravenous administration whereas the first true inhaled liposome-based formulation was approved in 2018. This was the case of Arikayce®, Insmed Inc., an inhaled (delivered via nebulisation) liposome amikacin

formulation for the treatment of Mycobacterium avium complex infections. The pulmonary administration of the encapsulated amikacin showed increased antibiotic exposure in the lungs compared to the effect obtained from the intravenous administration of the free amikacin (Zhang et al., 2018). When amikacin was delivered by nebulisation to rats in the liposome-encapsulated form, the drug exposure induced in lung tissue, airways and pulmonary macrophages was respectively ~ 42-, 69- and 274- fold higher compared to intravenous amikacin administration which provided very poor distribution of the drug in the same target areas. This clearly described the potential and the improvements that the nanoplatform provides over the conventional free drug formulation in the treatment of the infection caused by the non-tuberculous mycobacterium disease (Zhang et al., 2018).

46

47

48

49

50

51

52

53

54

55

56

57

58

35

36

37

38

39

40

41

42

43

44

45

The uniqueness of the LPNs is also represented by their chemical nature which allows the encapsulation of a wide range of drugs, both hydrophilic and hydrophobic therapeutics as well as ionisable cationic lipid. In addition, the small size they possess promotes their dissolution into the lung lining surface, whereas their composition makes them highly biodegradable and biocompatible. Extensive reviews highlighted the advantages and disadvantages of the LPNs as well the milestones during the LPNs development towards their success in the clinical use (Li et al., 2022; Rudokas et al., 2016). Despite the preliminary stage at which the investigation of albumin NPs for pulmonary delivery is at, the success gained by different type of nanocarriers mentioned above

59 60

of the nanocarriers' benefits over the conventional formulations and of pulmonary delivery over other routes of administration provide the rationale behind the experimental

represents an important milestone for the proof of concept for nanocarrier based

therapeutics over conventional formulations via the pulmonary route. The combination

work described in this thesis.

62 63

61

64

65

Design considerations for albumin nanocarriers for pulmonary 1.4 68 delivery: improving lung deposition

69 70

67

1.4.1 Appropriate particle size for lung delivery: design of nanoparticle embedded in microparticles (NEMs)

72

73

74

75

76

77

78

79

80

81

82

83

71

In the last decade, innovation has happened in the field of pulmonary delivery. The benefits of controlled and targeted delivery to the lungs are clear, but the development of new formulations is complicated by the challenges that must be overcome. The success of an inhalation therapy depends on many factors with the aerodynamic size of the particles being one of the most important of them (Figure 1.6). It is now well known that particles with an aerodynamic diameter larger than ~ 5 µm will likely deposit in the conducting region of the airways as the oropharyngeal region. In the respiratory tract particles will be subject to clearance mechanisms and eliminated very efficiently by cough or sneezing. In alternative, particles can also be swallowed and go through the gastrointestinal tract, binding to undesired targets which will result in side effects as previously mentioned in the case of PDE4 inhibitors (Robichaud et al., 2002).

84

85 86

87

88

89

90

91

Smaller particles $(1 - 5 \mu m)$ will deposit predominately in the lower airways and thereby avoid mucocociliary clearance. If macrophages clearance is also avoided, the encapsulated therapeutic will be released and exert the desired pharmacological effect. Particles with diameter less than 1 µm will more likely be exhaled as they would remain in the airstream without being deposited. Physical and aerodynamic size-related mechanisms that dictate the deposition of the particles in the airways will be further discussed in Chapter 6.

92

93

94

95

96

97

98

99

With further decrease of the particle size ($< 0.5 \mu m$ – ultrafine particle), lung deposition may increase (Chalupa et al., 2004; Heyder, 2004; Jaques & Kim, 2000). However, this does not apply to individual NP as such with a size within 100 - 200 nm, which interestingly will more likely be exhaled rather than deposited into the lungs. In addition, due to their high surface area and the strong interparticle cohesive forces they tend to aggregate which reduces their stability and dispersability – hence lack of their successful development as therapeutic inhaled dosage forms (Bailey & Berkland, 2009).

It is evident how the need for respirability makes NP design for pulmonary administration challenging and how an advanced formulation strategy is required. Alternative approaches that have been suggested to exploit their benefits by enabling effective pulmonary administration are the so-called Trojan particles and the nanoparticle embedded in microparticles (NEMs). The Trojan particles consists of a large porous carrier in the form of a powder containing NPs and allowing the NPs to be delivered in the lungs. This system possessed both the benefits of the large porous particles and those of the NPs with a resulting ease of flow, good aerosolization and drug delivery potential. The NEMs consists of a nanocomposite system obtained by inclusion of drug-loaded NPs within a microparticle system, using an inert carrier (excipient). This drug delivery system after deposition in the humid lung environment allows the dissolution of the matrix and the further release of the NPs containing the payload (Figure 1.6). This approach will be adopted in this thesis and albumin-based NPs converted into mannitol-based NEMs as formulation strategy to improve the respirability of RFM-HSA-NPs..

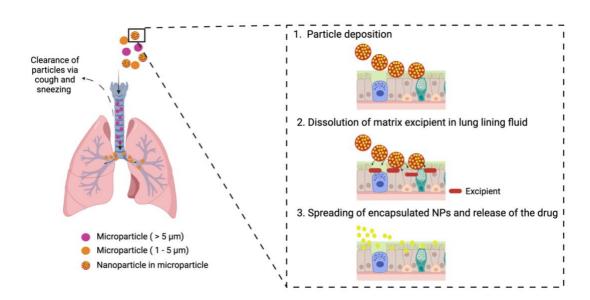


Figure 1.6 Site of deposition of inhaled particles based on the aerodinamic diameter and mechanims of NPs delivery through aerosol of nanoparticle embedded microparticles.

Selecting a nanocarrier based formulation and a suitable inhalation device

for pulmonary delivery

123

121

122

124 In addition to the pharmacological efficacy of the drug itself and the aerodynamic size of 125 the designed formulation, potential NPs must also be compatible with the devices 126 available on the market, especially in view of a potential translation to clinical use 127 (Biddiscombe & Usmani, 2018; Cazzola et al., 2020). There are four different types of 128 pulmonary inhalation pharmaceutical dosage forms on the market which differ for several 129 factors as the effort needed by the patient, the size of the aerosol obtained, the required 130 drug formulation - if solid (powder) or liquid (solution or suspension). Those are 131 nebulisers, pressurized metered dose inhalers (pMDI), dry powder inhalers (DPI) and soft-mist inhalers (SMIs) (Table 1.7). 132 133 The above-mentioned approach based on the NEMs represents a valuable formulation 134 strategy to improve the respirability of a NPs-based powder aerosol (Sung et al., 2007). 135 To convert NPs suspension into a dry powder formulation with good aerodynamic 136 characteristics (NEMs system) spray drying is often used. This process involves different 137 steps carefully controlled by specific temperature and pressure values. It starts with the 138 atomisation through a nozzle of a feedstock solution followed by the rapid evaporation 139 of the liquid components of the droplets into solid powder in a heated chamber. The 140 feedstock solution is represented by a mixture in variable ratio of the NPs suspension with 141 an excipient. Commonly used excipients are sugars (lactose, mannitol, trehalose), 142 synthetic polymers (polyethylene glycol), surfactants or amino acids (Alhajj et al., 2021). 143 Mannitol, a polyol, is widely used to develop inhalable spray dried microparticles from 144 NPs and its superiority over trehalose and L-leucine in the spray drying of albumin NPs 145 has been reported (Patel, 2018; Varshosaz et al., 2015). 147

146

148

149

150

151

152

153

154

The potential and the feasibility of the conversion of albumin NPs into NEMs as a delivery strategy to achieve their pulmonary delivery has been reported in the literature. For example, Papay and others (Pápay et al., 2017) investigated the potential as inhaled carrier of a drug powder formulation of bovine serum albumin (BSA)-apigenin-NPs. The NPs were spray dried with leucine and lactose and aerodynamic characterisation was carried out. Both the formulations showed good fine particle fraction (FPF) values which ranged between 58% and 66% for lactose-based and L-leucine formulations respectively suggesting that the particles had good potential to deposit into the lungs. Within the excipients tested, the use of L-leucine resulted in the powder with the most suitable mass median aerodynamic diameter (MMAD) (2.1 µm).

FPF as well as MMAD and geometric standard deviation (GSD) are some of the descriptors of the aerodynamic particle size distribution of an aerosol. The FPF corresponds to the fraction of the drug mass in the aerosol cloud that has a size lower than the cut-off size (usually considered 5 µm). Despite not corresponding to an exact prediction of the *in vivo* behaviour of the powder, for which full aerodynamic particle size distribution should be considered, FPF is a good parameter to describe the quality of a formulation for inhalation. An interesting review about the advantages and disadvantages of its use in the research and considerations about its application as a predictor of both drug pharmacokinetic and clinical response has been recently published (Newman, 2022). Further details on those parameters and their definitions will be discussed in Chapter 6. In addition, Varshosaz (Varshosaz et al., 2015) studied haloperidol targeted NPs of BSA loaded with doxorubicin. The conversion of the nanocarrier into a NEMs was investigated using three different excipients: trehalose, L-leucine and mannitol. Mannitol-based spray dried powder showed the most favourable aerodynamic characteristics over the three formulations with a MMAD equal to 4.58 µm and an FPF of 66%. A similar formulation strategy was also employed for the pulmonary delivery of rifampicin (Joshi & Prabhakar, 2021), a first-line drug for the treatment of tuberculosis. Rifampicin-loaded BSA NPs were first manufactured and then spray dried to obtain a dry powder inhaler formulation which showed promising results in terms of respirability with a MMAD of 3.21 µm and

The lung delivery of pharmaceutical powders obtained via spray-drying can be achieved with two different types of inhalers: DPIs or pMDI (**Table** 1.7 Advantages and disadvanategs of different type of inhaler devices). DPI are breath-actuated devices which delivery efficiency is highly dependent on the inspiration flow rate. Their use does not require coordination of actuation and inhalation hence are easier to use. Those devices also differ for the number of doses than can be loaded and delivered, with i) single or ii) multi-unit dose inhaler using one single gelatine capsule containing the drug of interest, or multiple sealed blisters; iii) multi-dose reservoir with a bulk supply of powder that is individually dosed at each actuation (Bailey & Berkland, 2009). Dry powders are

FPF equal to 52% (Joshi & Prabhakar, 2021).

considered very stable, but their formulation is challenging as those micronised particles possess a high surface energy which makes them cohesive with following aggregation and poor flowability when delivered. As a result, there is the need to work on the balance between the interparticulate forces in the bulk powder (Hoppentocht et al., 2014). In this thesis the use of spray-dried rather than micronised particles may represent a promising strategy to improve the stability of the formulation and facilitate its translation to the clinic.

pMDIs usually contain a drug dissolved or suspended in a pressure-liquefied propellent.

Those devices are portable and compact and offer some advantages as multi-dosing and

Those devices are portable and compact and offer some advantages as multi-dosing and consisten dosing. Chlorofluorocarbon were originally used in those formulations as propellants; however, after the discovery of their role in the depletion of the ozone layer, they were replaced by hydrofluoroalkane. After dispersion, the propellant evaporates forming an aerosol of dry agglomerated or in situ-precipitated material. pMDIs are more difficult to use as they require coordination between actuation and inhalation to provide a good deposition.

Besides DPIs and pMDIs, nebulisers are devices that can convert a liquid into an aerosol suitable for patient inhalation. This category can be further divided in jet, ultrasonic and mesh nebuliser. Moreover, the latest technology developed is represented by the SMI (Table 1.7). Mesh nebulisers (both static or vibrating) represents a fairly new category of nebuliser and are operated by battery or electricity, are small and silent. As identified by their name, those devices are characterised by the presence of a piezo element in contact with a mesh which produce vibrations. The vibration of the mesh induces its deformation into the liquid side which is pumped into the mesh holes. The ejected droplets can be then inhaled by the patients. However, the efficiency of this device in terms of aerosol output rate and inhaled fraction, defined as a percentage of nebulised volume loaded in the reservoir, is influenced by the type of the loaded formulations. Viscosity of the formulation can influence the nebulisation resulting in more or less fine droplets. Blockage of the mesh aperture due to precipitation and crystallisation of drug particles has been reported in case of highly concentrated drug suspension (Ari, 2014; Vecellio, 2006). On the other side, the device characteristics dictate the droplet size and their distribution. SMIs is the newest type of inhaler, and one example is the Respirat (tiotropium bromide). This is an easy and portable device which does not require

- propellants. However, it needs to be primed if it has not been used for some days
- 223 (Pleasants & Hess, 2018).

Table 1.7 Advantages and disadvanategs of different type of inhaler devices

| | Advantages | Disadvantages | | |
|---|---|--|--|--|
| Nebuliser | Convert liquid into aerosol | | | |
| Jet | • Easy to use | Difficult to cleanNeed compressed gas | | |
| Ultrasonic | • Easy to use | Large residual volumeDegradation of heat-sensitive materials | | |
| Mesh | Small and silentEasy to useOperated by electricity or power | Aerosol output rate and inhaled fraction influenced by type of formulation loaded (e.g. viscosity) | | |
| Soft mist | PortableMultidoseSlow velocity aerosolLong plume duration | No breath-actuated Need to prime if device has not been used in the past days | | |
| Metered pressurised dose inhaler (pMDI) | <u>-</u> | Drug dissolved or suspended in a pressure-liquefied propellent | | |
| | Portable and compactMulti-dosingConsistent dosing | Coordination between actuation and inhalation required Use of propellant | | |
| Dry powder | | Powder, breath-actuated device, delivery efficiency | | |
| inhaler (DPI) | dependent o | dependent on inspiration flow rate | | |
| | Coordination of actuation and inhalation not required > easier to use Single or multi-dose deliverable Formulation stability | Dry powder may aggregate > poor flowability when delivered | | |

Research into the nebulisation of NPs has most often concerned SLNs. Indeed, this is not surprising considering that as mentioned above those nanocarriers represent the most successful carrier that has reached the market. However, there have been some concerns regarding the negative effects that the nebulisation process may have on the structure of the nanocarriers. In fact, the latter must retain their physiochemical characteristics as well as the pharmacological activity of the payload in order to preserve their pharmaceutical acceptability. Therefore, studies should be performed to determine whether it is possible to produce an aerosol compatible with human use. This was the case of an investigation (Hureaux et al., 2009) which aimed to demonstrate that the encapsulation of paclitaxel in lipid nanocapsules and their nebulisation can potentially represent a promising pulmonary delivery strategy. The first part of this study aimed to determine which nebulisers can produce an aerosol of blank lipid nanocapsule unmodified in terms of size and polydispersity index compared to control. Six nebulisers were used: two jet nebulisers, two ultrasonic and two mesh nebulisers. Results showed that ultrasonic nebulisers were not able to produce the aerosol cloud, whereas jet nebulisers induce an alteration of the original particle distribution probably due to a destruction-rearrangement phenomenon correlated to the stress of the jet effect. In contrast, the mesh nebuliser resulted as the most suitable and it was used to further nebulise the formulation to investigate any changes in the drug payload and its pharmacological activity. Only a small reduction of the payload was reported with 1.65 mg/mL of paclitaxel in the not-nebulised formulation and 1.45 mg/mL in the nebulised volume, with the cytotoxic activity of the nebulised formulation similar to fresh paclitaxel nanocapsules.

In a different study investigating the effect of nebulisation on liposomes, Rudokas (Rudokas et al., 2016) indicated that the nebulisation and the ongoing shear forces impacted their physiochemical properties with resulting fragmentation of the lipid vesicles. Further investigation on liposome and on a possible strategy to overcome the impact of the nebulisation on the vesicle structure was conducted by Elhissi (Elhissi et al., 2007). Improvements in their stability when nebulised was achieved with the use of mesh nebulisers with a bigger pore aperture (Aeroneb Pro - 8 µm) over the air-jet nebuliser (Pari LC Plus) or the use of cholesterol in liposome formulations. Moreover, the effect of nebulisation on polymeric NPs was instead reported by Dailey (Dailey et al., 2003) in which research the use of different type of nebulisers (jet, ultrasonic and piezoelectric crystal nebuliser) influenced the NPs aggregation during the nebulisation.

1.5 Fate of inhaled NPs and microparticles: what happens to pulmonary delivered carriers?

Despite the advantages that the pulmonary route offers, current inhalation therapies are characterised by low availability and short half-life due to clearance mechanisms that take place in the lungs which are usually aimed to protect the lungs from foreign particles entering the body (El-Sherbiny et al., 2015). The type of clearance mechanism that the inhaled particle will undergo depends on the site of deposition. The respiratory tract can be divided into two regions: the upper respiratory tract (including nose, nasal cavity and pharynx) and the lower respiratory tract (larynx, trachea, bronchi, alveoli and lungs). Overall, soluble particles deposited in both the conducting airways and alveolar region will undergo dissolution followed by clearance of their components in solution according to pharmacokinetic principles; whereas insoluble particles will be eliminated by mucociliary escalator if deposited in the conducting airways and phagocytised by alveolar macrophages which will then transport the particles towards the mucociliary escalator (Oberdörster, 1993).

The main clearance mechanism that takes place in the upper region of the respiratory tract is called mucociliary escalator. Cilia and secretory cells are the two main components of this innate mechanism defence. The role of the cilia is to beat in a synchronised manner therefore moving the mucus and the entrapped particles to the pharynx to be swallowed; the secretory cells are responsible for the secretion of the mucus. The airway surface mucus layer is responsible for particle entrapment and overlies a periciliary layer, which allows the cilia to beat rapidly due to its low viscosity. The clearance rate is dependent on both the cilia and the lung lining layer with a faster rate in the central airways and slower with the increase of the airway generation. When particles larger than 6 μ m are inhaled, the combined activity of those two cell types results in the particles entrapment in the mucus layer and following elimination via swallowing or coughing due to the cilia movement. The rate of the cilia beating, and the mucus composition may be severely altered in presence of airways diseases, consequently altering the clearance mechanisms of inhaled particles and their deposition (Bustamante-Marin & Ostrowski, 2016; Munkholm & Mortensen, 2014).

Inhaled particles smaller enough to escape the mucociliary clearance, cough and sneezing may be eliminated from the lungs via macrophage clearance. The alveolar and the airway macrophages are considered as the first line of cellular host defence. Macrophages are derived from monocytes and are present in large number in the lungs. Based on the anatomical location, four different type of macrophages can be distinguished (Geiser, 2010): pleural macrophages, are moderately phagocyte and responsible for the influx of polymorphonuclear leukocytes (and consequent interleukin- 6 release) during inflammation; intravascular macrophages, rare in humans and rodent, are highly phagocytic and tend to form complexes with the endothelium; interstitial and surface (alveolar and airway) macrophages are well known for their role in the clearance of particles from the lungs. Interstitial macrophages are key in the release of mediators because of their location in direct contact with the interstitium. Because of their location on the surface of the lungs, surface macrophages are mainly involved in the removal of inhaled particles and in innate immune responses such as chemotaxis. Due to their crucial location on the inner surface of the airways, beneath the surfactant layer and immersed in the lung lining layer, the airway and alveolar macrophages play a primary role in the clearance of particles from the lungs. Usually, macrophages quickly respond to a particle insult, whereas their timing is dependent on the species. The surface macrophages are the cells usually recovered with bronchoalveolar lavage techniques and represent > 97% of recoverable cells from rodents except for guinea pigs, which bronchoalveolar lavage fluid (BALF) was reported to have a resident population of eosinophils (Warheit & Hartsky, 1993). The macrophages mediated phagocytosis of micrometre-sized particles appears consistently different from that of nanometre-sized particles. In the context of nanometresized carrier, Geiser and others (Geiser et al., 2008) evaluated the deposition of inhaled ultrafine TiO₂ particles (20 nm) in the lungs of rats. They found that the surface macrophages clearance was negligible and sporadic and that at 24 h after inhalation only 0.1% of the deposited particles were taken by macrophages, hence concluding that macrophages clearance is negligible in the peripheral lungs where the NPs were hypothetically deposited. However, in contrast, Takeneka and co-workers (Takenaka et al., 2012) showed that after inhalation macrophages engulfed 16-nm Au NPs, concluding that most of the macrophages analysed from the pellet of BALF on day 0 had internalised gold NPs and that this content decreased on day 7 after the inhalation day.

100

68

69

70

71

72

73

74

75

76

77

78

79

80

81

82

83

84

85

86

87

88

89

90

91

92

93

94

95

96

97

98

Considering how the clearance mechanisms can be altered in presence of airways diseases (Gohy et al., 2019; Munkholm & Mortensen, 2014b), it is interesting also to mention an additional study where the cellular uptake of 21-nm Au NPs was evaluated both in a COPD and wild type mice model (Geiser et al., 2013). Particles were mainly found attached on the epithelial surface in form of singlets or small aggregates (< 100 nm) or engulfed by macrophages. At time 0 h after the inhalation, 24% and 58% of the NPs were found in macrophages in the COPD and wild type animal model respectively, whereas the percentage increased in both models at 24 h time point after inhalation. Overall, the NPs uptake by surface macrophages was less efficient in the COPD model compared to the 'healthy' model.

The time course of the particle uptake mediated by the surface macrophages has been evaluated in healthy humans exposed to a bolus inhalation of radiolabelled sulfur colloid aerosol (0.2 µm colloid size delivered in 6 µm droplets) targeting the central airways (Alexis et al., 2006). Besides radiolabelled particle inhalation, induced sputum was used as technique to examine the particle uptake. Indeed, the use of the induced sputum technique allowed the recovery of cells in the central airways which in the case of healthy patients it is mainly composed of surface macrophages and neutrophils. Results showed that the particle uptake was minimal 40 min after inhalation and maximal (31%) at 100 min. Interestingly, the increased macrophage uptake recorded at 100 min corresponded to an increased number and proportion of macrophages, whereas this was not reported for the earlier time point (40 min). This difference was considered a consequence of the time needed to recruit a new population of macrophages after the particle deposition; in addition, they also concluded that consistent particle uptake can only occur in presence of a critical number of macrophages which is higher than the number of macrophages available 40 min after inhalation (Alexis et al., 2006).

The clearance kinetics reported in humans by Alexis (Alexis et al., 2006) was similar to the kinetics reported by Geiser in Syrian Golden hamster in an earlier study (Geiser et al., 1994). Animals were exposed to an aerosol of 6 µm polystyrene particles and lungs fixated 20 min, 40 min and 24 h after the beginning of the inhalation. They found that 40 min after the inhalation, the number of macrophages was increased between 2- and 3-fold whereas the increase was 1.5- and 2.5- fold higher after 24 hours, concluding that the airways macrophages are rapidly (as soon as 40 min) recruited to the site of deposition

| 136 | after the particle exposure. An additional study conducted on hamsters (Geiser et al., |
|-----|--|
| 137 | 1990) also reported that 15 - 20 min after the end of the aerosol exposure, about 29% of |
| 138 | the particles have already been taken by macrophages, whereas overall > 87% of particles |
| 139 | were taken after 24 h. The latter study was carried out in hamsters exposed to an aerosol |
| 140 | of monodisperse polystyrene microbeads of $5.85\mu m$ diameter and particle deposition was |
| 141 | evaluated by fixation of the lungs immediately after aerosol exposure or 24 h after |
| 142 | inhalation. |

Overall, the retention time of nano and microparticles will depend on the site of deposition and on the cells that the particles will encounter. The retention will be shorter if the particles deposit in the conducting airways due to the high efficiency of the mucociliary clearance and of the cough, whereas the retention time will increase with the increase of the airways generation due to the reduced velocity of the mucus.

1.6 Aims and scope of the thesis

- The aim of this thesis was to investigate the potential of HSA-NPs as nanocarriers for lung delivery using RFM, a PDE4 inhibitor, as payload. This included first the development of *in vitro* models suitable to investigate the NPs fate, the release of the payload and the conversion of the NPs into a respirable microparticle formulation for potential clinical translation. In addition, it included the optimisation of *in vitro* and *in vivo* inflammatory models using lipopolysaccharide as trigger agent to test the potential anti-inflammatory activity of RFM as inhaled therapy.
- 159 Specific objectives included:
 - Manufacture and characterisation of roflumilast -HSA-NPs (RFM-HSA-NPs)
 - Conversion of NPs suspension into a respirable powder formulation
- Investigation of the anti-inflammatory activity of inhaled RFM in vitro and in vivo

1.7 Research questions and objectives

- 166 Chapter 2: Can RFM-HSA-NPs be successfully manufactured and release the payload in an *in vitro* model of lung lining fluid?
 - Optimise suitable RFM-HSA-NPs manufacture and characterisation methods

| 169 | • Design of relevant <i>in vitro</i> models to investigate the NPs degradation and the drug |
|-----|---|
| 170 | release from the nanocarrier |
| 171 | |
| 172 | Chapter 3: Can RFM-HSA-NPs be converted into a nanoparticle embedded |
| 173 | microparticles (NEMs) system for pulmonary delivery? |
| 174 | Manufacture of a NEM formulation using a spray-drying method |
| 175 | • Evaluate the properties and respirability of the obtained spray-dried powder: in |
| 176 | vitro aerodynamic assessment |
| 177 | |
| 178 | Chapter 4: Does RFM exert an anti-inflammatory activity in an LPS-challenged |
| 179 | bronchial epithelial cell in vitro model? |
| 180 | • Establish and optimise an <i>in vitro</i> inflammation model using bronchial epithelial |
| 181 | cells and comparing different LPS concentrations and exposure regimes to |
| 182 | produce a robust inflammation model |
| 183 | • Apply the designed model to test the anti-inflammatory activity of RFM as |
| 184 | preventive treatment |
| 185 | |
| 186 | Chapter 5: Do LPS-challenged guinea pigs represent a valuable in vivo model to |
| 187 | mimic COPD exacerbations and demonstrate anti-inflammatory drug action? |
| 188 | Optimise an LPS inflammation whole-body chamber model in guinea pigs |
| 189 | • Validate the applicability of the model to demonstrate anti-inflammatory drug |
| 190 | effects via the oral administration of RFM |
| 191 | |
| 192 | Chapter 6: What is the potential of inhaled albumin-based NPs for topical lung |
| 193 | delivery of therapeutics? |
| 194 | • Manufacture and characterise a suspension suitable for in vivo lung delivery of |
| 195 | RFM to investigate inhaled activity |
| 196 | • Perform aerodynamic characterisation of the above-mentioned suspension to |
| 197 | validate the quality of the aerosol |
| 198 | • Evaluate the anti-inflammatory activity of nebulised RFM in an LPS-challenged |
| 199 | guinea pig model |
| 200 | • Investigate the impact of nebulisation using a mesh nebuliser on the |
| 201 | physiochemical properties of RFM-loaded and blank HSA NP. |

CHAPTER 2: Manufacture and characterisation of roflumilast albumin nanoparticles (RFM-HSA-NPs)

2.1 Introduction

Albumin NPs are a colloidal system that can be produced using simple manufacturing methods and have good physical stability during storage. Due to the high content of charged amino residues, albumin NPs are a good delivery system for both positively and negatively charged molecules. The NPs matrix system allows a sustained delivery when delivered to the target site. Albumin can be obtained from different sources including egg (ovalbumin, OVA), bovine serum (bovine serum albumin, BSA) and human serum (human serum albumin, HSA). Being an endogenous protein, albumin is biocompatible as demonstrated by its use in licensed medicines (Spada et al., 2021).

Serum albumin is the most abundant protein in the bloodstream, and it has important physiological functions as the maintenance of the osmotic pressure and the transport of vitamins, hormones and drugs. Albumin is characterised by three domains (I, II, III), each of them comprised of two subdomains (A and B). The subdomains IIA and IIIA contain two hydrophobic cavities (named Sudlow site I and Sudlow site II) which are the most important binding sites for ligands (Dockal et al., 1999) (Figure 2.1).

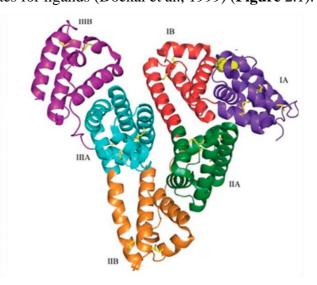


Figure 2.1 Structure of human serum albumin (HSA). Adapted from Spada et al., 2021

HSA is made up of a single chain of 585 amino acids and it is synthetised by the hepatocytes in the liver. It is the most abundant plasma protein, but its majority is stored in the interstitial space. Its biological half-life is of 19 days, despite it can last only 16-18

h in circulation. HSA can bind several molecules, both endogenous (as bilirubin, fatty acids, vitamins) and exogenous (molecules as anti-inflammatory or antibiotics drugs), therefore representing a valuable carrier (Spada et al., 2021).

Regarding the primary structure, BSA contains only 583 amino acids, and its molecular weight differs only by less than 1% compared to HSA's molecular weight. BSA is a globular protein as HSA, and it is negatively and positively charged at neutral and acidic pH respectively. BSA can bind both positively and negatively charged compounds due to the presence of both positive and negatively charged amino acids on its surface. It is a versatile carrier due to its water-solubility, high-loading capability and therefore its ability to bind both hydrophobic and hydrophilic drugs. One difference between those two types of serum albumin is the number of tryptophan residues which are responsible for the fluorescence of the molecule, often used in spectroscopic assays for ligand-binding affinity studies (Ketrat et al., 2020). Due to its low cost, BSA is widely used in research studies as drug carrier. However, its administration in humans is hindered by its immunogenicity linked to its molecular state. The antibody response is driven by the aggregate form and not by the monomer form.

OVA is extracted from the egg white of which is the main protein. It is composed of a single chain of 386 amino acids, and it has a molecular weight of 42-47 kDa. Its functions are still unknown and due to its immunogenicity, it is often used as antigen rather than as drug carrier for the manufacture of NPs (Spada et al., 2021)

2.1.1 Preparation techniques for albumin nanoparticles manufacture

Over the years, this topic has been well reviewed concerning the different available techniques but also the optimisation of the process to obtain a reproducible and simple manufacturing method that produces consistent physiochemical particle characteristics. The available mechanisms for manufacture of albumin NPs are desolvation, emulsification, thermal gelation, self-assembly, nano-spray drying and nab-technology. Error! Reference source not found. presents a summary of the techniques and their advantages and disadvantages. Detailed description of the manufacturing methods can be found in several reviews (Elzoghby et al., 2012) (Verma et al., 2018) (Lohcharoenkal et al., 2014) (Tarhini et al., 2017) (Sleep, 2015) (Karimi et al., 2016), (Sundar et al., 2010),

- original reports (Joshi et al., 2020), (S. H. Lee et al., 2011), (Galisteo-González & Molina-
- 59 Bolívar, 2014) (Pinto Reis et al., 2006) (Moinard-Checot et al., 2006), (Jahanban-
- 60 Esfahlan et al., 2016) and book chapters (Elzoghby et al., 2015), (Otagiri & Chuang,
- 61 2016; Pathak & Thassu, 2016).

Table 2.1 Advantages and disadvantages of albumin nanoparticles manufacture methods available in the literature.

| Albumin nanoparticle manufacture method | Advantages | Disadvantages | References* |
|---|--|--|---|
| Desolvation Emulsification | Easy and highly reproducible No need of specific device Easy process | Use of organic solvent Use of crosslinker Residual organic solvent and oil phase Thermal stabilization only for not heat sensible molecules | (Galisteo-González & Molina-Bolívar, 2014; Jahanban-Esfahlan et al., 2016; Kouchakzadeh et al., 2014; Langer et al., 2003; Sadeghi et al., 2014; Tarhini et al., 2017; von Storp et al., 2012; Weber et al., 2000) (Desai, 1999; Lomis et al., 2016a; Müller et al., 1996; Patil, 2003) |
| Thermal gelation | Good to obtain albumin nanoscale hydrogels | Need of surfactant - | (Yu Shaoyong, Yao Ping, Jiang Ming, 2006) |

| Self-assembly | High degree of drug loading | - | (Gong et al., 2009) |
|-------------------|---|---|---|
| Nano-spray drying | Suitable for sensible molecules | Need of specific device | (Arpagaus, 2018; S. H. Lee et al., 2011) |
| Nab-technology | Safe and solvent-free Suitable for intravenous administered nanoparticles Polymeric material or surfactant not required | Need of specific device | (Desai, 2011; Fu et al., 2009; Hawkins et al., 2008) |

^{*} Selected articles describing the manufacturing methodology and optimisation in detail

Of these methods, two of the most widely used, easily reproducible and not requiring specific technology will be explored in more detail: desolvation, which is the method of choice in this experimental work, and the emulsification process. These two methods will be compared, with an emphasis on the method optimisation regarding reproducibility and particle properties (**Figure** 2.2).

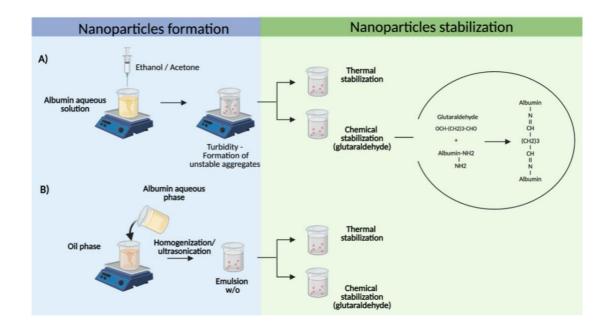


Figure 2.2 Illustration of the main steps in the desolvation (A) and emulsification (B) manufacturing methods.

2.1.2 Crosslinking techniques

Cross-linking is an essential step for NPs preparation, and it influences the drug release as well as the carrier biodegradability. There are some chemical cross-linkers that include the use of molecules like glutaraldehyde, but also glucose, ascorbic acid, tannic acid, citric acid, and sorbitol; alternatively, physical crosslinking methods include heating and ultraviolet (UV) irradiation (Amighi et al., 2020; Niknejad & Mahmoudzadeh, 2015).

Glutaraldehyde (GLU) is the molecule adopted experimentally in this chapter. GLU is included in aqueous solution and various concentration are reported in the literature as effective cross-linking methods. The amount of crosslinker to use is determined by the desired degree of crosslinking of the NP system. The stabilisation is effected by a condensation reaction between the aldehyde group of GLU and the amino moieties of the

albumin, forming a Schiff base (D. Zhao et al., 2010). In the case of NPs obtained by the emulsion method, the chemical stabilisation is based on the addition of GLU to the first emulsion or on the resuspension of first emulsion in ether containing formaldehyde or 2,3- butadiene. Alternatively, the first emulsion is added dropwise to heated oil phase under constant stirring to evaporate the aqueous phase. Different temperatures are reported in the literature. Weber and co-workers (Weber et al., 2000) performed a systematic study focussing on the relationship between the use of different amount of GLU for cross-linking and the resulting number of available amino groups on the surface of HSA NPs after cross-linking. Amount of GLU from 0 to 200% of the theoretic amount needed to the quantitative cross-linking of the total number of amino groups available in the HSA molecule (equal to 59) were employed. Results showed that the number of available amino groups on the NP surface decreased with GLU percentages from 40 to 200%, with the degree of crosslinking of NPs increasing with the increase of the GLU concentration. The use of percentage of GLU lower than 40% produced unstable NPs with an unexpectedly low number of amino groups on the NPs surface, hence concluding that stable NPs will be formed with GLU concentration not lower than 40% of the theoretical amount of GLU to cross-link the total number of amino groups available.

However, some concerns have arisen about the toxicity of GLU. As an alternative Niknejad and others (Niknejad & Mahmoudzadeh, 2015) evaluated methods including ultraviolet (UV) irradiation in combination or not with glucose. Their data support the idea that a combined UV and glucose technique can be a promising alternative to GLU, producing same size NPs as those produced by GLU crosslinking. The effect of different crosslinking agents in the preparation of BSA NPs was well described by Amighi (Amighi et al., 2020).

Heat stabilisation. As an alternative to the use of a cross-linker, heat stabilisation has also been investigated. The incubation of particles (obtained by desolvation method) for less than 48 hours at 50°C and at 60°C for less than 24 hours did not sufficiently stabilise the colloidal system, confirming that albumin resists cross-linking after being heated at 60°C for ten hours. Heating for two hours at 70°C however showed particles were cross-linked (Weber et al., 2000). Interestingly, in contrast to cross-linking by GLU, the heating does not change the number of amino groups available on the albumin surface. This could be explained by heating process only affecting the internal functional groups of albumin.

Heat leads to the formation of amide groups between amino and carboxyl groups of the protein whereas cross-linking involves the reaction of two amino groups of the protein by the aldehyde.

2.1.3 Determinants for a controlled size, PDI and zeta potential NPs population

The high reproducibility of the desolvation and emulsification processes reflects that the critical processing factors can be controlled to obtain a consistent size, with a narrow particle size distribution and consistent zeta potential. NPs' characteristics obtained by desolvation can be controlled varying GLU concentration, the rate of addition of desolvating agent and its ratio, albumin concentration and pH of albumin aqueous solution (**Table** 2.2). Extensive studies of NPs determinants for controlled size, polydispersity index (PDI) and zeta potential were conducted by J. M. Gallo (Gallo et al., 1984) and B.G. Müller and co-workers (Müller et al., 1996) and by L. Yang (L. Yang et al., 2007).

Glutaraldehyde concentration. Weber (Weber et al., 2000) reported that the GLU concentration and the denaturation time do not affect the size of NPs. Langer (Langer et al., 2003) reported the same results after a study that involved the use of different concentrations of GLU (40, 100 and 200%) of the theoretical amount needed to quantitatively crosslink the available amino groups on the albumin surface. On the other hand, the GLU concentration affects the zeta potential. The increased concentration of GLU reduces the positively charged amino groups and increase the negatively charged carboxyl groups, with a consequent decrease of zeta potential with increasing GLU concentration.

Desolvating agent. The volume of desolvating agent is positively correlated with particle size when the volume is up to 1.5-fold the initial volume of albumin aqueous solution. This effect does not persist with further increase of the ethanol volume. The increase of ethanol volume also positively affects the particle concentration. Langer and co-workers (Langer et al., 2003) confirmed that the amount of desolvating agent controls the particle size, but also that the variability at any given volume was high. Therefore, a controlled addition method was developed, switching from the manual addition to a pump-controlled system consisting of a syringe and a specific gauge needle.

pH of aqueous solution. It is also widely reported (Langer et al., 2003) how i) the pH strongly influences the size of albumin NPs and ii) particle diameter decreases away from the albumin isoelectric point (pI=4.9). Average particle diameters decreased from 275 nm at pH 7.5 to 180 nm at pH 9. At pI of protein, the net surface charge is zero, therefore there is no electrostatic repulsion and aggregates are formed only by non-specific interactions. At pH below the pI, the protein carries a positive net charge and as the pH deviates more positively from the pI, the net charge becomes more negative as the carboxyl groups of the protein undergo greater deprotonation. The surface charge provides an electrostatic repulsion that results in reduced aggregation and therefore smaller particles (Amighi et al., 2020). Thus, the pH of the aqueous solution also affects the stability of the particles and their zeta potential. For example, increasing the pH value, the zeta potential reduced from - 40 to - 50 mV at pH between 7.2 and 10. Tarhini and colleagues (Tarhini et al., 2018) showed a consistent positive zeta potential (15 mV) for pH equal to 3 and at higher pH in the range 5 to 11 the particles drop to negative values between - 18 and - 23 mV.

Albumin concentration. Albumin concentration also affects the size of NPs. Based on the study performed by Amighi (Amighi et al., 2020), particle size and PDI increase when the albumin concentration increases from 20 to 50 mg/mL and this is explained by the nucleation theory, which can be generally defined as the first step in a self-assembly process that allows a new structure to be formed. A detailed review of the mechanism of nucleation in relation to the growth of NPs in solution is reported in the literature (Thanh et al., 2014). Müller and colleagues (Müller et al., 1996) showed that the smallest particle size when manufacturing albumin nanospheres via an emulsion process was obtained at an albumin concentration of 5 to 20% w/v; no particle sizes below 300 nm cannot be obtained with albumin concentration higher than 20% w/v.

Aqueous to non-aqueous phase volume ratio. It has a consistent and remarkable effect on particles size. It was reported that no particle size below 300 nm can be obtained with an aqueous ratio higher than 9% v/v (Müller et al., 1996).

Table 2.2 Factors affecting size and zeta potential of albumin nanoparticles.

| | | Effect on |
|--------------------------|--|--|
| | Size | Zeta potential |
| Glutaraldehyde | No effect on size | Effect on zeta potential - increasing concentration of GLU |
| (GLU) | | reduced the positively charged and increased negatively charged |
| concentration | | groups with a following decrease of zeta potential |
| Desolvating agent | • Positive correlation when volume of | - |
| | desolvating agent is up to 1.5-fold initial volume | |
| | albumin solution; | |
| | • Positive correlation also on particle | |
| | concentration | |
| pH aqueous | Particle diameter decreases away from the albumin | Reduction of zeta potential with increasing pH values $(7.2 - 10)$ |
| solution | isoelectric point | |
| Albumin | Size and polydispersity index increase with increasing | - |
| concentration | albumin concentration (from 20 to 50 mg/ml) | |
| Aqueous to non- | Effect in particle size with no particle size < 300 nm | - |
| aqueous phase | achievable with a ratio > than 9% v/v | |
| volume ratio | | |

2.1.4 Degradation of albumin nanoparticles

| ٠, | |
|----|--|
| | |
| | |

1

3 The inclusion of trypsin or other proteases in drug release in vitro models is a useful tool 4 to analyse how albumin NPs undergo degradation. This is of particular interest when 5 considering the degradation of the albumin NPs and the drug release in a simulated lung 6 environment. The use of trypsin to investigate albumin-based drug delivery system degradation has been the subject of a number of studies. Wartlick and colleagues 7 8 (Wartlick et al., 2004) reported the incubation of HSA-NPs with trypsin and proteinase 9 K as method for quantitative evaluation of particle degradation aiming to quantify the 10 matrix-bound drug. Both the enzymes were found to be suitable to obtain fast and 11 complete degradation of the particles within 60 min. They reported that the rate of 12 degradation mediated by those two enzymes was dependent on the degree of cross-linking 13 and that maximum degradation efficiency was obtained with a NPs degree of crosslinking 14 equal to 40%. The effect of trypsin in the release medium was also investigated by 15 Merodio and co-workers who found that the addition of trypsin did not have a significant 16 effect on the release profile of ganciclovir (Merodio et al., 2000); in contrast the release 17 profile of Rose Bengal was dramatically enhanced by the protease activity (W. Lin et al., 18 2001b) as well as the release of 10-hydroxycamptothecin (HCPT) from BSA-NPs (L. 19 Yang et al., 2007). 20 Later, Langer and co-workers (Langer et al., 2008) performed a systematic study of the 21 enzymatic degradation of blank albumin NPs in presence of trypsin, proteinase K, 22 protease from bovine pancreas, pancreatin, pepsin and cathepsin B at different pH values. 23 The aim was to study the enzymatic degradation of blank albumin NPs to investigate 24 degradation under the assumption that it is a critical parameter for the release of the 25 embedded drug. Those enzymes were employed also to assess the NPs biodegradability. 26 Results showed that the degradation activity of trypsin was highly dependent on the 27 crosslinking degree, with only 9% of NPs having 100% degree of crosslinking being 28 degraded within 24 h. Specific attention was given to cathepsin B, because of its presence 29 in the lysosomes of cells, which is where drug release from the NP matrix will occur if 30 particles translocate to lysosomes after endocytosis and are therefore liable to degradation 31 by lysosomal enzymes such as cathepsin. The fastest NPs degradation was seen under 32 acidic pH, by pepsin and cathepsin B. Under neutral conditions, degradation was achieved 33 over a longer timeframe of 24 h by trypsin, proteinase K and protease. However, NPs 34 with 100% cross-linking degree were not fully degraded within 24 h by any of the

35 enzymes (trypsin, proteinase K, protease and cathepsin B), whereas quantitative 36 degradation was possible with lower cross-linking degree NPs by multiple enzymes. It 37 was concluded that trypsin, proteinase K, protease and pepsin were suitable to obtain 38 overall a rapid degradation of albumin NPs and to investigate in vitro the release of the 39 embedded drug. It is evident that the choice of the specific enzyme to be used should be 40 also made based on the stability of the drug under acidic or neutral conditions and on the 41 degree of the crosslinking of the NPs. These studies highlight clearly that protease 42 degradation is an essential parameter also for the release of a drug from an inhaled 43 formulation, and that it must be considered in pharmacokinetic studies. 44 In the context of how proteases affect the degradation of an albumin carrier deposited 45 into the lungs and therefore its drug release rate, an improvement in the understanding of 46 the albumin-based NPs fate after pulmonary administration was recently achieved by 47 Woods and colleagues (Woods et al., 2020). Predominant proteases were quantified in 48 BALF of healthy human volunteers. Four proteases model were defined: (i) trypsin only, 49 where the trypsin concentration adopted mimics the total protease concentration found in 50 BALF (100 µg/mL), (ii) healthy lung protease model, a complex model that 51 combined cathepsin D, cathepsin H, dipeptidyl carboxypeptidase I/ angiotensin-52 converting enzyme and dipeptidyl peptidase IV, (iii) neutrophil elastase only to model 53 the protease conditions in the lung during inflammation and (iii) inflamed lung protease 54 model, based on the healthy model with the addition of neutrophil elastase. It is interesting 55 to highlight how the presence of the proteases affected the degradation rate outcome in comparison with the incubation of particles in enzyme-free phosphate buffered saline 56 57 (PSB). Results showed that particles remained intact for over 48 h in PBS, but degradation 58 occurred more rapidly (50% reduction in 10 minutes) in the trypsin only model compared 59 to the healthy model (50% reduction in 150 minutes). The inflamed model showed a more 60 variable degradation profile. These studies illustrate the importance of considering the 61 effects of proteases on the stability of NPs for the delivery to the lungs and to include the 62 protease profile in predictive models. 63 It is therefore evident how the addition of a protease in a drug release or particle clearance 64 model represents an important factor to make the model more faithful and reliable in 65 terms of the lung simulated environment.

2.1.5 Drug loading into albumin nanoparticles

68 69

70

71

72

73

74

75

76

77

78

79

80

81

82

83

84

85

86

87

88

89

90

91

92

93

94

95

96

97

98

99

100

Albumin is known for its extraordinary binding capacity due to its highly adaptable binding sites. It can bind endogenous molecules, such as non -esterified fatty acids, thyroxine, hemin, and bilirubin (Peters, 1996), and drugs. In general, the loading of a drug in albumin NPs can be achieved either by encapsulation inside the NPs matrix or by interaction with the protein via numerous surface functional groups present on the albumin surface. Water soluble drugs can be loaded by either an incubation or incorporation method. The first is based on the incubation of the drug with the formed and hardened particles; the second on the incorporation of the drug in the albumin solution prior to NPs formation. Alternatively, the drug can be added to GLU solution before NPs formation and cross-linking. In contrast, water insoluble drugs are dissolved into the organic solvent if a desolvation method is used as in the context of this work. **Table** 2.3 summarises drugs that have been loaded in BSA or HSA-NPs according to the literature. The impact of the drug loading method on NPs characteristics was investigated by Merodio and colleagues (Merodio et al., 2000), who characterised three separate formulations where the drug was (a) incubated with the just formed albumin NPs, resulting in surface adsorption and little or no incorporation of the drug into the matrix; (b) added to an aqueous albumin solution; or (c) added to a solution of albumin and GLU prior the addition of desolvating agent and therefore formation of the carrier. They described that the lowest encapsulation efficiency was achieved by adsorption with 12.5 \pm 1.5%, followed by the model c where drug was incubated with albumin and GLU with $20.0 \pm 2.5\%$. The lower encapsulation efficiency in model c was attributed to a negative effect of GLU on the protein-drug interactions (Das et al., 2005; Merodio et al., 2000). The highest encapsulation efficiency at any specific drug/albumin ratio was achieved by model b with a value of $40.6 \pm 3.3\%$. In agreement to Merodio, also Lin and colleagues (Lin et al., 2001a) reported loading differences between NPs produced by incubation of the drug with albumin prior to particles formation and by addition of the drug post particle formation for Rose-Bengal albumin NPs. Merodio and colleagues (Merodio et al., 2000) also investigated the effect of the incubation time of the drug with the albumin NPs, albumin solution or albumin solution with GLU. The ganciclovir loading increased during the first four hours of incubation both in model (a) and (c), remaining constant despite further incubation. In contrast, the

drug loading behaviour for NPs formed using model (b) was characterised by a plateau reached after 30 min without a further increasing in the next four hours of incubation.

Overall, the drug loading content and encapsulation efficiency can be influenced by factors such as (1) affinity between drug and albumin; (2) drug solubility in water and (3) drug/albumin ratio.

Table 2.3 Examples of drugs that can be encapsulated in albumin NPs described in the literature.

| Drug encap | sulated | Drug MW (g/mol) | Drug LogP | Manufacture method- crosslinking technique | Drug loading method | Albumin source | Encapsulation Efficiency (%) [†] | Reference |
|-------------|-----------|--------------------|--------------|---|------------------------|-------------------|--|--------------|
| 10- | | 364.4 | 0.6** | Emulsion-heat | - | Bovine | 57.5 | (L. Yang et |
| hydroxycam | ptothecin | | | stabilization technique | | | | al., 2007) |
| (HCPT) | | | | | | | | |
| Aspirin | | 180.16 | 1.2 | Desolvation - | Incorporation | Bovine | 81.1 | (Das et al., |
| | | | | glutaraldehyde | | | | 2005) |
| Docetaxel | & | 807.9 | 1.6** | Desolvation - | Dissolution in | Bovine | o DTX-QT-BSA-NPs: | (Desale et |
| Quercetin | | 302.24 | 1.5** | glutaraldehyde | organic solvent | | 75.18 (DTX), | al. 2018) |
| | | | | | | | 68.09 (QT) | |
| | | | | | | | o DTX-BSA-NPs: | |
| | | | | | | | 80.4 (DTX) | |
| Ganciclovir | sodium | 277.21 | -1.5 | Desolvation - | Incubation, | Bovine | 12.5, 40.6, 20.0 †† | (Merodio |
| salt | | | | glutaraldehyde | incorporation, | | | et al., |
| | | | | | and incubation | | | 2000) |
| | | | | | with albumin | | | |
| | | | | | and crosslinker | | | |

| Methotrexate | 454.4 | -1.8 | 1-ethyl-3-(3- | Dissolution in | Human | - | (A. Taheri |
|----------------------|---------|-------|--------------------------|-----------------|--------|------------------|--------------|
| | | | dimethylaminopropyl) | organic solvent | | | et al., |
| | | | carbodiimide HCl | | | | 2011) |
| Noscapine | 449.9 | - | Desolvation - | Incorporation | Human | 97 | (Sebak et |
| hydrochloride | | | glutaraldehyde | | | | al., 2010) |
| Obidoxime dichloride | 359.2 | - | Desolvation - | Incubation | Human | 59.2 (adsorption | (Kufleitner |
| | | | glutaraldehyde | | | efficiency) | et al., |
| | | | | | | | 2010) |
| Paclitaxel | 853.9** | 2.5** | Desolvation- | Dissolution in | Human | 85.7; | (Lomis et |
| | | | intramolecular disulfide | organic solvent | | 81.80 – 97.96; | al., 2016a; |
| | | | bonds; | | | 95.3 | Ruan et al., |
| | | | Emulsion-solvent | | | | 2018; D. |
| | | | evaporation method; | | | | Zhao et al., |
| | | | Desolvation- | | | | 2010) |
| | | | glutaraldehyde | | | | |
| Docetaxel | 807.9 | 1.6** | Self-assembly – | Dissolution in | Human | 63.1 | (Qu et al., |
| | | | Sodium tartrate or | organic solvent | | | 2019) |
| | | | gluconate | | | | |
| Rose Bengal | - | - | Desolvation – | Incubation, | Human* | - | (W. Lin et |
| | | | glutaraldehyde | incorporation | | | al., 2001a) |

| Sorafenib | 464.8 | 4.1** | Desolvation - 1-ethyl-3- (3- dimethylaminopropyl) carbodiimide HCl | Dissolution in organic solvent | Human | 91.09 | (Gao et al., 2019) |
|------------|---------|-------|---|--|-------|-------|------------------------|
| Tacrolimus | 804.0 | 2.7** | Nab [™] -technology | Dissolution in organic solvent | Human | 79.3 | (Thao et al., 2016) |
| Colistin | 1155.45 | -2.4 | Double-emulsion (W/O/W) | Dissolved in aqueous solution of Span83 TM (1% w/v) | Human | 98.65 | (Scutera et al., 2021) |

^{106 *}Albutein

^{107 **} Values vary from the different sources used (PubChem and DrugBank).

[†] If multiple values of encapsulation efficiency are reported in the reference, only the one obtained by the optimal formulation and manufacture method is reported in the table.

^{††} Values are referred to a ratio of 250 µg ganciclovir/ mg initial protein.

2.1.6 Drug release from albumin nanoparticles

| 2 | |
|----|---|
| 3 | The method of incorporation of the drug into the carrier - whether being physically |
| 4 | entrapped within the cross-linked matrix, adsorbed on the surface, or chemically |
| 5 | conjugated to the particles -does not only affect encapsulation efficiency, but also drug |
| 6 | release. In general, drug release rate depends on factors like solubility of drug, |
| 7 | polymer/drug interactions, water absorption, drug diffusion through NPs matrix, |
| 8 | combination of erosion/diffusion process in the carrier (Mohanraj & Chen, 2006). A |
| 9 | detailed review of drug release mechanisms in poly (lactic-co-glycolic acid)-based NPs |
| 10 | is provided by Fredenberg and colleagues (Fredenberg et al., 2011). |
| 11 | |
| 12 | Desai (Desai, 2011) classified NPs into four different groups depending on binding and |
| 13 | loading mechanisms of the drug which can be a) covalently or b) noncovalently linked to |
| 14 | a cross-linked albumin matrix; c) noncovalently adsorbed on the surface of crosslinked |
| 15 | albumin matrix; d) in a core coated by albumin when the drug is hydrophobic, and a nab- |
| 16 | technology (nanoparticle albumin bound technology) method is used. The latter is an |
| 17 | additional technique to manufacture albumin NPs. It is usually applied for poorly water- |
| 18 | soluble drugs, and it requires the formed drug-albumin NPs to go through a jet under high |
| 19 | |

or absence of a crosslinker) and resulting in vitro drug release profiles for experimental

albumin NPs formulation reported in the scientific literature.

Table 2.4 Evaluation of correlation between drug loading methods in albumin NPs and resulting drug release profiles.

| Drug | rug Drug loading Cross- Drug release from method linker NPs | | Drug rele | Ref | | | | |
|------------------------|---|-------------------------------|------------------------|--|---|-------------------|----------------|-----------------------|
| | | | | | Method of experiment | Release medium | Trypsin Y/N | |
| | | Biphasic release | : initial b | urst release followed | by sustained relea | se over time | ; | |
| Docetaxel quercetin | & | Incubation in organic solvent | 5 μL of 25% GLU | Burst release up to 2 h for both drugs, followed by sustained release for up to 24 hours | shaking at 100 rpm, 1 mL samples withdrawn | 7.4 with | N | (Desale et al., 2018) |
| Gabapentin | | Dissolved in albumin solution | 100 μL of 4% GLU | Initial fast release due to the desorption and diffusion of the drug on the outer surface of the particles; the drug across the albumin matrix is released | shaking at 100 rpm; aliquots of 2 mL withdrawn and replaced with fresh | pH 7.4, 50 | N | (Wilson et al., 2014) |

slower in a sustained way up to 24h

| Oligonucleotides (PO) | PO-NPB Incubation with albumin solution | GLU: from 0.06 to 12.5 µg/mg | | NPs dispersed in different types of release media, shaking incubator at | pH 7.4 (0.05, 0.15 or 1 M) | N | (Arnedo et al., 2002) |
|--------------------------|--|--|---|---|----------------------------------|---|------------------------|
| Paclitaxel | Dissolved in organic solvent and later added to albumin solution; three different initial concentration of drug tested (0.5 – 1.0 and 1.5 mg/mL) | None | Initial burst release by the first 12 h (cumulative % of drug released by 12 h inversely proportional to the initial drug concentration); continuous slow increase of drug release by 48 hours. | PBS at 37 °C, shaking at 120 rpm, aliquots of 0.5 mL | PBS | N | (Lomis et al., 2016b) |
| Palladum complex (II) | _ | · | A percentage of 36.7% of the release within the first 20 h due to the | shaking at 170 rpm | - | N | (Karami et al., 2020b) |

| | | adsorbed drug complexes on the NPs surface | release removed and replaced with fresh | |
|-------------|---|---|---|--|
| Ganciclovir | A) Addition and A)1.56 incubation (2h) of µg/mg drug with HSA hardened formed B) 1.56 NPs µg/mg HSA B) Incubation of C) 1.56 drug with HSA µg/mg solution; GLU HSA added to coacervates already formed C) Drug added to HSA solution | followed by a step of slower release for all three NPs models over 5 days; however, the percentage of drug release over time differs within the three models due to the different fractions of drug on the surface of the NPs (initial burst release) or covalently linked to the protein matrix via GLU. The | eppendorf; at predetermined time point supernatant was collected after centrifugation; shaking at 37 °C – | N and Y (Merodio (9300 et al., U.I.) 2000) bovine pancreas trypsin added to NPs in PBS |
| | containing GLU with following incubation | presence of trypsin slightly increases the amount of drug released for each model. | | |

| | | Susta | ined release overtime – no | burst effect | | | |
|------------|--|-------|---|--|-----------------------|---|---------------------|
| Docetaxel | Incubation with ethyl alcohol and mixing with hydrogen phosphate and pre-heated HSA | none | Sustained drug release over 48 hours | shaking at 100 rpm, 0.5 mL sample | 0.5% v/v | N | (Qu et al., 2019) |
| Tacrolimus | nab- technology | none | Gradual release over 24 hours of tacrolimus content of HSA-NPs | 2 mL samples were | with 0.1% (v/v) Tween | N | (Thao et al., 2016) |
| Paclitaxel | PTX-PEG-HSA: drug cofused with PEG; mixing of the PTX-PEG solid dispersion with HSA solution PTX-HSA: dissolved in organic solvent | None | Steady and continuous release with no initial burst effect (35% and 53% of PTX released from PTX-HSA and PTX-PEG-HSA respectively over 4 days). Overall, the cumulative PTX released in 10 days is about 80%. | shaking at 100 rpm over 12 days, 1mL aliquots withdrawn and replaced with | 0.2% Tween | N | (Yin et al., 2015) |

| | | | | Monopha | sic release | | | |
|------------------|----------------|---------|------|-----------------|-----------------|------------------|---|-----------------|
| Phosphodiester | PO-NPA: | GLU: | from | Complete and | Eppendorf | PBS pH 7.4 | N | (Arnedo et al., |
| oligonucleotides | Incubation of | 0.06 to | 12.5 | instantaneous | tubes, NPs | (0.05, 0.15 or 1 | | 2002) |
| (PO) | PO with pre- | ug/mg | | release of | dispersed in | M) | | |
| | formed albumin | | | almost the | different types | Citrate buffer | | |
| | NPs | | | whole amount | of release | 0.19 M (pH 3, | | |
| | | | | of drug | media, shaking | 5, 6.5 or 7.4) | | |
| | | | | adsorbed on the | incubator at 37 | | | |
| | | | | particles | C, 60 | | | |
| | | | | surface | strokes/min | | | |
| | | | | | | | | |

The three most common particles conformations in terms of albumin-drug structure and the resulting three general release profiles are illustrated in **Figure** 2.3. According to these variables, three different drug release profiles can be identified: A) drug release from cross-linked albumin NPs is generally biphasic, with an initial quick release of the drug, followed by a slow-release phase (Arnedo et al., 2002; Desale et al., 2018; Gao et al., 2019; Karami et al., 2020a; Lomis et al., 2016a; Merodio et al., 2000; Wilson et al., 2014). One fraction of the loaded drug is physically bound to the surface of the NP, easily being removed, therefore leading to the initial burst release. Another fraction is incorporated deeper into the NP matrix or covalently linked to albumin with cross-linkers, being removed more slowly, leading to a prolonged sustained release; B) sustained release overtime with no burst effect (Qu et al., 2019; Thao et al., 2016; Yin et al., 2015); C) monophasic burst release when albumin NPs are prepared *via* surface adsorption post-particle production and the drug is only physically adsorbed on the particles (Kufleitner et al., 2010) (Figure 2.3).

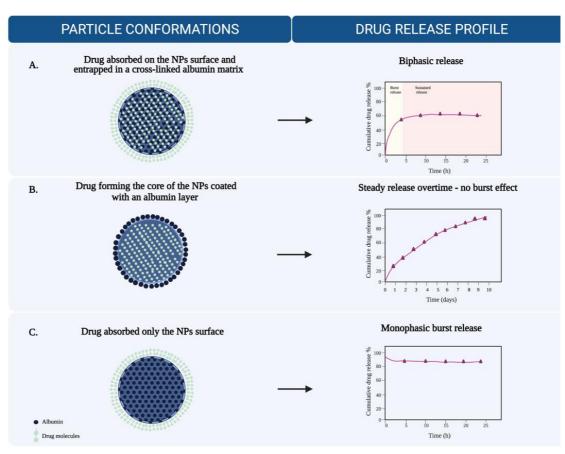


Figure 2.3 Schematic correlation between albumin nanoparticles conformations and drug release profiles.

2.2 Aims and objectives

1617

- 18 The overall aim of the experiments described in this chapter was to investigate the
- 19 development of a successful albumin-based drug delivery nanoplatform that can be
- 20 converted into a respirable formulation. The target product profile for the nanoplatform
- is that it is able to i) encapsulate RFM; ii) undergo degradation using a clinically relevant
- 22 model that is characterized by protease concentration comparable to the lung
- concentration; iv) release RFM in a sustained manner.
- 24 Specific objectives included:
- 1. Design a robust and reproducible lab-based manufacture technique for HSA NPs
- with small particle size, low polydispersity index and suitable encapsulation
- 27 efficiency;
- 28 2. Use a suite of characterisation techniques to evaluate the physiochemical
- 29 properties of the NPs;
- 30 3. Investigate the degradation rate of the NPs using a simplified *in vitro* model of
- 31 proteases;
- 4. Establish and optimise a robust method for quantifying the drug release from the
- NPs overtime.

34

2.3 Methods

3536

37 2.3.1 Manufacture of blank and drug-loaded albumin NPs via desolvation method

- 39 Blank and drug-loaded albumin NPs were manufactured using a desolvation method,
- schematically represented in **Figure** 2.4. Human serum albumin (HSA) (50 mg) was
- dissolved in 1 mL of Tris buffer HCl 0.01 M pH 8.9 and gently shaken for 10 min (shaker
- 42 Model R100 Rotatest shaker Luckham) to allow complete dissolution of the powder. An
- aliquot (25 µl) of sodium hydroxide 1 N was added to the hazy albumin solution under
- gentle stirring to increase the pH to 9 prior to the ethanol addition. For blank (RFM-free)
- 45 NPs, ethanol (4 mL) was added dropwise to the albumin solution under stirring (850 rpm,
- 1 cm magnet) until turbidity appeared and the NPs suspension appearance turned to milk
- 47 colour. The change of the albumin solution colour from haziness to milky appearance
- 48 corresponded to NP formation. For drug loaded albumin NP, roflumilast (RFM) (1 mg)
- 49 was dissolved in the ethanol (4 mL). For both the formulations, controlled addition of

ethanol was achieved using a 10 mL syringe (without piston) attached to a 21 G needle. The addition of the total volume of ethanol was performed in 1.25 mL increments at an infusion rate of ca 1.25 mL/min. The suspension was left stirring (without lid) for 15 min. Finally 47 μ L of freshly prepared gluteraldheyde 5% w/v in water was added to crosslink and stabilize the NPs. The suspension was left stirring overnight (with a reduced stirring rate ~ 300 - 400 rpm) to allow ethanol evaporation. The obtained final NP suspension had a brown cloudy appearance.

Residual ethanol, non-encapsulated drug and any undissolved albumin and not cross-linked GLU were removed by ultracentrifugation. Prior to ultracentrifugation, the volume of the NP suspension was increased to 8 mL, by the addition of milliQ water. The NPs were purified by three cycles of centrifugation at 20,000 g for 60, 30 and 30 minutes at 20 °C (Optima XE Ultracentrifuge, Beckam Coulter) with redispersion of each pellet to the original volume (8 mL) in double distilled water via ultrasonication (1 min). The pellet obtained from the third cycle of centrifugation was resuspended in 4 mL of water. Each supernatant was collected and stored for further analysis to quantify the albumin and RFM that was not encapsulated.

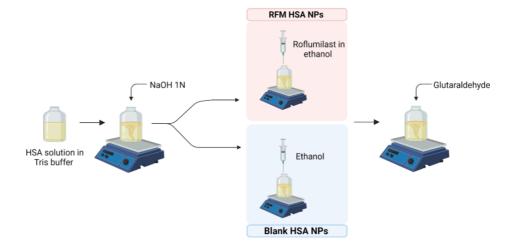


Figure 2.4 Schematic representation of the manufacture process of blank and roflumilast (RFM)-loaded human serum albumin nanoparticles (HSA-NPs).

2.3.2 Calculation of degree of cross-linking of HSA NPs

The calculation of the NPs degree of crosslinking was carried out based on previously reported methods (Langer et al., 2008; Weber et al., 2000).

- A molecule of HSA has 60 amino groups with only the Lys- amino group being available
- to be crosslinked. Considering that GLU is a bifunctional molecule, one molecule of GLU
- can react with two amino group of the HSA. Therefore, to crosslink the 60 -NH₂ of one
- 75 molecule of HSA, 30 molecule of GLU will be required. This ratio will result in a degree
- of crosslinking equal to 100%.
- Firstly, the number of molecules of HSA available was calculated using the following
- 78 equation:

80

Equation 2.1 Calculation of number of HSA molecules available

N° molecule $HSA = n \mod \times N_A$

81

- 82 With *n mol* being the number of HSA moles obtained as mass of HSA divided by the
- molecular weight (MW) of HSA and N_A being the Avogadro number (6.023 x 10²³). To
- 84 calculate the number of GLU molecules required to have 100% crosslinking, the
- 85 following formula was used:

86

87

Equation 2.2 Number of GLU molecules

N° molecule glutaraldehyde = n° molecule HSA × 30

88

- 89 The number of molecules of GLU available based on the volume used in the manufacture
- process was calculated using the **Equation** 2.2 to investigate if the degree of cross-linking
- of the NPs was equal to 100%.

92 93

2.3.3 Physiochemical characterisation of nanoparticles suspension: Dynamic Light

94 Scattering and Nanoparticle Tracking Analysis (NTA)

95

- 96 Particle hydrodynamic diameter, polydispersity index (PDI) and zeta potential were
- 97 determined by Dynamic Light Scattering (DLS) using the Zetasizer Nano Series ZS
- 98 (Malvern Instruments, UK). The analysis was performed at a scattering angle of 173 °
- and at 25 °C. For size and zeta potential measurements, NPs were diluted 100-fold with
- double distilled water. Zeta potential was measured in double distilled water at 37 °C and
- at a concentration of 0.02 mg/mL.

The NPs size was also investigated with the Nanoparticles Tracking Analysis (NTA). NPs were diluted 50,000 or 100,000-fold with ultrapure water to achieve a final ideal particles/frame of 20-80. The video data for each measurement were collected for 30 sec and repeated three - four times for each sample.

2.3.4 Quantification of encapsulated albumin

2.3.4.1 Yield and albumin quantification via bicinchoninic acid (BCA) protein assav

NP yield was calculated using a bicinchoninic acid (BCA) protein assay. The amount of albumin encapsulated was obtained using an indirect method, knowing the total amount of albumin used in the NPs manufacture and the total free amount (not-desolvated) recovered in the supernatants (I and II) obtained from the first 2 purification cycles. If needed, supernatants I and II were diluted with milliQ water to match the concentration range adopted in the calibration curve. The amount of albumin in supernatant III was determined to be negligible in preliminary experiments and therefore not included in the evaluation.

A calibration curve was made each time an assay was performed using an HSA standard solution. Albumin (10.2 mg \pm 0.11) was dissolved in 5 mL of ultrapure water (2 mg/mL, n=3) and serial dilutions were made in the range 200 - 2000 μ g/mL. The blank consisted of ultrapure water without protein. The required volume of the working reagent (WR) was calculated using the following formula:

Equation 2.3 Calculation of working reagent required

 $WR = (\# \text{ standards} + \# \text{ unknown}) \times (\# \text{ replicates}) \times (\text{volume of WR needed})$

The WR reagent was prepared by mixing 50 parts of BCA reagent A with 1 part of reagent B. For microplate measurements, the WR (200 μL) was added to each unknown sample or standards (25 μL). To mix the reagents, the plate was placed on a plate shaker (R100 Rotatest shaker, Luckham, England) for 30 seconds. Plate was covered and incubated at 37°C for 30 minutes. The plate was cooled at room temperature and absorbance measured at 562 nm using a spectrophotometer (Spark®, Tecan, Switzerland). The average absorbance of the blank was then subtracted from the absorbance of each individual

standard and unknown sample. Blank-corrected measurements were plotted against the

concentration (µg/mL). The NP yield was calculated using the equation below:

136 Equation 2.4 Calculation of NPs yield

$$Yield (\%) = \frac{Total \ mass \ HSA - free \ mass \ HSA}{Total \ mass \ HSA} \times 100$$

Where total mass HSA is the total mass of albumin used in the manufacture process and

138 free mass HSA is the sum of the albumin masses recovered and quantified in the

supernatant I and II during purification.

140141

2.3.5 Bicinchoninic acid (BCA) protein assay validation

142

143 Linearity was assessed by the construction of HSA calibration curves across the

144 concentration range of $200 - 2000 \,\mu\text{g/mL}$ (200, 350, 500, 750, 1000, 1500, and 2000

145 μg/mL) (n=3, measurements in triplicate). The absorbance at 562 nm was plotted against

known concentration to determine the linear equation and the regression coefficient (R^2) .

Limit of detection (LOD) and limit of quantification (LOQ) were calculated using the

Equation 2.5 where F is a factor of 3.3 or 10 for LOD and LOQ respectively, SD is the

standard deviation of the net absorbance of the lowest concentration (200 μ g/mL) and b

the slope of the regression line.

151

152 Equation 2.5 Limit of detection/quantification formula

$$LOD/LOQ = \frac{F \times SD}{b}$$

153 The accuracy was defined as the closeness of agreement between the value accepted as

conventional true and the value observed. It was calculated using the difference between

theoretical (T) and experimental (O) values, taken at three separate concentration values

(200, 750, and 2000 µg/mL which are here defined as low, medium and high) across the

assay in triplicate. Accuracy was calculated using the % relative error (RE) (Equation

158 2.6, **Equation** 2.7).

159

154

155

156

160 Equation 2.6 Calculatin of accuracy expressed as error

$$Error(E) = O - T$$

1 and day 3.

Equation 2.7 Calculation of sampling accuracy expressed as % relative error

$$\% RE = \frac{E}{T} \times 100$$

Sampling accuracy was expressed as percentage relative error (% RE) and it was calculated using thirty determinations (ten samplings for three concentrations; 200, 750 and 2000 µg/mL) on day 1.

and 2000 µg/mL) on day 1. Precision is a measure of the closeness of agreement between a series of measurements obtained from multiple sampling of the same sample under a set of prescribed conditions. In this body of work, precision was calculated at two levels: *repeatability* (intra-assay precision) and *intermediate precision*. Repeatability is the precision under the same operating conditions over a short period of time. Three concentrations (low, medium and high; 200, 750 and 2000 µg/mL) were tested on the same day. Results from day 1 are expressed as percentage relative standard deviation (% RSD) (**Equation** 2.8) using nine determinations. Intermediate precision assessed the within-laboratories variations as multiple BCA assays were performed on different days. The samples were tested on day

177 Equation 2.8 Relative standard deviation (%)

$$\% RSD = \frac{SD}{mean} \times 100$$

2.3.6 In vitro model of lung protease to investigate the stability of albumin NPs

The stability and the degradation rate of albumin NPs in a simulated lung environment were investigated using a modified method reported elsewhere (Woods et al., 2020). The evaluation of the proportion of intact NP overtime in the protease model was monitored using two parameters: i) derived count rate (kilo counts per second, kcps) and ii) particle size distribution. The derived count rate has been showed to be proportional to the NP concentration (Tantra et al., 2010). The validation of this relationship was performed preparing a calibration curve of HSA in PBS (0.125, 0.25, 0.5, 1.0 and 2.0 mg/mL).

- Samples were diluted 1:10 with PBS prior to measurement and analysed at 25°C using
- the Zetasizer Nano Serie ZS.
- 190 Trypsin (0.1 mg, 0.25 mg and 0.5 mg) (Type I, ~ 10,000 BAEE units/mg protein) was
- dissolved in 1 mM of HCl and added to blank NPs (1.6 mg); the resulting mixture was
- incubated at 37°C under shaking (120 rpm) (Incu-Shake MINI, SciQuip, UK) for 4 hours.
- 193 Blank NPs in PBS alone at 37°C were used as controls. At allocated time points, aliquots
- 194 (50 µL) of the enzyme-particles mixture were withdrawn, diluted with PBS (10-fold), and
- analysed immediately using the Zetasizer Nano Series ZS (Malvern).

197 **2.3.7 Quantification of encapsulated roflumilast**

198

- 200 2.3.7.1 Roflumilast quantification using a high-performance liquid chromatography (HPLC) detection method
- The amount of encapsulated RFM (encapsulation efficiency; EE) was calculated by
- measuring the amount of drug not encapsulated recovered in the supernatants I, II and III
- obtained from the purification process using **Equation** 2.9.

204

205 Equation 2.9 Encapsulation efficiency (%)

$$EE\% = \frac{Total \ drug - free \ drug}{Total \ drug} \times 100$$

- Where total drug is the mass of RFM weighed at the beginning of the manufacture
- process and dissolved in ethanol; *free drug* is the sum of masses of RFM in each of the
- three supernatants.

- 210 The process to quantify the amount of RFM encapsulated in the NPs was firstly carried
- out using a method (method 1, **Figure 0.1**) based on the use of acetonitrile and on a
- centrifugation cycle. An alternative method (method 2, **Figure 0.2**) employed the use of
- 213 trypsin to obtain a direct quantification of roflumilast using acetonitrile (**Figure 0.3**).
- However, both the methods resulted in unsatisfactory outcomes and an indirect
- 215 quantification was considered more reliable and therefore preferred as definitive method.
- The optimised and final method used in this thesis is represented in **Figure** 2.5. An aliquot
- of 1 mL of each supernatant resulting from the purification step was placed in a
- borosilicate glass tube and the total volume evaporated using a Rotary Evaporator (water

bath temperature 40° C). The resulting dried sample was reconstituted in a mixture of water-acetonitrile (1 mL, 30:70 v/v), vortexed for 1 min and centrifuged (10,000 rpm x 5 min). The resulting supernatant was collected and diluted with the required volume of a mixture of water:acetonitrile (30:70) and the drug present in the samples calculated using a reversed-phase HPLC method described in detail in section 2.3.8. A calibration curve of RFM in the same solvent mixture in the range $0.5 - 150 \,\mu\text{g/mL}$ was constructed.



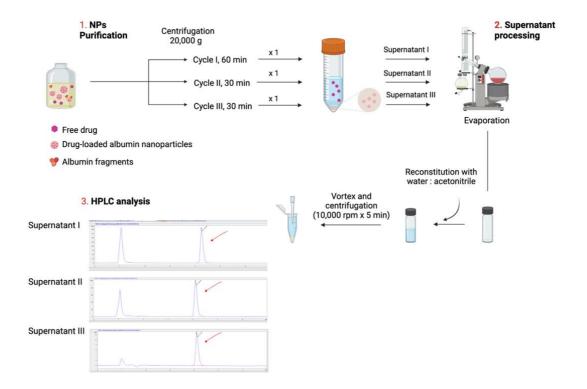


Figure 2.5 Schematic diagram of the indirect method of roflumilast quantification: (1) Separation of free drug and encapsulated roflumilast; (2) processing of non-encapsulated drug; (3) analysis of non-encapsulated drug using an HPLC method.

2.3.8 Validation of High-Performance Liquid Chromatography (HPLC) detection method

The Agilent Technology 1260 Infinity was used for the purpose of this study. The system consisted of a binary solvent system, flow through needle sample and a column thermostat with the analytical column kept at 40° C. The analytes were separated on a YMC Triart C18 column (150 mm x 4.6 mm, 3 μ m particle size) with YMC-Triart C18 Guard Cartridge (10 x 4 mm, 12 nm or 3 μ m particle size) using isocratic elution. Mobile phase

A consisted of 70% of HPLC-grade acetonitrile and mobile phase B of 30% of HPLC-grade water with 0.1% of trifluoroacetic acid (TFA). The flow rate was set to 1 mL/min and the injection volume was 50 μ L and the detection wavelength 252 nm (**Table** 2.5).

Table 2.5 Summary of HPLC method for roflumilast detection and quantification.

| | ROFLUMILAST |
|--------------------------|---|
| Structure | F F CI HN O |
| Molecular weight | 403.207 g/mol |
| | |
| Assay method: | HPLC |
| Column: | YMC Triart C ₁₈ 3µm 150-4.6 mm |
| Mobile phase: | 30:70:0.1 H ₂ O:ACN:TFA |
| | Isocratic |
| Sample diluent: | 30:70 H ₂ O:ACN |
| Oven Temperature: | 40°C |
| Run time: | 7 minutes |
| Flow rate: | 1.0 mL/mL |
| Autosampler temperature: | Ambient |
| Injection volume: | 50 μL |
| UV wavelength: | 252nm |

238239

240

241

244

Stock solution was prepared in HPLC grade water-acetonitrile mixture (30:70, v/v) at a concentration of 150 μ g/mL (n=1) with further dilutions over a concentration range of 0.5 – 150 μ g/mL.

The intra-assay precision (repeatability) was evaluated with ten consecutive injections of 150 μg/mL performed on the same day and under the same experimental conditions.

Repeatability was represented by standard deviation and relative standard deviation. LOD

and LOQ were calculated on the "standard deviation of the response of and the slope" using the Equation 2.5.

247

- The SD value adopted was equal to the standard deviation of the lowest concentration
- $(0.5 \,\mu g/mL)$ and b is the slope of the regression line.
- 250 The stability of RFM in the mobile diluent was investigated comparing the area response
- of the three samples solution $(0.5 5.0 \text{ and } 150 \,\mu\text{g/mL})$ analysed on day 1, 2, 3, and 7 to
- 252 the area response of the same concentration samples obtained on day 0 when the sample
- 253 was freshly prepared (n=1). Samples were stored in capped volumetric flasks at 4°C
- during the stability study.

255

2.3.9 Optimisation of a dialysis bag release method for RFM

257

256

- 258 The release of RFM from albumin NP was studied by a dialysis bag method (**Figure** 2.6).
- 259 Dialysis bags were placed in a small beaker and submerged in 10 mL of release media
- 260 (PBS 0.01 M + 0.8% Tween 80). The samples were incubated at 37°C under shaking for
- the duration of the assay. Samples were RFM loaded and blank NPs with trypsin from
- bovine pancreas (Type I, ~ 10,000 BAEE units/mg protein) in different trypsin: albumin
- ratio (1: 100, 1: 2). Mass of HSA used was equal to 3.25 mg and 2 mg when the trypsin:
- albumin ration was equal to 1:100 and 1: 2 respectively. Controls were i) free RFM
- solution (0.2 mL in dimethyl sulfoxide (DMSO) or 1 mL in DMSO and release medium);
- 266 ii) RFM with albumin solution; iii) RFM with blank NPs.
- The potential enhancement of the RFM-HSA-NPs degradation in the assay mediated by
- 268 trypsin was investigated via the 'activation' of the enzyme. Trypsin solution was prepared
- on ice and away from the light. The acid pH of the solution was changed to 7-9 via the
- addition of NaOH.
- 271 Samples (1 mL) were withdrawn from the release medium (receiver fluid) at
- 272 predetermined time intervals and the same volume was replaced with fresh medium to
- 273 maintain sink conditions. RFM was quantified in the samples by HPLC (section 2.3.8)
- and the cumulative percentage mass of roflumilast release over time was calculated.

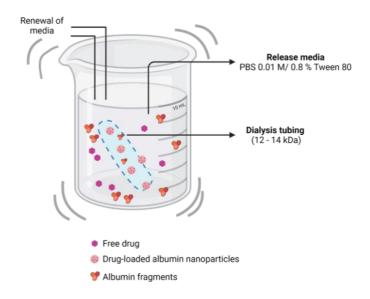


Figure 2.6 In vitro drug release model. Schematic representation of the in vitro drug release study experimental set up.

2.4 Results

2.4.1 Physiochemical characterisation of NPs via Dynamic Light Scattering (DLS)
 and Nanoparticles Tracking Analysis (NTA)

Blank and drug loaded HSA-NPs were manufactured using a desolvation method. In order to optimise the manufacture process and the physiochemical properties of the NPs, stirrer speed and rate of ethanol addition were investigated. Nine different formulations were manufactured using three stirrer speeds (500, 850 and 1250 rpm) and three different ethanol addition rates (0.25, 1.25 and 2.0 mL/min) (**Table** 2.6). The combination of 850 rpm and 1.25 mL/min resulted in the formulation with the most appropriate physiochemical properties, as small size, low PDI and negative zeta potential (**Table** 2.7). The highest and lowest speeds resulted in sticky formulations and particle size greater than 200 nm.

Table 2.6 Schematic representation of the different combination of stirring rate (rpm) and ethanol addition rate (mL/min) tested in the optimisation of the NPs manufacture process.

| | | STIRRER SPEED (rpm) | | | | |
|--------------------------------|------|---------------------|-----|------|--|--|
| | | 500 | 850 | 1250 | | |
| ETHANOL ADDITION RATE (mL/min) | 0.25 | | | | | |
| | 1.25 | | | | | |
| | 2.0 | | | | | |

Size, PDI and zeta potential of blank and drug-loaded HSA-NPs were characterised using a Dynamic Light Scattering technique. The physiochemical properties of both blank and drug-loaded NPs were very similar, with size in the range of 140 nm, PDI < 0.1 and negative zeta potential (- 42.5 mV and - 36.8 mV for blank and drug loaded NPs respectively) (**Table** 2.7).

Table 2.7 Size, polydispersity index (PDI) and zeta potential of blank and drug loaded albumin nanoparticles. Data represents mean (SD) of n = 3 - 8 independent experiments.

| | Size (nm) | PDI | Zeta potential (mv) |
|-----------------|--------------|-------------|---------------------------|
| Blank NPs | 139.2 (15.7) | 0.09 (0.04) | -42.5 (3.23) |
| RFM-HSA- NPs | 147.3 (6.78) | 0.05 (0.01) | -36.8 (4.93) |

The DLS measurement performance was evaluated and compared to results obtained from the NTA analysis. In an NTA measurement, the particles' movements are tracked in consecutive video frames (**Figure** 2.7 right panel). The overlapping of NTA and DLS size measurements of drug loaded NPs described particles with good size and in accordance with results from table 2.6 (**Figure** 2.7 left panel).

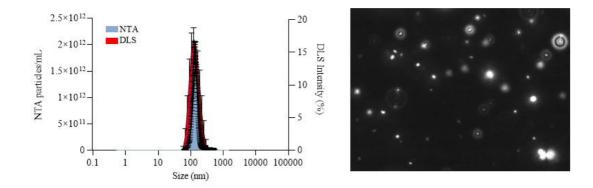


Figure 2.7 Size distribution from NTA and DLS measurements of monodisperse roflumilast albumin NPs (left panel) with an illustrative NTA video frame of one of the samples analysed (right panel). Error bars represents standard deviation (DLS) and standard error (NTA) obtained from three different independent samples (n = 4 measurements for the NTA measurements).

The degree of crosslinking of the manufactured HSA NPs was calculated using the formula described in section 2.3.2. The number of HSA molecules available based on the mass of HSA employed in the manufacture process resulted equal to 4.53×10^{17} . Based on this value the number of molecules of GLU required to obtained NPs with 100% degree of crosslinking was calculated to be equal to 1.36×10^{19} . Therefore based on the calculated number of molecules of GLU available when using $47 \mu L$ of 5% w/v (1.50×10^{19}), the degree of crosslinking of the HSA-NPs resulted equal to 100%.

2.4.2 Evaluation of albumin yield and roflumilast encapsulation into NPs

2.4.2.1 NPs albumin yield and validation of a BCA assay

The albumin entrapment in the RFM-HSA-NPs was calculated using a BCA assay and found to be 73% (n=2). The HSA assay was validated, and results are shown in **Figure** 2.8 and in **Table** 2.8. The calibration curves for HSA were constructed by plotting the net absorbance versus the concentration. A linear correlation between absorbance and concentration was found in the range $20 - 2000 \,\mu\text{g/mL}$. LOD and LOQ were calculated and equal to $50.1 \,\mu\text{g/mL}$ and $152.3 \,\mu\text{g/mL}$, respectively.

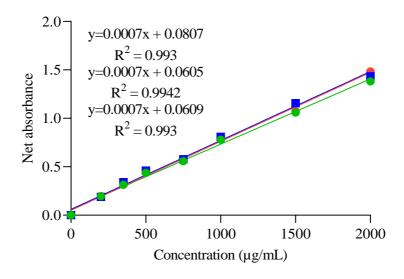


Figure 2.8 Intra-day validation of linearity of human serum albumin (HSA) in the concentration range $200 - 2000 \,\mu\text{g/mL}$. Data represents n = 3, each measurement in triplicate.

The BCA assay was validated in terms of intra-day (repeatability) and inter-day precision. Three concentrations (low, medium and high) were tested on the same day (intra-day) and on two different days (day 1 and day 3) and absorbance measured. Results from day 1, expressed as percentage relative standard deviation (% RSD), were 5.3, 6.2 and 3.7 %, respectively, for low, medium and high concentrations. When tested over two days, the RSD% were equal to 1.4, 5 and 0.2 % for the same concentrations.

Accuracy was calculated using the **Equation** 2.6 and **Equation** 2.7 for the same low, medium and high concentrations. The corresponding RE were 2.5, 2.4 and 1.8 %. The sampling error was also calculated using ten determinations of the three concentrations. The highest RE % were reported for the low and medium concentrations.

Table 2.8 Validation of BCA assay as method for albumin yield over three concentrations (low, medium and high). Data represents mean (SD) of n=3 independent experiments.

| Concentration (µg/mL) | Net absorbance mean (SD) | | Precision | | Accuracy | Sampling accuracy | LOD | LOQ |
|-----------------------|--------------------------|---------------|---------------------|----------------------|--------------------|-----------------------|--------------|---------|
| | Intra-day | Inter-day | Intra-day (%RSD) | Inter-day (% RSD) | (% relative error) | (% relative error) | $(\mu g/mL)$ | (µg/mL) |
| 200 | 0.194 (0.01) | 0.192 (0.003) | 5.3 | 1.4 | 2.5 | 11.1 | | |
| 750 | 0.570 (0.04) | 0.591 (0.03) | 6.2 | 5 | -2.4 | 11.2 | 50.281 | 152.366 |
| 2000 | 1.443 (0.05) | 1.431 (0.003) | 3.7 | 0.2 | -1.8 | 0.8 | | |

2.4.2.2 Roflumilast encapsulation into HSA-NPs and validation of an HPLC quantification method

The encapsulation efficiency of RFM in HSA-NPs was calculated using the method described in section 2.3.7 and was equal to 30%, with an amount of encapsulated RFM being 19.9 μ g for each mg of albumin entrapped, albeit with a high amount of variability between preparations (SD = 12 μ g; n=8).

The HPLC method for RFM quantification was validated for LOD, LOD, precision and RFM was evaluated for stability over 7 days. Firstly, a linear correlation between the concentration and the area under the curve was establish ($R^2 = 0.9995$) (**Figure** 2.9).

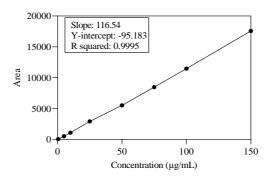


Figure 2.9 Linear relationship between RFM concentration and area under the curve in the range $0.5-150 \,\mu\text{g/mL}$.

LOD and LOQ were calculated using Equation 2.5 and were equal to 8.65 ng/mL and 27.39 ng/mL. Stability was measured for three concentrations of solution (0.5, 50 and 150 μ g/mL) on day 0, 1, 2, 3 and 7. No significant changes were recorded over the period and the RSD % for the low, medium and high concentrations analysed was equal to 0.99, 0.35

and 0.20% (**Table** 2.9). In addition, the precision of the assay was evaluated at the level of repeatability with ten consecutive injections of the highest sample concentration under the same method conditions and the RSD was 0.18%.

Table 2.9 Stability of roflumilast in water-acetonitrile solution over 7 days. Data represent n=1indipendent experiment, with measurements in triplicate. Sample solutions were stored in capped volumetric flasks at 4°C during the length of the stability study.

| Concentration | Day | | | | | Sample | | |
|---------------|--------|--------|--------|--------|--------|--------|------|-------|
| | 0 | 1 | 2 | 3 | 7 | mean | SD | RSD % |
| 0.5 | 1.27 | 1.27 | 1.27 | 1.27 | 1.24 | 1.26 | 0.01 | 0.99 |
| 50 | 48.23 | 48.07 | 47.90 | 47.90 | 47.74 | 47.97 | 0.17 | 0.35 |
| 150 | 151.58 | 151.30 | 152.09 | 151.46 | 151.98 | 151.68 | 0.30 | 0.20 |

2.4.3 In vitro model of lung protease to investigate the stability of albumin NPs

The degradation of RFM-HSA-NPs mediated by proteases was investigated using the relationship between albumin NP concentration and derived count rate. The NPs used had the same physiochemical properties described previously. A schematic representation of the size and PDI is showed in **Figure** 2.10 **a**. The technique was validated by preparing a calibration curve in the range 0.125 - 2.0 mg/mL. The linear relationship between albumin NP concentration and derived count rate (kcps) was described ($R^2 = 0.9839$) (**Figure** 2.10 **b**).

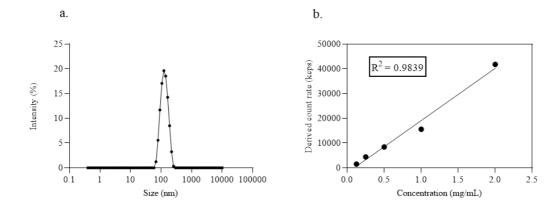


Figure 2.10 Characterisation of HSA NPs for degradation studies. (a) Representative particles size distribution obtained from albumin nanoparticles at 100x dilution in double distilled water at 25°C; (b) Representative linear relationship between derived count rate (kcps) and HSA NPs concentration. Nanoparticles samples are diluted 1:10 with phosphate buffered saline (PBS). Data n=1independent experiment, with measurement in triplicate.

RFM-HSA-NP were incubated at 37°C with three different concentrations of trypsin (0.1, 0.25 and 0.5 mg/mL) and the degradation rate of NP investigated. The effect of increasing trypsin concentration could not be detected as increasing degradation rate when a time window of 4 hours was adopted. At each concentration, the count rate was massively reduced by 1 hour from the starting time of the incubation and remained constant and close to zero until the end of the experimental window. However, a time-dependent degradation profile could be observed in the time frame 0 - 1 h. The investigation of the NP degradation using the same experimental conditions over the shorter period demonstrated that the albumin degradation took place gradually from 0 to 40 min (**Figure** 2.11 D). Thus, it was concluded that the degradation takes place gradually in the first interval of time and that after 1 hour the NPs were almost completely degraded and fragmented.

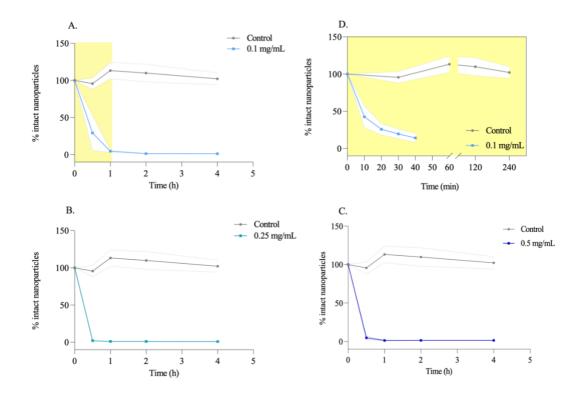


Figure 2.11 Degradation profile of RFM-HSA-NPs following exposure to 0.1 (A), 0.25 (B) and 0.5 mg/mL (C) of trypsin compared to phosphate buffered saline at 37° C (control); (D) Degradation profile of RFM-HSA-NPs following exposure to 0.1 mg/mL of trypsin over 40 minutes only. Degradation is illustrated as reduction of the initial percentage of derived count rate using dynamic light scattering. Dotted lines ("") represent the standard deviation from the mean. Data represents mean \pm SD (n = 3 independent experiments).

The albumin NPs degradation rate was also investigated in terms of change of particle size distribution. The impact of three different trypsin concentrations on the NPs PDI was compared for each time point (0-0.5-1-2-4 h) to the control (NPs without trypsin). At time 0, NPs resulted intact as when incubated without trypsin. The quick and consistent reduction of derived count rate showed in Figure 2.11 when NPs were incubated with 0.25 and 0.5 mg/mL is in agreement with results reported in **Figure** 2.12. After 30 min, multiple peaks were detected highlighting the presence of several aggregates being formed. The particle population became consistently polydisperse especially after 1 hour with aggregates in the size range of 10 nm, 1000 nm and 10,000 nm. The tracking of particle size changes overtime provided a further look at the sample degradation to complement the evaluation of the derived count rate. Indeed, over the time period from 1 to 4 hours ongoing degradative changes were detected to be taking place beyond the initial

405 particle degradation indicated by the constant low derived count rate being reported in 406 Figure 2.11. 407 Incubation with 0.1 mg/mL also resulted in a polydisperse particle population, with 408 multiple peaks at different size highlighting the presence of aggregates and fragments. 409 However, when NPs were incubated with 0.1 mg/mL, these changes in PDI were not 410 observed at the 30 min incubation showing that particle count provides a more sensitive 411 measure of initial NP degradation before the detection of albumin fragments and 412 aggregates becomes apparent.

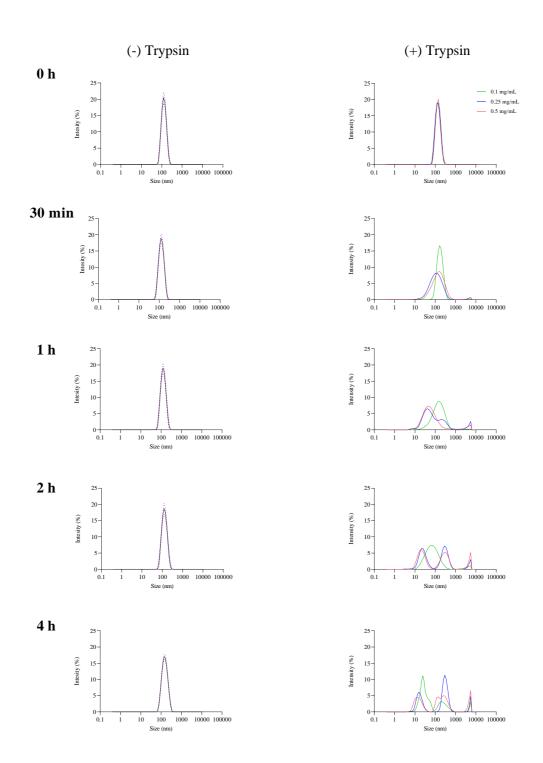


Figure 2.12 Degradation, aggregation and increase in polydispersity index of the RFM-HSA-NPs following exposure to different concentrations of trypsin (0.1, 0.25 and 0.5 mg/mL) at 37°C for up to 4 hours. Data represents mean of n=3 independent experiments and SD (dotted line) for the control and mean only for the positive trypsin samples.

2.4.4 Roflumilast release over time from albumin NPs

RFM release from HSA-NPs was assessed over a period of 7 hours. The amount of RFM released from the NPs was calculated using a dialysis bag system combined with a sample preparation method and an HPLC quantification method. A calibration curve of RFM in the release media (PBS 0.01 M/ 0.8% Tween 80) was prepared in the range 0.5-20 µg/mL and linearity were confirmed ($R^2=0.9987$) (n=1 independent experiment). The chromatogram showed a symmetrical peak at 4.138 min **Figure** 2.13 and a linear relationship between RFM concentration and area under the curve was observed.

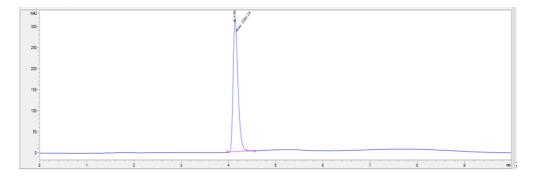


Figure 2.13 Representative chromatogram of RFM (20 μ g/mL) in phosphate saline buffer (PBS) 0.01 M/ 0.8% Tween 80.

The optimisation of the drug release assessment included the evaluation of a suitable drug release media. RFM is poorly soluble in water (0.52 – 0.56 μ g/mL at 22°C) (European Medicines Agency, 2010) and therefore different solubility enhancers were tested before choosing Tween 80 as the most suitable. Indeed, the RFM solubility at 37°C in the aforementioned medium (PBS 0.01 M/ 0.8% Tween 80) was experimentally determined to be 25 μ g /mL, i.e. the use of 0.8% Tween 80 resulted in a ~ 45x increase of RFM solubility in water at 22°C (European Medicines Agency, 2010). However, the solubility remained considerably low and therefore a volume of release medium of 10 mL was required to ensure the maximum RFM concentration released was always 10x less than the RFM solubility in the same medium.

The release of RFM loaded in a dialysis bag was first assessed. In order to avoid misleading results induced by the increased solubility of RFM in the medium when dissolved in DMSO, the percentage of DMSO in the system when used was kept below

2%, a level that was considered negligible. The mass of RFM loaded in the bag at time 0 was calculated to be 16.11 μg using an HPLC method. The cumulative RFM release in terms of percentage and mass increased gradually and peaked at 24 h at ~ 80% (**Figure** 2.14).

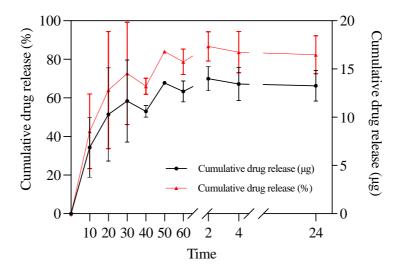


Figure 2.14 In vitro drug release of roflumilast solution in DMSO (100%). A dialysis bag with 200 μ L of RFM in DMSO was submerged in 10 mL of release media (PBS 0.01 M/0.8% Tween 80). Data represent mean \pm SD of n=3 independent experiments.

The transfer of RFM in solution (DMSO) was further investigated adjusting the volume of the dialysis bag content. The volume was increased from 0.2 mL to 1 mL via dilution with the release medium. Despite achieving the same percentage of drug release, the profile shape was affected by the total volume in the dialysis bag (**Figure** 2.15). It was hypothesized that the presence of Tween 80 micelles provided a favourable environment and reduced the transfer of RFM through the pore membranes affecting the release profile.

Confirmation of bag mass content at time 0 and 24 h was provided by RFM quantification by HPLC. A total amount of 19.90 µg of RFM was loaded in the dialysis bag and after 24 h 18.21 µg had transferred to the release medium and a small amount of drug (2.64 µg) remained entrapped in the bag (**Table** 2.10).

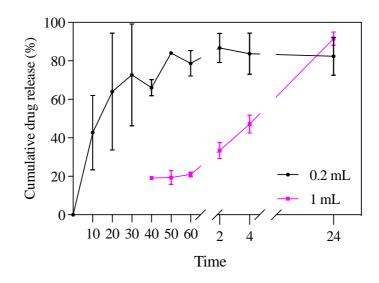


Figure 2.15 Impact of different volumes of dialysis bag content on the free drug release. (\circ) A total volume of 0.2 mL of RFM solution in DMSO and (\Box) RFM solution diluted in release media (1 mL) in a dialysis bag were submerged in 10 mL of release medium (PBS 0.01 M/ 0.8% Tween 80). Data represents mean \pm SD of n=3 independent experiments.

Table 2.10 Calculated mass balance in the dialysis bag at time 0 and after 24 h. Data represent mean of n=3 independent experiments.

| RFM mass in the bag at T0 | 19.90 μg |
|------------------------------|----------|
| Mass released at T 24h | 18.21 μg |
| Mass left in the bag at T24h | 2.64 μg |

The potential formation of complexes between free RFM and albumin in solution was evaluated by incubating the mixture in presence and absence of trypsin. The presence of trypsin did not impact the drug release rate as the albumin was free and not in forms of aggregates or particles. A total percentage of 80% of drug was released both in presence and absence of trypsin (**Figure** 2.16).

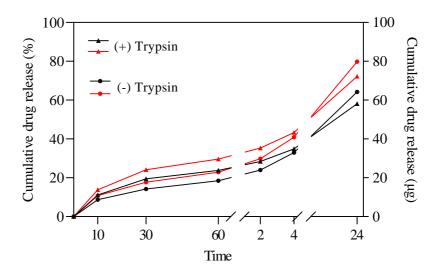


Figure 2.16 Drug release of free RFM and human serum albumin (HSA) solution in presence and absence of trypsin (0.0325 mg) (trypsin:albumin ratio = 1:100). A dialysis bag of a total volume of 1 mL containing 0.9 mL of HSA in Tris HCl buffered and 0.1 mL of RFM in DMSO was submerged in 10 mL of release medium. Aliquots of release medium withdrawn at allocated time point and replaced with fresh medium to maintain sink conditions. Cumulative drug release (%) and mass are represented by red and black lines respectively. Data represent n=1 independent experiment.

The same experimental conditions were used to investigate the potential for aggregate formation of free RFM when incubated with albumin NPs in presence or absence of trypsin (**Figure** 2.17). The percentage of RFM released from the inner side of the dialysis bag when incubated in presence of albumin NPs was not affected by the presence of trypsin, while the size and PDI of the HSA-NPs at the beginning and at the end of the trypsin incubation showed that the NPs underwent degradation (**Table** 2.11). This confirmed that the albumin NPs in the conditions adopted undergoes degradation when incubating with trypsin but does not affect RFM transfer.

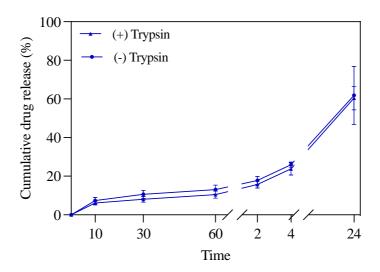


Figure 2.17 Drug release of free RFM incubated with human serum albumin (HSA) NPs in presence and absence of trypsin (0.0325 mg) (trypsin:albumin ratio = 1:100). In each dialysis bag (1 mL) HSA NPs were incubated with free drug in presence or absence of trypsin; each bag was submerged in 10 mL of release media. Aliquots of 1 mL were withdrawn at allocated time point from the receiver chamber and replaced with fresh medium to maintain sink conditions. Data represent mean \pm SD of n=3 independent experiments.

An increase in size and PDI from time 0 (124.14 nm; 0.09) to time 24 hours (387.07 nm; 0.40) occurred (Table 2.11) and albumin NP degradation was further confirmed by the drop in the derived count rate of the mixture. In terms of percentage of drug release, 60% was detected to transfer with the remaining 40% presumed to be lost to adsorption and interaction with the albumin aggregates.

Table 2.11 Size, PDI and derived count rate of NPs at time 0 (- trypsin) and at time 24 h of incubation (NPs left in the dialysis bag). Data represent mean (SD) of n=3 independent experiments.

| | Size | Polydispersity index (PDI) | Derived count rate (kcps) |
|-------------|---------------|----------------------------|---------------------------|
| (-) trypsin | 124.14 (2.2) | 0.09 (0.02) | 7572.43 (153.6) |
| (+) trypsin | 387.07 (55.0) | 0.40 (0.1) | 918.75 (135.4) |

RFM release from albumin NPs degradation was investigated in presence of trypsin both activated and inactivated. The trypsin:albumin ratio was adapted to 1:2. Drug-loaded albumin NPs were incubated with 'activated' and 'inactivated' trypsin and the resulting drug release profiles are shown in **Figure** 2.18. The NP released an initial burst of RFM consistent with the degradation of the particle followed by a steady increase in RFM in the receiver medium reaching a peak percentage at 4 h of about 30% and 15% when 'activated' and 'not activated' trypsin was used respectively. In the range between 4 and 24 h no further drug release was detected (data not shown).

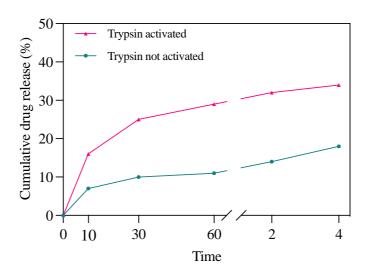


Figure 2.18 Drug release of RFM-HSA-NPs in presence of trypsin activated or not activated. Trypsin activation was performed changing the pH to 7 - 9 via the addition of 1 N NaOH. An aliquot of 2 mL of RFM-HSA-NPs was incubated over 24 h with 1 mg of trypsin (trypsin: albumin ratio = 1:2). Data represent n = 1 independent experiment.

The particle degradation was corroborated by the changes in size, PDI and derived count rate (**Table** 2.12). Generally, the incubation with trypsin resulted in particles degradation as size and PDI increased consistently, whereas the derived count rate number decreased from time 0 to time 24h. Consistent differences were reported between the use of 'activated' or 'not activated' trypsin especially in terms of size and PDI.

Table 2.12 Variation of size, PDI and derived count rate after 24 h of incubation with trypsin activated and not activated were recorded using dynamic light scattering. Data represent n = 1 independent experiment.

| | Size | Polydispersity index (PDI) | Derived count rate (kcps) |
|-----------------------|--------|----------------------------|---------------------------|
| Т 0 | 137.23 | 0.10 | 23321.0 |
| | | Trypsin activated | |
| T 24 h | 364.87 | 0.71 | 107.47 |
| Trypsin not activated | | | |
| T 24 h | 205.33 | 0.45 | 246.60 |

As the 'activated' form of trypsin showed improved activity in the degradation of the HSA-NPs and therefore in enhancing the drug release, it was used for a further confirming experiment using the same protocol. The incubation of RFM-HSA-NPs with 'activated trypsin' induced a sustained release of the drug reaching a maximum of ~ 30% after 4 hours of incubation, with negligible release occurred between 4 and 7 h (**Figure** 2.19).

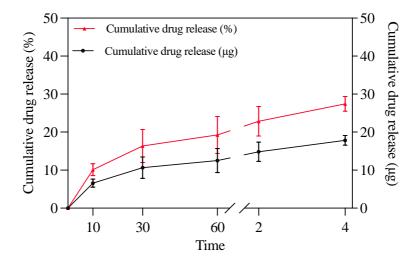


Figure 2.19 Drug release of RFM-HSA-NPs in presence of activated trypsin. An aliquot of 2 mL of RFM-HSA-NPs was incubated over 4 h with 1 mg of trypsin (ratio trypsin: albumin = 1:2). The activation was performed via change of the pH to 7-9.

Data represents mean ± SD of n=1 independent experiment (single batch of NPs)

(measurements in triplicate).

Again, the size, PDI and derived count rate changes confirm the degradative activity of trypsin on the NP (**Table** 2.13). Despite the size and PDI underwent only a small increase, the extensive reduction in the derived count rate demonstrated that the NPs were fully converted into fragments and aggregates.

Table 2.13 Variation of size, PDI and derived count rate after 7 h of incubation with trypsin were recorded using dynamic light scattering.

| | Size | Polydispersity index (PDI) | Derived count rate (kcps) |
|-------|---------------|----------------------------|---------------------------|
| Т0 | 137.23 (-) | 0.10 (-) | 23321.20 (-) |
| T 7 h | 173.96 (5.31) | 0.23 (0.01) | 261.53 (47.13) |

The NPs designed in this experimental chapter showed good size, PDI and zeta potential,

2.5 Discussion

with minor variability throughout the batches manufactured. The evaluation of the optimal manufacture process included the study of different parameters. In agreement with studies reported in the literature (Jahanban-Esfahlan et al., 2016; Langer et al., 2003), the successful formation of NPs with good physiochemical properties was described highly dependent on stirrer speed and ethanol addition rate. For example, it was described that the combination of stirrer speed of 1250 rpm with ethanol addition rate of 2 mL/min or 1.25 mL/min resulted in NPs too polydisperse to carry out a distribution analysis and with presence of large or sedimentary particles.

The investigation of the potential of a nanocarrier system must also include the evaluation of its encapsulation efficiency. The calculation of the total amount of drug that can potentially be loaded in the carrier compared to the total amount of drug used at the beginning of the manufacture process is fundamental to predict the therapeutic potential of the NPs. As for RFM, the use of a poorly water-soluble drug represents a challenge for the EE evaluation. The 'indirect' method is widely used and allows to quantify the EE based on the amount of drug washed out during the purification process. This process was

employed in this experimental chapter and resulted in a high variability of the amount of RFM per mg of HSA (19.9 µg of RFM for each mg of albumin entrapped). The reported SD value equal to 12 µg was considered a result of the lower accuracy of the indirect method of drug quantification.

A valuable alternative for the calculation of the EE is represented by a method that directly determine the amount of drug entrapped in the NPs via the calculation of the amount of drug being released from the nanocarrier. Trypsin, proteinase K, protease and pepsin are reported as adequate enzymes to obtain overall a rapid degradation of albumin nanoparticles and to investigate *in vitro* the release of the embedded drug (Langer et al., 2008).

In this experimental work trypsin was used as key component in two separate assays: the

545546

540

541

542

543

544

2.5.1 Investigating the degradation of albumin NPs via the use of trypsin

548

549

550

551

552

553

554

555

556

557

558

559

560

561

562

563

564

565

566

567

568

569

547

evaluation of the degradation rate of blank NPs in a biorelevant environment and the investigation of the rate of release of RFM from the NPs. The degradation of HSA-NPs is fundamental for the release of the active ingredient and the following therapeutic activity, but also for the clearance and metabolism of the carrier itself. Despite the critical role that proteases have in the lung health and metabolism in presence of albumin-based carrier, research studies concerning this topic are lacking and not sufficient. However, a recent investigation (Woods et al., 2020) evaluated the total protease concentration in the human lung fluid of volunteers using proteomic analysis and found 14 proteolytic species of proteases, of which the four most abundant were cathepsin D, cathepsin H, dipeptidyl peptidase IV and dipeptidyl carboxypeptidase I/angiotensin-converting enzyme (ACE). From those data four in vitro models were developed and the rate of degradation of the HSA-NPs designed in this experimental chapter was described using one of those models reported in the literature (Woods et al., 2020). The NPs were incubated at a concentration relevant to approximate their concentration in the epithelial lung lining fluid at the no observed adverse effect level (NOAEL) reported in pre-clinical study (Woods et al., 2015). The incubation with 0.1 mg/mL of trypsin at 37°C and under shaking induced a slow and full degradation of the NPs from time 0 to 1 h. Those results are in agreement with what reported in this experimental chapter. Although the analysis of the occurred degradation was carried out only via photon correlation spectroscopy, two parameters were used which showed to

570 being complementary. The analysis of the reduction of the derived count rate showed 571 high sensitivity allowing to report a slow and minimal reduction of the total number of 572 particles overtime; in contrast, the changes of the particle size distribution allowed a 573 rather macroscopic analysis which markedly showed the formation of the aggregates. 574 These results further support the interest in HSA-NPs as a controlled release formulation 575 for inhaled and overall provided an informed prediction of the fate of the NPs in a lung 576 simulated environment. They will also inform next studies which will focus on the 577 investigation of the designed HSA-NPs in the disease models reported in the literature 578 (Woods et al., 2020).

579

580

581

2.5.2 HSA-NPs provided a sustained release of the encapsulated RFM compared to the release of free RFM

582

583 Results from the investigation of the rate of release of RFM from the NPs have showed 584 that the NPs designed in this experimental thesis can release the drug overtime in a 585 sustained manner. In the *in vitro* assay designed, the amount of RFM released increased 586 from time 0 to 4 h with 20% of cumulative drug released after 60 min and a total of 34% 587 detected at 4 h. The sustained drug release was only described for RFM-HSA-NPs as it 588 is confirmed by the different release profile obtained for free RFM. In this case, a total ~ 589 80% of drug was released by 24 h, of which almost 70% was released already after 30 590 min. 591 Interestingly, the release profiles obtained when RFM was dissolved in DMSO only or in 592 DMSO and release medium (containing Tween 80) were considerable different. Although 593 the cumulative percentages release by 24 h were comparable, the kinetic of release 594 appeared slower in presence of Tween 80. Surfactants as Tween 80 are characterized by 595 the critical micelle concentration (CMC) which is defined as the concentration of 596 surfactant above which micelles forms in the given dispersant. Considering that the 597 concentration of Tween 80 adopted exceeded the CMC of Tween 80, the distinct kinetic 598 of release obtained may have been the result of the formation of 'RFM-embedded 599 micelles' which hindered the rate of transport of RFM from the dialysis bag to the receiver 600 medium. 601 In this context, the choice of the release medium often represents a key challenge in the 602 design of an *in vitro* assay investigating the rate of release of the drug from the carrier 603 especially when using a poorly water-soluble drug, as in the case of RFM. A preliminary

investigation (data not shown) showed that PBS 0.01 M/ Tween 80 was the optimal receiver medium adequate to mimic a biorelevant receiver medium as well as to ensure a suitable RFM solubility in the medium (Siepmann & Siepmann, 2020). In contrast to this experimental approach, many studies reported as strategy to overcome the poor water solubility of the molecules of interest the use of a mixture of PBS and ethanol as receiver medium. This is the case of a study (Craparo et al., 2022) which investigated the release of RFM from lipid-polymer hybrid NPs using a dialysis tubing immersed in 30 mL of PBS/ ethanol (80/20 v/v); similar receiver medium was employed in a study (Fang et al., 2015) in which the *in vitro* rolipram release was carried out via the use of Franz Cell having a receptor compartment with 5.5 mL of 30% ethanol in pH 7.4 buffer.

2.5.3 NPs degradation rate is affected by the pH of trypsin solution

The investigation of the rate of drug release from the NPs required as key aspect the optimisation of the trypsin: albumin ratio as well as of the pH of trypsin solution. Those variables are fundamental for the effective proteolytic activity of trypsin. The mechanism of action of the substrate hydrolysis at the active site of trypsin is complex and is based on a series of biochemical reactions as substrate binding, nucleophilic attack, protonation and ester hydrolysis (Kaur & Singh, 2022). The rate of hydrolysis mediated by trypsin on the albumin substrate depends on many factors as temperature, pH, concentration of substrate and the ratio of enzyme to substrate (Shi et al., 2005). pH affects the hydrolytic activity of trypsin as it influences the dissociation of the functional groups, which consequently affects the banding of enzyme and substrate. It was reported that the BSA hydrolysis is slowest at pH 7 and fastest at pH 9, with a fast reduction with time at pH 10 (Shi et al., 2005). In agreement with these results, in this experimental chapter changing the pH of the trypsin solution resulted in a modified proteolytic activity and therefore in a different total amount of drug released. The incubation of RFM-HSA-NPs with 'activated' trypsin induced an almost 2-fold higher total cumulative release by 4 h compared to 'not activated' trypsin, when the ratio of trypsin:substrate was kept constant. Therefore, it is evident how changes in the experimental protocol – as the pH of the enzyme adopted to enhance the NPs degradation- can impact the total amount of drug released and can result in misleading outcomes if not properly optimised.

As mentioned above, the cumulative percentage of RFM released overtime was equal to 34%. Some hypotheses can be drawn to investigate the rationale behind the achievement of a total cumulative release overtime not near 100%.

Firstly, based on the release profile obtained, the distribution of RFM within the NP matrix and on the NPs surface can be hypothesized. A fraction of RFM may be entrapped in the matrix system and the remaining fraction is covalently and not-covalently bound to the surface of the NPs. One hypothesis is that the amount of drug released detected (34 %) only corresponds to the surface-bound drug, whether the other fraction remained attached to the albumin molecules while those were being degraded by trypsin. The formed albumin-drug fragments may be not physically able to be transferred from the dialysis bag to the receiver medium, hence that fraction of drug is not encountered in the total amount of drug released. In order to further confirm or reject this hypothesis, further studies evaluating the exact distribution of the drug within the NPs matrix and on the surface must be carried out.

Langer and co-workers (Langer et al., 2008) investigated the kinetic of enzymatic degradation of HSA-NPs. The latter was described as highly dependent on the crosslinking degree of the NPs, with only 9% of NPs having 100% degree of crosslinking being fully degraded within 24 h. As the calculated degree of cross-linking of the NPs developed in this experimental chapter was equal to 100%, it can be argued that the crosslinking degree may have hindered the full degradation of the NPs and the achievement of a total cumulative release of 100%. However, in contrast to Langer's study, the evaluation of the changes of size, PDI and derived count rate throughout the assay confirmed that the NPs were fully degraded despite the degree of crosslinking equal to 100%. This outcome was also confirmed by the full degradation of blank NPs incubated with RFM in presence and absence of trypsin. As anticipated, the rate of RFM release did not change upon trypsin addition in the dialysis bag as the drug was not embedded in the NPs, but the full occurred degradation of the blank NPs was confirmed by a 4-fold increase in the PDI and a 4-fold increase in the size compared to time 0. However, it is also interesting that the evaluation of size, PDI and derived count rate changes more closely resembles a qualitative assay rather than quantitative. Therefore, further studies could focus on the development of an assay that simultaneously combines the quantitative analysis of drug release (HPLC) with the quantification of the remaining albumin fragments.

On the other side, the lack of a full (100%) release of the drug from the nanocarrier may be not relevant if the mass of RFM released is sufficient to achieve a therapeutic activity. Considering the total amount of albumin entrapped in the system and its EE, the total mass of RFM achievable is equal to ~727 µg. Taking into account that *in vitro* the amount of drug released overtime was equal to 34%, it can be concluded that the mass of RFM available to produce a therapeutic activity would be equal to ~247 µg.

The intended aim of the designed NPs system is the investigation of its potential

The intended aim of the designed NPs system is the investigation of its potential pulmonary delivery. The use of pulmonary delivery often involves a reduced total dose administered compared to oral administration of the same drug (which in the case of RFM is 500 µg daily). This is due to the avoidance of the first pass metabolism and the release of the drug at the target site with a following reduction of the unbounded plasma fraction of the drug and its systemic exposure. Therefore, the EE achieved in this experimental work and the cumulative % released described in the *in vitro* assay provided initial evidence of the potential of a formulation strategy for RFM and can inform further evaluation mainly focussed on the optimisation of RFM content and calculation of the dose achievable when administered to the lungs using a suitable inhalation device.

687

688

689

690

691

692

693

694

695

696

697

698

699

700

701

702

703

704

678

679

680

681

682

683

684

685

686

Moreover, evidence from the literature also corroborates the successful therapeutic suitability of NPs with EE values and a cumulative drug release from the carrier in an in vitro assay lower than 100%. Craparo and colleagues (Craparo et al., 2022) investigated the release of RFM from the lipid-polymer hybrid NPs system for lung delivery and found that the drug was slowly released without any burst effect and that the max amount of RFM obtained in the aqueous medium was about 40 % wt of the total amount after 24 h of incubation. Slightly higher (60%) but not near 100% was the amount of rolipram released from a vesicle carrier (Fang et al., 2015). Both the formulations tested (with and without PEG) exhibited an initial burst and were then able to maintain a sustained released overtime (12 h). In this case, the authors commented the lack of total (100%) release was due to the limited volume of receptor compartment in the Franz cell used to investigate the in vitro drug release. For cilomilast, similar percentages of drug released were obtained in two different studies investigating the release from phosphatiosomes and from oleic acid and lipid matrix nanocarriers respectively (C. Y. Lin et al., 2019; Liu et al., 2018). Cilomilast was fully and rapidly released from the control (free drug) by 24 h whereas the nanovescicular encapsulation of the drug allowed a sustained and controlled release overtime. However, only 26% of cilomilast was released at 24h. The release behaviour of the same drug from the NPs was evaluated using Franz diffusion cells, using a receiver medium that contained 30% of ethanol to enhance the drug solubility. Free drug was represented by cilomilast solubilised in 100% DMSO. Interestingly, although the percentage of cilomilast released from the carrier achieved in 24 h was only 14%, the use of the encapsulated drug still represented an advantageous formulation choice due to the sustained released that cannot be achieved with any other formulation strategies.

Although in this experimental work the degradation of the carrier and the following drug release rate are investigated in two distinct *in vitro* experimental models, it is more likely that in a living system the two events will take place simultaneously, with the drug being released while the carrier undergoing degradation. Further studies will focus on the development of a combined *in vitro* assay which employs analytical techniques as the HPLC to accurately quantify the amount of drug released overtime and fluorescence microscopy to monitor the degradation of the HSA-NPs at is happens.

2.6 Conclusion

This chapter describes the development of an albumin based- nanoplatform that can encapsulate and release RFM in a sustained manner after deposition and degradation in the lungs for PDE4 inhibition as a treatment for a lung inflammatory disease. The NPs suspension developed is suitable for its conversion in a respirable form which will be investigated and described in Chapter 3. An easy lab-based and reproducible manufacturing method was developed for the consistent manufacture of the albumin nanocarrier which physiochemical properties were characterised using different techniques. The NPs showed small particle size, uniformity and negative zeta potential. The formulation underwent degradation in an in vitro model of lung proteases which employed trypsin as a model enzyme to investigate the NPs fate after degradation. Trypsin was used similarly to establish and optimised a drug release method, which showed that complete RFM release from the HSA-NPs occurred over 4 h. The next step is for the formulation to undergo biological testing to determine whether the encapsulation efficiency and drug release achieved are sufficient to produce therapeutic effects in the lungs. It is estimated that the pulmonary dose required will be much lower than the oral dose currently adopted in clinical use. Development of a respirable dosage form and development of an animal model of lung disease are the next steps to determine whether further optimisation of the NP formulation is needed.

CHAPTER 3: RFM-HSA-NPs in mannitol-based microparticles powder for inhalation

771

769

770

3.1 Introduction

772773

774

775

776

777

778

779

780

781

782

783

784

785

786

787

788

789

790

791

792

Even for drugs characterised by high potency, their effectiveness can be severely hindered by low or very low water solubility, as in the case for the prototype drug used in this work. NPs are a useful platform to deliver those drugs and can improve the systemic or local drug bioavailability allowing a controlled onset of therapeutic action. Indeed, where low-soluble drug cannot dissolve in the lung lining fluid, NPs with their higher surfaceto-volume ratio can dissolve much faster than the free drug, enhancing its solubility and facilitating pharmacological activity in the lungs. The use of the pulmonary route of drug delivery to target the lungs or the systemic circulation is a promising method which requires delivery of a pharmaceutical aerosol with particles with suitable aerodynamic size. Particles with an aerodynamic diameter less than 1 µm are more likely to reach the alveolar region but possess low mass and do not deposit efficiently. Although, their low mass hinders their deposition by impaction and sedimentation allowing them to reach the alveoli, deposition by diffusion is slow and they are subject to exhalation and a consequent loss of contribution to the therapeutic dose. A further difficulty for inhaled delivery aerosols composed of sub-micron particles is the high surface area, which enhances the free energy with a resulting possible aggregation between particles (Heyder, 2004; Praphawatvet et al., 2020). These disadvantages of NPs for inhalation can be tackled using an alternative delivery systems called Trojan particles and nanoparticle embedded microparticles (NEMs).

793

794

3.1.1 Trojan particles

795 796

797

798

799

800

801

The development of dry powder for inhalation containing NPs is very challenging to achieve due to aggregation that would take place in the drying phase. Large porous carriers containing NPs called Trojan particles, have been investigated as alternative approach to deliver NPs to the lungs in the form of dry powders (**Table** 3.1). This approach was firstly reported by Tsapis and co-workers (Tsapis et al., 2002), who developed a system based on large porous nanoparticles (LPNPs) with improved

aerosolization and physical properties and avoidance of phagocytosis in the lungs. Tsapis and colleagues developed system of **LPNPs** composed a dipalmitoylphosphatidylcholine (DPPC), dimyristoylphosphatidylethanolamine (DMPE) and lactose using spray drying. The LPNPs possessed both the benefits of the large porous particles (LPPs) (D. A. Edwards et al., 1997) and those of the NPs with a resulting ease of flow and aerosolization and drug delivery potential. LPPs are characterised by low mass density ($< 0.4 \text{ g/cm}^3$) and high geometric diameters ($> 5 \mu \text{m}$). Compared to smaller nonporous particles, LPPs have an improved aerosolization efficiency from DPI and have the potential avoidance of macrophage clearance after deposition. NPs have instead a typical geometric size of a couple of hundred nanometers and can remain in the lung lining fluid after deposition for extended periods and release the active ingredient which can exert the pharmacological activity.

3.1.2 Nano-embedded microparticles (NEMs)

Although Trojan particles possess many advantages for pulmonary delivery, there are some drawbacks correlated to the preservation of the particle aerodynamic properties and integrity during the drying process of the NPs suspension. An alternative approach is represented by the nano-embedded microparticles (NEMs) system which consists of nanocomposite particles obtained by inclusion of drug-loaded NPs within a microparticle system, using an inert carrier (excipient) (**Table** 3.1) (Silva et al., 2014; Ungaro et al., 2012). The specific advantage of this systems is the degradation of the excipient on the pulmonary epithelium after deposition and following release of the NPs. Some of the most used polymers are PLGA and chitosan, whereas mannitol and lactose are widely used excipients. Mannitol is advantageous compared to lactose for its low hygroscopicity, no reducing effect and non-toxicity (Ungaro et al., 2012). Lactose is the only FDA-approved sugar carrier for dry powder aerosol formulations. NEMs are characterised by superior aerodynamic characteristics and pulmonary deposition compared to simply drug encapsulated in NPs; they provide a higher stability over time and a higher deposition of encapsulated APIs in the lungs (Anton et al., 2012; Tsapis et al., 2002).

Table 3.1 Features of nanoparticles (NPs), large porous particles (LPPs), large porous nanoparticles (LPNPs) and nano-embedded microparticles (NEMs).

| Nanoparticles (NPs) | Large porous particles (LPPs) | Large porous nanoparticles (LPNPs) (Trojan system) | Nano-embedded microparticles (NEMs) |
|---|--|--|--|
| Geometric size ∽ 100-200 nm | Geometric size > 5 μm | Dissolve to produce NPs | Dissolve to produce NPs after reaching deep lung |
| Potential to remain in the lung lining fluid | Mass density ≤ 0.1 g/cm ³ | Improved flow and aerosolization properties typical of LPPs | Inert excipients used (mannitol, lactose, trehalose) |
| Low inertia | Aerosolization efficiency | Long-term residence in situ, prolonged drug release typical of NPs | Improved aerodynamic properties and stability |
| Potential avoidance of mucociliary and macrophage clearance | Potential avoidance of macrophage clearance | | |
| Inter-particle interactions > potential aggregation | Dissolve to produce molecular components | | |

Spray drying is a common technique used to manufacture NEM usually in combination with excipients such as mannitol (Praphawatvet et al., 2020). Alternatives such as wet milling, supercritical fluid extraction or electrospray can be used, but in this body of work, the NEMs were manufactured in two steps: first, the NPs are produced using techniques such as nanoprecipitation or emulsification and then spray-dried with an excipient (Bohr et al., 2014). The resulting dry powder formulations are characterized by greater stability and pulmonary delivery potential compared to NPs. An additional advantage sought by the delivery of an API entrapped in a NEM system over a conventional formulation is the controlled release that can be achieved.

Spray drying is a very convenient tool to transform a liquid feedstock solution, suspension, or emulsion in dry particles in a highly controllable way. The fluid phase is forced through high pressure nozzles to produce a fine mist from which the aqueous content evaporates, leaving behind a powder (Bailey & Berkland, 2009). This method obtains well-controlled characteristics at the particle and powder level. An extensive review of the impact of excipients and processing parameters on the spray drying of particles for inhalation was recently published by Alhajj and colleagues (Alhajj et al., 2021).

The final NEMs appearance and morphological structure is dependent on the drying phase of the spray drying process and its kinetics. The Peclet number (Pe) (**Equation** 3.1) is a dimensionless mass transport number which gives an idea of the final structure of the NEMs, whether based on a matrix or hollow system. It also allows the understanding of the relationship between the drying process and the resulting particle morphology. The Pe is equal to the ratio between two characteristics times: the time required by the solute (single molecule or NP) to diffuse from the edges of the droplet to its centre (R^2/D , with R^2 being the radius of the droplet and D the diffusion coefficient of the molecule or NP) and the time required for a droplet to dry (τ_d).

Equation 3.1 Peclet number

$$Pe = \frac{R^2}{\tau_d D}$$

If Pe is $\ll 1$, the drying phase will be very slow providing sufficient time to the molecule or NP component within the droplet to redistribute by diffusion, hence obtaining relatively dense dried particles. Vice versa, $Pe \gg 1$ corresponds to a quicker drying phase, which will result in the components not having adequate time to move towards the centre hence remaining on the edges of the dried particle (hollow structure). The NPs will then be locked in place due to Van der Waals forces.

In other words, the distribution of the NEMs components within the particles is affected by how the solid content of a droplet and the solvent molecules behave during two critical drying phases of the spray drying process: the constant drying rate and the falling drying rate. During the constant drying period, the role of the solid content of the droplet is

negligible whereas key role is played by the solvent. Simultaneously molecules of solvent on the surface evaporates while others migrate from the centre of the droplet to its surface. The completion of the solvent molecules evaporation launches the second drying phase – falling drying rate- which is characterized by the particle solidification. How the various components of the particles will redistribute within a droplet during the evaporation process depends on the recession process of the droplet surface. The reduction of the solvent at the particles surface leads to an increase in the local concentration of the solute and results in a concentration gradient between the surface and the centre of the particle. The above mentioned Pe can also described this process. A high Pe corresponds to a higher surface recession than solute diffusion resulting in surface enrichment which corresponds to hollow particle; in contrast, a low Pe will often corresponds to dense particle resulting from a solute diffusion rate higher than the surface recession. There are two different kinetics of drying that can result in two different particle structures: hollow particles are the product of a fast droplet surface recession than solute diffusion which results in surface enrichment; the opposite condition leads to dense particles (**Figure 3.1**). Furthermore, additional morphological changes can take place after the solidification phase (Alhajj et al., 2021; Tsapis et al., 2002).

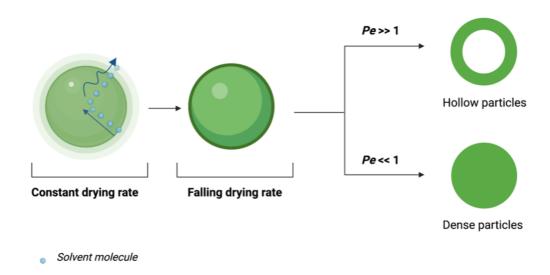


Figure 3.1 Schematic representation of critical phases of spray drying process which regulate the final particle morphology: constant drying phase and falling drying phase. Pe is Peclet number.

876

877

878

879

880

881

882

883

884

885

886

887

888

889

890

891

892

Therefore, based on the drying kinetic, NEMs can have a dense structure, a thick shell or there can be a crust rich in NPs resulting from insufficient time for the NPs to migrate towards the centre of the structure, enclosing the remaining solution. The latter escapes by evaporation from the shell, with the remaining NPs onto the surface of the shell, frequently puncturing it and producing porosity.

900901

902

903

904

905

906

907

908

909

910

911

912

913

914

915

916

917

918

919

920

921

922

923

924

925

895

896

897

898

899

The advantages of those embedded NPs when delivered to the lungs are dependent on the type of excipient used and, on the degradation kinetic of the whole system. Indeed, the microparticles represent a delivery system that due to the high-water solubility of the bulk excipient used (such as mannitol) can be easily dissolved in the lung lining fluid and release the NP system which will disperse and function as designed to dictate the release of the drug. This step is fundamental to maintain the benefits provided by the nanocarrier and control the onset and duration of the therapeutic action. Despite its importance, the investigation of the disintegration rate of the microparticles lacks extensive research. Often researchers evaluate the NEMs disintegration dissolving the system in high volume of water and applying forces such as stirring or mixing. However, this set up does not represent the conditions in the lungs, particularly regarding the lung fluid's composition and its volume. In order to improve the investigation of the NEMs disintegration, an innovative in vitro model was designed by Ruge and colleagues (Ruge et al., 2016) who studied the disintegration of a NEMs system after deposition onto a static or dynamic layer of mucus. The study of the microparticle onto a static layer of mucus did not result in release of the NPs from the NEMs system, whereas the individual polymeric NPs were successfully released when forces were applied in the dynamic model (Ruge et al., 2016). Those findings suggest that mechanical forces may be required to overcome the attractive interactions that exists within the NPs. The question that remains unaddressed is to what extent the lung mechanics will enhance the disintegration of the NEMs. An alternative in vitro model to investigate the disintegration of the microparticles in set up closer to the real lung condition was designed by Torge (Torge et al., 2017). The model was based on the incubation of spray dried powders with different content of mannitol at 37°C in > 90% of relative humidity (RH). This innovative model was shown to allow the NEMs disintegration, releasing unchanged nanoparticles.

926

3.2 Aims and objectives

The aim of the work in this chapter was to investigate the use of mannitol, a highly water soluble sugar alcohol, as an excipient in a microparticle system composed of 40% w/w RFM-containing HSA-NP and 60% w/w of mannitol. The physiochemical and aerodynamic characterisation of this formulation was carried out focussing on the particle size distribution of the powder, its thermal behaviour, as well as the impact of the spray drying process on the properties of the embedded NPs. The overall aim of these series of experiments was to investigate the potential of RFM-HSA-NPs to be embedded in a respirable formulation, a key step in facilitating their translation to clinical use.

Specific objectives included:

- 1. Establish a spray-drying protocol to convert the albumin NPs suspension in a nanoparticle embedded microparticles (NEMs) respirable formulation;
- 2. Characterise the manufacturing process and the obtained powder in terms of yield, particle size distribution and aerosol performance;
 - 3. Investigate the physiochemical spray-dried powder characteristics using dynamic vapour sorption (DVS) and dynamic scanning calorimetry (DSC).

3.3 Methods

3.3.1 Spray-drying conditions of manufacture

For the preparation of HSA-NPs embedded in microparticles, the NPs manufacture process described in Chapter 2 was scaled up and an amount of 600 mg of mannitol was added to the NP suspension (10 mL) and the volume increased to 25 mL with double distilled water. The suspension was then spray dried using a laboratory scale spray dryer according to a previously reported method (Patel et al., 2020). **Table** 3.2 shows the operating conditions for the spray-drying process. The solution was pumped into the spray-dryer and the resultant powder was separated from the airstream using a cyclone separator. The obtained powder was collected, weighed, and stored at room temperature in a desiccator.

Table 3.2 (A) Spray dried feedstock (FS) solution and solvent composition. (B) List of parameters adopted in the spray-drying process.

| Excipient name | % w/w in dry product | |
|-------------------------------------|----------------------|--|
| Feedstock (FS) solution composition | | |
| RFM-HSA NPs | 40 | |
| Mannitol | 60 | |
| Total dry % w/v (including active) | 100 | |
| Solvent composition | | |
| Main solvent | Water | |
| FS total solid content (% w/v) | 4 | |
| Total volume (mL) | 25 | |
| FS storage | Ambient | |

| Spray drying conditions | |
|-------------------------------------|-----|
| Feed solution concentration (% w/v) | 4 |
| Inlet temperature (°C) | 106 |
| Outlet temperature (°C) | 65 |
| Feed rate (mL/min) | 2 |
| Atomisation flow (L/min) | 17 |
| Atomisation pressure (bar) | 2.5 |
| Drying air flow (kg/h) | 17 |
| Drying air pressure (bar) | 2.5 |
| Pulsing nozzle | No |
| Estimated duration (min) | 14 |
| Pump speed (rpm) | 4.1 |

| 963 | 3.3.2 Physiochemical and aerodynamic characterisation of microparticles | | |
|-----|---|--|--|
| 964 | | | |
| 965 | 3.3.2.1 Impact of spray-drying on size and polydispersity index (PDI) of embedded | | |
| 966 | NPs | | |
| 967 | Any changes in the size and polydispersity index of the NPs embedded in microparticles | | |
| 968 | after the spray-drying were evaluated. The spray-dried powder was reconstituted by | | |
| 969 | dispersing 10 mg of the powder in distilled water (2 mL). After centrifugation at 2,000 | | |
| 970 | g for 10 min, 1.5 mL supernatant was removed and changes of the size and zeta potential | | |
| 971 | of the NP after the spray-drying were determined by | | |
| 972 | dynamic light scattering (Zetasizer nano ZSP, Malvern Instruments, UK). Size, PDI | | |
| 973 | and zeta potential were measured at 25°C. | | |
| 974 | | | |
| 975 | 3.3.2.2 Fast Screening Impactor (FSI) studies | | |
| 976 | Aerosol performance of spray dried formulations was assessed using a Fast Screening | | |
| 977 | Impactor (FSI, Copley Scientific, UK) with a 5 µm cut point insert. Hand-filled sealed | | |
| 978 | aluminium blisters containing 10.76 ± 0.37 mg spray dried powder were dispersed at 60 | | |
| 979 | L/min for 4 seconds using a unit dose dry powder inhaler (Vectura Ltd, UK). Fine | | |
| 980 | particle fraction (FPF % $\leq 5~\mu m)$ and blister evacuation (% fill mass) were determined | | |
| 981 | gravimetrically (n=3). | | |
| 982 | | | |
| 983 | 3.3.2.3 Particle size distribution | | |
| 984 | The particles size distribution (D_{10} , D_{50} and D_{90}) of the obtained spray-dried powder was | | |
| 985 | measured using the Hydro MV on the Malvern Mastersizer. The microparticles (9.4 mg) | | |
| 986 | were weighed and dispersed in 10 mL of 0.1% lecithin in iso-octane with sonication for | | |
| 987 | 3 minutes. | | |
| 988 | | | |
| 989 | 3.3.2.4 Dynamic Vapor Sorption (DVS) and differential scanning calorimetry | | |
| 990 | (DSC) | | |
| 991 | The water sorption/desorption behaviour of the spray dried powder was determined using | | |
| 992 | a DVS Advantage instrument (SMS Ltd, UK). Spray dried powder (~30 mg) was weighed | | |
| 993 | into a sample pan and equilibrated at 0% RH at 25°C until change in mass was less than | | |
| 994 | 0.002%. Incremental 10% step changes in relative humidity from 0 - 90% RH and from | | |
| 995 | 90 - 0% RH were performed at 25°C. Progression to the next step occurred once change | | |
| 996 | in mass was less than 0.002%. Two cycles were performed. | | |

997 998 Thermal events were measured using differential scanning calorimetry (Discovery DSC, 999 TA instruments). A mass of 3 - 5 mg of the spray dried powder was filled in 1000 aluminium DSC pans and hermetically sealed with a sample encapsulation press. Heating 1001 rate was 10°C/min from 20-300°C. 1002 3.4 Results 1003 1004 1005 3.4.1 Physiochemical and aerodynamic characterisation of microparticles 1006 1007 A feedstock solution of 40% w/w of RFM-HSA-NPs and 60% w/w of mannitol dissolved 1008 in water was spray-dried and the obtained powder was collected and the yield % 1009 calculated as \sim 46%. The FPF of the resulting powder measured using a cut-off of 5 μ m 1010 using a Fast Screening Impactor was 67%, highlighting that a significant portion of the 1011 obtained powder had size below 5 µm and could therefore be considered as 'respirable' 1012 for potential lung administration. Blister evacuation of the obtained powder from hand-1013 filled sealed aluminium blisters was showed to be of 95% (Table 3.3). 1014 1015 The impact of spray-drying on the physiochemical properties of the NPs was evaluated 1016 using dynamic light scattering. Spray-drying did not impact the size and PDI of the 1017 embedded NPs which remained mostly unchanged except for an increase in the PDI.

Table 3.3 Properties and aerodynamic performance of spray-dried powders composed of 40% (w/w) RFM-HSA-NPs embedded in a mannitol matrix. Values reported are derived from the mean of three consecutive measurements performed on a single batch of spray dried particle (n = 1 independent experiment).

| | SPRAY DRIED POWDER | | |
|------------------------|---------------------|---------------------|--|
| Feedstock solution | 40 % w/w RFM-HSA | A-NPs with mannitol | |
| Yield (g) | 0.4586 | | |
| Yield (%) | 45.9 | | |
| Fine Particle Fraction | 67.05 ± 1.72 | | |
| (%) ± SEM | | | |
| Blister evacuation (%) | 94.16 ± 0.67 | | |
| \pm SEM | | | |
| | Before spray-drying | After spray-drying | |
| Size (nm) | 173.1 | 164.6 | |
| PDI | 0.043 | 0.108 | |

3.4.2 Particles size distribution (PSD)

Particle size distribution of the obtained spray-dried powder is summarized in **Table** 3.4. Laser diffraction analysis of the spray-dried powder showed that 50% of the total mass had a geometric size below 2.21 μ m while 90% of the total mass of particles had a size below 4.53 μ m indicating promising characteristics for pulmonary delivery, which were confirmed by aerodynamic measurements.

Table 3.4 Particle size distribution (D_{10} , D_{50} and D_{90}) expressed as equivalent volume diameters of the spray died powder measured with using the Hydro MV on the Malvern Mastersizer. Refractive index of the material was 1.480; refractive index of the dispersant is 1.391. Values reported are derived from the mean of six consecutive measurements performed on a single batch of spray dried particles (n = 1 independent experiment).

| | D ₁₀ | D ₅₀ | D ₉₀ | Below 5 µm (%) |
|-----------|-----------------|-----------------|-----------------|----------------|
| Mean (µm) | 0.937 | 2.21 | 4.53 | 92.68 |
| RSD % | 0.272 | 0.254 | 0.219 | 0.07 |

3.4.3 Differential scanning calorimetry (DSC) and dynamic vapour sorption (DVS)

1034

1035

1036

1037

1038

1039

1040

1041

1042

1043

1044

1045

1046

1047

1048

1049

1050

1051

1052

1053

The thermal properties of the NEMs were evaluated using DSC. Figure 3.2 shows the thermal traces associated with the spray-dried powder, highlighting the corresponding exothermic or endothermic events. The profile shows a broad endothermic peak located at ~ 60°C associated with water loss from the system followed by a re-crystallisation event (exothermic peak). Despite not confirmed by a DSC analysis of the pure drug, RFM, the endothermic peak was attributed to the drug itself, with the justification that DSC traces of RFM reported in the literature (Mahmoud et al., 2018) showed a similar endothermic peak (at 69.55°C) and an additional sharp peak at 161.8°C related to its melting point. DSC curves of RFM have also been reported by Viertelhaus and coworkers (Viertelhaus et al., 2013). RFM at room temperature exists in only one crystalline form and a phase transition is reported at 50°C; peak maxima of the phase transition was observed at 51.47 ± 0.05 °C (heating) and 48.7 ± 0.9 °C (cooling). The melting point peak was reported to be at 159.94 \pm 0.11°C. Using different analytical techniques, they also showed that RFM undergoes a reversible phase transition. A value in agreement with the above mentioned is also reported in the patent document of Daxas where RFM melting point is stated at 159.7°C (European Medicines Agency, 2010).

Exothermic event (crystallization) Water loss

Endothermic event

(melting)

250 Exo Up Figure 3.2 Dynamic scanning calorimetry (DSC) thermogram of RF-HSA-NPs (40% w/w) embedded in mannitol microparticles (60% w/w) (NEMs). Two measurements were performed on a single batch of spray dried particles (n =1 independent

In addition, it is assumed that the crystallisation event is related to the mannitol present in the formulation. D-mannitol is a material that has different morphological phases (polymorphism) which produce changes on the melting point. The forms include α with a melting point of 165.3°C/166 °C, β with a melting point of 166.7°C/166.5°C and δ where a discrepancy was reported regarding the melting point values (either 146.8 – 156.2°C or 150 – 158°C). **Table** 3.5 indicates the different melting points of each polymorphic forms reported in the literature.

1061

1054

1055

1056

1057

1058

1059

1060

-0.5

-1.0

-3.0

-3.5

-5.0

experiment).

Flow (Normalized) (W/g) -2.0 -2.5

Table 3.5 Melting points of mannitol polymorphic forms reported in the literature.

| Mannitol polymorphic forms | Reported melting point peak (°C) | Refs | |
|----------------------------|---|---|--|
| α | $167; 165.6 \pm 0.1; 166$ | (Barreneche et al., 2013; | |
| β | 155 and 166; 166.0 ± 0.5 ; 166.5 | Benetti et al., 2021; Y Yang et al., 2022) | |
| δ | $155; 157.1 \pm 0.2; 155$ | 1 ang et an., 2022) | |

Moreover, the thermogram lacked evidence of the glass transition temperature of mannitol; hence we could argue that this event is overlayed by the larger water loss peak. On the other hand, the endothermic event at 161.13°C can be attributed to the melting of mannitol. Unfortunately, the melting points values reported in the literature for each of the forms of mannitol were not helpful to understand in which form the mannitol existed in the spray-dried powder. However, in a study investigating the crystallinity of inhalable siRNA powder formulation having HSA as dispersion enhancer (Chow et al., 2019), the DSC trace of raw mannitol showed - as reported in the results of this experimental chapter - a sharp endothermic peak at around 167°C which corresponds to the melting point of mannitol in its β form. Indeed, as the material of interest that has been analysed is not a pure material (mannitol only) but rather a combination at a fixed ratio of mannitol and RFM-HSA-NPs, we could conclude that the melting event is associated with the mannitol and the drug both undergoing melting. Based on the qualitative analysis that the DSC provided and on the presence of endothermic events associated to both drug and mannitol, the hypothesis is that the spray dried powder existed in form of a crystallised powder. Further studies based on the comparison of multiple DSC analysis (raw mannitol, raw roflumilast, raw HSA, HSA-NPs) will help to evaluate the solid-state profile of the obtained powder.

The study of the spray dried mass behaviour, and whether this was amorphous or crystalline, in presence of increasing percentages of humidity was performed using a DVS technique. The adsorption isotherm curve showed the gravimetric changes of the spray dried powder while receiving increasing amount of water in form of vapour. The typical DVS isotherm shows the sequence of the increased humidity values (blue, reference) and the recorded mass changes of the sample of interest (red curve) (**Figure 3.3**). It was showed that the powder only retained a small portion of vapour. Indeed, the red profile mostly overlapped the blue profile except for the final section describing that only a small percentage of water was retained with a consequent increase in the mass. These results are further explored in **Figure 3.4** where the hysteresis (i.e. how much water is retained or expelled from the sample during specific points of the humidity cycle) is reported.

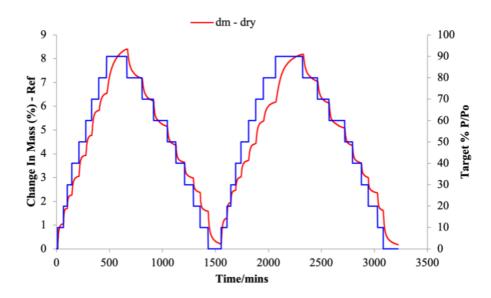


Figure 3.3 Dynamic vapour sorption isotherm of roflumilast albumin nanoparticles embedded in mannitol (NEMs) (blue reference). One measurement was performed on a single batch of spray dried particles (n = 1 independent experiment).

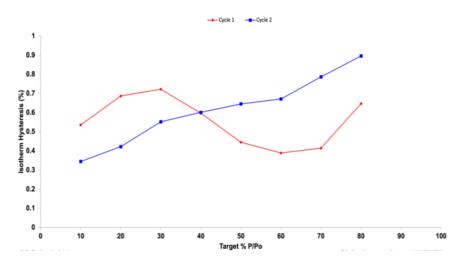


Figure 3.4 Dynamic vapour sorption isotherm (hysteresis) of RFM-HSA-NPs embedded in mannitol (NEMs).

3.5 Discussion

1093

10941095

1096

1097

1098

NP can be an effective drug delivery system to treat locally airway diseases, but the potential of this nanometer size range carrier is hindered by the impact that the aerosolization may have on the NP's stability and physiochemical properties. A detailed

study of the influence of nebulisation process on NPs suspension was carried out by Dailey and co-workers (Dailey et al., 2003). Biodegradable NPs were nebulised using jet, ultrasonic and piezo-electric crystal nebulizer. In agreement with other studies performed on liposomes (Leung et al., 1996), shear forces and high energy generated during jet nebulisation and ultrasonic nebulisation respectively were shown to alter the characteristics of the nanometric system. The NPs were small and normally distributed before nebulisation, whereas after nebulisation, the suspension had a bimodal distribution pattern, with signs of aggregation that happened during the nebulisation. Hence, it is evident that nebulisation can have a negative impact on the physiochemical properties of the NPs which therefore would not be suitable in this form to be used clinically. On the other side, the delivery of NPs as dry powder also has drawbacks. Aerodynamic particle diameter is one of the critical product attributes of the orally delivered inhaled drug products. NPs would not deposit in the lungs neither by sedimentation or by impaction, nor substantially by diffusion. In addition, interparticle cohesive forces may lead to uncontrolled aggregation in the powder and variability in product quality and any therapeutic effect.

To overcome those disadvantages and being able to deliver therapeutic drugs to the lungs an alternative formulation strategy has been achieved. Described by Tsapis (Tsapis et al., 2002), NPs have been shown to successfully be incorporated into microparticles system and delivered to the airways. An example of the improvements that the incorporation of a free drug in NPs first and then in microparticles can bring is provided by the study of Yu and colleagues (Yu et al., 2021). They used colistin and ivacaftor, drugs characterized by low-water solubility. As strategy to increase the drug solubility and therefore improve the therapeutic activity of the drugs, they encapsulated the drugs in a NPs formulation which was then converted to a microparticle. Their studies demonstrated that colistin acted as a matrix material to bind the NPs of ivacaftor into inhalable microparticles. The powder formulation obtained via spray-freeze-drying was characterized by high FPF and superior emitted dose. Importantly, the formulation provided a very significant increase in dissolution rate compared to the free drug. The superiority for pulmonary delivery of the NEMs compared to NPs was therefore demonstrated in this study.

The use of the NEM has also been reported in the field of the photodynamic therapy. Elias Baghadan (Baghdan et al., 2019) developed an inhalable formulation consisting of NPs

loaded with a photosensitizer. The formulation of NPs into microparticles was performed via spray-drying using mannitol as a bulking agent and resulted in a FPF of 65% and MMAD of 3.02 µm (Baghdan et al., 2019).

1136

1137

1138

1139

1140

1141

1142

The superiority of the NEMs aerodynamic properties compared to the NP-containing powders alone and to the raw micronized drug was further demonstrated by Pilcer and co-workers (Pilcer et al., 2009). Particle dispersion during the inhalation was improved when the NEMs system was used and the FPF of the formulation increased form 36% for the raw micronized drug (tobramycin) to about 61% for the most effective NEMs formulation.

1143

1144

1145

1146

1147

1148

1149

1150

1151

1152

1153

1154

1155

1156

1157

1158

1159

1160

1161

1162

1163

1164

1165

1166

The concept of converting HSA-NPs into microparticles investigated in this thesis has also been reported elsewhere. In the study conducted by Varshosaz and co-workers (Varshosaz et al., 2015), haloperidol targeted-BSA NPs were manufactured via desolvation method and loaded with doxorubicin. The NPs were converted via spraydrying to microparticles using different inlet temperatures (between 80 and 120°C) and excipients (mannitol, L-leucine and trehalose). The best results were obtained when HSA-NPs were spray dried with mannitol at 80°C (inlet temperature), showing a mean aerodynamic diameter of 4.58 µm and FPF of 66%. Despite the difference in the inlet temperature used (80 °C in Varshosaz's study (Varshosaz et al., 2015) and 106 °C in this experimental work), FPF value obtained (66 %) corresponds to the FPF obtained in this experimental study (67 %). The potential of mannitol as a bulking excipient, described by Varshosaz and co-workers, was also explored in a similar investigation where three different excipients – mannitol, leucine and trehalose – were used to evaluate the best spray dried powder containing HSA-NPs (Patel, 2018). Varshosaz and others also investigated the morphological structure of the nanocomposites (M₈₀ and M₁₂₀, when albumin NPs were spray dried with mannitol using 80°C and 120°C respectively as inlet temperature in the spray drying process). Nanocomposite of mannitol appeared approximately round and smooth, and this structure was not impacted by the increase in temperature (from 80 to 120 °C). Despite any morphological analysis were performed in this experimental work, a previous scanning electron microscopy analysis of a spray-dried powder incorporating both blank

and RFM-HSA-NPs (Patel, 2018) showed spherical particles for both formulations, with

NP-containing formulation appearing to have a slight rougher surface. Further particle

surface analysis would need to be carried out to better evaluate how the NP influence the morphology of the final NEM structure.

As mentioned above, the rate of two critical phases in the spray drying process – constant drying rate and falling drying rate- will highly impact the final structure of the NEMs. In this context it would be interesting to investigate first the morphology of the pure mannitol microparticle and then the result of the co-spray dried particles. The distribution of both blank and RFM-loaded HSA NPs in the mannitol spray-dried matrix (NEMs) could be achieved using a confocal laser scanning microscopy. This technique allows – previous labelling of components with fluorescent dyes – to visualize the surface and the core of the particles. The resulting three-dimensional picture would enable to study the spatial distribution of the component within a particle.

There are several excipients that can be used to manufacture microparticles via spray drying and the choice of the most appropriate one for lung administration is mainly based on the potential toxicological concerns and on the physiochemical properties that relate to product quality and the desired kinetics of drug release from the particle. When formulating a NEMs system for lung delivery, it is recommended to achieve low aggregation of the NPs in the microparticles in order to get rapid disaggregation once deposited into the lungs. Those features are usually obtained adding an excipient which provides spatial separation within the individual colloidal NPs ensuring a lower extent of NP-NP interaction (Ruge et al., 2016).

The interactions between excipient and NP must be 'weak enough' to allow the excipient dissolution and dissociation from the NPs after deposition, but on the other hand those interactions need to be strong enough to hold the system together also withstanding the stress of the spray drying process. Neither the excipient nor the spray drying process should alter the physiochemical properties of the NPs and the kinetics of drug release which are designed to be dictated by the NP system.

The investigation of the fate of the administered spray-dried powder is a key step in the development of an inhalation delivery system as it allows the spreading of the embedded nanometric system into the target area. The hypothesis is that after deposition into the lung lining fluid, the NEMs dissociate into multiple primary NPs system which evade clearing mechanisms and deliver drug. The re-dispersibility of the aggregate system

chemical characteristics of the excipient and its ability to make bridges with the NPs system – rather than the attractive forces (van der Waals) among the NPs; ii) the degree of microparticle wetting in the medium. However, it is important to highlight that dissolution of the matrix components in the lung lining fluid is not automatically associated with the disintegration of the NPs and that the understanding of this phenomenon may vary based on the *in vitro* model used and whether it is biorelevant or not. In a study of Ruge and co-workers (Ruge et al., 2016), polymeric (polystyrene) NPs were manufactured and then spray dried with trehalose forming NEMs. The aqueous redispersibility of the system was firstly studied in a model based simply on the redispersion of the NEMs powder in water with following vortexing and Dynamic Light Scattering analysis. Results showed that the NEMs were successfully disintegrated into the single NPs which were efficiently detected by light scattering. However, when a more complex in vitro model was used, the NEMs aerosolization onto a static mucus of layer resulted in the NEMs remaining in their microparticulate state. The authors raised the hypothesis that the NEMs were dissolved in the mucus due to the excipient solubility, but the polymeric (polystyrene) NP did not disperse upon NEM disintegration remaining in agglomerates form. This may be due to the interparticulate attractions within the NPs agglomerate such as van-der-Waals or capillary forces. The aqueous re-dispersibility of the NEMs is dependent on the 'excipient bridges' between carrier and NPs, but it is also governed by the degree of particle wetting in an aqueous medium. The latter is influenced by the nano-aggregate surface hydrophilicity and by the shell thickness to particle radius ratio, where particles with thicker shells have less re-dispersibility due to the reduced surface area (Kho & Hadinoto, 2010a).

depends on i) the strength of the NEMs binding forces – which is governed by the

12241225

1226

1227

1228

1229

1230

1231

1232

1233

1201

1202

1203

1204

1205

1206

1207

1208

1209

1210

1211

1212

1213

1214

1215

1216

1217

1218

1219

1220

1221

1222

1223

Regarding disintegration, the methods usually adopted by researchers to investigate the particles wettability such as application of high-intensity forces or ultrasonication do not resemble the conditions that particles are exposed to in the lungs. The need for more complex biorelevant models was addressed by Kho and co-workers in 2010 (Kho & Hadinoto, 2010a). The wettability of hollow spherical silica mannitol-based nanoaggregates was calculated with a method based on a series of dilutions and centrifugations combined with a turbidity measurement, as a function of particle size. This correlation was based on the wetting of particles and their 'excipient bridges' leading

to dissociation of the primary NPs with a concomitant reduction of the aggregate size and therefore reduction of level of turbidity.

A detailed description of the dispersibility assay was also reported in another research study (Kho & Hadinoto, 2010b). The same authors also investigated the re-dispersibility of a nanoaggregate manufactured for the delivery of the antibiotic polycaprolactone using and testing different ratio of three excipients: mannitol, leucine and lactose (Kho et al., 2010). They concluded that the re-dispersibility is highly dependent on the excipient formulation and only the nanoaggregates with lactose-leucine as excipients resulted in highly re-dispersible formulation. Similar results were obtained in another study where multiple-excipients formulation involving leucine and lactose produced successful formulations in terms of morphology and aqueous re-dispersibility (Kho & Hadinoto, 2010b).

In this experimental study, the mannitol-based nanoaggregates were dissolved to release albumin NP, which were observed to be of consistent size and PDI before and after the spray-drying, which represents successful re-dispersibility of the nanoaggregates and indicates that the NPs retained their properties through formulation as NEMs. Further studies could focus on the redispersability of the designed system in more biorelevant models which implicate the aerosolization of the NEMs onto a static and dynamic mucus layer.

Often the *in vitro* models used by researchers to investigate the re-dispersibility of the nanoaggregates involves the use of shaking, for example as in the quantitative evaluation of dispersibility performed by Torge (Torge et al., 2017) in presence of excess of simulated lung fluid. The use of stirring or shaking in *in vitro* models is often claimed to reproduce the lung dynamicity as they undergo movement associated with breathing cycles. Besides this, also the motion of ciliary beat should also be considered. The influence of force that exceeds the cohesion forces between the particles, is in providing a source of shear stress that will contribute to the disintegration of the particle aggregates with subsequent spreading of NP on the mucus layer and in the lung lining fluid.

Based on previous studies in the literature which employ mannitol as excipient, we may anticipate for the system designed in this experimental chapter a good and promising redispersibility behaviour *in vivo*; however further works are required to fully characterise the disintegration kinetic of the embedded microparticles in a biorelevant assay, e.g. using lung simulated fluid. One promising technique to discriminate the performance of the system may be represented by the isolated lung technique (Beck-Broichsitter et al., 2016). In addition, further investigation could focus on the *in vivo* distribution of the NEMs in an LPS-inflammation model. For pre-clinical studies, *in vivo* administration could be achieved firstly via aerosolization using the Penn Century device. A valuable alternative for the *in vivo* administration is also represented by the use of a system called PreciseInhale (Inhalation Sciences, Sweden). The latter allows to generate a dispersed aerosol and deliver it to an individual specie with minimal loss of drug and an accurate administration which is constantly monitored via a software. Following this first preliminary investigation, the adoption of a more complex and reliable method based on the use of a commercially available Vectura DPI device would be recommended.

3.6 Conclusion

A key step when investigating the potential of a NPs system aimed for inhalation delivery to the lungs is evaluating its respirability. Hence the main objective of this chapter was to find a strategy to overcome the issues related to the pulmonary administration of a delivery system in the nanometre range. A spray-drying manufacture process was used which, despite being a precedented method, has not been extensively studied for HSA-NPs embedded in microparticles systems. This chapter presents a successful manufacturing approach for HSA-NPs in mannitol matrix microparticles. The spray drying conditions adopted resulted in good process yield and did not impact the physiochemical properties (size, PDI and zeta potential) of the original NP system. This is a key aspect when formulating a microparticles system, as its disintegration will release the NPs which ultimately control the release of the drug. Preliminary aerodynamic investigation resulted in a promising FPF equal to 67% and PSD analysis also demonstrated that 90% of the particle population has a geometric diameter below 5 μ m. These data indicate that the microparticles are suitable for delivery and deposition in the lungs.

CHAPTER 4: Anti-inflammatory activity of roflumilast in an in vitro respiratory epithelial cell assay

4.1 Introduction

BEAS-2B cells are respiratory epithelial cells isolated from normal human bronchial tissue derived from autopsies of non-cancerous individuals, transfected with an adenovirus 12-SV40 virus hybrid and cloned. They have been used as two-dimensional in vitro airway model to mimic the epithelium and in the drug development for the screening of the biopharmaceutics of new compounds (Villandre et al., 2022; M. Zhang et al., 2022). In addition, other two cell lines commonly used as 2D-in vitro models of the airways are A459 cells, an adenocarcinomic human alveolar basal epithelial cell line and the bronchial adenocarcinoma-derived Calu-3 cell line. Despite their widespread use as starting point in the *in vitro* evaluation of new compounds, a recent review highlighted the limitations that 2D models have compared to 3D models. In 2D cellular models, cells are forced to adapt to an environment that differs from the physiological one. In particular, BEAS-2B fail to express tight junction formation and secrete airway mucins with consequences on their ability to form an effective barrier (Yaqub et al., 2022). Despite the limitations that 2D models may have, BEAS-2B are often utilised in research as model for the airways and in studies to understand the interaction of new drugs with the airway epithelium.

One of the most common *in vitro* models used for COPD involves the exposure of cells to an endotoxin. Endotoxins of gram-negative bacteria can induce potent pathophysiological effects in mammalian cells. The endotoxins are lipopolysaccharide (LPS) composed of an O-specific chain, a core oligosaccharide and a lipid component called lipid A which is responsible for the endotoxic activities. The mechanism of endotoxic activity of LPS involves an active response of the host cells such as endothelial, mononuclear cells or macrophages. The recognition between LPS and host cells results in the secretion of various mediators which activate other cellular inflammatory pathways (Rietschel et al., 1994). In 1990, Wright and colleagues demonstrated that leukocytes respond to LPS by the secretion of cytokines such as TNF- α . The mechanism of action involves the binding of LPS to a glycoprotein found in human serum called

1335 lipopolysaccharide binding protein (LBP) followed by recognition and binding of the complex LPS-LBP to the receptor CD14 anchored to the cell membrane (mCD14) (S. D. 1336 1337 Wright et al., 1990). 1338 1339 Although mCD14 is not expressed in endothelial or epithelial cells, Pugin and co-workers 1340 demonstrated that the stimulation of those cells by LPS was via a specific mechanism 1341 which involved LBP and soluble CD14 (Pugin et al., 1993). Further investigation of the mechanism of action of LPS in BEAS-2B cells showed that in these cells there can be a 1342 1343 CD14-indipendent activation and that other proteins may be involved or direct TLR-LPS 1344 interactions happens. They concluded that airway epithelial cells respond to LPS in a 1345 concentration dependent manner and that the effect is augmented by the presence of 1346 serum, supporting the hypothesis that cofactor(s) are necessary to initiate the stimulation 1347 (Schulz et al., 2002). 1348 1349 After the confirmation of the involvement of TLR4 in the LPS activation signalling 1350 pathway, the same signalling in pulmonary epithelial cells was investigated by Guillott 1351 and colleagues (Guillott et al., 2004). They demonstrated: i) the expression of TLR4 and 1352 MD-2 in respiratory epithelial cells; ii) the intracellular presence of TLR4; iii) the 1353 signalling of LPS in epithelial cells shares some elements with the activation of myeloid 1354 cells such as MyD88, IRAK, TRAF6 and MAPK. They demonstrated the expression of 1355 TLR4 in human alveolar and bronchial epithelial cells and its intracellular localization of 1356 this receptor; in addition, they confirmed that the activation pathway of LPS involves and is dependent on the TLR4 signalling (Guillott et al., 2004). 1357 1358 Therefore, current understanding of the activation pathway for LPS in airway epithelial 1359 cells implicates the activation of a complex association of receptors composed by TLR4, 1360 MD-2 and CD14 in the case of mononuclear phagocytes. 1361 1362 Besides the LPS inflammation model, another common model for COPD is based on the 1363 exposure to cigarette smoke extract (CSE) (Krimmer & Oliver, 2011). The inflammation 1364 may differ depending on the number of cigarettes burned - if commercially available or 1365 research grade – or by the presence or the absence of filter. As for the LPS, CSE can 1366 modulate the release of cytokines and chemokines from the lungs and immune cells. 1367 Moreover, as viral infection is an important feature of COPD that can result in

exacerbations, the combination of CSE and rhinovirus has also been modelled in vitro in

1370 Hudy & Proud, 2013). 1371 1372 In the inflammation model designed and adopted in this chapter, the level of specific 1373 extracellular signalling proteins (IL-8, interleukin- 6 (IL-6) and TNF- α) secreted by 1374 bronchial epithelial cells was chosen as a measure of inflammation. In inflammatory lung 1375 diseases, cytokines play a key role sustaining the inflammation and recruiting further cells 1376 into the lungs, orchestrating the chronic inflammation (Chung, 2001). The pivotal role of 1377 cytokines in the pathophysiology of COPD is supported by their increased level found in 1378 the induced sputum of patients, plasma or exhaled breath. More than 50 cytokines have 1379 now been identified to be involved in the molecular pathology of diseases such as COPD. 1380 Clinical studies have demonstrated that TNF- α (Aaron et al., 2001; Keatings et al., 1996), 1381 IL-6(Bhowmik et al., 2000; Bucchioni et al., 2003) and IL-8(Aaron et al., 2001; Barnes, 1382 2008; Barnes et al., 2015; Fischer et al., 2011; Keatings et al., 1996) can be found in the 1383 induced sputum of COPD patients. 1384 According to the literature, TNF- α and IL-6 are also good biomarkers of systemic 1385 inflammation in COPD patients (Karadag et al., 2008). The serum level of those markers 1386 has been reported to be higher in both COPD patients with a stable condition or with 1387 exacerbations phases than in healthy controls, supporting their use as biomarkers of 1388 systemic inflammation in COPD patients. Increased levels of TNF- α , IL-8 and IL-6 were 1389 also reported in bronchioalveolar lavage fluid from 14 healthy smokers compared with 1390 16 healthy non-smokers (Kuschner et al., 1996) 1391 Overall, the role that IL-8, IL-6 and TNF- α play in COPD further corroborate the choice 1392 of using the above-mentioned cytokines as representative COPD markers in the in vitro 1393 model of lung inflammation disease designed and optimised in this experimental chapter. 1394 1395 The level of cytokines released by LPS-stimulated BEAS-2B has been reported to vary 1396 in presence or absence of serum. Indeed, multiple cell culture conditions are used in the 1397 literature with a consequent lack of consistency within studies. According to the literature, 1398 cell culture conditions for BEAS-2B include the use of i) serum free bronchial epithelial 1399 cell growth medium (X. Wang et al., 2012) or Dulbecco's Modified Eagle Medium 1400 supplemented with 10% fetal bovine serum (FBS). The latter was used to study heavy 1401 metals induced carcinogenesis (Laulicht et al., 2015; Park et al., 2015), to investigate the 1402 relations between chronic arsenic exposure, reactive oxidative species production and cell

BEAS-2B with a consequent upregulation of interleukin- 8 (IL-8) (Hudy et al., 2010;

- transformation (Carpenter et al., 2011; Chang et al., 2010) or to investigate the protective
- effect of angiotensin converting enzyme 2 against LPS-induced injury in mice (Ye & Liu,
- 1405 2020).
- 1406 Indeed, the exposure of BEAS-2B to serum can alter the response to toxic agents and the
- 1407 cytokine secretion. It is also associated with the cell squamous differentiation.
- 1408 The design of the *in vitro* model described in this chapter also focussed on the relationship
- between increasing concentration of serum in the culture medium and concentration of
- 1410 cytokine secreted. This hypothesis was further corroborated by a study carried out by
- 1411 Veranth (Veranth et al., 2008). The hypothesis that the secretion of IL-6 from BEAS-2B
- can vary based on the cell model used was tested. Three different culturing media were
- 1413 tested: Lechner and Laveck medium (LHC-9), KGM and LHC-9 with FBS. Results
- showed how the IL-6 secretion can be titrated by increasing amount of serum added to
- 1415 KGM media in absence of particulate matter or in presence of soil dust treatment. The
- 1416 evidence that BEAS-2B used in airways models can be successfully cultured using
- 1417 different conditions, led us to preliminary need of studying the effect of different
- percentages of serum on the cytokine production.

1419

4.2 Aims and objectives

14201421

- 1422 The overall aim of this series of experiments was to build an *in vitro* inflammation model
- in bronchial epithelial cells (BEAS-2B) to enable investigation of the anti-inflammatory
- 1424 activity of RFM. LPS-induced inflammation was chosen for this work to enable
- progression of the research into animal models that are based on the same inducer of
- inflammation.

- 1428 Specific objectives included:
- 1. Optimise BEAS-2B culture conditions, including the amount of FBS used in the growth medium;
- 2. Optimise the LPS concentration and exposure time that result in a sustained and detectable secretion of cytokines into the culture medium over time;
- 3. Investigate the anti-inflammatory activity of RFM applied in a pre-treatment protocol for 1.5 h, 3 h or 24 h.
- 1435 4.

1436 **4.3 Methods**

substrate.

1437

1438 **4.3.1** Cell culture conditions

1439

Bronchial epithelial cells (BEAS-2B) were grown at 37°C with 5% CO₂ in 75 cm² Falcon tissue culture flasks in culture medium (RPMI 1X [+] glutamine, 10% fetal bovine serum and 1% penicillin/streptomycin) which was replaced with fresh medium every three days. Cells were passaged or seeded into 24-well plates when > 70% confluent by washing with Ca²⁺ and Mg²⁺ free PBS before using trypsin 0.25% to dissociate cells from their

14451446

1447

4.3.2 Experimental design

1448

On day 0, cells were seeded in 24-well plate (Greiner CELLSTAR®) in growth medium 1449 1450 (0.5 mL) and allowed to adhere to the base of the well overnight; medium was replaced 1451 on day 1 and, unless stated otherwise, treatment started on day 2. After each specific 1452 treatment, cell supernatant from each well was withdrawn and immediately centrifuged 1453 at 1,000 g x 5 min at 4°C to eliminate any cell debris. Supernatants were aliquoted and 1454 stored at - 80°C for assay of IL-8, IL-6, or TNF-α level using commercial sandwich 1455 enzyme-linked immunosorbent assay (ELISA) kits (DuoSet, R&D, Biotechne, 1456 Minneapolis). Every experiment was performed with three replicate wells for each 1457 experimental variable, with the experiment being repeated in duplicate or triplicate. Cells 1458 used for those experiments were between passages 29 and 43. The optimal seeding 1459 density (day 0) to obtain a confluent monolayer of cells on day 2 was investigated and 1460 found to be 2.5 x 10⁵ cells/well (data not shown) which was then used as seeding density 1461 for every experiment mentioned in this chapter.

14621463

4.3.3 Effect of fetal bovine serum concentration on cytokine release

- 1465 Cells were seeded in 24-well plate at 2.5 x 10⁵ cells/well in growth medium (day 0).

 1466 Medium was replaced with fresh containing a combination of either 2 or 10% FBS on

 1467 day 1 and day 2. After 72 h in the medium (day 3 in total), cell supernatants were
- 1468 withdrawn and processed as described above (Figure 4.1). The impact of different

1469 concentration of FBS on the levels of IL-6, IL-8 and TNF- α release was measured using a commercial sandwich ELISA kit.

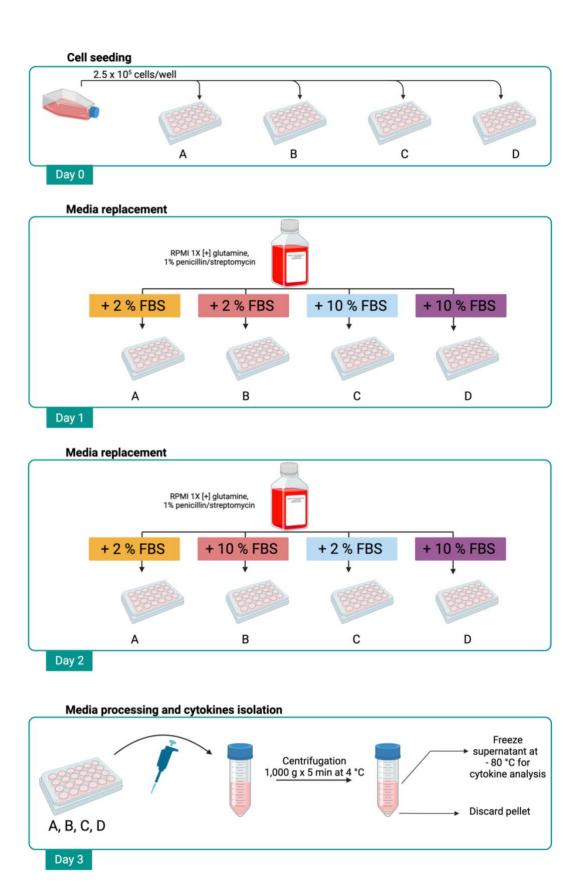


Figure 4.1 Schematic representation of the experimental design adopted in the evaluation of the effect of serum on cytokine secretion.

| 1473 | 4.3.4 Optimisation of LPS- induced inflammation model |
|------|--|
| 1474 | |
| 1475 | The LPS inflammation model was optimised in terms of LPS concentration, LPS |
| 1476 | exposure time and concentration of FBS in culture medium. Based on preliminary results, |
| 1477 | experiments to evaluate the most suitable concentration and exposure time were |
| 1478 | performed using 10% FBS in the culture medium throughout. |
| 1479 | On day 0, cells were seeded in culture medium, which was replaced with fresh medium |
| 1480 | on day 1. On day 2, an aliquot of the LPS (O111:B4) stock solution (5 mg/mL) previously |
| 1481 | prepared was thawed and serial dilutions performed in RPMI 1X [+] glutamine, 10% FBS |
| 1482 | and 1% penicillin/streptomycin to produce concentrations of 10, 100, 200, 300, 500, 800, |
| 1483 | 1000 ng/mL. Cells were exposed and incubated with LPS or cell medium (0.5 mL) |
| 1484 | (negative control) at 37°C. Following 24 h incubation, the medium was withdrawn and |
| 1485 | processed for assay for cytokine detection as described in paragraph 4.3.2. |
| 1486 | |
| 1487 | The impact of different concentrations of FBS in the cell medium on day 1 and day 2 was |
| 1488 | investigated when cells were exposed to LPS. On day 0, cells were seeded in growth |
| 1489 | medium. Medium was replaced on day 1 and on day 2 cells were exposed to 800 ng/mL |
| 1490 | and $1000 \text{ ng/mL} \ (0.5 \text{ mL})$ of LPS in medium with different percentages of FBS (Figure |
| 1491 | 4.1). Following 24 h incubation, culture medium was withdrawn and processed as |
| 1492 | described in paragraph 4.3.2. |
| 1493 | |
| 1494 | The effect of LPS incubation time on the IL-6 levels released by BEAS-2B cells was |
| 1495 | investigated. Cells were seeded on day 0, and medium replaced on day 1. On day 2, cells |
| 1496 | were incubated with 800ng/mL (0.5 mL) of LPS for 2, 4, 6, 15, 24 and 48 h. A percentage |
| 1497 | of 10% of FBS was used in the medium on both days 1 and 2. Control cells were incubated |
| 1498 | with growth medium only. Following LPS exposure, medium was withdrawn and |
| 1499 | processed as described in paragraph 4.3.2. |
| 1500 | |
| 1501 | 4.3.5 Exposure of LPS-exposed BEAS-2B cells to roflumilast |
| 1502 | |
| 1503 | The anti-inflammatory activity of RFM in the BEAS-2B cell inflammatory model was |
| 1504 | investigated using a protocol designed to test a preventative effect whereby cells were |
| 1505 | exposed to the drug for different period of time before LPS was applied for 24 h. |
| 1506 | Dexamethasone pre-treatment was used as positive control to confirm the ability of the |

1507 model to report anti-inflammatory activity. The concentration of LPS used in these drug 1508 treatment experiments was 800 ng/mL. To ensure that each well had the same total cell 1509 number, a 'modified protocol' was adopted for the drug exposure of 1.5 - 2 or 3 h (**Figure** 1510 4.2). 1511 1512 For RFM and dexamethasone pre-treatment of 24 hours, cells were seeded on day 0 in 1513 24-well plate and cells fed with fresh medium on day 1. On day 2, cells were exposed to 1514 the drug dissolved in the culture medium. After 24 h (i.e on day 3 in total) conditioned 1515 medium was withdrawn and discarded, and cells exposed to LPS for 24 h. On day 4 the 1516 experiment was terminated, and samples processed as described in section 4.3.2. For 1517 RFM and dexamethasone pre-treatment of 1.5, 2 or 3 h, the protocol was adapted, and the 1518 drug exposure started on day 3 rather than on day 2. After the allocated exposure time, 1519 culture medium was withdrawn, and cells were exposed to LPS. On day 4 the experiment 1520 was terminated, and samples processed as described in section 4.3.2. 1521 1522 RFM stock solution (0.01 M) in DMSO (100% v/v) was prepared and aliquots frozen. On 1523 the day of the experiment, an aliquot was thawed and serial dilutions in growth medium 1524 were performed to produce concentration of 0.001, 0.1, 1.0, 100, 1,000 and 10,000 nM. 1525 The percentage of DMSO in each sample was calculated to be < 0.1%. Controls samples 1526 were represented by control cells exposed to drug- and LPS-free culture medium 1527 (negative control) or cells exposed to drug-free culture medium containing 0.1% DMSO, 1528 then exposed to LPS (positive control). 1529 1530 A stock solution of dexamethasone (21,600 µg/mL) was prepared in DMSO (100% v/v) 1531 and aliquots stored at -80 C°. On day of the experiment serial dilutions were performed 1532 to produce dexamethasone concentrations of 0.1, 1.0, 10, 100 µg/mL in culture medium. 1533 The percentage of DMSO in each sample was calculated to be < 0.5%. Controls samples 1534 were cells exposed to drug- and LPS-free culture medium cells exposed to growth culture 1535 medium containing 0.5% DMSO, then exposed to LPS (positive control). 1536 1537 RFM and dexamethasone pre-treatments were evaluated by incubating the cells with the 1538 drug at the chosen concentrations for 1.5 h, 3 h and 24 h for RFM and 2 h and 24 h for 1539 dexamethasone. 1540

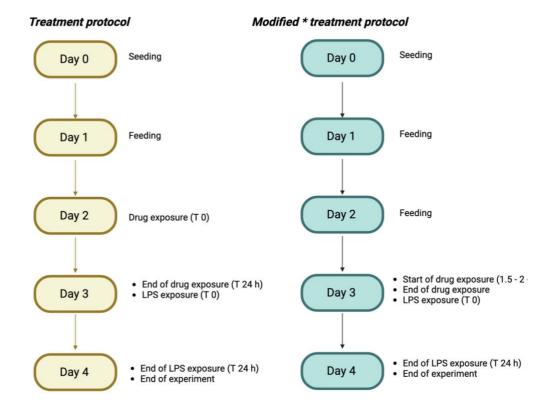


Figure 4.2 Schematic representation of 'treatment protocol' and 'modified treatment protocol' adopted.

4.3.6 Statistical analysis

Data were expressed as mean \pm SD. Where appropriate, data were analysed using GraphPad Prism version 9, (GraphPad Software, San Diego, USA). Normal distribution of data was firstly evaluated and the statistical significance between groups was determined using parametric tests. Statistical significance was evaluated with unpaired test within two conditions, ordinary one-way or two-way ANOVA multiple comparisons. Statistically significant differences are represented by asterisks as follow: *, p \leq 0.05; **,

 $p \le 0.01$; ***, $p \le 0.001$. Where stated that a statistical analysis was performed, absence

of asterisks indicates non-statistically significant results.

4.4 Results

15561557

1558

1559

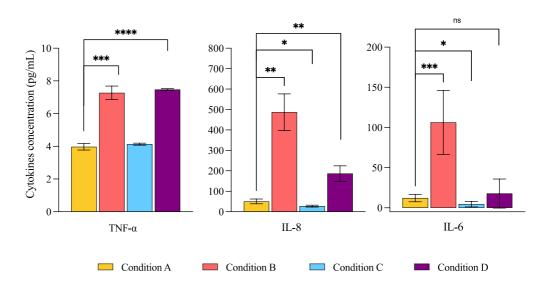
4.4.1 Effect of fetal bovine serum concentration on IL-8 and IL-6 basal release from BEAS-2B cells

1560

1561 The incubation of BEAS-2B cells with different concentration of serum (2% or 10%) on 1562 day 1 and 2 after seeding resulted in a basal production of cytokines. The basal release of 1563 TNF- α , IL-6 and IL-8 varied according to the concentration of FBS and the duration of 1564 exposure (Figure 4.3). Overall, there was a consistent trend for the cytokine 1565 concentrations released in response to different FBS exposure across the three cytokines 1566 evaluated, although the levels of TNF- α detected were considerably lower (between 3.9 1567 and 7.47 pg/mL) compared to IL-8 and IL-6 (<u>IL-8</u>: A) 50.4 pg/mL; B) 486.9 pg/mL; C) 1568 27.7 pg/mL; D) 186.7 pg/mL. IL-6: A) 12.2 pg/mL; B) 106.3 pg/mL; C) 4.6 pg/mL; D) 17.8 pg/mL) (Figure 4.3 a). For both IL-8 and IL-6, the exposure to low (2%) and high 1569 1570 (10%) percentages of serum on day 1 and day 2 respectively resulted overall in the highest 1571 concentration of secreted cytokines. Lower than the latter but still elevated concentration 1572 of cytokines were released when the cells were fed with the highest concentration of 1573 serum on both days. In contrast, the exposure to 10% and 2% on day 1 and 2 respectively 1574 resulted in the lowest level of cytokines released by the BEAS-2B cells. Results showed 1575 that the concentration of TNF- α and IL-8 – but not IL-6 - released in presence of high 1576 percentage of serum on day 1 and day 2 were higher and significantly different compared 1577 to those released by cells exposed to the lowest percentage of serum on day 1 and 2. In 1578 addition, results showed that if cells were exposed to 2% on day 1, the further exposure 1579 on day 2 to 10% of serum significantly 'boosted' the sensitivity of the cells inducing an 1580 increased level of cytokine released compared to cells exposed to 2 % on day 2. 1581 Among the four culturing conditions tested, the addition of 10% of serum to the growth 1582 medium both on day 1 and day 2 was considered the most appropriate and adopted for 1583 the drug treatment exposure experiment. Indeed, when using the optimised seeding 1584 density, those percentages of serum can stimulate the cells to secrete cytokine 1585 concentrations adequate to be efficiently detectable using commercial ELISA kits and 1586 low enough to work as control (no treatment) in the drug treatment protocol.

1587

a.



b.

| | % of serum added to growth media | | | | | |
|---------------|---|------|-----|------|--|--|
| | Condition A Condition B Condition C Condition D | | | | | |
| Feeding Day 1 | 2 % | 2 % | 10% | 10 % | | |
| Feeding Day 2 | 2 % | 10 % | 2 % | 10 % | | |

Figure 4.3 (a) Effect of fetal bovine serum (2% or 10%) in cell culture medium on secretion level of TNF- α , IL-8 and IL-6. (b) The different regimes for exposing cells to fetal bovine serum. Cells (BEAS-2B) were seeded in 24-well plate on day 0 in growth medium (0.5 mL). On day 1 and 2, cell medium was replaced with fresh medium containing either 2% or 10% of FBS. Twenty-four hours later, conditioned medium was withdrawn, and levels of cytokine detected with commercial sandwich ELISA kit. Statistical significance was evaluated with student t-test. Data represent mean \pm SD of one (TNF- α) or two (IL-8 and IL-6) independent experiments (for each experiment, each sample was in triplicate (three wells)).

4.4.2 Effect of LPS on IL-8 and IL-6 production in BEAS-2B

A positive LPS dose-response relationship for IL-8 and IL-6 in BEAS-2B cells was observed (**Figure** 4.4). The exposure of BEAS-2B cells to increasing concentrations (10 – 1000 ng/mL) of LPS induced an increased secretion of both cytokines compared to control. The exposure to the lowest LPS concentration (10 ng/mL) already induced a

significant increase of IL-8 and IL-6 compared to control as well as when cells were exposed to 800 and 1000 ng/mL. Higher variability in the IL-6 response to LPS was observed at the concentration range tested. In both cases, the highest concentrations of LPS used (800 and 1000 ng/mL) resulted in a robust response from BEAS-2B cells.

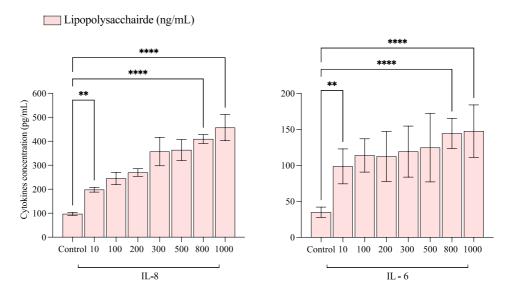
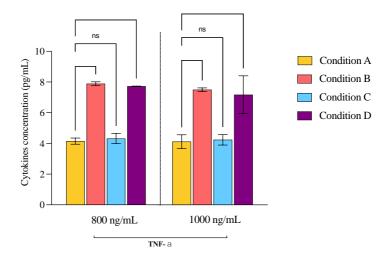


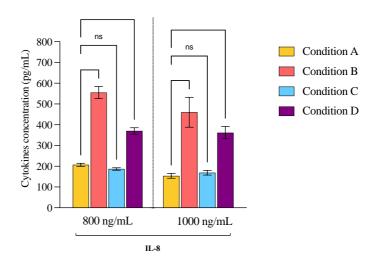
Figure 4.4 Effect of lipopolysaccharide exposure (24 h) on IL-8 and IL-6 production in BEAS-2B. Cells were grown in culture medium for 2 days then exposed to culture medium (control) or LPS (10, 100, 200, 300, 500, 800, 1000 ng/mL) for 24 h. After LPS exposure, medium was withdrawn and assayed for cytokine concentration. Statistical significance was evaluated with ordinary one-way ANOVA multiple comparisons. Data represent mean \pm SD of one (IL-8) or two (IL-6) independent experiments, using one or two different passage number (for each experiment, each sample was in triplicate (three wells)).

Following the dose-response study, 800 and 1000 ng/mL LPS were selected for further investigation. The correlation between LPS doses and serum percentages on day 1 and on day 2 was evaluated measuring the concentration of IL-8 and TNF- α released by the cells (**Figure** 4.5). The exposure to 800 and 1000 ng/mL for 24 h using different concentrations of FBS resulted in the same trend showed in Figure 4.3 (a). The highest level of TNF- α and IL-8 was detected when cells were exposed to any of the percentages investigated on day 1 (2 or 10%), but to 10% on day 2. The levels of TNF- α detected were considerably lower compared to IL-8 concentrations, with values between 4.12 and 8.0 pg/mL, while IL-8 concentrations (day 1: 10% FBS, day 2: 10% FBS) were in agreement with those obtained in the LPS dose-response (Figure 4.4). Overall, for both IL-8 and TNF- α the

1619 concentration of cytokines released by the cells was similar, regardless of the 1620 concentration of LPS used to stimulate the cells. 1621 A multiple comparison was carried out to investigate if the exposure of BEAS-2B to 1622 percentages of serum different from 2% on both days resulted in significant differences. 1623 For both IL-8 and TNF- α the increase of serum only on day 2 resulted in significant 1624 difference compared to the use of low percentage of serum on both days and vice versa. 1625 Significantly different was also the concentration of cytokines (IL-8 and TNF- α) released 1626 when BEAS-2B were exposed to 10% of FBS on both days compared to 2% of FBS on 1627 both days. In contrast, the increase of FBS percentages on day 2 if on day 1 cells were 1628 exposed to 2% of FBS resulted in not significant differences of cytokines concentrations. 1629 The concentration of 800 ng/mL was considered adequate to sufficiently stimulate the 1630 secretion of the cytokines of interest from BEAS-2B. It was therefore selected as the LPS 1631 dose to be used in the treatment schemes which results are described in paragraphs 4.4.3 1632 and 0.

a.





b.

| | % of serum added to growth media | | | | | | |
|---------------|---|------|-----|------|--|--|--|
| | Condition A Condition B Condition C Condition D | | | | | | |
| Feeding Day 1 | 2 % | 2 % | 10% | 10 % | | | |
| Feeding Day 2 | 2 % | 10 % | 2 % | 10 % | | | |

Figure 4.5 (a) Effect of lipopolysaccharide (800 and 1000 ng/mL) on TNF- α and IL-8 production in BEAS-2B when cells are incubated with different percentages of fetal bovine serum (2 % or 10%) on day 1 and 2. (b) The different regimes for exposing cells to fetal bovine serum. Statistical significance was evaluated with ordinary one-way

ANOVA multiple comparisons. Data represents mean \pm SD of one independent experiment (one passage number) (each sample in triplicate (three wells).

To optimise the inflammation model, the effect of the duration of LPS exposure was also investigated. The time-dependency of the release of IL-6 induced by LPS (800 ng/mL) was determined. A robust time-dependent relationship was observed between IL-6 secretion and duration of LPS exposure (**Figure** 4.6). The difference between IL-6 concentration in control samples and LPS-challenged samples was significantly different for each time point considered, except for the 2 h exposure (control 27.8 pg/mL vs LPS 193.4 pg/mL, control 31.9 pg/mL vs LPS 349.9 pg/mL at 24 h and 48 h time points, respectively). The concentration of IL-6 detected in the cell supernatant increased from 2 h to 48 h with values of 15.9 pg/mL at 2 h to 349.9 pg/mL at 48 h. According to these results, 24 h was selected as LPS exposure time due to its suitability to induce a robust release of cytokine which modulation by anti-inflammatory drugs will be described in the next paragraph.



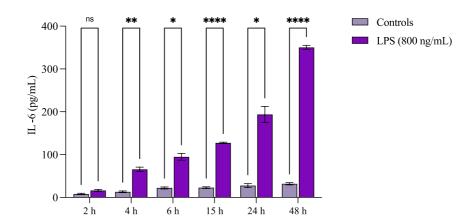


Figure 4.6 Effect of different exposure times to lipopolysaccharide (800 ng/mL) on IL-6 production from BEAS-2B cells. Cells were seeded on day 0 in culture medium which was replaced with fresh medium on day 1; on day 2 cells were exposed to LPS (800 ng/mL) or culture medium (control) for the allocated exposure times. Statistical significance was evaluated with two-way ANOVA multiple comparisons. Data represent mean \pm SD of one independent experiment, with measurements in triplicate (three wells).

| 1655 | 2B model |
|------|--|
| 1656 | |
| 1657 | The exposure of BEAS-2B to a pre-treatment of dexamethasone for 2 or 24 h followed |
| 1658 | by LPS stimulation resulted in the reduction of the IL-6 levels compared to non-drug |
| 1659 | treated control (Figure 4.7). For the 2 h pre-treatment, the dose-response relationship is |
| 1660 | less evident with values of 117.5 pg/mL, 73.5 pg/mL, 54.3 pg/mL and 53.0 pg/mL for |
| 1661 | $0.1,1.0,10$ and $100\mu\text{g/mL}$, respectively. Interestingly, dexamethasone was less effective |
| 1662 | in reducing IL-6 secretion when the cells were pre-exposed for 24 h to the same range of |
| 1663 | concentrations, requiring higher concentrations to achieve the same suppression of IL-6 |
| 1664 | levels seen at 2 h. i.e. after cells were exposed to 1.0, 10 and 100 μ g/mL (positive control: |
| 1665 | 311.8 pg/mL; 1.0 µg/mL: 173.3 pg/mL; 10 µg/mL: 130.4 pg/mL; 100 µg/mL: 61.6 |
| 1666 | pg/mL). |
| 1667 | For both the pre-treatment regimes, the concentration of IL-6 released from cells exposed |
| 1668 | to LPS (800 ng/mL) was significant different compared to control (growth media only). |
| 1669 | The exposure to each dexamethasone concentrations significantly reduced the IL-6 levels |
| 1670 | compared to positive control when cells were exposed to the 2 h pre-treatment, whereas |
| 1671 | the treatment with $0.1~\mu g/mL$ for 24 h did not significantly reduce the IL-6 levels |
| 1672 | compared to positive control. |

4.4.3 Anti-inflammatory activity of dexamethasone in an LPS-challenged BEAS-

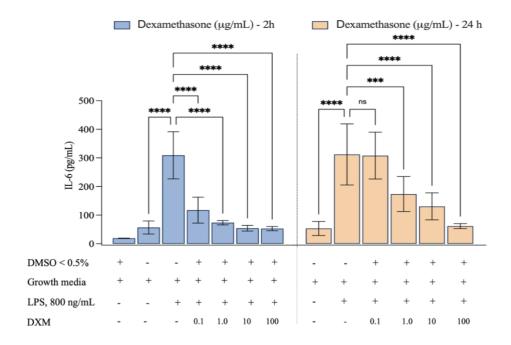


Figure 4.7 Effect of dexamethasone pre-treatment on IL-6 production from LPS-challenged BEAS-2B cells. For the 2 h pre-treatment, cells were seeded on day 0 and medium changed on day 1 and 2. On day 3, cells were exposed to dexamethasone following by exposure to LPS (24 h); for the 24 h pre-treatment, cells were seeded on day 0 and medium changed on day 1. On day 2, cells were exposed to dexamethasone (24 h). On day 3, supernatant was withdrawn, and cells stimulated with LPS (24 h). Statistical significance was evaluated with one-way ANOVA multiple comparisons. Data represent mean ± SD of three independent experiments (using three different passage number) (with measurements in triplicate (three wells)).

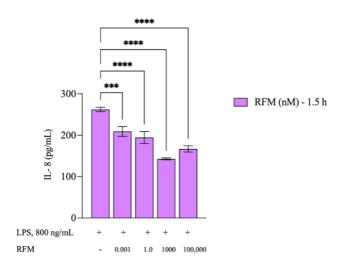
4.4.4 Investigating the anti-inflammatory activity of roflumilast pre-treatment in an LPS-challenged BEAS-2B model

The effect of the PDE-4 inhibitor RFM on the LPS-induced release of IL-8 and IL-6 from BEAS-2B was investigated (**Figure** 4.8 and **Figure** 4.9). LPS strongly stimulated the release of IL-8 which was partially and weakly reduced by RFM. The pre-treatment of RFM for 1.5 h at doses of 0.001 – 1 and 10,000 nM significantly reduced the levels of IL-8 compared to control. In terms of percentage, the reduction was equal to 20%, 25%, 45% and 36% respectively compared to LPS alone (Figure 4.8). However, IL-6 levels were not reduced by any of the concentration of RFM tested, over any of the exposure

times explored (1.5, 3 or 24 h). Interestingly, higher concentrations of IL-6 over control samples were recovered in the supernatant after pre-treatment with 1000 and 10,000 nM (Figure 4.9). A hypothesis is that the 'over release' reported in presence of 1000 and 10,000 nM of RFM may have caused a toxic effect in BEAS-2B as those concentrations were considerably higher than the clinically-relevant plasma concentration of RFM (1 – 2 nM). The latter (free, not bound to plasma proteins) was calculated in a clinical study based on the oral administration of RFM at the clinical dose of 500 μ g/mL daily (Bethke et al., 2007). Levels of TNF- α detected after different pre-treatment exposure time regimens (1.5, 3

and 24 h) with RFM were lower than the lowest point of the recommended standard curve (< 15.6 pg/mL) (data not shown).

a.



b.

| I411 0 | | | | | |
|----------------------------|-------------------|----------------|----------------|-------------------|---------------|
| Interleukin-8 | 0 | 0.001 nM | 1 nM | 1000 nM | 100,000 nM |
| Concentration (pg/mL) | 262.07 ± 5.30 | 208.77 ± 11.75 | 194.42 ± 14.56 | 142.70 ± 2.43 | 166.94 ± 7.54 |
| Reduction from control (%) | - | 20 % | 25 % | 45 % | 36 % |

Figure 4.8 IL-8 level released by LPS-stimulated BEAS-2B cells in presence or absence of roflumilast treatment. BEAS-2B were pre-treated with growth media (vehicle) or roflumilast (RFM) (0.001, 1, 1000, 10,000 nM) for 1.5 h before being stimulated with LPS (800 ng/mL) for 24 h. Statistical significance was evaluated with one-way ANOVA

multiple comparisons. Data represents mean \pm SD of n=1 independent experiment, with measurements in triplicate (three wells). The results are also expressed as the percentage inhibition vs vehicle (LPS alone).

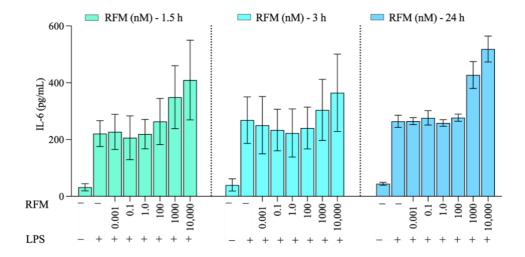


Figure 4.9 Effect of roflumilast pre-treatment (1.5 - 3 - 24 h) on IL-6 production from LPS-challenged BEAS-2B. For the 1.5 and 3 h pre-treatment, cells were seeded on day 0 and media changed on day 1 and 2. On day 3, cells were exposed to dexamethasone following by exposure to LPS (24 h); for the 24 h pre-treatment, cells were seeded on day 0 and media changed on day. On day 2, cells were exposed to dexamethasone (24 h). On day 3, supernatant was withdrawn, and cells stimulated with LPS (24 h). Data represents mean ±SD of one independent (24 h exposure) or two (1.5 and 3 h exposure) independent experiments, using one or two distinct passage number. For every experiment, each measurement was in triplicate (three wells).

4.5 Discussion

In this work, BEAS-2B cells were used to form an *in vitro* model of inflammation in which to investigate the ability of RFM to reducing the levels of IL-8 and IL-6 secretion which were chosen as inflammatory biomarkers. In the context of BEAS-2B cell culturing conditions, it was first necessary to consider the impact that FBS has on the BEAS-2B cell phenotype, as well as on the response to agents such as LPS. The suitability of BEAS-2B cells as experimental model of arsenic toxicity was assessed by Zhao and others (Zhao & Klimecki, 2015). They showed that FBS changes the cell phenotype with consequences such as an increase in the total glycolytic capacity of the cells, increase in the basal

1715 respiration and in the oxygen consumed for ATP production. Earlier studies (Ke' et al., 1716 1988) highlighted how BEAS-2B cells undergo squamous differentiation in presence of 1717 serum which results in cell senescence and loss of immortality, whereas more recent 1718 studies further investigated the cellular and molecular biological changes that take place 1719 in presence of serum. 1720 A change in the phenotype of the cells when exposed to FBS was also reported by Malm and co-workers (Malm et al., 2018). In this case, a mechanism called epithelial-1721 1722 mesenchymal transition was described. They demonstrated that the exposure of BEAS-1723 2B cells to serum induces the loss of specific markers of epithelial identity and the gain 1724 of markers of mesenchymal cell identity. This process is reversible if serum is removed. 1725 This finding was partially supported by others (Han et al., 2020). They also showed that 1726 BEAS-2B cells shared the expression profile of surface markers with mesenchymal cells, 1727 exhibited osteogenic and adipogenic differential potential, but it was unclear for them 1728 whether those properties were the result of epithelial-mesenchymal transition induced by

transforming growth factor- β 1, which is abundant in serum.

1730

1731

1732

1733

1734

1735

1736

1737

1738

1739

1740

1741

1742

1743

1744

1745

1746

1747

1729

Despite these studies raised concerns about the suitability of BEAS-2B cells as an in vitro epithelial model, many researchers are still using these cells with the addition of serum to the growth medium to model the airway epithelium successfully. Studies have showed that BEAS-2B cells can be cultured with Dulbecco's Modified Eagle Medium supplemented with 10% FBS to study heavy metals induced carcinogenesis (Laulicht et al., 2015; Park et al., 2015), to investigate the relations between chronic arsenic exposure, reactive oxidative species production and cell transformation (Carpenter et al., 2011; Chang et al., 2010) or to investigate the protective effect of angiotensin converting enzyme 2 against LPS-induced injury in mice (Ye & Liu, 2020). The use of RPMI 1640 in presence of serum is also widely reported and multiple studies have adopted these cells and these culturing conditions to model the airway epithelium. In a study (Schulz et al., 2002), BEAS-2B were used as epithelial cells to investigate the molecular pathway induced by the LPS stimulation, using experimental conditions in agreement to the one adopted in this experimental chapter. Same culturing conditions were also adopted in two other studies (M. Wang et al., 2019; Y. Wang et al., 2015) which described the role of two transient receptor potential protein ion channels in mediating airway tissue injury and inflammation besides the expression profile and function of miRNAs in acute lung injury.

1748 They concluded that miR-18b may be involved in the process of LPS-induced

inflammation in BEAS-2B.

1750 In this experimental study, specific investigation of any serum induced epithelial

1751 mesenchymal transition or expression of mesenchymal features was not carried out as

this was not the aim of the study. However, the experimental study was conducted based

on the assumption that the cells maintain an epithelial phenotype throughout the whole

experimental window. Indeed, the culturing conditions (growth medium and addition of

serum) used in this experimental study were in agreement and similar to those reported

by others (Schulz et al., 2002; M. Wang et al., 2019; Y. Wang et al., 2015) which

1757 successfully designed airway models.

1758

1762

1754

1755

1756

1759 The percentages of serum at which the cells have been exposed on day 1 and 2 after

seeding impacted the basal level of IL-6 and IL-8. A basal level of cytokine released by

BEAS-2B has been also reported by others (Schulz et al., 2002) who have shown that

despite the basal cytokine expression being low, it can be increased by approximately 10-

fold in presence of serum. The addition of 10% of serum on day 1 and on day 2 of the

culturing protocol was chosen as the final experimental condition because it resulted in a

low basal level of cytokines on day 2 and enabled growth of cells to approach confluency

on the day that drug treatment was applied.

1767 The effect of the exposure of LPS on BEAS-2B in presence of different percentages of

serum was also investigated. The presence of LPS, amplificated the response of BEAS-

2B cells with a 'serum concentration – dependency' comparable to that reported for the

basal level of cytokine release. It is known that LPS sensitizes BEAS-2B cells via a

1771 complex pathway of molecular mechanisms. Schultz and colleagues (Schulz et al., 2002)

investigated the effect of LPS exposure (10 µg/mL) on BEAS-2B cells in presence of

different concentrations of serum (2, 5 or 10%), describing the component of serum

1774 responsible for the sensitization of BEAS-2B cells to LPS. They found that the addition

of soluble CD14 alone to BEAS-2B did not alter the production of IL-8 and IL-6, whereas

the addition of sCD14 in presence of LPS resulted in increased levels in a concentration

1777 dependent manner.

1778

1779 The LPS- stimulation of BEAS-2B resulted in dose and time-dependent release of IL-6

and IL-8. The LPS-challenge of BEAS-2B cells for 24 h with increasing concentrations

of LPS resulted in dose-dependent increased levels of IL-8. The exposure to a constant

1782 concentration for different exposure times resulted in time-dependent increased of IL-6 1783 levels compared to control sample. These findings are in agreement with those of Guillott 1784 and colleagues (Guillott et al., 2004) which showed that the exposure to LPS and in 1785 presence of serum strongly stimulates the release of IL-8 and IL-6 from BEAS-2B cells 1786 in a concentration-dependent manner. Although, the magnitude of the cytokine release 1787 was not comparable. In Guillot's study the stimulation of BEAS-2B for 24 with 100 1788 ng/mL and 1000 ng/mL of LPS resulted in ~ 400 pg/mL and 800 pg/mL respectively for IL-8 and ~ 300 pg/mL and 900 pg/mL respectively for IL-6; whereas in this experimental 1789 1790 chapter the stimulation of BEAS-2B with the same conditions (LPS, length of exposure) 1791 induced the release of 245.3 pg/mL and 457.2 pg/mL for IL-8 and 113.8 pg/mL and 147.5 1792 pg/mL for IL-6. 1793

Reasons for this discrepancy and the lower magnitude reported in this experimental chapter may be related to the different number of cells used in the experiments and the different serotype of LPS (*P. Aeruginosa*) which may have resulted in different responses (Guillott et al., 2004).

1797

1794

1795

1796

1798 The use of LPS-challenged BEAS-2B cells to model a wide range of inflammatory-based 1799 lung conditions induced by diseases or exposure to environmental toxin or smoke has 1800 been reported previously in the literature (L. Chen et al., 2021; Fuentes-Mattei et al., 1801 2010; H. H. Jang et al., 2016; Laan et al., 2004; Veranth et al., 2004, 2007). The main 1802 differences within these studies are related to the serotype of LPS used which may impact 1803 the concentration of cytokines detected, the concentration of LPS used and the length of 1804 exposure to LPS. Fuentes-Mattei and colleagues (Fuentes-Mattei et al., 2010) used an 1805 LPS-BEAS-2B model to investigate the immunological markers resulting from exposure 1806 to PM2.5 organic extract from Puerto Rico and found that the stimulation of BEAS-2B 1807 cells for 24 h with 10,000 ng/mL of an unspecified strain of LPS resulted in 942.8 (± 1808 10.9) pg/mL and 1274.1 (± 10.9) pg/mL of IL-6 and IL-8 respectively, whereas 1809 stimulation for 24 h with LPS from E. Coli 055:B5 (10 – 1,000 ng/mL) induced the 1810 secretion of IL-6 concentrations from 200 pg/mL to 550 pg/mL and IL-8 from 10,000 1811 pg/mL to 16,000 pg/mL (Schulz et al., 2002).

1812

Beside the use of LPS from *P. Aeruginosa*, many studies report the use of LPS from *Escherichia Coli*. LPS from *E. Coli* O55:B5 was also adopted by Jang and co-workers (B.-K. Jang et al., 2020). The stimulation of BEAS-2B cells for 48 h with 1,000 ng/mL

1816 of LPS resulted in increased levels of TNF-α, IL-8 and IL-6 compared to controls (13 1817 pg/mL, 180 pg/mL and 1600 pg/mL, respectively). A time-dependent increase of IL-8 1818 levels when BEAS-2B cells were exposed to LPS from E. Coli (1,000 ng/mL, O26:B6) 1819 for 2, 4, 6, 8 and 10 h was also reported by Laan and others (Laan et al., 2004) in a more 1820 complex experiment where LPS treatment was associated to CSE exposure in an 1821 inflammation model. 1822 1823 Increased levels of TNF- α and IL-6 were reported also when BEAS-2B cells were 1824 stimulated by LPS from E. Coli but of a different strain (O127:B8) (L. Chen et al., 2021). 1825 They reported the use of LPS at a concentration of 30,000 ng/mL for 24 h which is 1826 considerably higher compared to concentrations used by previously mentioned studies. 1827 Compared to control, the production of TNF- α by BEAS-2B was elevated from 96.7 to 1828 433.6 pg/ml by stimulation with LPS while the IL-6 concentration was reported to be 1829 136.7 and 678.3 pg/mL in absence and presence of LPS, respectively. 1830 1831 Additional uses of BEAS-2B cells to investigate airways diseases and pathological 1832 mechanisms of action are also reported in the literature, i.e. the effects of TNF- α and IL-1833 1β stimulation (Stecenko et al., 2001) or respiratory syncytial virus and adenovirus (Yoon 1834 et al., 2007). 1835 1836 The ability of the LPS model to respond to an anti-inflammatory intervention was 1837 successfully demonstrated with dexamethasone. Both regimens used (2 and 24 h pre-1838 treatment) reduced the elevated levels of IL-6 induced by LPS stimulation (800 ng/mL). 1839 The use of dexamethasone as positive control has been reported in other studies that have 1840 investigated the anti-inflammatory potential of new pharmaceutical entities. For example, 1841 the potential anti-inflammatory activity of Salvia plebeian R. Br extract was compared to 1842 dexamethasone activity (10 and 100 μ g/mL) in LPS and TNF- α stimulated BEAS-2B 1843 cells (H. H. Jang et al., 2016). The use of the glucocorticoid as positive control is also 1844 reported in a study that aimed to show the potential of cannabidiol in the regulation of 1845 basal and LPS-induced inflammation responses in macrophages, lung epithelial cells and 1846 fibroblast (Muthumalage & Rahman, 2019) and in an additional study where the potential 1847 anti-inflammatory activity of flavonoids in the airways was evaluated (P. Zhang et al., 1848 2019).

The anti-inflammatory activity of RFM in an airway model using LPS-stimulated BEAS-2B was investigated by studying the ability to suppress increased levels of IL-8 and IL-6 after LPS stimulation using the same protocol that was used with dexamethasone. The pre-treatment for 1.5 h with RFM resulted in a partial and weak reduction of IL-8 with the highest suppression mediated by 1000 nM. The weak suppression of IL-8 was also reported by Edwards and colleagues (M. R. Edwards et al., 2016), who stimulated BEAS-2B with rhinovirus and compared the potential anti-inflammatory activity of a new compound CHF6001 to that of RFM. The suppressive activity of the CHF6001 as a pre-treatment only in reducing the IL-8 levels was 48-fold higher compared to RFM and overall the new compound had the same level of efficacy of a combined RFM pre and post treatment. Furthermore, RFM tested in a concentration range between 0.001 and 1000 nM also exhibited suppressive activity against IL-29, IL-28, RANTES and IP-10 mRNA expression. (M. R. Edwards et al., 2016)

The results obtained in this research are partially in agreement also with a more recent study conducted by Salvator and colleagues (Salvator et al., 2020) who used a different airways model: bronchial explants resected from human lungs instead of bronchial epithelial cell line. Same serotype of LPS as well as similar range of concentrations of LPS were adopted (O111:B4, 1000 ng/mL) in both studies. In addition, RFM was used in a pre-treatment regimen of 1 h exposure to concentrations in the range 0.1 – 1000 nM followed by LPS stimulation for 24 h. Results showed that the LPS-induced release of IL-8 was reduced by 20% at a concentration of 1 nM and this well correlates with our findings (20% IL-8 reduction with 1 nM of RFM). On the other side, in contrast to our findings that described an absence of IL-6 reduction after RFM pre-treatment, Salvator demonstrated that the LPS-induced IL-6 level was reduced by 35 % at 100 nM.

of IL-8 may not be sensitive to cAMP modulators (Dent et al., 1998; Yoshimura et al., 1997). In addition, Buenestado (Buenestado et al., 2013) showed that the levels of chemokine involved in the recruitment of neutrophils such as IL-8 are not reduced by RFM in a human lung parenchymal explant model.

The weak or absent inhibition of LPS-induced IL-8 levels may suggest that the production

The RFM pre-treatment schemes did not suppress the increased levels of IL-6 induced by exposure to LPS. This result is in agreement with a study conducted by Lea and coworkers (Lea et al., 2019), which investigated the activity of RFM in alveolar

macrophages from COPD patients and in whole lung tissue explants (Lea et al., 2019). Macrophages and lung tissue from COPD patients and smoking controls were used in the method design. RFM (0.000001 – 10 nM) pre-treatment (1h) followed by LPS stimulation (1000 ng/mL for 24 h) produced a reduction of TNF- α levels in alveolar macrophages and lung tissue. However, levels of IL-8 and IL-6 in alveolar macrophages or lung explants were not reduced by RFM (1000 nM). Besides IL-6 and IL-8, other researchers have conducted studies on the TNF- α suppression mediated by RFM. It has been widely reported that RFM reduced the LPS-induced TNF- α levels in a concentration dependent-manner in BEAS-2B and in other cellular systems as well (Hatzelmann et al., 2010; Salvator et al., 2020). Buenestado and colleagues (Buenestado et al., 2013) showed that RFM inhibits in a concentration-dependent manner the increased release of TNF- α from lung macrophages isolated from resected human lungs and stimulated with LPS for 24 hours (Buenestado et al., 2012). However, in the airway model used in this thesis, TNF- α levels detected were always considerably low and often below the calibration range of the commercial ELISA kit used. For this reason, TNF- α was not utilised an endpoint in the treatment scheme, but only in the optimisation of the growing conditions and LPS concentration.

4.6 Conclusion

The human bronchial epithelial cell line model was established to investigate whether RFM can inhibit the inflammation triggered by LPS in a human bronchial cell line (BEAS-2B) cultured in presence of serum. Initially, the BEAS-2B cells culturing conditions and how those impact the sensitivity of the cells to LPS-stimulation, including different exposures to serum as a key component to the medium, were investigated. Results demonstrated that the serum has an impact on the BEAS-2B cytokine secretion when cells are exposed to different concentrations for different duration and that unstimulated cells release basal IL-8, IL-6 and TNF- α at concentrations that are dependent on the concentration of serum (2 or 10%) to which the cells have been exposed to on day 1 and 2 after being seeded in 24-well plate. The key finding of this chapter is represented by the sustain detectable release of IL-6, IL-8 and TNF- α from BEAS-2B induced by multiple concentrations of LPS (10 – 1000 ng/mL) and exposure time (2 – 48 h), with 800 ng/mL and 24 h being considered the most suitable experimental conditions to adopt.

The established model was used to investigate pre-treatment with RFM as potential anti-inflammatory therapy. Dexamethasone was used as a positive control to demonstrate the ability of the *in vitro* lung inflammation model to respond to drug activity. Two regimens for pre-treatment of cells (2 and 24 h) were used and resulted in concentration-dependent reduction of IL-6 and IL-8 over the range of concentrations tested (0.1 – 100 μ g/mL). RFM pre-treatment for 1.5 h at doses of 0.001 – 100,000 nM reduced the levels of IL-8 by 20%, 25%, 45% and 36% compared to untreated control. Thus, RFM was only able to moderately reduce the levels of chemokines involved in the recruitment of neutrophils, such as IL-8. There was even less effect on the LPS-induced increase of IL-6 which was not suppressed at any concentrations or time regimens by RFM.

The research aims for this chapter were achieved as BEAS-2B culture conditions were optimised and used in an LPS model. A sustained and detectable release of cytokines in the cell medium overtime was obtained, which was suppressed by dexamethasone and partially by RFM. Overall, this chapter provide a suitable foundation for the use of this model in the investigation of the anti-inflammatory activity of other molecules. However, the model was not suitable to study RFM activity and act as a bioassay to guide formulation strategy as required in this thesis, i.e. to evaluate the potential of RFM-HSA-NPs to confer a drug delivery advantage. Due to uncertainty whether this is an *in vitro* artifact and how the model might be optimised, the development of an *in vivo* model in which to evaluate RFM activity was preferred.

CHAPTER 5: A guinea pig model of lung inflammation for evaluation of roflumilast anti-inflammatory activity

5.1 Introduction

The purpose of this experimental chapter was to establish an animal model representing the inflammation associated with COPD. For continuity, the same trigger agent for inducing inflammation, LPS, which was used in Chapter 4 for the *in vitro* respiratory epithelial cell assay was used to establish the animal model. Furthermore, the model was tested for its responsiveness to orally administered RFM to verify whether it had potential as a preclinical model to evaluate the anti-inflammatory effect of RFM administered via the pulmonary route.

Indeed, it is fundamental to use a model that mimics most of the pathophysiological

profile of COPD in order to develop effective treatment options. There are several animal models and due to the complex molecular features of COPD, often no model recapitulates all the features of the disease. Therefore, it was of utmost importance to choose the most relevant model and demonstrate its responsiveness to RFM, while also considering the model's feasibility in terms of time, costs, and laboratory equipment available. In this experimental chapter, a model replicating a COPD exacerbation was adopted.

The way an episode of exacerbation in a patient with COPD is defined has not changed hugely over the years. A panel of experts have tried to improve the definition of exacerbation, providing an updated definition and severity classification of exacerbation of COPD (ECOPD) (Celli et al., 2021). The purpose of the meeting was to overcome the shortcomings of the current definition in an attempt to positively improve clinical and healthcare decision. It was in 1821 that the first definition of ECOPD appeared, followed by an update by Anthonisen and colleagues (Anthonisen et al., 1987) which remained almost unchanged over the last 35 years and forms the basis of the current definition of the European Respiratory Society/ American Thoracic Society definition of exacerbation. The latter states that an exacerbation is "an episode of increasing respiratory symptoms, particularly dyspnoea, cough and sputum production and increased sputum purulence" (Wedzicha et al., 2017). More general is the definition adopted by the Global Initiative

1985 for Chronic Obstructive Lung Disease (GOLD) which states that an exacerbation 1986 corresponds to "an acute worsening of respiratory symptoms which results in additional 1987 therapy" (Vestbo et al., 2013). 1988 1989 Despite there being no universal agreement on the definition of exacerbation, it can be 1990 considered as an event characterized by an acute burst of airway inflammation due to 1991 bacteria, viruses, or environmental pollutants. Airway inflammatory markers such as IL-1992 6 and IL-8 increase during an exacerbation, although not consistently enough to provide 1993 markers for disease severity (Barnes et al., 2015; Celli & Barnes, 2007; Roca et al., 2013; 1994 Segal et al., 2015). 1995 A study focussed on the differences between patients with stable COPD or ECOPD 1996 phases was conducted (Karadag et al., 2008) where the biomarkers of systemic 1997 inflammation in stable (83 patients) and exacerbation phases (20 patients) COPD patients 1998 were compared to healthy controls (30 patients). Levels of TNF- α and IL-6 were higher 1999 in COPD and ECOPD patients than controls, concluding that those are biomarkers of the 2000 systemic inflammatory response in stable COPD patients. 2001 Bronchoalveolar lavage fluid and induced sputum of COPD patients usually have an 2002 increased number of neutrophils and macrophages; increased levels of pro inflammatory 2003 cytokines such as IL-8, IL-6 and TNF- α have been observed in the same specimens 2004 (Chung, 2001). 2005 The importance of biomarkers and their variation over the course of the disease was 2006 highlighted in an extensive review (Barnes et al., 2006). A summary of significance of 2007 the biomarkers in bronchial biopsies, BAL, sputum and exhaled condensate breath was 2008 reported. It was found that the cellular component of BAL in individuals with COPD is 2009 mostly made of macrophages with some neutrophils and T lymphocytes (O'Donnell et 2010 al., 2006). Increased levels of IL-8 were also reported. Sputum IL-8 and TNF- α have 2011 been studied and shown to be increased in the sputum of COPD patients compared to 2012 healthy smokers (Barnes et al., 2006). 2013 2014 Current species used to investigate COPD include rodents, guinea pigs, dogs, and larger 2015 animals such as sheep. A methodological review conducted by Ghorani and others 2016 highlighted that the most used COPD pre-clinical models are based on mice, guinea pigs 2017 and rats which however are considered a poor model due to their resistance to develop

COPD condition hallmarks. Animals can be exposed to different inducers of lung

inflammation such as cigarette smoke, LPS or elastase (Ghorani et al., 2017). This review also includes an extensive comparison between the different methods used to build COPD animal models (e.g. number of cigarettes used, length of exposure to trigger agent etc). An additional comprehensive review of the different pre-clinical models and their advantages and disadvantages has been published by Tanner and colleagues (Tanner & Single, 2019). COPD and lung fibrosis pre-clinical models based on rodent species are summarized in **Table** 5.1. Advantages, disadvantages, and pathophysiological features expressed by each model are included. It is not uncommon that animals are exposed to multiple COPD inducers simultaneously; this is the case of the study conducted by Yang where mice were exposed to cigarette smoke only, LPS only or a combination of both (Y. Yang et al., 2021). Despite relevant for the understanding of COPD pathophysiology and related treatments, those combinations will not be covered in this chapter and therefore were not included in the Table 5.1.

Table 5.1 Rodent models reflecting COPD and related respiratory disorders/ fibrosis described in the literature with their advantages, disadvantages, and corresponding pathophysiological features.

| Trigger agent | Route of administration | Animal model (rodent only) | Main pathophysiological features of the model | Advantages | Disadvantages |
|--|--|---|--|--|---|
| Lipopolysaccharide (various strains available) | IntravenousPulmonary (Instillation, inhalation) | MouseRatGuineapigs | Inflammation Cell influx (macrophages, neutrophils) Structural changes in the lungs (chronic exposure) | Short period of of time required to induce the inflammation Very representative of COPD-related exacerbations | Variability within lot and strain |
| Elastase | Instillation | RatMouse | Lung damageLoss of alveolar wall | Short time required to induce the damage Low cost of reagent The degree of severity can be easily adjusted varying the | window Different mechanism of action of the two elastase enzymes available to be used |

| | | model |
|--|--|--|
| Bleomycin (BLM) Subcutaneous Rats Intraperitoneal Pulmonary (intratracheal or intranasal) Oropharyngeal | Acute lung inflammation Systemic administration induces more homogeneous pattern of fibrosis Less strong | Lung fibrosis induced by BLM considered not fully representative of idiopathic pulmonary fibrosis Spontaneous resolution of the fibrosis induced by single-dose BLM Different timing of the disease development in animal model vs clinical disease Development of fibrosis limited to Balb/c mice |

amount of enzyme o Poor impact of

immune

involvement in this

cell

administered

| Cigarette smoke extract | Pulmonary (whole- body of nose-only) | MouseRatGuineapigs | Pulmonary infiltration of macrophages and neutrophils Airway fibrosis Emphysema | Can induce many COPD features in animals | High variability of the model outcome due to lack of a standardized protocol for animal exposure Requires long time exposure |
|--|--|---|---|--|---|
| Fluorescin isothiocyanate (FITC) | o Intratracheal | o Mice | Acute lung injury Edema and inflammation (with presence of neutrophil) Fibrosis Localized pattern of inflammation like bleomycininduced Long-term effects (up top 5 months) | Long-term effects (durable fibrotic response) Fluorescent imaging | o Absence of consistent results due to difficulties in preparing FITC (different time of particle sonication induce variable particle size which lead to not consistent toxicity) |
| Silica particles | Pulmonary route (intratracheal administration, aerosolization) | MiceRats | Inflammatory responseLung fibrosis | Induce similar effects in human and mice The lung damage persists after the | Expensive equipment required Lack of IPF-like lesions |

Oropharyngela aspiration termination of the silica particles exposure

- Persistent, toxic inflammatory response
- Intratracheal model easy and less expensive

References

2032

2033

(Degryse & Lawson, 2011; Ghorani et al., 2017; Jenkins et al., 2017; Jones et al., 2017; Moeller et al., 2008; Moore et al., 2013; Tanner & Single, 2019; Tashiro et al., 2017; Wright et al., 2008)

- 1 Instillation of the proteolytic enzyme elastase can induce and maintain an inflammatory
- 2 response in the rodent lungs with immediate and marked loss of alveolar wall structure.
- 3 This model consists of instillation of enzymes such as porcine pancreatic elastase, human
- 4 neutrophilic elastase and papain (elastase activity depending on its purity and source).
- 5 Despite the time advantage provided by this model (a single dose of elastase results in
- 6 immediate lung damage), it has a very narrow dose window, and it results in 'artificial'
- 7 lung tissue damage.

- 9 Cigarette-smoke (CS) exposure is another model that can be used. Details of the CS
- 10 model and its variability within laboratories have been mentioned in Chapter 4. An
- additional source of variability for CS models is represented by the type of exposure;
- whether nose-only or whole-body. As later will be mentioned for the LPS model as well,
- a downside of the whole-body model is the deposition on the animal fur of the CS
- constituents which can be ingested by the animal and eventually influence the results.
- 15 The poor control of the dose exposure when a chamber model is used can be overcome
- with the nose-only exposure, which however can be stressful for some animal species as
- it requires constraints.

- 19 Bleomycin (BLM) is a chemotherapeutic antibiotic that is pro-fibrotic such that
- 20 pulmonary fibrosis developed after the intravenous administration of the drug to patients
- 21 with lymphoma (Sleijfer, 2001). BLM can be administered systemically (intravenous,
- subcutaneous or intraperitoneal administration) or directly to the lungs (intratracheal or
- oropharyngeal administration). Generally, three or four weeks after a single dose of BLM
- 24 directly to the lungs, an acute lung damage can be visualized followed by localized
- 25 inflammation and fibrosis at the site of the agent administration. In contrast, systemic
- administration induces a more homogeneous fibrosis throughout the lungs, but a lower
- state of lung inflammation. In this case, the BLM induced fibrosis will be detectable
- within 4 12 weeks from the exposure. The initial site of damage when delivered
- 29 intravenously is the pulmonary vascular endothelium, followed by the alveolar
- 30 epithelium.
- 31 In terms of dosing regimens used, a wide range is reported in the literature. For single
- dose exposure, mice can receive from 1.25 U/kg (Hecker et al., 2014) to 4 U/kg (Rojas et
- 33 al., 2005) usually suspended in 50 100 μL of PBS via intratracheal administration. In
- one of the few studies that has investigated repetitive BLM injury (chronic exposure),

- 35 mice were exposed to intratracheal administration of BLM (0.04 U) biweekly for a total
- of 4 months (eight total doses) (Degryse et al., 2010).
- 37 Chronic pulmonary exposure to BLM induces a more robust fibrosis compared to one
- 38 single exposure, with an attenuation of the neutrophilic inflammation as the model
- 39 timeline progresses. The repetitive dosing more closely resembles the recurrent nature of
- 40 lung injury that occurs in patients with idiopathic pulmonary fibrosis (Degryse & Lawson,
- 41 2011). Although BLM can be delivered via multiple routes, the intratracheal is the most
- 42 frequent route used by researchers.

- 44 Besides those models, the administration of fluorescein isothiocyanate (FITC)
- 45 (Christensen et al., 1999) and silica particles (Lakatos et al., 2006) have also been used
- 46 to induce lung damage leading to fibrosis. FITC administration induces a localised
- 47 inflammation pattern similar to that induced by BLM. Interestingly, it conjugates to lung
- 48 parenchymal proteins, remaining localized to the area of initial injury and allowing the
- 49 use of immunofluorescence to better investigate the lung damage. However, the main
- disadvantage of this model is represented by its variability which is correlated to the FITC
- 51 lot used and to the size of the FITC particulate number or surface characteristics obtained
- via sonication (Moore et al., 2013; Moore & Hogaboam, 2008). Christensen (Christensen
- et al., 1999) reported a significant increase in the early mortality for intratracheal
- 54 inoculation and increase acute toxicity when a FITC preparation protocol that required
- long sonication time to ensure better dispersion was used. These difficulties are correlated
- 56 to the variability within studies in different laboratories and different research studies.
- 57 Finally, silica particles induce a fibrotic damage that more closely resembles the
- occupational induced silicosis with the presence of fibrotic nodules. The silica particles
- 59 tend to not being easily cleared from the lungs, hence inducing a persisted stimulus.
- 60 However, besides the expensive equipment required, the development of the fibrotic
- 61 nodules can take between 40 and 120 days after exposure.

- Besides the above-mentioned agents used to induce lung damage, LPS can also be used
- as a COPD model. LPS is a component of the wall of Gram-negative bacteria and its
- characteristics were described in Chapter 4. Its use in animal models is common and it
- 66 quickly produces lung damage, which usually persists after the exposure is ceased
- 67 (Ghorani et al., 2017; Tanner & Single, 2019).

Acute (single administration) exposure to LPS induces a lung inflammation characterized by cellular influx whereas chronic exposure is often associated with structural changes of the lungs. This is a valuable model to understand exacerbation-related COPD mechanisms. Indeed, bacterial colonisation of the lower airways is an important factor in determining the degree of airway and systemic inflammation in stable COPD patients and is highly related to the development of exacerbations. Bacterial endotoxins, such as peptidoglycan fragments, activate the immune response exacerbating the lung inflammation. Patients with a high level of bacteria colonisation in the lungs have an increased level of neutrophils and pro inflammatory cytokines in the induced sputum (Celli & Barnes, 2007; Roca et al., 2013; Segal et al., 2015). This makes the use of LPS as inducer in preclinical models of COPD relevant as bacteria isolated from lungs fluids of patients with COPD immediately after exacerbation are mainly Gram-negative (Tanner & Single, 2019).

The administration of LPS into the airways or systemically is a commonly used model to induce lung inflammation. A narrative review describes the molecular dynamics of LPS-induced lung injury in the rodent model (Domscheit et al., 2020). When delivered via the pulmonary route, LPS damage occurs principally to the alveolar epithelium. Moreover, LPS induces a strong migration of cells into the lung tissue which terminates 72 hours after the challenge followed by secondary fibrosis (Bozinovski et al., 2004). When LPS is administered systemically it acts primarily on the vascular endothelium causing interstitial edema (Domscheit et al., 2020).

In pre-clinical models, the exposure to LPS is known to cause severe tissue injury characterized by accumulation of inflammatory cells in the alveolar and interstitial space and alveolar well thickening (Matuta Bella et al., 2011). The activation of the signalling

and alveolar wall thickening (Matute-Bello et al., 2011). The activation of the signalling molecules involved in the LPS-mediated inflammation is very complex and time dependent. It is very likely that multiple signalling molecules are present in the lung tissue at different time points after the LPS challenge. The signalling molecules related to LPS pathophysiological pathways are time-dependent, being activated at different time points during the disease progression (Domscheit et al., 2020b). The kinetics of cell influx after LPS exposure are discussed further in the paragraph 5.5.

Generally, pulmonary drug administration to pre-clinical COPD models can be achieved using a whole-body exposure system (chamber) or a nose-only exposure system (**Table**

102 5.2). A whole-body chamber model is represented by full or partial immersion of animals 103 in an atmosphere containing the agent. This is advantageous when a large number of 104 animals are used, or a chronic study performed. However, sometimes it is recommended 105 to house animals individually in chambers as they tend to huddle, which can be a source 106 of increased variability in the dose inhaled due to reaction with the animal fur or filtration 107 by it. In addition, if allocated in groups, animals can inhale air which has been exhaled 108 and cleaned by other animals, which is a further mechanism of dose variability. 109 An alternative is represented by nose- or head-only exposure. Such systems are designed 110 to reduce the deposition of the test compound on the animal fur as only the head or the 111 nose/mouth of the animals is exposed to the test compound. However, this model also 112 possesses some downsides and requires trained investigators as well as specific and 113 expensive equipment. 114 To improve the pulmonary exposure of test compound in animals, Wong and others 115 (Wong et al., 2008) developed a single-animal whole-body exposure system for 116 inhalation for use when neither a conventional large whole-body exposure model nor a 117 nose-only were suitable. They combined a series of chambers connected together in a 118 manifold system and exposed mice and rats by inhalation to compounds over a 13-weeks 119 period. They found out that the test compound distribution was uniform, and the 120 compound measured concentrations were 2% within the target concentration, concluding 121 that the method designed was effective when a low amount of test substance is available. 122 Generally, the chamber model is usually the least stressful method for animals as they do 123 not require restraint. However, it is characterized by high variability in terms of dose and 124 concomitant routes of exposure (skin, eyes and oral). In contrast, the nose-only exposure 125 system allows exposure principally to the respiratory tract with less dose variability. However, for some species the restraint may present a source of stress and training is 126 127 recommend before the exposure to reduce the stress and produce normal physiological

128

states (Phalen et al., 2014).

Table 5.2 Advantages and disadvantages of different exposure methods that can be adopted in the pulmonary exposure of the disease inducing substance in pre-clinical animal models.

| Exposure method | | Advantages | | Disadvantages |
|------------------------|-----|--|-----|---|
| Whole-body | 0 0 | Can allocate large number of animals (allocate single animals is usually recommended) Long term studies No restraint for animals > less stress | 0 0 | Multiple routes of exposure (skin, eye, oral) Dose variability Compound of interest may interact with excreta |
| Nose- or head- only | 0 | More accurate deposition of the product into the respiratory tract | 0 | Stress to some species (acclimatation recommended) |
| Intratracheal | 0 | High control of deposition of compound of interest | 0 | Unrealistic deposition in the respiratory tract |

130

131

132

133

134

135

136

137

138

139

140

141

142

143

144

145

Different animal species can be used to model the pathological features of COPD. However, the pre-clinical model designed in this chapter was based on the use of guinea pigs. Guinea pigs possess many similarities to humans, making them a valuable species in the design of COPD models. An extensive review of the use of guinea pigs in studies relevant to asthma and COPD was published in 2008 (Canning & Chou, 2008). Receptor pharmacology in guinea pigs is more similar to that of humans compared to other species and the guinea pig lung anatomy and physiology very closely resembles that of humans. Guinea pigs have goblet cells and mucus glands, with a subepithelial vasculature both between the epithelial and the smooth muscle layer. In both species the trachea, mainstream bronchi and large intrapulmonary bronchi are lined with a pseudo-stratified epithelium. The physiology and the anatomy of the airway smooth muscle of guinea pigs also resembles those of humans. However, the major drawback of the use of guinea pigs in COPD model is represented by the axon reflex (Kroll et al., 1990). This reflex is the response to activation of peripheral terminals of capsaicin sensitive nerves in the airways of rats and guinea pigs, which results in the release of tachykinin which induces many features of asthma such as mucus production, bronchospasm, and inflammatory cell

recruitment. However, it has been reported that the way the axon reflex works in guinea pigs and rats is dissimilar to humans. In guinea pigs the axon reflex it is likely to be relevant to responses to experimental challenges whereas it has a limited role in the human airway function.

150

146

147

148

149

5.2 Aims and objectives

151152

- 153 The overall aim of the work reported in this chapter was to illustrate how an LPS-induced
- guinea pig model of lung inflammation can be used to model inflammatory lung disease
- and can be modulated by orally administered RFM. This will provide a platform for the
- investigation of the pulmonary delivery of RFM in the same preclinical model.
- 157 Initially the dose-finding studies were performed for LPS-induction of inflammation
- using a whole-body chamber inhalation model. This was followed by the evaluation of
- the anti-inflammatory activity of the positive control, orally administered RFM.
- 160 Specific objectives included:
- 161 1. Establish a whole-body exposure chamber model for delivery of LPS to guinea pigs nebulised via an Aerogen Pro (ultrasonic mesh nebuliser);
 - 2. Investigate the dose-response to LPS using biomarkers including the total and differential count of the cells infiltrated into the lungs as consequence of the endotoxin exposure;
 - 3. Confirm the responsiveness of the model by measuring reduction of inflammation by the oral administration of RFM.

168

163

164

165

166

167

5.3 Methods

170171

169

5.3.1 Preliminary and qualitative assessment of LPS exposure: intratracheal administration

- 174 Two male Dunkin-Hartley guinea pigs (250–299 g) were exposed to an intratracheal
- administration of a blue dye in order to investigate the variability often related to this
- specific way to achieve pulmonary exposure in preclinical studies. Animal received an
- overdose of sodium pentobarbital (1 g/kg) via an intraperitoneal injection and then they
- were placed vertically on a bar to facilitate the visualization of the trachea. The
- administration was carried out using a pyrogen free 1 mL syringe attached to a stain steel

gavage needle. This study was aimed to gain qualitative information and therefore was carried out only on two animals. Both animals were intratracheally instilled with 200 μ L of Evans Blue (0.02%) above the carina whereas one animal received only the Evans Blue bolus and the second animal received the volume of the dye followed immediately by 1 mL of air. The vertical position was retained for one minute after the distribution to allow complete and uniform delivery of the liquid into the lungs.

5.3.2 Design of a whole-body chamber LPS-induced inflammation model in guinea pigs

5.3.2.1 Preparation of Lipopolysaccharide stock solution

Lipopolysaccharide (LPS) (O111:B4, Sigma L2630) was dissolved in ultrapure water (5 mg/mL) under gentle stirring, aliquoted and stored at – 20°C in Eppendorf®, protected from direct light. Immediately before the experiment, an aliquot was thawed and diluted to the desired working concentration in sodium chloride 0.9% w/v.

5.3.2.2 Nebuliser setting

LPS was nebulised using a nebuliser Aerogen Pro[®] (Aerogen Ireland Ltd., S/N 297, volume median diameter with sodium chloride 0.9% 4.44 μm, average flow rate 0.4 mL/min (Aerogen ® Pro System Instruction Manual)) attached to an ISO 22 mm t-piece fixed inside the lid of the chamber box and directed towards the inside of the glass box (470 (L) x 200 (H) x 200 (D) mm) (**Figure** 5.1). The nebulisation of sterile sodium chloride 0.9% w/v (control) was performed using a nebuliser Aerogen Pro® (Aerogen Ireland Ltd., S/N 356, volume median diameter 4.82 μm, average flow rate 0.4 mL/min (Aerogen ® Pro System Instruction Manual) with the same set up above mentioned. If stated otherwise, LPS (0.1 mg/mL, 20 mL) was nebulised using an Ultra-Neb 2000 ultrasonic nebuliser (Devilbiss, Germany). The nebuliser was connected to the side of same box mentioned above via a connecting tube.

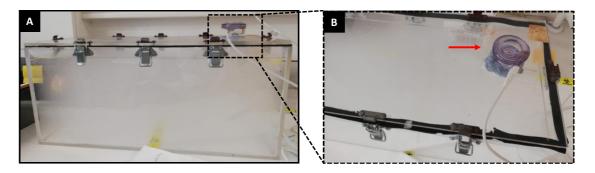


Figure 5.1 Experimental set up used in the design of a whole-body chamber model: an Aerogen Pro® nebuliser is fitted on the top of a plexiglass chamber.

211

212

213

214

215

216

217

218

219

220

221

222

223

224

225

226

227

228

229

5.3.2.3 LPS dose-response in guinea pigs using a whole-body chamber model

At time 0, male Dunkin-Hartley guinea pigs (250–299 g) were placed individually unanaesthetised and without restraint in the exposure chamber. Animals were allocated to one of three treatment groups which were exposed to i) 0.1 mg/mL, ii) 0.2 mg/mL or iii) 0.5 mg/mL of LPS. The volume of the LPS solution and the length of the exposure were 10 mL and 30 min respectively for all the treatment groups. After the LPS exposure, animals were returned to the housing boxes; four hours later they were exposed to an overdose of sodium pentobarbital (1 g/kg) via an intraperitoneal injection. The trachea was cannulated and bronchoalveolar lavage was performed using 5 mL of filtered PBS (pH 7.3 \pm 0.2 at 25 °C) which was gently instilled and withdrawn 3 times using a 5-mL syringe (Figure 5.2). An aliquot of the recovered BAL was immediately centrifuged (4000 rpm), the supernatant was collected and stored at - 80 °C for cytokine evaluation using a commercial sandwich ELISA kit. For differential cell count evaluation, an aliquot of 100 µL of BAL was placed on a microscope slide and immediately processed using a cytocentrifuge (1000 rpm x 1 min). The microscope slides were air-dried and stained using Reastain Quick-Diff following the manufacturer's instructions. Differential cell count was performed using light microscopy. A total of 200 cells were counted for each slides using four different field of view and under 400x magnification. The total cell number was calculated by counting a stained (50% v/v Turk's stain) aliquot (10 μL) under a microscope using a haemocytometer.

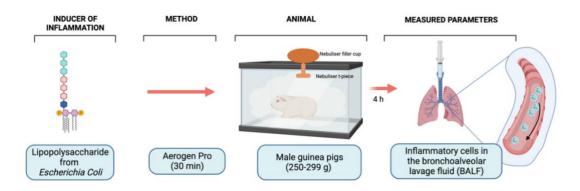


Figure 5.2 Schematic representation of the designed inflammation whole-body chamber model in male Dunkin-Hartley guinea pigs.

5.3.3 Oral administration of roflumilast in LPS-exposed guinea pigs

5.3.3.1 Preparation of roflumilast suspension for oral administration

For oral administration, RFM was suspended in polyethylene glycol 400 (PEG₄₀₀) by continuous stirring at 70°C. Once fully dissolved, the stock solution was diluted with an equal proportion of 4% w/v methyl cellulose (methocel) until a homogenous milky suspension was obtained.

Methocel 4% w/v was prepared the day before the *in vivo* study. To make a 100 mL preparation of 4% w/v methocel, half of the volume of water needed was refrigerated on ice to cool at 1 - 4°C; the other half was heated at about 30°C in a glass beaker. The weighed powder was added to the heated methocel and stirred using a glass rod obtaining a white and sticky paste. The ice-cold water was then added, stirred vigorously on a plate. Once the dispersion had reached the temperature at which the methocel becomes water soluble, the powder began to hydrate with following increase of the viscosity. The obtained preparation was allowed to cool at 5°C overnight before used to prepare the drug suspension for *in vivo* administration.

5.3.3.2 Oral administration of roflumilast suspension in an LPS-inflammation model

Male Dunkin-Hartley guinea pigs (250–299 g) were exposed to a preventive protocol of RFM administered via the oral route (p.o.). The p.o. administration volume was 1 mL/kg of body weight. Animals were divided in three groups, with four animals in each group: i) *saline challenge:* animals treated with vehicle (PEG₄₀₀ + methocel 4% w/v) and challenged with sterile sodium chloride 0.9%; (ii) *LPS challenge:* animals treated with

- vehicle (PEG₄₀₀ + methocel 4% w/v) and challenged with LPS; (iii) *drug-treated*: animals
- treated with RFM at a dose of 0.5 mg/kg and challenged with LPS.
- 257 RFM or vehicle were administered p.o. at time 0 to conscious animals. One hour later,
- animals were placed in the plexiglass chamber and exposed to nebulised LPS from E.
- 259 Coli. LPS (0.1 mg/mL, 20 mL) using a Devilbiss nebuliser. At the end of the LPS
- 260 exposure, animals were placed in their housing boxes; four hours later they were exposed
- 261 to an overdose of sodium pentobarbital (1g/kg) via an intraperitoneal injection. The
- trachea was cannulated and bronchoalveolar lavage was performed using 5 mL of filtered
- 263 phosphate buffer solution that was gently instilled and withdrawn 3 times using a 5 mL
- syringe. Bronchoalveolar lavage fluid was processed as mentioned in paragraph 5.3.2.3.

- All experimental procedures and conditions were reviewed and approved by the ethics
- 267 committee of King's College London and conducted in accordance with the United
- 268 Kingdom Animal Scientific Procedures Act, 1986. Procedures were conducted under the
- 269 Project Licence PEF229300 and the Personal Licence no. I8232C275. The Project
- 270 Licence holder is Prof. Clive Page and the Protocol adopted is no. 2 (Studies of lung
- pathophysiology) which has a moderate severity category. The author thanks Dr Sandra
- 272 Rudman for having conducted some of the experimental procedures described as well as
- for her support during those.

274

275

5.3.3.3 Statistical analysis

- Data were expressed as mean \pm SD. Where appropriate, data were analysed using
- 277 GraphPad Prism version 9, (GraphPad Software, San Diego, USA). Normal distribution
- of data was firstly evaluated and the statistical significance between groups was
- determined using one-way ANOVA with Šídák's, multiple comparison tests where
- appropriate. Statistically significant differences are represented by asterisks as follow: *,
- 281 $p \le 0.05$; **, $p \le 0.01$; ***, $p \le 0.001$. Where stated that a statistical analysis was
- performed, absence of asterisks indicates non-statistically significant results.

283

5.4 Results

284285

286 5.4.1 Lung distribution of a dye after intratracheal administration

The intratracheal route is often reported in studies in which the lungs are the target organ for both the development of the inflammatory model and for the investigation of the anti-inflammatory treatment. This assessment was carried out to determine the pattern of distribution of a liquid administered to the lungs via the intratracheal route and how this is affected by a minor protocol modification. **Figure** 5.3 describes the different patter of distribution if only the liquid was instilled (Figure 5.3 A, B) or if the administration of the liquid was immediately followed by 1 mL of air (Figure 5.3 C, D). The absence of air resulted in a highly localized dye with accumulation mainly in the trachea and a patchy and uneven distribution; in contrast the addition of air after the delivery of the volume of dye had a considerable positive impact on the distribution. The colour was well distributed into the airway and Figure 5.3 C and D show how the colour, despite being mainly located in the lower lobes, is well distributed in the alveolar structure.

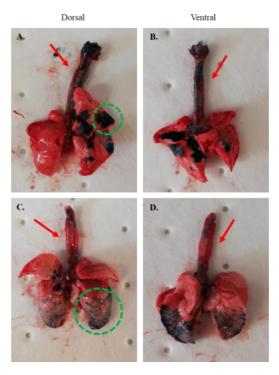


Figure 5.3 Representative pictures (dorsal and ventral views) of guinea pig lungs showing how the specific technique of intratracheal administration used can impact the distribution of an instilled solution. (A, B) Administration of 200 μ L of Evans Blue (0.02%) only; (C, D) Administration of 200 μ L of Evans Blue (0.02%) followed by 1 mL of air bolus. The experimental procedure was carried out on two animals receiving the intratracheal administration using the two different technique. Pictures were taken from two different animals, one per technique used.

5.4.2 LPS-induced lung inflammation in guinea pigs

To determine the potential of nebulised LPS to induce an inflammation in the lungs of guinea pigs, the total and differential cell number infiltrated into the lungs of the animals after the exposure to LPS were determined (**Figure** 5.4). In this experimental study, the outcome was measured 4 hours after the exposure to LPS. At this time point the neutrophils influx has already started and, despite possibly not being at their peak concentration (Domscheit et al., 2020b), inflammatory cells were significantly present.

Macrophages Neutrophils Lymphocytes Eosinophils

Figure 5.4 Representative morphology of cells recoverable from the BAL of guinea pigs.

The total and differential cells collected in BALF four hours after the exposure to LPS are shown in **Figure** 5.5. The exposure to increasing LPS doses resulted in 175.0 x 10⁴ cells/mL, 324.25 x 10⁴ cells/mL and 350.25 10⁴ cells/mL for 0.1, 0.2 and 0.5 mg/mL LPS respectively. The recovered total number of cells was similar when animals were exposed to the two highest doses of LPS. The number of eosinophils did not change when animals were exposed to increasing concentrations of LPS, nor was there clear relationship between number of macrophages and dose of LPS as the dose 0.2 mg/mL corresponded to the lowest number of macrophages with the lowest and the highest doses resulting in

similar number of macrophages. Compared to eosinophils and macrophages, the number of neutrophils was highly impacted by the LPS exposure and by the different concentrations tested. The neutrophils recovered in the BALF increased from 128.8 x 10⁴ cells/mL to 291.75 x 10⁴ cells/mL and 294.75 x 10⁴ cells/mL with increasing LPS dose. Indeed, differential cell count analysis highlighted that the increased total cell number was mainly determined by neutrophils with lesser impact of the smaller numbers of macrophages and eosinophils.

The dose of 0.2 mg/mL was considered optimal for these experimental studies as it resulted in a clearly detectable influx of inflammatory cells. Therefore, it was adopted as LPS dose for nebulisation in the following *in vivo* experimental studies.

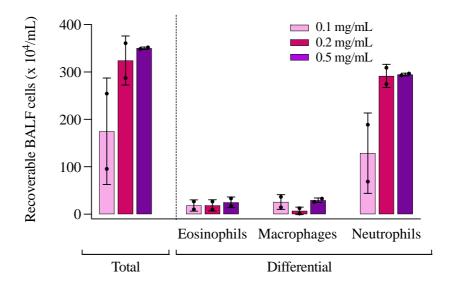


Figure 5.5 Total and differential cell count from bronchoalveolar lavage fluid (BALF) of guinea pigs exposed to increasing concentration of lipopolysaccharide from E. Coli. Cells were recovered four hours after the exposure to LPS. Cell populations were identified on air-dried cytocentrifuged smears after staining with Diff-Quick stain. Differential cell counts were performed on 200 total cells using four different fields of view. Data represent mean \pm SD of n=1 independent experiment, (n=2 animals/group).

The impact of LPS on the levels of TNF- α in the BALF was investigated using a commercial ELISA kit. The concentrations of TNF- α detected were 1.6 x 10⁴ pg/mL, 1.47 x 10⁴ pg/mL and 1.78 x 10⁴ pg/mL when animals were exposed to 0.1, 0.2 and 0.5 mg/mL LPS, respectively (**Figure** 5.6). The concentration of TNF- α did not vary accordingly to the increasing concentrations of LPS to which the animals were exposed.

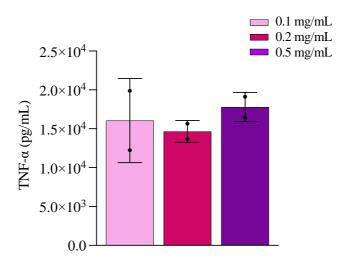


Figure 5.6 Levels of human tumour necrosis factor alfa (TNF- α) in bronchoalveolar lavage fluid (BALF) from guinea pigs four hours after the exposure to increasing doses of Lipopolysaccharide (LPS). Cytokine levels were detected using a commercial ELISA kit. Data represents mean \pm SD of n=1 independent experiment, (n=2 animals/group).

5.4.3 Anti-inflammatory activity of orally administered roflumilast in LPS-exposed guinea pigs

To evaluate the anti-inflammatory activity of orally administered RFM in LPS-exposed guinea pigs, the characteristics of the cell population infiltrated into the lugs after four hours from the LPS nebulisation was studied. Evaluation of leukocytes included a total white blood cell count and a differential count, with absolute numbers of each type of leukocytes. Representative guinea pigs BAL cytospin preparations showing the different cell population infiltrated in the lungs can be visually recognised based on the type of treatment or challenge received (**Figure** 5.7). In the cytospin of saline-challenge guinea pigs (Figure 5.7 A) a predominance of macrophages can be described. Macrophages possess a large size and high cytoplasm to nuclear ratio. A prevalence of neutrophils can be highlighted in Figure 5.7 B, whereas neutrophils are identifiable due to their segmented nuclear morphology. The reduced ratio of neutrophils in the Figure 5.7 C makes easier to identify also eosinophils (with less segmented nuclei and round, red cytoplasmatic granules) and lymphocytes (with their little cytoplasm) (Siegel & Walton, 2020).

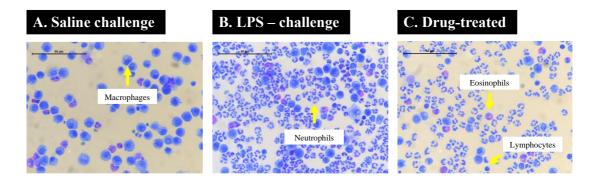


Figure 5.7 Representative guinea pig BAL cytospin preparations. a) Predominance of alveolar macrophages in BAL of healthy guinea pigs exposed to saline challenge and treated with vehicle; the photomicrographs also show a number of eosinophils (red staining); b) BAL neutrophils predominance in guinea pigs challenge with 0.2 mg/mL, 10 mL of LPS and treated with vehicle; c) Reduced number of neutrophils in combination with a small number of eosinophils, macrophages and lymphocytes in drug-treated guinea pigs' BAL.

362

363364

365

366

367

368

369

370

371

372

373

374

375

376

377

378

379

380

The exposure to nebulised LPS induced a significant increase of the total cells recovered in the BALF compared to the number of cells in the lungs after exposure to nebulised saline (Figure 5.8). The oral treatment with roflumilast at a dose of 0.5 mg/kg significantly reduced the total number of cells, highlighting the anti-inflammatory activity of roflumilast in the model of interest. The exposure to LPS induced a very significant increase in the number of neutrophils compared to saline-challenge, highlighting the efficacy of LPS to initiate a state of inflammation in the lungs of the animals. In contrast, the exposure to LPS had no impact on the number of both eosinophils and macrophages. Roflumilast pre-treatment significantly reduced the number of eosinophils (LPSchallenge vs drug-treated: 89.18 x 10⁴ cells/mL vs 16.96 x 10⁴ cells/mL) and neutrophils (LPS-challenge vs drug-treated: 841.15 x 10⁴ cells/mL vs 224.84 x 10⁴ cells/mL) recovered in the BALF 4 hours after the LPS challenge, demonstrating the antiinflammatory activity of RFM when delivered via the oral route in the model of lung inflammation that was established. In summary, exposure to LPS resulted in an increased number of neutrophils that infiltrated the lungs and this inflammatory response was effectively reduced by treatment with RFM. This demonstrates both the potential of the LPS as inflammation inducer and confirms the activity of roflumilast as a drug with anti-inflammatory activity when delivered via the oral route in the preclinical model.

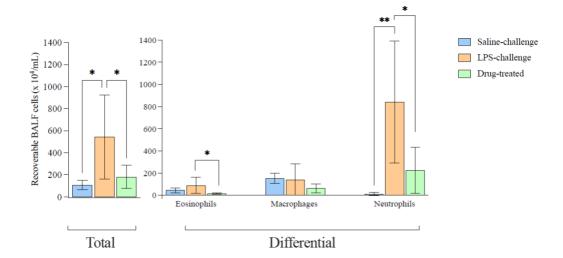


Figure 5.8 Oral administration of free RFM. Total and differential count of cells recovered from bronchoalveolar lavage fluid of guinea pigs. Cell populations were identified on air-dried cytocentrifuged smears after staining with Diff-Quick stain. Differential cell counts were performed on 200 total cells using four different fields of view. Data represent mean \pm SD of n=2 independent experiments, (n=4-8 animals/group). One-way ANOVA followed by Sidak's multiple comparison test was used to examine differences between groups. Significant differences are shown as: $*, p=\leq 0.05; **, p=\leq 0.01;$ no bar = not significant.

5.5 Discussion

In this work, guinea pigs and LPS were used to design and optimise a model that replicates the conditions and related markers of a COPD exacerbation. The final aim was to obtain a robust inflammation in the lungs detected mainly via the total white blood cell and the differential count and to confirm that the oral administration of RFM in the same model resulted in significant reduction of the induced inflammation. The model was designed and optimised in terms of i) LPS dose and ii) how the animals were exposed to LPS – whole-body chamber and inhalation exposure.

As mentioned in the introduction section of this current chapter, LPS represents only one of the possible agents that can be used to induce a model that resemble most of the COPD and the related exacerbations features. The use of LPS in a whole-body chamber model is well-known as well as the molecular pathway related to its cascade activation. The

cellular response to LPS is associated with the activation of the TLR4 receptor and corresponding pathway. A detailed review about LPS and its molecular pathway activation was written by Lu and others (Lu et al., 2008). LPS is one of the most studied immunostimulatory compound and as mentioned elsewhere is a component of the outer membrane of Gram-negative bacteria. The activation of the LPS-related cellular signalling involves multiple molecules: LPS binding protein (LBP), CD14, MD-2 and toll-like receptor 4 (TLR4). The association between LPS and CD14 is mediated by LBP. CD14, also present in a soluble form, mediates the binding of LPS to the complex TLR-4/MD-2 whereas MD-2 is a soluble protein that can directly form complexes with LPS. Upon LPS recognition, TLR4 undergoes oligomerization with following recruitment of adaptors using the domains of its receptor (TIR). There are five different TIR domainscontaining adaptor proteins (MyD88, TIRAP, TRIF and TRAM) and they are all necessary for the TLR functioning. It has been demonstrated that the TLR4 signalling correlated to the activation of pro-inflammatory cytokines is a MyD88 - dependent pathway. Upon LPS recognition and activation of the TLR4 pathway, several death domain-containing kinases are activated and responsible for the transcription of proinflammatory cytokines (Lu et al., 2008).

The experimental preclinical model developed in this chapter successfully resulted in a measurable lung inflammation using 4 hours as total time window after LPS exposure. Other studies have investigated the kinetic of cells influx looking at how the concentration of pro inflammatory cells was changing over time in a longer period. Toward and Broadley (Toward & Broadley, 2000) evaluated the relation between aerosolized LPS exposure and extent of leukocyte infiltration at 0.5 h, 1 h, 2 h, 4 h, 24 h and 48 h after the LPS exposure. Male Dunkin-Hartley guinea pigs were exposed for 1 h to aerosolized LPS (*E. Coli*, O26:B6) (30 μg/mL) or vehicle (0.9% w/v saline) in a sealed chamber (620 x 300 x 420 mm) using a Wright nebulizer (flow rate 0.5 mL/min). They showed that after the above mentioned LPS exposure (concentration and length) an increased number of neutrophils was detectable already after 0.5 h (~ 8 x 10⁶ cells/mL). The neutrophils concentration increased throughout, peaking at 24 h (~ 35 x 10⁶ cells/mL) and decreasing at 48 h (~ 15 x 10⁶ cells/mL). Macrophages increased up to 48 h after the LPS challenge, with a minor increase in the number of eosinophils (Toward & Broadley, 2000). Our findings are in agreement with those of Toward and Broadley as after 4 hours from

the LPS exposure a measurable and significant change in the total cell count was detected.

However, the exact concentrations of neutrophils at 4 hours in the two studies are not in agreement. The number of neutrophils recovered in our study was between 3 x 10⁶ cells/mL and 8 x 10⁶ cells/mL, whereas ~ 30 x 10⁶ cells/mL neutrophils were recovered in Toward and Broadley's study. In addition, compared to the study of Toward and Broadley, our method adopted a smaller chamber (470 mm (L) x 200 mm (H) x 200 mm). These results are interesting as we would have expected an opposite outcome with higher concentration of LPS and smaller chamber resulting in increased air concentration of LPS and stronger neutrophilia. This outcome may be attributed to the different strain of LPS use within studies, nebuliser and resulting particle size as well as the specific setting of the chamber used. Although 0.9 mg of LPS results in a peak of neutrophils at 24 h, it is possible that the combination of a higher dose of LPS (2 mg) and a smaller chamber result in an earlier detectable peak of neutrophils. This hypothesis was not explored, but the use of 4 h was determined to be a suitable time point at which there was a robust increase in the number of neutrophils in the lungs in response to LPS in the model that was established and was suitable as tool to investigate the anti-inflammatory activity of a drug. In contrast the lack of significant changes in the macrophages number in our results (saline challenged vs LPS challenged) corresponded to little changes in macrophage numbers reported previously at 4 h compared to 48 (Toward & Broadley, 2000).

Another study that evaluated the effect of the time elapsed from 0 h to 72 h after LPS intranasal instillation was conducted by Lee and others (S.-Y. Lee et al., 2018). Female BALB/c mice were exposed to 20 μ g/20 μ L of LPS (strain not specified) via intranasal instillation and biomarkers of COPD severity including the total white blood cell and neutrophils count in the BAL were measured at time 0, 3 h, 24 h, 48 h and 72 h. They found that the total number of cells increased over time, becoming significant different 48 h after the LPS exposure. Despite an increase in the number of eosinophils overtime, only the change in the neutrophil number was statistically significant at 48 h and 72 h post-challenge. They also investigated how the level of pro-inflammatory cytokines changed overtime and found that they all increased overtime from 3 to 72 h after the LPS instillation. The changes recorded in the IL-8 levels were the largest compared to TNF- α and others and its expression was dramatically increased at 72 h. On the other hand, the levels of TNF- α were increased at 3 h after the challenge compared to control, followed by a decrease at 24 h and a further and robust increase at 48 h and 72 h after the challenge.

465 These data are in agreement with the TNF- α kinetic described by others (Bozinovski et 466 al., 2004). Mice were exposed to intranasal instillation of 10 µg/mice of LPS (E. Coli, 467 O26:B6) at time 0 with TNF- α levels detected at 0, 5 h and 24 h. The TFN- α levels 468 increased sharply from 0 to 5 h (5 ng/mL) with a following decrease overtime until 24 h 469 post-challenge. In both studies an early increase was reported which is in agreement with 470 the fact that the release of this cytokine represents an early event in response to LPS 471 stimulation. Moreover, in both studies a decrease at 24 h was described. 472 These data suggest that although the time point used in this experimental chapter was 473 demonstrated to be suitable to detect a significant change in the neutrophils number, it 474 may not be suitable to detect changes in the level of TNF- α and a longer period of time 475 including earlier and later time points might be required to detect increases of its level. 476 Bozinovski and co-workers (Bozinovski et al., 2004) also investigate the kinetic of 477 neutrophilia overtime. Evident increase of neutrophils number was detected as early as 2 478 h post-challenge with a robust increase 6 h after instillation of LPS, and the highest concentration reached after 24 h (1.3 x 10⁶ cells/mL); 48 h after the challenge, the 479 480 concentration of neutrophils declined and completely resolved by 72 h (Bozinovski et al., 481 2004). It was also reported that the number of macrophages steadily increased from 6 h 482 to 48 h post challenge, with a following robust further increase at 72 h post-challenge. 483 This latter increase was in contrast with the kinetic reported for the neutrophils and it was 484 considered associated to the *in situ* replication of the macrophages. 485 Although experimental conditions may vary within studies (mode of LPS exposure, LPS 486 concentration etc.), it is evident how after a LPS challenge the influx of inflammatory 487 cells is always described. The neutrophils mobilisation and release of pro-inflammatory 488 cytokines is an early event and 4 hours represents a suitable time point at which the 489 neutrophils activation has already started. In some studies that considered a wider time 490 window, the neutrophils concentration was showed to peak 24 h after the challenge with 491 a further decline at 48 h. Additional studies are required to further elucidate the kinetic in 492 the model used in this experimental chapter and those will consider a longer time range 493 with multiple time points analysed. 494 495 The design and optimisation of the LPS model in this experimental chapter considered 496

variables as animal welfare, severity of the procedure (3R) as well as the dose of the trigger agent the animals had to be exposed to. The animals should receive a dose that yet produces a measurable change in the endpoint or marker of interest, despite not causing

497

side effects that may hinder the detection of the pharmacological effect or bring to misinterpretation of the results or cause unnecessary and suffering events to the specie.

501

502

503

504

505

506

507

508

509

510

511

512

513

514

515

516

517

518

519

520

521

522

523

499

500

In a dose-response and kinetic study carried out by Larsson (Larsson et al., 2000), C57BL/6JBom mice were exposed to different nebuliser concentration of LPS (range of 0.001 to 1 mg/mL) (E. Coli, O128:B12) using a nose-only Battelle exposure chamber. The study showed that the increase of the LPS concentration resulted in an increased accumulation of leukocytes recovered 16 h after the LPS exposure. Despite the different species used, exposure mode and the time window adopted (16 h vs 4 h), the LPS dosedependency detected in this experimental chapter is in agreement with the finding of Larsson and others. In this context, it is important to highlight that a systematic comparison of LPS doses and corresponding outcomes used in preclinical models and available in the literature is often challenging. There is a lack of consistency in how the LPS concentration is reported. This can be described as the value of the concentration (mg/mL) loaded in the nebuliser reservoir or as the dose administered directly to the lung if an intratracheal administration is performed. In other studies, the delivered dose (mg/kg) is reported with a theoretical estimation of the lung deposition equal to 20 %. In the same study, the kinetics of the inflammatory response were studied using a low (0.1 mg/mL) and high dose (1 mg/mL) of LPS. The accumulation of neutrophils and eosinophils after the low and high dose exposure did not differ significantly during the first 12 h. At high dose, the total neutrophils and eosinophils number further increased and peaked at 24 h, whereas the inflammation peaked and resolved 12 h after the challenge for the low-dose group. This demonstrated an early cell influx at the low dose and sustained cell influx overtime for the high dose. The number of cells returned to prechallenge levels 48 h after the challenge.

524

525

526

527

528

529

530

531

532

In this experimental chapter the LPS dose-dependency was described using three different doses of LPS (0.1-0.2-0.5 mg/mL). In agreement with other scientific studies, results shows that the exposure to increasing concentration of LPS results in increased number of leukocytes recovered. However, it would be beneficial to newly carry out the experiment increasing the number of subjects in each group. Indeed, the small number of animals in each group (n=2) did not allow to evaluate whether the data follows a normal distribution or not. Therefore, the statistical difference within groups was not investigated.

Larsson and co-workers showed that the LPS-induced inflammation was also correlated to an increased level of pro-inflammatory cytokines when the profile of cytokines in the lung tissue was evaluated after low and high dose. The low dose induced a transient and early (2 h after the challenge) onset for the pro-inflammatory chemokine analysed; in contrast the high dose induced a delayed but more sustained release of the same cytokines (Larsson et al., 2000). The expression of TNF- α and other cytokine was strongly exhibited in the late phase (20 h) of the inflammation process after high-dose exposure. The key role of TNF- α in the recruitment of the neutrophils in the lungs is discussed and demonstrated by Kips and co-workers, who showed that its inhibition in rats exposed to LPS reduced the neutrophil influx (Kips et al., 1992). Multiple rats were placed in a whole-body chamber and exposed to aerosolized LPS (0.001 mg/mL and 0.01 mg/mL) for 30 min. Lungs were lavaged 1.5 h after the endotoxin exposure and concentrations were detected. The exposure to the low and high dose of LPS resulted in 17.9 \pm 6.9 and 80.5 ± 7.8 U/mL, respectively, with no TNF- α detected when the rodents were exposed to saline. Interestingly, the exposure to a pre-treatment with anti-TNF antibodies resulted in partial inhibition of the neutrophil influx, indicating that TNF- α is a mediator of the endotoxin-induced inflammation (Kips et al., 1992)

As previously mentioned, two of the possible routes to achieve pulmonary exposure of LPS in preclinical models are intratracheal instillation and inhalation. More generally, the use of intratracheal instillation when administering an endotoxin to establish an inflammation model or a drug to treat the inflammation represents a source of variability especially when comparing findings obtained from different studies and carried out in different laboratories. One source of variability is represented by the use of a fixed volume of air immediately after the instillation of the agent of interest. Results reported in this experimental chapter showed that this minor protocol modification consistently impacted the final distribution of the substance of interest. The use of 1 mL air allows a more uniform distribution of the instilled volume, which otherwise deposit in an uneven pattern throughout the lungs. Those results highlighted how the use of the intratracheal administration increases the variability of the outcome, concluding that the inhalation is a superior route of administration for LPS in the designed inflammation model.

The variability of lung response after exposure to LPS via intratracheal instillation (5 mg/kg) and nose-only inhalation of an aqueous LPS aerosol (concentration 100 mg LPS/m³) for 6 h was investigated in another study (F. Liu et al., 2013). It is not surprising

that the inhalation route provided a more uniform type of injury, whereas the dose needed to induce lung injury was lower when using inhalation compared to intratracheal instillation. The total cell count and cytodifferentiation in BAL were measured alongside other endpoints at 1, 3, 7, and 14 days after intratracheal bolus instillation or after inhalation of LPS. The total cell count and polymorphonuclear neutrophils differ according to the method (bolus intratracheal or inhalation) not in the LPS - dosed animals, but rather in the control - dosed animals. A difference was noticeable for the control groups, with groups receiving vehicle via intratracheal administration showing a higher number of infiltrated cells (total and differential) compared to inhalation, highlighting an inflammation induced by the instillation method itself compared to inhalation. Hence concluding that the inhalation method appeared superior compared to the intratracheal method. In addition, the study demonstrated that the same quantitative outcome was achievable by using a lower dose by inhalation compared to intratracheal administration. Indeed, the same conclusion was drawn by Smith and others in two different studies (Foster et al., 2003; Smith et al., 2011) where LPS was administered via intratracheal route or inhalation.

Indeed, when investigating the benefits of the pulmonary route in pre-clinical models, intratracheal instillation is one of the most well-known and used methods. However, the use of an excessive volume of substance of interest (either endotoxin or therapeutic drug) may affect the results and lead to misinterpretation and cause a lung damage itself. It could result in uneven lung distribution and responses caused by non-homogeneous distribution of the substance of interest. In addition, the administration of high volume may alter the lung clearance mechanisms and impact any kinetic study of the instilled material, making the pulmonary delivery via instillation considerably less controlled than the inhalation.

The exposure to an inhaled material requires an estimation of the dose used. Indeed, in preclinical as in clinical models only a percentage of the total dose delivered will impact the lungs of the subject and be available to exert a therapeutic effect. For example, Larsson and co-workers (Larsson et al., 2000) assumed that only 20% of the delivered dose via inhalation (nose-only system) was deposited into mice lungs. Therefore, they calculated that the lung burden provided by the concentrations of 0.1 mg/mL and 1 mg/mL was of 0.02 and 0.2 mg/mouse respectively. An alternative way to estimate the

delivered dose is using the equation developed by a working group of the Association of Inhalation Toxicologists. The equation (**Equation** 5.1) defines the delivered dose (DD) and takes into account the concentration of substance in the air (mg/L), the respiratory minute volume or the volume of air inhaled in one minute (RMV) (L/min), the duration of exposure (D) (min), the proportion by weight of particles that are inhalable by the test species i.e. inhalable fraction (IF) and the body weight (BW).

Equation 5.1 Calculation of the delivered dose achievable via inhalation

$$DD = \frac{C \times RMV \times D \times IF}{BW}$$

The RMV for different species (mice, rats, dogs and non-human primates) can be calculated using the formula below (**Equation** 5.2):

Equation 5.2 Calculation of respiratory minute volume

$$RMV(L/min) = 0.608 x BW(kg)^{0.852}$$

where BW does correspond to specie bodyweight expressed in kg.

breathing zone areas.

This equation represents an extremely valuable tool to estimate the dose at which the specie is exposed which usually differ from the theoretical dose. This is the case of a study conducted by Liu (F. Liu et al., 2013). Rats were exposed to an LPS intratracheal dose equal to 5 mg/kg. However, the lung burden or thoracic dose calculated using the Equation 5.1 resulted of 2.6 mg/kg.

In addition to the use of this equation which enables to have an estimation of the delivered dose, an ideal inhalation system in preclinical studies should be characterized by controlled temperature and humidity of the nebulised solution. The integrity and stability of the aerosol generation and exposure should be monitored real time as well as the total mass of the API of interest at which the animal species is exposed to. Usually this is allowed by the gravimetric determination of the inhaled molecule via filters located at the

The inhalation system built in this experimental chapter was less controllable as not coupled with a real time analysis of the breathing zone area of the guinea pigs. Despite it was unlikely to have an estimation of the deposited dose of LPS, successful deposition of the endotoxin particles was confirmed by the increased inflammatory cells recovered in the BALF. The Equation 5.1 will be used in Chapter 6 to evaluate the deposited dose of inhaled RFM.

The anti-inflammatory activity of RFM in COPD models is well-known. In 2005, orally administered RFM was shown to partially improve lung inflammation and completely prevent the parenchymal destruction induced by CS (Martorana et al., 2005). Indeed, these therapeutic actions of RFM were evaluated in an acute and chronic mice model. The anti-inflammatory activity of orally administered RFM was also described in Brown Norway rats as RFM inhibited eosinophilia and LPS-induced circulating TNF-α (Bundschuh et al., 2001). The activity of RFM in attenuating the pulmonary inflammation has also been demonstrated clinically. Healthy subjects were challenged with segmental endotoxin and treated for 28 days with placebo or orally RFM (500 µg). After 29 days a baseline BALF was performed followed by exposure to segmental endotoxin challenge (4 mg/kg). After 24 h, cells in the lungs were collected and counted. RFM was showed to reduce by 39% and 74% the number of eosinophils and neutrophils respectively compared to placebo. The number of macrophages and lymphocytes showed unchanged if subjects received placebo or RFM (Hohlfeld et al., 2008). The model established in this chapter was able to demonstrate similar anti-inflammatory activity of RFM, where a single oral dose was shown to significantly reduce the lung

5.6 Conclusion

A preclinical model was established which mimics the lung inflammation associated with COPD exacerbations. A dose-dependency was described with increasing LPS doses (0.1, 0.2 and 0.5 mg/mL) resulting in increased total and differential cell count recovered from the BAL. The responses measured for the biomarkers selected to investigate the modulation of the inflammation were comparable with those reported in the literature. The results illustrated that a single exposure via nebulisation to LPS (nebuliser concentration of 0.2 mg/mL) can elicit an acute and significant increase of cell infiltration

inflammation expressed as neutrophilia in the lungs of LPS challenged guinea pigs.

into the airway, making this model useful for studying inflammation. The model has ease of use and the cost effectiveness, especially when compared to the laboratory equipment that a nose-only system or a chronic exposure to CS would require. The main limitations, which adds to the intrinsic variability of LPS response in preclinical models, concern the calculation of the aerosol concentration and the guinea pig lung function monitoring which was not performed. The modulation of inflammation by orally administered RFM (0.5 mg/kg) was demonstrated. The LPS-induced neutrophilia was reduced by a preventive protocol of RFM in the designed model, highlighting its suitability to investigate the exposure of the same drug by the pulmonary route. This response will serve in Chapter 6 to investigate the potential of inhalation to deliver RFM effectively for an anti-inflammatory action and to test formulation strategies. In summary, this model was shown to be fit for purpose to investigate the anti-inflammatory activity of therapeutic agents and be used to study their administration by pulmonary delivery.

CHAPTER 6: In vivo anti-inflammatory activity of 678 nebulised roflumilast 679 680 6.1 Introduction 681 682 The design of a formulation for lung delivery as opposed to oral or intravenous 683 684 administration comes with particular challenges. The deposition of a formulation in the 685 lungs and local therapeutic activity depends on a complex series of factors, including 686 particle properties (density, aerodynamic diameter), respiratory physiology, fluid 687 dynamics, the physical deposition mechanisms and type of inhalation device employed 688 (Hofmann, 2011). 689 Despite the airway system and the particle deposition being dependent on multiple 690 factors, three main mechanisms dictate particle deposition in the lungs: impaction, 691 sedimentation, and diffusion (Carvalho, Peters, et al., 2011; Darquenne, 2012; Heyder, 692 2004; Hofmann, 2011). To a lesser extent interception and electrostatic precipitation are 693 also relevant, particularly for elongated fibrous particle or chain-like aggregates and for 694 electrically charged particles, respectively. 695 Diffusion is the mechanism that dictates the deposition of particles smaller than 0.5 µm, 696 albeit these carry little mass and are less relevant in terms of pharmaceutical aerosols. 697 Deposition is correlated to particle size and to respiratory rate, and increases when longer 698 distances are travelled by particles with smaller size under the influence of increasing 699 respiratory cycle period. The total diffusional deposition decreases with increasing 700 particles size up to 1 µm. 701 Particles larger than 0.1 µm deposit by diffusion but also by sedimentation, which is under 702 the influence of gravity, which increases with increasing particle mass, particle density 703 and respiratory cycle period, whereas particles with a diameter >1 µm deposit by both 704 sedimentation and by impaction, producing the typical U shape of the total deposition 705 curve (Figure 6.1).

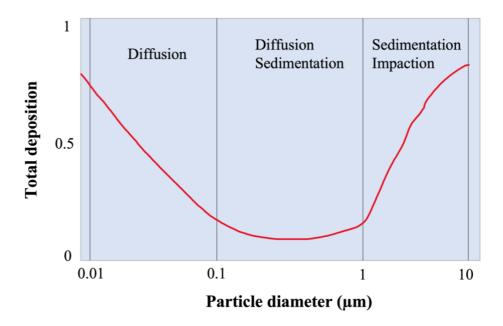


Figure 6.1 Schematic representation of relationship between particle deposition mechanisms in the lungs and particle aerodynamic diameter.

Impaction plays an important role in the deposition of particles in the tracheobronchial region – where the air speed is high, and the flow is turbulent - whereas the gravitation sedimentation predominates in the smaller bronchi and bronchioles. In the alveolar region particles deposit by both sedimentation and diffusion (Heyder, 2004; Labiris & Dolovich, 2003). A schematic representation of the mechanisms of particle deposition in the relationship with the particle size is displayed in **Figure** 6.2.

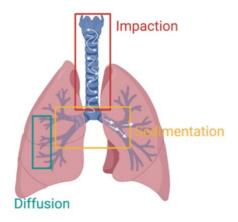


Figure 6.2 Schematic representation of three main mechanisms of particles deposition in the lungs based on the particle aerodynamic diameter: impaction, sedimentation and

715 diffusion. The figure also schematically represents the turbulent flow (oro-tracheal

716 region) and the laminar flow (respiratory airways).

717 Inertial impaction is the predominant deposition mechanism for particles with an

aerodynamic diameter $>5 \,\mu m$ as particles have enough momentum to keep their trajectory

despite changes in the airflow and are not able to follow airstream direction changes

resulting in impaction of the particles on the walls of the airways, especially in the upper

airways and at the bifurcations. The probability of a particle depositing by impaction is

described by the Stokes number (**Equation** 6.1) – the higher the Stokes number the higher

723 the probability of impaction into the airways.

724

725

719

721

722

Equation 6.1 Stokes' number equation

$$Stk = \frac{\rho \times d^2 \times V}{18 \times \eta \times R}$$

Where ρ is the particle density, d² is the particle diameter, V is the air velocity, η is the

air viscosity and R the airway radius. Larger particles are transported by inertial impaction

which increases with particle size, particle density and airflow rate as well (Heyder,

729 2004).

730

728

731 The gravitational sedimentation is correlated to the gravity. It mainly occurs in the small

airways or in the alveolar cavities where the space is restricted. The settling velocity is

expressed by **Equation** 6.2 and increases with particle size and residence time, hence

breathing manoeuvres such as breath-holding increases the probability of particle

735 deposition by this mechanism.

736

737

Equation 6.2 Settling velocity

$$Vs = \frac{\rho \times d^2}{18\mu} \times g$$

738 With g being the gravitational acceleration.

In contrast, smaller particles ($< 0.5 \ \mu m$) are characterized by Brownian motion (motions of particles due to their collision with gas molecules) and will more likely deposit into the lungs by diffusion (Williams et al., 2011). Opposite to impaction and sedimentation, the deposition by diffusion is inversely related to particle size (Darquenne, 2012; Williams et al., 2011).

The aerodynamic diameter is determined mainly by measuring deposition by impaction. It is defined as the diameter (d_{ae}) of a sphere with density of 1 g/cm³ and with the same velocity in the air as the particle of interest. It is dependent on the actual diameter of the sphere (d) and the spherical particle density (ρ) by the following equation (**Equation** 6.3):

Equation 6.3 Aerodynamic particle diameter (dae)

$$dae = d \times \sqrt{\frac{\rho}{\rho 0}}$$

One the most useful and used parameters to describe the particle size of an aerosol is the mass aerodynamic diameter (MMAD). It divides the particle population in two, with 50% of the particle population being smaller and 50% larger of the stated value. The geometric standard deviation (GSD) describes the dispersity of the particle size distribution around the MMAD value. It can be summarized that particles with a MMAD between $5-10~\mu m$ are mainly deposited in the large conducting airways and oropharyngeal region, whereas smaller particles with a MMAD between 1 and 5 μm will likely deposit in the small airways, with > 50% of the particle with aerodynamic diameters of 3 μm deposited in the alveolar region. Smaller particles (< 3 μm) have a higher chance (80%) to deposit into the lower airways (of which 50 - 60% in the alveoli) (Labiris & Dolovich, 2003).

Parameters as the MMAD, the GSD and the FPF - defined as the amount of the deposited dose that lies below the 5 µm range - are key to assess the likely distribution pattern of an aerosol in the human respiratory tract. One of the most used and well-known *in vitro* tests to provide those metrics is the deposition in a multistage cascade impactor, called Next Generation Impactor (NGI) (Marple Virgil A., 2003). Combined to a vacuum pump set at a clinically relevant flow rate recommended by the Pharmacopeia (General Chapters_ 601_ Aerosols, Nasal Sprays, Metered-Dose Inhalers, and Dry Powder Inhalers. United Stated Pharmacopeia (USP) 35, 2012) and matched to the inhalation

device of interest, this equipment can fractionate the aerosol based on the aerodynamic diameter. Particles with sufficient inertia, will deviate from the air stream, go through several nozzles with specific particle size cut-off and impact on plates (also called stages). The presence of multiple nozzles, each with a specific cut-off size, will allow the particles to impact and deposit on specific stages according to their aerodynamic diameter, providing a particle distribution. Importantly, the flow rate through the impactor determines the cut-off diameters which are function of nozzle geometry, particle density and air velocity in the nozzle (de Boer et al., 2002). There are eight stages in the NGI and the measurement of mass deposited in each stage allows metrics to be calculated from the cumulative mass-weighted aerodynamic particle size distribution (Marple et al., 2004; Marple Virgil A., 2003). This equipment is a valuable tool for measuring particle size distribution and providing an estimation of regional particle deposition in the lungs, despite the NGI not providing an exact replica of lungs' sections. In addition, the measurements provided by the NGI represent only a single approach that must be combined with other *in vitro* investigations. Indeed, the cascade impactor has some limitations: i) in contrast with the human inspiratory profile which has a varying flow rate, the NGI operates at constant flow in order to preserve the effective cut-off diameter; ii) temperature and humidity of human

lungs are not replicated in the apparatus (Mitchell et al., 2007).

A detailed prediction of the aerosol deposition is extremely complex because it depends on many factors including the airway calibre and the lung anatomy. In particular it should be considered that: i) the presence of a lung disease, such as COPD or cystic fibrosis is usually associated with alteration of normal physiology and structure hence the need to consider them in the prediction of particle deposition; ii) often a particle deposition prediction takes into account the physiology and structure of the human lung whereas *in vivo* models often use rodents (as in this thesis) as the first species to investigate the therapeutic potential of inhaled medicines.

Inflammatory lung conditions, such as COPD are characterized by obstruction of the airways, increase production of mucus and a general and consistent alteration in the lung architecture (Barnes et al., 2015). The lungs of COPD patients are characterized by narrowing of the bronchioles (bronchiolitis) or enlargement of distal airspace (emphysema), and these modifications may alter the normal deposition pattern (Labiris & Dolovich, 2003). When designing a drug delivery system for the lungs of patients with

similar conditions, the deposition pattern in presence of those alteration is a key aspect as there is a possibility that the drug delivered will not deposit in the obstructed region which can also be the target region. Laube (Laube et al., 1989) studied the lung distribution of 0.9% saline labelled with ^{99m}Tc sulphur colloid in healthy subjects and patients with CF. Subjects were exposed to a polydisperse radiolabelled aerosol (MMAD = $1.12 \mu m$) and the distribution of aerosol was uniform in the healthy subjects, whereas aerosol distribution in the lungs of CF patients appeared non uniform with regions of higher, lower, or no deposition. On the other side, Jakobsson (Jakobsson et al., 2018) studied the particle deposition pattern in healthy and COPD subjects exposed to a nanometer size range aerosol and reported an altered deposition of inhaled NPs between the groups. Healthy never-smoking subjects, asymptomatic active and former smokers and subjects with COPD were exposed to an inhaled aerosol of monodisperse polystyrene latex nanospheres (50 and 100 nm) and lung deposition was measured after a 10 s breath-hold; results showed no difference between healthy never-smokers and former smokers but subjects with emphysema had a lower deposition fraction mainly due to the emphysema and to the alterations of the lung morphology. There are, however, discrepancies within the lung deposition studies of NPs reported in the literature (especially important in the matter of pollution and environmental studies) as different methodologies are used or different degree of lung inflation or residence time of the aerosol are considered.

The weak link between preclinical models and clinical studies in terms of prediction of particle deposition, translocation and response is related to the differences of airway morphology and breathing parameters between human and the rodent species which are often used as pre-clinical models. As particles that are inhalable for humans may not be inhalable to rodents, experimental adjustments may be necessary. In addition, rodents and rabbits are compulsive nose breathing species, making the nasal route rather than oral inhalation the means of aerosol administration. Nasal filtration in rodents influences the total amount of particles available for lung deposition and since particle clearance in the nasal region can be rapid, longer exposure period may be required to increase the delivered dose.

In addition, for nasal breathing the inhalability is correlated and dependent on the size and orientation of the nasal opening hence it can be determined when comparing animals 839 and human deposition studies. Another factor is the minute ventilation which is used to 840 estimate the delivered dose. 841 A critical aspect in terms of differences in particle deposition is the geometry of the lungs, 842 which is dissimilar between animals and humans. Detailed nasal geometry in Fischer 344 843 rats has been described in the literature (Kimbell et al., 1993). Raabe and colleagues 844 (Raabe et al., 1988) investigated the deposition pattern of aerosol particles with an 845 aerodynamic diameter up to 10 µm in multiple species including mice, guinea pigs, 846 hamsters and rabbits. Animals were exposed to monodisperse aerosol of fused 847 aluminosilicate particles labelled with radioactive ¹⁶⁹Yb via a modified vibrating liquid 848 stream generator for 45 minutes. Results showed that particles with MMAD > 3 µm 849 mainly deposited in the nasal-pharyngeal region whereas particles with MMAD > 10 µm 850 completely deposited in the nasal-pharyngeal and laryngeal region with no deposition in 851 the pulmonary tract. 852 The advantages of combining the newest tools of the nuclear medicine to allow a more 853 detailed evaluation of particle deposition with the use of a polydisperse aerosol population 854 which more closely resembles the currently pharmaceutical aerosol used were explored 855 by Kuehl in 2012 (Kuehl et al., 2012). Aerosol deposition pattern was investigated as a 856 function of particle size in rats and mice using radiolabelling techniques applied to a 857 polydisperse aerosol of radio labelled particles with MMAD of 0.5, 1.0, 3.0 and 5.0 µm, 858 which were nebulised via air jet nebuliser to four mice and four rats using a nose-only 859 exposure system in combination with SPECT/CT imaging. Unsurprisingly, results 860 showed that the deposition fraction decreases with the increasing particle size with higher peripheral deposition for smaller particles. Smaller particles showed an increase 861 deposition in the lungs and in the peripheral lungs compared to bigger particles. 862 863 A similar and very extensive study was conducted by Asgharian (Asgharian et al., 2003) 864 which exposed fifty-five female Long-Evans rats to a monodisperse radiolabelled aerosol 865 with MMAD in the range 0.9 to 4.2 µm. Deposition data revealed that the particle 866 deposition fraction, defined as the amount of material deposited in the tissue of interest 867 divided by the total amount of material inhaled, decreased with increasing particle size 868 due to a reduction in respirability correlated with an increase in particle size. 869

This chapter aims to explore the therapeutic potential of an inhalable NPs-based

formulation encapsulating RFM using a model of lung inflammation in guinea pigs. The

870

871

experimental methods and formulations adopted have been described in the previous chapters, in which the suitability of those methods was established.

The choice of the inhalation device used for the pulmonary administration to guinea pigs was based on the need to aerosolise a liquid formulation, which is the approach typically used in early development. The device employed in this investigation was a mesh nebuliser (Aerogen Pro), which is commonly used in hospital settings to administer medical aerosols to patients. Generally, a nebuliser is a device that can convert a liquid into a droplet aerosol suitable for inhalation. There are three types of nebulisers: air-jet, ultrasonic and mesh nebuliser (Ari, 2014). Jet nebuliser required large (2 to 10 L/min) volume of pressurized gas to draw medication up through a capillary tube; however, they can be difficult to use due to the need of compressed gas and additional tubing. In the ultrasonic nebuliser the aerosol is produced due to the vibration of a piezo electric crystal, and they can be large-volume or small-volume. Downsides of those devices include large residual volume and degradation of heat-sensitive material. On the other hand, mesh nebuliser represents newer technology with a mechanism of aerosolization based on the vibration of a mesh with multiple apertures with a specific diameter (in the case of the device used in this work, the aperture range was between 3.5 and $5 \mu m$).

In contrast to ultrasonic and jet nebuliser, the mesh nebuliser employs single-pass technology, avoiding recirculation of the droplets, avoiding heating and reducing the extent of shear forces while in the reservoir. These characteristics have made them suitable also for delivery of labile molecules such as proteins and mAbs (Matthews et al., 2020).

The aerosol delivery of NPs to the lungs represents an interest topic of the nanomedicine as it includes both the advantages of the pulmonary route and those of the nanocarriers (N. Osman et al., 2018; N. M. Osman et al., 2020). The administration of a therapeutic directly to the lungs allows to bypass the gastrointestinal tract and deliver a higher dose to the target site while using a smaller total dose compared to other routes of administration. The advantages of delivering drug in a nanocarrier, include a longer retention at the site of action, the possibility of sustained release and a reduction of the systemic side effects, the option to improve drug solubility due to the encapsulation of the drug in the nanocarrier, and the avoidance of the clearance mechanisms which may further prolong the residence time.

Rather than immediately assess the delivery of a nanocarrier to the lungs based on the NPs in microparticle (NEMs), preliminary experiments focussed on a formulation strategy based on the delivery via a simple nebulisation of drug *in vivo* and the nanoparticle suspension *in vitro*.

909

910

911

912

913

914

915

905

906

907

908

To our knowledge, there are no currently clinical trials investigating therapies based on inhalable albumin NPs and pre-clinical studies investigating the pulmonary delivery in rodents species are very few, usually employing basic strategies to deliver the nanocarrier to the lungs such as the intratracheal route (often achieved via the use of a powder insufflator called PennCentury). A detailed overview of the downsides of the intratracheal route of administration were highlighted in Chapter 5.

916

917

918

919

920

921

922

923

924

925

926

927

928

929

930

931

932

933

934

935

936

937

938

In contrast, liposome delivery via the pulmonary route has gained considerable success in pre-clinical and clinical studies (Carvalho, Carvalho, et al., 2011). A liposomal amikacin suspension, Arikayce® for the treatment of the Mycobacterium avium complex lung disease via nebulisation has been approved by the EMA and the FDA (Arikayce Liposomal - Product Information; Khan & Chaudary, 2020). Various studies have also successfully demonstrated in vivo the potential of inhalable liposome compared to other routes of administration or formulation. An example is provided by one of the studies conducted by Koshkina (Koshkina et al., 1999) where three different strains of mice (C57BL/6, Swiss nu/nu and BALC/c mice) were exposed to inhaled camptothecin formulated in dilauroylphosphatidylcholine liposomes via Aerotech II nebuliser (MMAD of 1.6 µm). The drug deposition in the lungs was demonstrated to be higher when the drug was administered in liposomes via inhalation compared to intramuscular administration of camptothecin (control). Interestingly, prior to this study the intramuscular administration of camptothecin was considered the most effective route of administration in immunodeficient mice in cancer models, whereas this study concluded that the aerosol was more advantageous. In addition, they showed that the drug concentrations achieved at 30 min following inhalation in the aerosol-treated mice were greater compared to those in the non-aerosol-treated mice. The same liposome-based formulation was adopted in a different study (Koshkina et al., 2001) to encapsulate paclitaxel as treatment for a murine renal carcinoma pulmonary metastases model. The liposomes were nebulised with an Aero-Mist jet nebuliser and the therapeutic efficacy compared to intravenous administration (control). Results showed higher concentration

| 939 | of pac | clitaxel in the lungs when administered via inhalation compared to control | | | | |
|-----|--|--|--|--|--|--|
| 940 | (intravenous administration), with a slower clearance of the drug from the lung as well. | | | | | |
| 941 | | | | | | |
| 942 | 6.2 | Aims and objectives | | | | |
| 943 | | | | | | |
| 944 | The overall aim of this series of experiments was to investigate the anti-inflammatory | | | | | |
| 945 | activity of RFM delivered by the pulmonary route as a precursor to optimising this | | | | | |
| 946 | therapeutic effect by formulating as RFM-HSA-NPs. The first experimental step carried | | | | | |
| 947 | out was based on the formulation and characterisation of a RFM suspension in a | | | | | |
| 948 | biocompatible vehicle of saline, Tween® 80 and DMSO and its nebulisation to reduce the | | | | | |
| 949 | lung inflammation in LPS-challenge guinea pigs. The practicality of NPs suspension | | | | | |
| 950 | admin | stration via nebulisation was also investigated in vitro by determining the impact | | | | |
| 951 | of the nebulisation on the physiochemical characteristics of the nanocarrier. | | | | | |
| 952 | Specific objectives included: | | | | | |
| 953 | 1. | Formulate a RFM suspension and evaluate of particle size and geometric diameter | | | | |
| 954 | | using Morphologi 4; | | | | |
| 955 | 2. | Aerodynamic assessment of the nebulised roflumilast suspension using the Next | | | | |
| 956 | | Generation Impactor; | | | | |
| 957 | 3. | Calculate the RFM delivered dose (DD) to guinea pigs during the nebulisation | | | | |
| 958 | | cycle; | | | | |
| 959 | 4. | Evaluate the effect of nebulised RFM on lung inflammation using the guinea pigs | | | | |
| 960 | | LPS model; | | | | |
| 961 | 5. | Investigate the physiochemical stability of NP to nebulisation using Dynamic | | | | |
| 962 | | Light Scattering. | | | | |
| 963 | | | | | | |
| 964 | 6.3 | Methods | | | | |
| 965 | | | | | | |
| 966 | 6.3.1 | Manufacture and characterisation of roflumilast suspension prior to in vivo | | | | |
| 967 | admin | istration | | | | |
| 968 | | | | | | |
| 969 | 6.3.1.1 | Manufacture of roflumilast suspension | | | | |
| 970 | RPM s | suspensions (100 and 500 μg/mL) were prepared by suspending the drug powder in | | | | |
| 971 | a vehic | a vehicle of sodium chloride $0.9\%/0.2\%$ Tween 80 and 0.05% DMSO (Nials et al., 2011; | | | | |

Villetti et al., 2015). Firstly, RFM was weighed and suspended in the appropriate volume

of sodium chloride 0.9%/0.2% Tween 80 by a sonication process (10 minutes). Then an aliquot of DMSO corresponding to 0.05% of the total volume was added and the suspension was probe sonicated for 30 minutes (amplitude 30 mA).

The development and characterisation process of RFM suspensions prior to *in vivo* administration is illustrated in **Figure** 6.3.

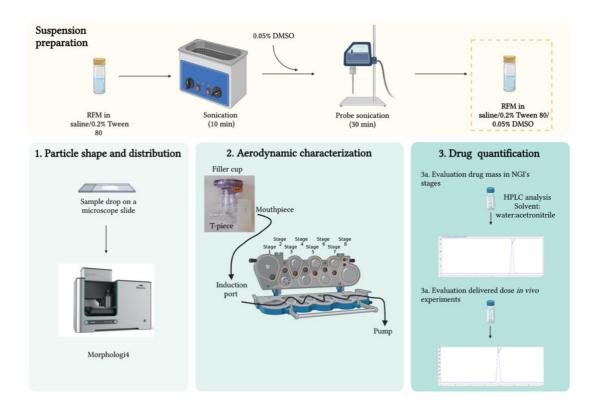


Figure 6.3 Schematic representation of manufacture, characterisation, and aerodynamic assessment of nebulised aerosols of roflumilast suspension prior to in vivo administration. After the preparation, the size and the shape of the particles were evaluated using Morphologi4, the aerodynamic characteristics evaluated with the Next Generation Impactor (NGI).

6.3.1.2 Ensuring dose homogeneity, investigating particle shape and geometric size distribution using Malvern Morphologi 4 system and drug concentration

Size and shape of the drug solid particles in the RFM suspension (500 µg/mL) prepared as described above were investigated. This analysis was carried out using a Malvern Morphologi 4 system (Malvern, UK) particle characterisation device. For each analysis,

an aliquot (10 μ L) was placed on a microscope glass slide and covered with a cover slip. The area of analysis (1.779 mm²) as well as the volume used was kept constant. The analysis was carried out at 50x magnification (0.5 – 50 μ m). Particles with elongated shape resulting from sample impurities and aggregates of particles (diameter 31 – 50 μ m) were excluded from the analysis. Stock solutions were prepared in triplicate and analysed in triplicate.

Furthermore, an assessment of the dose homogeneity within samples was carried out by investigating the concentration of RFM in each sample using the HPLC quantification method mentioned in paragraph 2.3.8. This ensured that the drug concentration achieved in each sample was consistent over time as multiple stock solutions were manufactured during the *in vivo* experiment. RFM stock solutions (100 and 500 μ g/mL) were prepared, and dilutions were carried out to produce suspensions of range 50, 100, 200, 300, 400 and 500 μ g/mL. Sodium chloride 0.9% + 0.2% Tween 80 was used as diluent. Prior to HPLC analysis, an aliquot (100 μ L) of each suspension (100 μ g/mL and 500 μ g/mL) was mixed with an aliquot (900 μ L) of HPLC grade acetonitrile. The samples were vortexed and the amount of drug in the sample calculated using the HPLC method described in section 2.3.8.

6.3.1.3 Aerodynamic characterisation of nebulised roflumilast using the Next Generation Impactor (NGI)

6.3.1.3.1 NGI settings

The aerodynamic characteristics of nebulised RFM suspension (100 and 500 μ g/mL) were evaluated using the Next Generator Impactor (NGI) attached to an Aerogen Nebuliser Pro (Aerogen Ireland Ltd., S/N 356, volume median diameter with saline 0.9% 4.82 μ m, average flow rate 0.38 mL/min) via a mouthpiece. The nebuliser was attached to an ISO 15 mm t-piece which was directed towards the induction port with a mouthpiece and the NGI system attached to a vacuum source. The experimental set-up (apart from the vacuum pump) is illustrated in **Figure** 6.4. The assembled impactor coupled with the induction port and the mouthpiece were refrigerated at 5°C in a cold room for 90 min prior to use in order to control the evaporation of droplets produced during the nebulisation (United Stated Pharmacopeia (USP) 35, 2012). The system was used within 5 min from the impactor removal from the refrigerator and the nebulisation of 2 or 4 mL RFM suspension was completed within 10 - 12 minutes of removal of the system from

the refrigerator. The NGI was coupled with a vacuum pump (Gast, Benton Harbor, USA) and the airflow was adjusted prior to refrigeration to 15 L/min using a flow meter attached to the induction port. The flow rate value was used as this value is a good approximation of the mid-inhalation flow rate achievable by a healthy adult breathing at 500 mL tidal volume (United Stated Pharmacopeia (USP) 35, 2012).

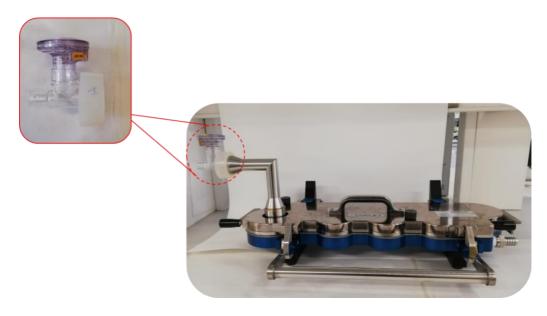


Figure 6.4 Experimental set-up for Next Generation Impactor (NGI) testing. (From left to right of picture) Aerogen® Pro nebuliser (Aerogen Ireland Ltd, S/N 356, volume median diameter with saline 0.9% 4.82 µm, average flow rate 0.38 mL/min) attached to an ISO 15 mm t-piece directed toward the induction port through a mouthpiece adapter (in the focused section).

6.3.1.3.2 Evaluation of the respirability of nebulised roflumilast suspension

The volume of RFM suspension to be nebulised was selected in order to ensure good drug detection in each stage of the cascade impactor whilst avoiding the streaking phenomena in the system stages. This was investigated by nebulisation of different volumes (2, 3 and 5 mL) of the RFM suspension (100 μ g/mL).

For each determination of the aerodynamic particle size distribution produced by nebulisation of the RFM suspension a fixed aliquot (2 mL or 4 mL for 500 and 100 μ g/mL, respectively) was added into the nebuliser reservoir and nebulised to dryness. To ensure a constant flow throughout the system, vacuum pump was activated 1 min prior to the nebulisation. After achieving nebulisation to dryness, vacuum pump and nebuliser

were switched off. The amount of drug deposited onto each stage was calculated using a previously validated HPLC method (section 2.3.8). Complete recovery of the deposited drug was achieved by rinsing each stage with a fixed volume of HPLC water-acetonitrile (ratio 30:70). The mouthpiece was washed with 1 mL, induction port and stages 1 to 5 with 5 mL and t-piece and stages 6 to 8 with 3 mL. These volumes were selected to provide a concentration of RFM that was readily quantified (data not shown). The suitability of the method used to recover the drug deposited in each section of the NGI was evaluated via nebulisation of 2 mL of saline/ 0.2 % Tween 80 + 0.05% DMSO (control) with following addition to each section of the impactor of a fixed volume of a known concentration of a RFM stock solution in water:acetonitrile (30:70) (50 μ g/mL). The amount of drug in each of those sample was calculated as described previously.

The linearity of the RFM concentration curve in water:acetonitrile (30:70) was determined in the range 0.05 - 150 μ g/mL by HPLC. To increase sensitivity, two calibration curves were built: a) 0.05 - 4.0 μ g/mL; b) 5 - 150 μ g/mL. Working dilutions were obtained from stock solutions of RFM in water:acetonitrile (30:70) (50 μ g/mL and 500 μ g/mL for the low range and high range concentrations).

The aerodynamic parameters calculated from the NGI assessment were FPF, fine particle dose (FPD), MMAD and GSD (**Table** 6.1).

Table 6.1 Definitions of the most used parameters for aerosol characterisation.

- FINE PARTICLE FRACTION (FPF): Fine particle dose Total emitted dose
- FINE PARTICLE DOSE (FPD): Mass of particles less than 5 μm in size within the total emitted dose
- MASS MEDIAN AERODINAMYC DIAMETER (MMAD): Diameter at which 50% of the particles of an aerosol by mass are larger and 50% smaller
- GEOMETRIC STANDARD DEVIATION (GSD): standard deviation of the logarithm of particle diameter

1062 Exposure of LPS-challenged guinea pigs to a pre-treatment of roflumilast via 1063 nebulisation using a whole-body chamber model 1064 1065 6.3.2.1 Calculation of *in vivo* delivered dose (DD) of roflumilast 1066 Guinea pigs were exposed to nebulised LPS and RFM via the use of a whole-body 1067 chamber model. As described in Chapter 5, an estimation of the dose of drug that animals 1068 have been exposed to is required. Hence, the delivered dose (DD) of nebulised roflumilast 1069 was calculated using Equation 5.1 and Equation 5.2. 1070 1071 6.3.2.2 Nebulised roflumilast administered to LPS-challenged guinea pigs 1072 Unanaesthetised Male Dunkin-Hartley guinea pigs (250 – 299 g) were placed individually 1073 and without restraint in the exposure chamber (47 cm (L) x 20 cm (H) x 20 cm (D)). In 1074 order to achieve the target delivered dose, the RFM stock solution of 500 µg/mL was used 1075 rather than the 100 µg/mL. The nebuliser filler cup was loaded with two aliquots of 2 mL 1076 each, for a total volume of 4 mL. The first aliquot was nebulised first followed 1077 immediately by the second aliquot. 1078 RFM and vehicle (control) were nebulised using Aerogen Pro® (Aerogen Ireland Ltd., 1079 S/N 356, volume median diameter with saline 0.9% 4.82 µm, average flow rate 0.38 1080 mL/min) attached to an ISO 22 mm t-piece fixed inside the lid of the chamber box and 1081 directed towards the inside of the glass box (470 (L) x 200 (H) x 200 (D) mm). LPS was 1082 nebulised following the same nebulisation settings mentioned in paragraph 5.3.2.2. 1083 1084 Subjects were divided in two groups which were exposed at time 0 to i) nebulised RFM 1085 (calculated delivered dose: 50 µg/kg); ii) nebulised sodium chloride 0.9%/ 0.2% Tween 1086 80 + 0.05% DMSO (control). The length of the total drug/vehicle exposure was 20 min. 1087 One hour after the drug exposure, animals were again placed in the exposure chamber 1088 and exposed to nebulised LPS (0.2 mg/mL, 10 mL). Four hours after the inflammatory 1089 challenge, animals were euthanized with an overdose of pentobarbital (1 g/kg) via an 1090 intraperitoneal injection. The trachea was cannulated and bronchoalveolar lavage was 1091 performed using 5 mL of filtered PBS that was gently instilled and withdrawn 3 times to 1092 flush the lungs using a 5 mL syringe. Bronchoalveolar lavage fluid was processed and 1093 analysed for cytokine and cell content as mentioned in paragraph 5.3.2.3.

| 1093 | An experimental procedures and conditions were reviewed and approved by the editics | | | | | |
|------|---|--|--|--|--|--|
| 1096 | committee of King's College London and conducted in accordance with the United | | | | | |
| 1097 | Kingdom Animal Scientific Procedures Act, 1986. Further details are mentioned in | | | | | |
| 1098 | section 5.3.3.2. | | | | | |
| 1099 | | | | | | |
| 1100 | 6.3.3 Physiochemical characterisation of nebulised NPs using the Dynamic Light | | | | | |
| 1101 | Scattering | | | | | |
| 1102 | | | | | | |
| 1103 | The impact of the nebulisation on the size, PDI and zeta potential of blank and drug loaded | | | | | |
| 1104 | HSA-NPs was investigated. An aliquot (0.4 mL) was placed in the filler cup of a Aerogen | | | | | |
| 1105 | Pro (S/N 356) attached to an ISO 15 mm t-piece which was tightly connected a 15 mL | | | | | |
| 1106 | falcon tube. The nebulisation was started, and the emitted aerosol collected as a | | | | | |
| 1107 | condensate in a 15 mL tube after the nebulisation. For size and PDI evaluation, an aliquot | | | | | |
| 1108 | of $100\mu\text{L}$ of the condensate fluid was collected and diluted 100-fold with double distilled | | | | | |
| 1109 | water to match the dilution adopted for NPs analysis pre-nebulisation (paragraph 2.3.3). | | | | | |
| 1110 | For zeta potential measurement, an aliquot of 5 μL was collected form the condensate | | | | | |
| 1111 | fluid and diluted 200-fold with double distilled water. Size, polydispersity index and zeta | | | | | |
| 1112 | potential were measured using the Dynamic Light Scattering (using a method described | | | | | |
| 1113 | in paragraph 2.3.3). | | | | | |
| 1114 | | | | | | |
| 1115 | 6.4 Results | | | | | |
| 1116 | | | | | | |
| 1117 | 6.4.1 Optimisation of roflumilast suspension prior to in vivo administration: | | | | | |
| 1118 | particle size, geometric diameter, and aerodynamic assessment | | | | | |
| 1119 | | | | | | |
| 1120 | 6.4.1.1 Particle shape and geometric size distribution of roflumilast suspension | | | | | |
| 1121 | The particle shape and geometric size distribution of RFM suspension prior to in vivo | | | | | |
| 1122 | administration was studied by Morphologi 4, using the circular equivalent diameter which | | | | | |
| 1123 | is the diameter of a circle calculated from the equivalent area of the measured particles | | | | | |
| 1124 | and the average D_{10} , D_{50} and D_{90} values. | | | | | |
| 1125 | The aspect ratio of the drug particles in the RFM suspension (500 $\mu g/mL$) appears with | | | | | |
| 1126 | irregular symmetry with some particles having an elongated aspect, whether others are | | | | | |
| 1127 | smaller and rounder. Moreover, most of the particles have rougher outlines (Figure 6.5). | | | | | |
| | | | | | | |

The investigation of the particle morphology of raw RFM was not performed but further studies may investigate this aspect to provide evidence for the evaluation of the effect of sonication (time and amplitude) performed during the suspension preparation on the particle aspect form.

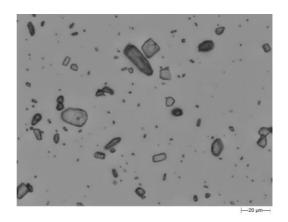


Figure 6.5 Representative particles images of 500 μ g/mL RFM suspensions using Malvern Instrument (50x). Scale bar is 20 μ m.

The geometric particle size was also evaluated and provided useful information regarding the quality of the formulated suspension prior to its nebulisation in a preclinical model. Results showed that 10%, 50% and 90% of the sample is smaller than 6 μ m, 13.2 μ m and 24.6 μ m respectively. Therefore, the particles in the suspension are in a size range between 6 and 24.6 μ m, although the obtained standard deviation of D₉₀ value is equal to 12.0 highlighting variability within measurements (**Table** 6.2). Unfortunately, any information about the raw material (roflumilast) and whether this was micronized or not was provided by the supplier (Sigma).

Table 6.2 Volume distribution statistics over 9 measurements for the RFM suspensions (500 μ g/mL) calculated using Morphologi 4 Malvern Instrument. Values are reported as mean and standard deviation (SD) of n=3 independent experiments, measurements performed in triplicate.

| | D [v, 0.1] | D [v, 0.5] | D [v, 0.9] |
|------|------------|------------|------------|
| Mean | 6.0 | 13.2 | 24.6 |
| SD | 2.15 | 3.83 | 12.0 |

The mesh aperture pores of the Aerogen Pro^{\circledast} nebuliser adopted for the RFM nebulisation have a size between $3-5.5~\mu m$. Based on the described geometric particle size, the nebulisation of the suspension will likely result in loss of a fraction of the total mass of RFM available which may be retained on the mesh. However, the aerodynamic assessment of the RFM suspension will provide further details on its respirability. It will also serve to estimate the delivered dose at which the species will be exposed to in the preclinical model.

6.4.1.2 Aerodynamic assessment of roflumilast suspension using the Next Generation Impactor (NGI)

The aerodynamic assessment of RFM in suspension was investigated using the NGI. The detection of the drug concentration in each stage of the cascade impactor was carried out using the method described in paragraph 6.3.1.3 combined with an HPLC method. For a more accurate detection of small RFM concentrations deposited in some of the stages, calibration curves were constructed in the ranges $0.05 - 4.0 \,\mu\text{g/mL}$ and then over the range $5.0 - 150 \,\mu\text{g/mL}$ ($R^2 = 0.9998$ and $R^2 = 0.9974$ respectively).

The method validation included the evaluation of the volume of RFM suspension that provided good quantification of RFM without overloading the impactor stages with the volume of liquid deposited (**Figure** 6.6). This analysis was carried out using the suspension of $100~\mu g/mL$. The visual inspection of the impactor stages after the nebulisation cycle did not reveal any overloading. In addition, the RFM recovered from each stage of the impactor was not affected by different volumes used, providing another indication that overloading or streaking was not occurring.

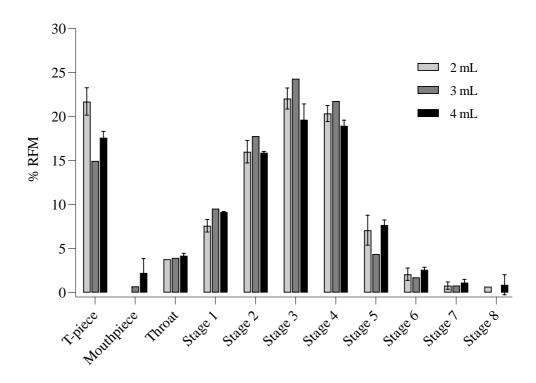
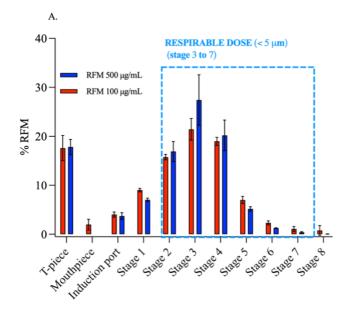


Figure 6.6 Evaluation of streaking phenomena. Roflumilast (%) recovery after the nebulisation of different volumes (2, 3, and 4 mL) of 100 μ g/mL roflumilast suspension. Results are shown as percentage of the total mass recovered from each compartment, represented as mean \pm SD of 1-2 independent experiments for each volume considered.

RFM suspensions were recovered in terms of percentage of drug deposited on each NGI stage when both the suspensions were separately nebulised at 15 L/min. The nebulisation of both the suspensions concentration resulted in \sim 17% loss of drug in the t-piece, with the highest amount of drug deposited in the stage 2 – 3 and 4 (**Figure** 6.7 **A**). The cut-off diameters of the NGI under its operating conditions are shown in **Figure** 6.7 **B**. The stages of interest when estimating the respirable dose are stages 3 to 7. With a cut off size from 5.39 μ m to 0.98 μ m, the nebulisation of 100 μ g/mL resulted in \sim 22% - 19% - 7% - 3% - 1% and 0.8% of drug deposited in stages 3 - 4 - 5 - 6 and 7 respectively. Nebulisation of the higher drug concentration resulted in the same % of mass recovered deposition trend, with percentages of RFM deposited in stage 3 of 28%, stage 4 of 21%, stage 5 of 6%, stage 7 of 0.4% and stage 8 of 0.07%.



| Stage | Cut-off Diameter (µm) |
|-------|--------------------------|
| 1 | 14.1 |
| 2 | 8.61 |
| 3 | 5.39 |
| 4 | 3.30 |
| 5 | 2.08 |
| 6 | 1.36 |
| 7 | 0.98 |

B.

Figure 6.7 A) Roflumilast mass (%) stage deposition from NGI when 100 μ g/mL (red) and 500 μ g/mL (blue) suspensions are nebulised at 15 L/min using an Aerogen Pro; (B) Cut-off sizes of Next Generation Impactor system at 15 L/min. Data is represented as mean \pm SD of five independent experiments. The percentage of the mass fraction in each stage has been calculated considering as total mass the sum of masses recovered in each part of the apparatus (t-piece, mouthpiece, throat and stages).

In terms of mass distribution across the stages of the NGI, the nebulisation of 4 mL of 500 μ g/mL (calculated concentration of RFM added to the nebuliser filler cup (mean \pm SD): 878.23 μ g/mL \pm 116.17) resulted in the following values of mass recovered from tpiece to stage 8: 37.3 μ g, 8.0 μ g, 14.9 μ g, 36.2 μ g, 57.4 μ g, 43.1 μ g, 11.1 μ g, 2.7 μ g, 0.9 μ g and 0.125 μ g (**Table** 6.3).

Table 6.3 Mass distribution across NGI stages recovered after the nebulisation of a volume of 4 mL of RFM suspension (500 μ g/mL). Data represent mean \pm SD of five independent experiments.

| NGI stage | Mass (µg) recovered |
|-----------------------|---------------------|
| T-piece | 37.3 ± 5.60 |
| Induction port | 8.0 ± 2.79 |
| Stage 1 | 14.9 ± 3.07 |
| Stage 2 | 36.2 ± 9.59 |
| Stage 3 | 57.4 ± 14.22 |
| Stage 4 | 43.1 ± 11.91 |
| Stage 5 | 11.1 ± 2.91 |
| Stage 6 | 2.7 ± 0.66 |
| Stage 7 | 0.99 ± 0.44 |
| Stage 8 | 0.125 ± 0.07 |

The aerodynamic parameters calculated from the NGI assessment were FPF, FPD, MMAD and GSD. Considering the FPF as the fraction or percentage of particle having an aerodynamic diameter less than 5 µm and therefore being suitable for lung deposition, the nebulisation of RFM suspension resulted in a FPF of 35% and 30.27% when the lower and higher drug concentrations suspensions were nebulised. In terms of mass of RFM that may deposit into the lung, a mass of 18.47 µg and 57.08 µg (FPD) was recovered for lower and higher drug suspension respectively. Besides this, the MMAD values calculated showed that 50% of the particles of the obtained aerosol have a size smaller than 6.42 µm and 6.59 µm for the 100 and 500 µg/mL drug suspension (Table 6.4). Although the suspension included particles with geometric size clearly greater than those that would pass through the mesh, there were more particles in the size range that would. The aerodynamic particle size may have differed from the geometric due to the non-spherical nature of the suspended particles and shear forces that operate during nebulisation. The evaluation of the geometric particle size of nebulised particles recovered from the NGI was not performed but it could inform the impact of the

nebulisation on the physical particle size distribution, and it can represent the focus of future studies.

The GSD is a measurement of the spread of the size in the population. The values were 1.95 and 1.76 for 100 μ g/mL and 500 μ g/mL (**Table** 6.4) showing a relatively tight aerodynamic particle size distribution after nebulisation.

Table 6.4 Aerosol performance parameters of two different concentrations of RFM suspensions in 0.9% saline/0.2% Tween 80 + 0.05% DMSO when nebulised with Aerogen Pro. Data represents mean (SD) of five independent experiments for 100 µg/mL (4 mL); four independent experiments for 500 µg/mL (2 mL).

| | 100 μg/mL | 500 μg/mL |
|----------------|--------------|--------------|
| FPF (%) | 35.00 (2.7) | 30.27 (3.0) |
| FPD (µg) | 18.47 (3.36) | 57.08 (6.43) |
| MMAD (µm) | 6.42 (0.18) | 6.59 (0.18) |
| GSD | 1.95 | 1.76 |

Total emitted dose used calculated as mass recovered from the mouthpiece, induction port and stages of the NGI (t-piece excluded as that mass could be considered as lost and it will not be available for lung deposition).

Nebulisation of 4 mL of 100 μ g/mL resulted in the recovery of 65.05 μ g of RFM while the nebulisation of 2 mL of 500 μ g/mL resulted in the recovery throughout the impactor (from t-piece to stage 8) of ~ 212 μ g of drug. When the RFM high dose suspension was nebulised, the mass of RFM deposited in stages 3 to 7 and therefore that can be considered as respirable was equal to 115 μ g (**Table** 6.5).The latter information is key when estimating the total mass of drug that will deposit in the lungs of the specie treated. These results will be used for the calculation of the DD described in the next paragraph.

Table 6.5 Evaluation of calculated masses available over different stages of the NGI after nebulisation. Data represent mean and (SD) for n=5 independent experiments for both concentrations.

| | 100 μg/mL | 500 μg/mL |
|---|---------------|-----------------|
| Total volume nebulised | 4 | 2 |
| (mL) | | |
| Total mass recovered from t-piece to S8 | 65.05 (14.63) | 211.7 (38.79) * |
| Mass recovered from | | |
| S3 to S7 (respirable | 33.21 (8.09) | 115.15 (21.47) |
| fraction/dose) | | |

^{*}Mass deposited in the mouthpiece not recoverable.

6.4.2 Pulmonary administration of roflumilast to LPS-challenged guinea pigs using a whole-body chamber model

6.4.2.1 Calculation of *in vivo* delivered dose (DD)

The calculation of the dose of nebulised RFM to which the guinea pigs were exposed was calculated using the Equation 5.1 and Equation 5.2. This estimation was carried out using the data obtained from the aerodynamic assessment of the nebulised drug suspension. As schematically represented in **Figure** 6.8, the delivered dose (and more precisely the concentration of drug in the air, C) was calculated as the total mass of RFM recovered from stage 3 to stage 7 – and equal to 115.15 μ g – divided by the total volume of the plexiglass chamber used as whole-body chamber (18.8 L).

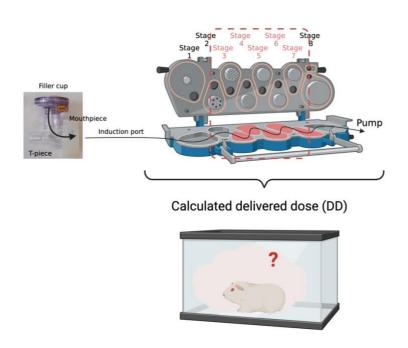


Figure 6.8 Estimation of the delivered dose (DD). Schematic representation of the calculation of the concentration of substance in the air (C).

The average animal weight was (0.316 kg \pm 0.008), calculated from the weight of each animal on the day of the experiment. The duration of each nebulisation cycle was equal to 5.5 min. The calculation of the delivered dose when taking into consideration two cycles of nebulisation (two aliquots, 2 mL each) resulted in a total delivered dose of 48.6 μ g/Kg, approximated to 50 μ g/kg. A dataset used to calculate DD is reported in **Table** 6.6 and a summary of the derivation of aerosol parameter used to calculate delivered dose is described in **Table** 6.7.

Table 6.6 Dataset of values used to calculate the delivered dose (DD).

| TABLE | |
|---|----------|
| Respirable mass presented to each animal (mg) | 0.115 |
| Volume whole-body exposure chamber (L) | 18.8 |
| C (mg/L) | 0.006125 |
| RMW (L/min) | 0.228 |
| D (min) | 5.5 |
| Average body weight (kg) | 0.316 |

Table 6.7 Summary of details of the in vivo administration of RFM suspension using the nebulisation as route of administration.

| Stock solution nebulised (µg/mL) | Time of nebulisation (min) | Total calculated delivered dose* (µg/kg) |
|--|----------------------------|--|
| 500 | 5.5/nebulisation cycle | 50 μg/kg** |

^{*}Amount per unit of body weight that is presented to the animal

6.4.2.2 Pulmonary delivery of roflumilast in LPS-challenged guinea pigs

The anti-inflammatory activity of RFM suspension when delivered to the lungs via nebulisation was investigated. The exposure to nebulised vehicle followed by LPS, induced an increased level of total cells in the BALF which was mainly represented by an increased level of neutrophils. Indeed, the number of the other white blood cells could be considerable negligible. However, the condition of lung inflammation induced by LPS was not fully or significantly reduced by a single prior pulmonary administration of RFM at a dose of $50 \,\mu\text{g/kg}$ (**Figure** 6.9).

^{**}Exact calculated value is 48.58 µg/kg

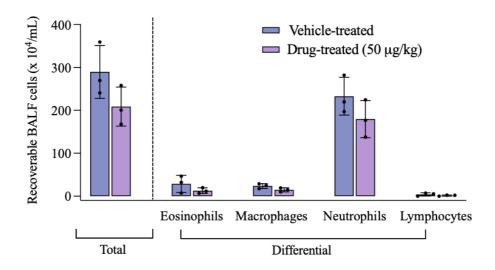


Figure 6.9 Nebulisation of RFM suspension (saline + 0.2% Tween 80 + 0.05% DMSO) in LPS-challenged guinea pigs. Total and differential count of cells recovered from bronchoalveolar lavage fluid (BALF) of guinea pigs. Groups represent vehicle: animals treated with vehicle (saline/0.2% Tween 80 + 0.05% DMSO) and challenged with LPS; drug-treated: animals treated with two consecutive aliquots (2 mL each) of nebulised RFM suspension and challenged with LPS. Data represents mean \pm SD of one independent experiment (3 animals/group).

Similar outcomes were achieved in test and control groups when evaluating the level of TNF- α in the BAL of guinea pigs. As observed for the number of white blood cell recovered in the BAL, the exposure of guinea pigs to an aerosol of RFM did not affect the level of TNF- α detected in the control sample (vehicle) **Figure** 6.10.

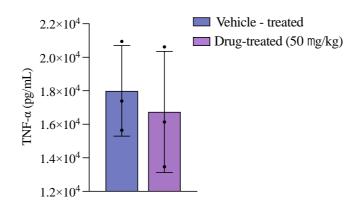


Figure 6.10 Levels of human tumour necrosis factor alfa (TNF-alfa) in bronchoalveolar lavage fluid (BALF) of RFM treated LPS-challenged guinea pigs. Animals were treated with nebulised vehicle (saline/0.2% Tween 80 + 0.05% DMSO) or drug (50 µg/kg). After 1 h animals have been exposed to LPS (0.2 mg/mL) and four hours after animals have been euthanized and lungs lavaged. Cytokine levels were detected using a commercial ELISA kit. Data represents mean \pm SD of one independent experiment (3 animals/group).

6.4.3 Impact of nebulisation on the HSA-NPs physiochemical characteristics

The impact of nebulisation on the physiochemical properties of the blank and drug-loaded HSA-NPs were investigated. The nebulisation induced a minimal decrease in the size, PDI and zeta potential values for both blank and drug-loaded NPs. Derived count rate remained overall constant compared to pre-nebulisation measurement, with only a negligible increase of the derived count rate of the blank NPs (pre-nebulisation: 130220.40 kcps; post-nebulisation: 151824.17 kcps) (**Table** 6.8).

Table 6.8 Size, polydispersity index (PDI) and zeta potential of blank and drug loaded nanoparticles (NPs) prior and after nebulisation with Aerogen Pro®. A 15 mL falcon tube was connected with tape to the inlet of a 15 mm ISO t-piece. A fixed volume of NPs (0.4 mL) was nebulised for 1 min and the condensation fluid in the falcon tube was recovered and diluted with double distilled water. Physiochemical properties were evaluated with Dynamic Light Scattering. Data represent mean \pm SD of 1 – 4 independent experiments performed on one single batch of nanoparticles.

| | | | PRE-NEBULISATION | | | POST-NEBULISATION | | | |
|--------------------|---------|--------------|------------------|---------------------------------|---------------------------|-------------------|------|---------------------------|---------------------------|
| | | Size (nm) | PDI | Derived count rate (kcps) | Zeta potential (mV) | Size (nm) | PDI | Derived count rate (kcps) | Zeta potential (mV) |
| Blank NPs | Average | 180.67 | 0.08 | 130220.40 | -32.09 | 173.17 | 0.06 | 151824.17 | -31.75 |
| | SD | - | - | - | 0.49 | 0.67 | 0.01 | - | 7.24 |
| Drug-loaded NPs | Average | 170.20 | 0.04 | 165822.90 | -33.93 | 170.30 | 0.03 | 168834.63 | -32.18 |
| | SD | - | - | - | 1.33 | 3.51 | 0.01 | - | 0.59 |

6.5 Discussion

The aim of this experimental chapter was to investigate the anti-inflammatory effect of inhaled RFM and the hypothesis that delivery of RFM formulated as inhaled albumin NPs can enhance this activity. The discussion of the results obtained will be divided in two sections. Initially the effect of the nebulisation on the HSA NPs was investigated. Indeed, the nebulisation was used as methodology to deliver RFM *in vivo* first and to evaluate *in vitro* the potential delivery of the blank and drug-loaded HSA NPs afterwards. The second part will discuss the absence of a significant reduction in the number of inflammatory cells recovered in the BAL after exposure to nebulised RFM in an LPS-challenged guinea pigs model.

6.5.1 *In vitro* nebulisation of blank and RFM-HSA-NPs

The nebulisation of blank and drug-loaded NPs described in paragraph 6.3.3 showed that the physiochemical properties investigated (size, PDI and zeta potential) remain unchanged after a cycle of nebulisation using a mesh nebuliser (Aerogen Pro®). As those features are key for the benefits provided by the NPs, it can be assumed that their

properties are retained and that they would be delivered to the lungs as an intact nanocarrier platform.

Only a small increase of the derived count rate of blank NPs after the nebulisation was detected, whereas the derived count rate of RFM-HSA-NPs remained unchanged. It is very likely that the ~ 15% increase in the count rate of blank NPs described depends on to the NPs being more concentrated after nebulisation due to a processing issue when collected from the tube. Therefore, those results showed that the nebulisation does not impact the physiochemical properties of the NPs, nor their concentration. However, in contrast with our results Aeroneb Pro® has been reported to fragment latex spheres into smaller particles in combination with uncontrolled aggregation after nebulisation (Najlah et al., 2014). As the count rate has been demonstrated to be proportional to particle concentration (Tantra et al., 2010), it can be hypothesized that the aggregation and fragmentation of nebulised HSA-NPs would result in a consistent reduction of the derived count rate. In fact, although the different experimental settings adopted and the NPs not being nebulised, this relationship was described in Chapter 2 (paragraph 2.4.3) where the occurred trypsin-mediated degradation induced aggregation and fragmentation of the NPs, which corresponded to a decrease of the derived count rate. Therefore, further confirming that the nebulisation did not impact the physiochemical properties of the NPs which did not undergo fragmentation or aggregation.

Interestingly, a study investigating the impact of nebulisation on NPs characteristics was conducted by Dailey (Ann Dailey et al., 2003). NPs made of four different polymers were manufactured and characterised before nebulisation using a jet, ultrasonic or piezo-electric crystal nebulisers. Results showed that the technique of aerosol generation had an impact on the NPs aggregation and the latter was dependent on the hydrophobicity of the particle surface. The nebulisation of NPs with high surface hydrophobicity showed high level of aggregation, which was reduced when using ultrasonic nebuliser or NPs with a more hydrophilic surface.

The suitability of a mesh nebuliser to deliver labile drugs such as proteins or mAbs without degradation has been demonstrated (Cunningham & Tanner, 2020; Forde et al., 2019; Respaud et al., 2014), hence further corroborating that the physiochemical properties of the HSA NPs are likely to remain unchanged and the NPs structure unmodified.

umnoumed

Effect of inhalad RFM on lung inflammation in vivo

| 1340 | 0.5.2 Effect of inflated KFWI on lung inflationation at vivo |
|------|---|
| 1341 | |
| 1342 | To investigate the activity of RFM delivered to the lungs the intratracheal administration |
| 1343 | was originally chosen as optimal technique. As discussed in Chapter 5, the instillation |
| 1344 | directly above the carina represents a convenient approach which does not require specific |
| 1345 | laboratory devices and does provide straightforward results. Although it comes with some |
| 1346 | disadvantages, it allows complete and controlled delivery of the total intended volume |
| 1347 | above the carina, without the challenges correlated to the nebulisation process using a |
| 1348 | whole-body chamber model. Therefore, the intratracheal instillation represented the |
| 1349 | preliminary chosen approach to investigate whether RFM in the designed model could |
| 1350 | exert a therapeutic anti-inflammatory activity. |
| 1351 | As discussed in Chapter 2, RFM is characterized by a poor water solubility $(0.52-0.56$ |
| 1352 | $\mu g/mL$ at 22 °C) (European Medicines Agency, 2010) which represents a challenge for |
| 1353 | its in vivo administration. In contrast, RFM is highly soluble in DMSO (~ 20,000 $\mu \text{g/mL})$ |
| 1354 | (Cayman Chemical, n.d.). However, due to the well-known toxicity of DMSO in high |
| 1355 | concentrations and the side effects that causes in vivo (Rubin, 1975), the instillation of |
| 1356 | solutions of RFM in 100% DMSO was not considered a suitable option. It was also not |
| 1357 | adequate to prepare a SS in 100% DMSO and dilute it with an aqueous based solvent. |
| 1358 | Based on the average weight animal and the target required dose, the percentage of |
| 1359 | DMSO in the final suspension would have been too high for in vivo administration, |
| 1360 | perhaps causing side effects |

Therefore, the adopted formulation strategy which was described in this chapter was 1361 based on the use of a saline/0.2% Tween 80 with the addition of a small percentage of 1362 DMSO equal to 0.05% v/v. This value lies in the wide range of percentages of DMSO 1363 1364 used in preclinical studies and reported in the literature (from 20% to 0.01 % v/v) (Fung 1365 et al., 2011; Ito et al., 2002). On the other side, the use of saline and 0.2% Tween 80 as 1366 vehicle for the intratracheal instillation of poorly water-soluble molecules was also 1367 reported in research studies which investigated the anti-inflammatory activity in vivo of 1368 two test compounds (GSK256066 and CHF6001) as new PDE-4 inhibitors (Nials et al., 1369 2011; Tralau-Stewart et al., 2011; Villetti et al., 2015).

1370

The two preliminary target doses were 30 and 60 µg/kg and the instillation volume equal 1371 1372 to 200 µL. Those doses were obtained via dilution from one of the three SS freshly

prepared (50, 100 and 200 μ g/mL) based on the body weight of the specie on the day of the intratracheal instillation.

As the preclinical study of RFM required multiple days and the suspensions were prepared on different days, the consistency of the preparation method and of the obtained final RFM suspension was fundamental to minimize the inter-specie variability. The evaluation of the geometric particle size showed that the particle possessed similar characteristics to those described for the highest concentration (500 µg/mL) in paragraph 6.4.1.1 (data not shown). As the intratracheal instillation provides the controlled exposure of the lungs (or sections of them) to the volume of interest, the geometric particle size of the RFM suspension had a lower impact overall compared to when administered via nebulisation.

Although intratracheal instillation was chosen as the original intended administration approach to achieve RFM lung exposure in guinea pigs, the newly laboratory availability of two different mesh nebulisers allowed to adopt a more complex and sensible lung exposure model based on the combined use of nebulisation and whole-body exposure chamber.

The calculation of the target delivered dose was carried out applying the equation designed by the Association of Inhalation Toxicologists (Alexander et al., 2008) discussed in Chapter 5. In order to achieve the target dose, a more concentrated RFM suspension (500 μ g/mL) was formulated and characterized. The geometric particle distribution analysis of RFM suspension revealed that 50% of the particles had a geometric size below 13.2 μ m (D₅₀) and therefore bigger than the mesh aperture pore size (3 – 5.5 μ m), whether 10% had a geometric size below 6 μ m (D₁₀). Those results anticipated that the nebulisation would have resulted in the loss of the fraction of RFM with an inappropriate size to pass through the mesh; however, on the other hand those results showed that a fraction of the evaluated suspension had a geometric size compatible with the pore mesh aperture, providing sufficient evidence of its nebulisation via mesh nebuliser and its potential deposition in the lungs.

In fact, the aerodynamic assessment confirmed that the nebulisation of 2 mL of RFM (500 $\mu g/mL$) resulted in the successful deposition of the drug in each stage of the impactor and this was validated via complete drug recovery and HPLC quantification. The respirable

dose calculated as the total mass recovered after nebulisation from stages 3 to 7 of the 1408 NGI was equal to 115.5 µg. The *in vitro* aerodynamic assessment showed that RFM had 1409 the potential to deposit in the lung of the specie and that the fraction with a suitable aerodynamic size was sufficient to induce a therapeutic effect. Confirmation of the potential deposition of nebulised RFM in the lungs was provided also by an MMAD equal 1412 to ~ 6 µm.

1413

1407

1410

1411

1414 In this experimental chapter the adopted delivered dose was equal to 50 µg/kg. The 1415 selection of this dose was performed based on two aspects. Limited results exist on the 1416 efficacy of inhaled roflumilast and few studies have been published in this field. 1417 However, an interesting research (Chapman et al., 2007) investigated the effect of RFM 1418 delivered to Brown Norway rats intratracheally or via nose-only inhalation in an 1419 ovalbumin model. Rats were exposed to intratracheal administration (20 - 60 - 200 µg/kg) 1420 5 h before or 24 h after the antigen challenge. Both treatment protocols resulted in the 1421 reduction of the total number of inflammatory cells in the BAL, with effects also on 1422 eosinophils and neutrophils number (except for the lowest dose $-20 \mu g/kg$). The ED₅₀ to 1423 inhibit the increase in total cells was 50 µg/kg. A partial reduction of the inflammatory 1424 cells in the BAL was also reported with a different dose regime (intratracheal 1425 administration 600 µg/kg, 24 h after the antigen challenge). 1426 Similar results were described for the nose-only delivery of RFM which inhibited the 1427 increase in total cells, neutrophils and eosinophils. The estimated pulmonary deposition 1428 ED₅₀ was calculated from the particle size distribution and equal to 10 μg/kg. In terms of 1429 formulation administered, intratracheally administered RFM was formulated as 1430 micronized powder admixed with lactose into a drug powder microspray needle (Penn 1431 Century), whereas the nose-only exposure was based on a micronized roflumilast with 1432 lactose. 1433 Doses in the same range were also tested in the investigation of the anti-inflammatory 1434 activity of a test compound developed as PDE-4 inhibitor (GSK256066). GSK256066 1435 was administered intratracheally to LPS-challenged rats as aqueous suspension (instilled 1436 volume: $200 \,\mu\text{L}$) at doses $0.1 - 100 \,\mu\text{g/kg}$. The test compound induced a dose-dependent 1437 inhibition of the LPS-induced neutrophilia with statistical significance detected at 3 µg/kg 1438 and maximal (72%) inhibition of lung neutrophilia at 30 µg/kg. As GSK256066 is a more 1439 potent drug than RFM, the described effective doses were lower compared to those of 1440 RFM (Nials et al., 2011; Tralau-Stewart et al., 2011).

Although being in agreement with doses reported in the literature, the target dose employed in this experimental chapter (50 μ g/kg) did not significantly reduce the lung influx of neutrophils induced by the validated LPS exposure, unlike when delivered orally (0.5 mg/mL).

Despite the lack of inhalable HSA-NPs' investigations, the benefits that the pulmonary delivery of a drug using nanoplatform provides over the oral and intravenous administration has been extensively demonstrated in literature studies for other type of nanocarriers. Therefore, the aim of this study was to further investigate if the inhaled delivery of RFM provides benefits over its oral administration, but most importantly if lower or comparable doses of inhaled RFM-HSA-NPs can exert an anti-inflammatory effect equivalent to the effect induced by inhalation of RFM. It is clear how this comparison would have been sensible only with RFM-HSA-NPs doses in the same range of those used for the administration of inhaled RFM.

Therefore, the second key factor considered in the evaluation of the target dose of inhaled RFM was correlated to the dose of RFM achievable when delivered as RFM-HSA-NPs in a whole-body chamber. As mentioned in Chapter 5, the calculation of the estimated delivered dose can be achieved via the application of an equation that considers several factors. Firstly, to calculate the concentration of RFM in the air (C), yield and mass of RFM encapsulated per mg of HSA should be considered. The yield described for RFM-HSA-NPs is equal to 73% which corresponds to ~ 9 mg/mL of total entrapped albumin (section 2.4.2.1). The amount of RFM encapsulated for each mg of albumin is equal to 19.9 µg (section 2.4.2.2). Assuming the use of the same plexiglass box (18.8 L), the nebulisation of 2 mL of RFM-HSA-NPs would produce a RFM concentration in the air (box) of 0.02 mg/mL. Considering the average body weight equal to 0.316 kg, the RMW would be equal to 0.228 L/min. Based on the average flow rate of the Aerogen Pro (0.4 mL/min) the duration of the nebulisation of 2 mL of NPs suspension would last 5.5 min. The resulting delivered dose would be equal to $\sim 80 \mu g/mL$ which eventually could be doubled if two aliquots of 2 mL were nebulised. However, the Equation 5.1 also includes a factor called inhalable fraction (IF) whereas incorporation of this parameter is not essential provided that the aerosol has reasonable respirability for the intended specie. In fact, this value was not included in the calculation of the DD of inhaled RFM as the concentration in the air already considered only the respirable fraction (obtained via aerodynamic particle distribution – stages 3 to 7). However, as the aerodynamic distribution of RFM-HSA-NPs was not performed in this experiment study, it is likely that the achievable target dose would be lower than 80 μ g/mL (2 mL) or 160 μ g/mL (4 mL). This estimation further rationalise the target dose adopted in the evaluation of the anti-inflammatory activity of RFM (50 μ g/kg) in this chapter as it allows the future assessment of the potential improved therapeutic activity of RFM in a nanocarrier using as positive control the administration of inhaled RFM and comparable doses.

Used in both *in vitro* and *in vivo* experiments, roflumilast showed to reduce the LPS-induced IL-8 increase in BEAS-2B (dose: 0.001 – 100,000 nM - Chapter 4) and neutrophilia in BAL of orally administered guinea pigs (dose: 0.5 mg/kg - Chapter 5) hence suggesting that it may be able to exert an anti-inflammatory activity when delivered via inhalation in a preclinical model. Inhalation of RFM in 100% DMSO at dose of 500 µg/mL for 15 min once day for five days was described to reduce the ovalbumin-induced lung inflammation in mice (Murad et al., 2017). However, in this experimental chapter the limitations correlated to the application of the nose-breathing preclinical models besides others may have restricted the deposited dose. Nasal filtration in rodents influences the total amount of particles available for lung deposition and longer exposure period may be required to increase the delivered dose.

The target dose investigated in this experimental chapter was in agreement with some of the doses used in previous studies which successfully showed RFM anti-inflammatory activity. It is likely that the lack of significant reduction of the LPS-induced neutrophilia described in this Chapter was the result of an insufficient dose of RFM that is also characterized by very low solubility in the lung lining fluid. This may have hindered its dissolution and binding to the PDE4 intracellular enzyme. In this context, the encapsulation of RFM in NPs will induce a much faster dissolution of the drug due to their higher surface area-to-volume ratio, thus overcoming the low solubility issue (Bohr et al., 2014) and increasing the drug availability. Future studies investigating the *in vivo* administration of inhaled RFM-HSA-NPs may confirm this hypothesis.

Although the potential of RFM in reducing the neutrophilia was reported by Chapman (Chapman et al., 2007) at doses of 60 - 200 and $600 \,\mu\text{g/kg}$, it is also relevant to mention that the *in vivo* models adopted within studies were different (antigen vs LPS challenge)

and the raw powder used was micronized. In addition, in this study milling of the RFM raw powder could represent an approach to improve the drug availability via optimisation of the geometric size of the particles, thus also improving i) their dissolution in the lung lining fluid; ii) the aerodynamic assessment of the RFM suspension via improvement of the percentage of particles liable to go through the mesh pores.

Future studies will further investigate the dose-response of inhaled RFM using a

Future studies will further investigate the dose-response of inhaled RFM using a combined approach that improves the geometric and aerodynamic particle size of the suspension besides the application of a bigger population of species in the same LPS model.

1518

1515

1516

1517

6.6 Conclusion

15191520

1521

1522

1523

1524

1525

1526

1527

1528

1529

1530

1531

1532

1533

1534

1535

1536

1537

1538

1539

1540

1541

1542

This experimental chapter aimed to the investigation of the potential anti-inflammatory activity of nebulised RFM as a precursor to optimising this therapeutic effect by the encapsulation of RFM in HSA-NPs. A RFM suspension for nebulisation was formulated that when nebulised using a mesh nebuliser resulted in its deposition across all the stages of a cascade impactor, depositing a respirable mass of 115 µg. The RFM suspension resulted was employed for the evaluation of the anti-inflammatory activity when nebulised to the LPS-challenged guinea pigs model of inflammation described in the previous chapter. Nebulised RFM did not induce a significant reduction of the number of inflammatory cells infiltrated into the lungs at the dose (delivered dose: 50 µg/kg) and protocol adopted. It is unclear whether the lack of a substantial therapeutic activity has a biochemical or pharmacological basis or is due to insufficient delivered dose. Although the lack of significant anti-inflammatory activity at the dose and protocol adopted, overall the outlined approach proved to be useful for the investigation of the potential lung delivery of RFM and in future studies of RFM-HSA-NPs. Furthermore, the potential of HSA-NPs as carrier for pulmonary delivery was corroborated by the lack of changes in their physiochemical properties that was reported for the blank and RFM-HSA-NPs after nebulisation. Overall those results highlighted the importance of the demonstration of the potential of inhaled RFM first before an optimisation using a formulation approach such as RFM-HSA-NPs can be undertaken. The data provided in this chapter provided initial evidence that demonstrating the

effectiveness of RFM via the inhaled route is essential before extending studies to the

CHAPTER 7: General Discussion

7.1 Original premise

Pulmonary delivery of therapeutics has gained increasing interest over the past decades due to the advantages that it provides over other routes of administration. The lungs possess a large surface area which represents an excellent target for local therapeutic activity and absorption for systemic delivery (Patton & Byron, 2007). Delivery to the lungs avoids first pass metabolism which can result in the reduction of the total dose available. Moreover, lung delivery of the rapeutics allows to use a reduced dose compared to other routes of administration, resulting in lower side effects and higher efficacy (Gulati et al., 2021; Praphawatvet et al., 2020). However, often the delivery to the lungs comes with challenges if the drug has a low solubility or if it is liable to degradation or losses by the multiple lung clearance mechanisms. The encapsulation of the API in a nanocarrier via an engineered formulation and modified release represents an extremely useful delivery strategy that allows to overcome the challenges associated with the delivery or pharmacokinetic of a drug (Abdelaziz et al., 2018; Anderson et al., 2020). The encapsulation of a drug in a NPs-based formulation allows for example i) to modify the release of the drug overtime; ii) to obtain the precise targeting of cells or organs of interest by functionalised nanocarriers; iii) to protect the payload from degradation.

The commercialisation of paclitaxel HSA-NPs for intravenous administration (Abraxane) for the treatment of various type of cancers in 2005 has made the potential of this carrier for clinical use clear (Hornok, 2021; Spada et al., 2021). Despite the successful and extensive investigation of albumin NPs for intravenous administration for cancer therapy (Hassanin & Elzoghby, 2020; Kunde & Wairkar, 2022), the use of albumin NPs for pulmonary delivery has not been completely or extensively explored yet. It was hypothesised that NP formulation might be a strategy to improve the therapeutic profile of the PDE inhibitors (Crocetti et al., 2022), the need for which was described in paragraph 1.2.4. The pulmonary delivery of PDE inhibitors to treat COPD associated exacerbations represents an unmet goal.

A strategy was developed in this thesis to first encapsulate RFM in HSA-NPs, then explore their delivery via the pulmonary route. This may allow to overcome both the

unfavourable therapeutic profile of this class of drugs while RFM being a drug prototype that will allow the investigation of the potential use of this carrier as a PK-modifying formulation for inhalation.

7.2 Drug-loaded albumin NPs for lung delivery

The aims of this thesis were achieved by optimising an RFM-HSA-NPs manufacture method first and by characterising the obtained NPs via the design of *in vitro* models to investigate the nanocarrier degradation in a simulated lung environment as well as the release of the payload overtime. RFM-HSA-NPs were converted into a respirable form based on NPs-embedded-microparticles (NEMs) as key 'feasibility' step to facilitate their translation to clinical use. Moreover, before RFM-HSA-NPs can be established as clinically acceptable enabling formulation for pulmonary drug delivery purposes, the potential anti-inflammatory activity of RFM when delivered to the lungs was investigated via the design of an LPS-challenged BEAS-2B *in vitro* model first and an LPS-challenged guinea pig *in vivo* model later. The key findings are outlined below in relation to the experimental chapter within this thesis.

In Chapter 2, the main research question centred around the potential of the successful manufacture of RFM-HSA-NPs as good nanocarrier being able to be RFM-loaded, undergo degradation and efficiently release the payload. The data clearly demonstrated that the manufacture method parameters adopted resulted in the production of NPs with a consistent size of ~140 nm, PDI < 0.1 and negative zeta potential which prevents aggregation. As the proteases play an important role in the pathogenesis of lung disease as well as in the function of healthy lungs (Abboud & Vimalanathan, 2008; Fischer et al., 2011; Greene & McElvaney, 2009; Pandey et al., 2017; Stockley, 1999), the use of trypsin at a total lung concentration of 0.1 mg/mL (Woods et al., 2020) in an in vitro model represented an informative approach to predict and investigate the HSA-NPs degradation in the lungs. The degradation of the HSA-NPs occurred gradually in the first interval of time and after 1 hour the NPs were almost completely degraded and fragmented. These results are in agreement with others previously reported in the literature (Woods et al., 2020). Interestingly, we employed as parameters to monitor the NPs degradation the PDI and the derived count rate, with the latter providing a more sensitive measure of initial NP degradation before the detection of albumin fragments and aggregates becomes

apparent via the alteration of the PDI value. Furthermore, the novelty of this model is represented by the general lack in the literature of accepted simulant models to represent the protease activity in the lungs.

The results highlighted in Chapter 2 also confirmed the potential of the HSA-NPs manufactured via the method adopted to successfully release the payload without which no therapeutic action would occur. Considering that RFM is a very poorly water-soluble drug (European Medicines Agency, 2010), the investigation of the rate of release of the payload from the NPs while still employing a biorelevant model represented an experimental challenge. Results showed the importance of the optimisation of the in vitro drug release model in terms of release medium adopted, concentration and pH of trypsin solution as well as ratio of trypsin: substrate. The superiority of HSA-NPs over notencapsulated RFM to achieve a sustained release overtime was clearly demonstrated. The release kinetics in the window time investigated (0 to 4 h) was in agreement with the degradation rate of the nanocarrier, with most of the drug being released by 60 min followed by a slower release until 4 h. Although there are differences in the model and protocol adopted, these results do not concord with the report by Langer (Langer et al., 2008) that HSA-NPs with a 100% degree of cross-linking (as those designed in this thesis) showed only a 9% degradation within 24 h. Overall, the research objectives of **Chapter 2** were achieved, and enabled further work in Chapter 3 to pursue the manufacture and characterisation of RFM-HSA-NPs embedded in microparticles as a key feasibility assessment to facilitate their translation to clinical use by demonstrating a marketable pharmaceutical formulation.

The key objective in **Chapter 3** was to investigate whether the designed RFM-HSA-NPs could be converted successfully in a formulation that could be manufactured as a stable dosage form suitable for clinical use. The aerodynamic diameter highly influences the deposition in the lungs of inhaled material. The manufacture of NPs embedded in microparticles (Tsapis et al., 2002) is a widely known formulation strategy to improve the respirability of NPs which was achieved successfully in this experimental work. The obtained spray-dried powder possessed good aerodynamic characteristics for pulmonary delivery with a FPF equal to 67% and a geometric particles size (D_{50}) equal to 2.21 μ m.

After deposition into the lungs, the NEMs must disintegrate to release the embedded NPs. Results showed that mannitol-based nanoaggregates were dissolved rapidly to release HSA-NPs although further studies employing a more biorelevant model should be carried out to more precisely investigate the rate of degradation (Ruge et al., 2016).

In the context of investigating formulation strategies to achieve pulmonary delivery of RFM-HSA-NPs, **Chapter 6** also focussed on the impact of the nebulisation on the physiochemical properties of blank and drug-loaded NPs. Indeed, pulmonary delivery can be obtained with different inhalation devices in which the APIs can be loaded in different type of formulations. Besides the investigation of NEMs as spray-dried powder, the nebulisation of RFM-HSA-NPs with a mesh nebuliser (Aerogen Pro) was carried out. Interestingly, in contrast with an expected reduced derived count rate due to the loss of NPs during the nebulisation, results described an unchanged formulation. Size, PDI and zeta potential remained overall constant, indicating the preservation of the NPs' key properties after aerosolization by mesh nebuliser.

Overall, the ultimate objective of this thesis was to investigate the anti-inflammatory activity of RFM delivered by the pulmonary route as a precursor to optimising this therapeutic effect by formulating as RFM-HSA-NPs. This was achieved firstly in **Chapter 4** by investigating whether RFM can exert an anti-inflammatory activity in an LPS-challenged bronchial epithelial (BEAS-2B) *in vitro* model. The two following chapters focussed i) on the design of an LPS-challenged guinea pig model employed to confirm the suitability of the model itself via the anti-inflammatory activity of orally administered RFM (**Chapter 5**); ii) on the *in vivo* evaluation of the effect of nebulised RFM afterwards (**Chapter 6**). The continuity throughout this part of the research was provided by the use of the same trigger agent (LPS O111:B4 from *E. Coli*) for inducing inflammation. LPS was selected as a clinically relevant inducer of inflammation in COPD exacerbation. Endpoints and outcomes used to measure the extent of the lung inflammation were also designed to provide consistency and add to value of those chapters.

In **Chapter 4**, the objectives were accomplished, with the caveat that RFM significantly reduced only the levels of IL-8 released by LPS-challenged BEAS-2B in a pre-treatment protocol (1.5 h), whereas the levels of IL-6 were not impacted by any of the protocols

adopted (pre-treatment: 1.5 h, 3 h and 24 h). The sensitivity of BEAS-2B to serum and LPS (at different concentrations and exposure times) in releasing cytokines has been identified in other studies (Guillott et al., 2004; Schulz et al., 2002). Our findings regarding the weak reduction of IL-8 levels achieved by RFM have also been seen with some studies (M. R. Edwards et al., 2016; Salvator et al., 2020). In contrast, IL-6 level was reported to be reduced by RFM treatment in bronchial explants (Salvator et al., 2020), but not in alveolar macrophages (Lea et al., 2019).

Results described in **Chapter 5** showed that LPS challenged guinea pigs represented a valuable *in vivo* model to mimic COPD exacerbations. Among the *in vivo* COPD models applied by others, the whole-body exposure model is a useful approach to achieve lung exposure in the specie. Moreover, the applicability of the model in the field of RFM lung delivery research was confirmed by the reduced neutrophilia induced by a pre-treatment of orally administered RFM (0.5 mg/kg).

Finally, the data presented in **Chapter 6** found that 50 µg/kg RFM delivered to the lungs in an LPS model does not induce a significant anti-inflammatory effect. Although it is difficult to accurately verify the delivered dose, the aerosol of RFM produced by nebulisation possessed good aerodynamic characteristics and had the properties required to deposit into the lungs. This was demonstrated by the aerodynamic assessment of RFM and generation of a respirable dose equal to 115 µg. Considering the data presented in this Chapter and the lack of success over the past decade in the investigation of new inhaled PDE inhibitors reported in the literature, it can be argued that perhaps PDE4 can provide an anti-inflammatory activity only when delivered systemically. On the other hand, it can be argued that the unchanged levels of IL-6 in BEAS-2B in vitro model after RFM pre-treatment anticipated the lack of anti-inflammatory activity of nebulised RFM in vivo. On the other hand, it should also be considered that the poor water-solubility of RFM may have hindered its dissolution in the lung lining fluid with a consequent lack of PDE4 inhibition. Although different limitations and ethical considerations hindered the in vivo testing of the RFM-HSA-NPs and the evaluation of its potential in improving the RFM solubility, it can be argued that a slow dissolving suspension would work as well as a nanocarrier that enhances the drug solubilisation. Clearly further investigation is required to confirm this hypothesis, and it is interesting how the sustained release

enhanced by the encapsulation of RFM in HSA-NPs described in Chapter 2 was well 1744 resembled by the release of RFM suspended in Tween 80 and DMSO.

1745

1743

7.3 Contribution to knowledge

1746 1747

1748

1749

1750

1751

1752

In the existing literature there is a lack of studies concerning the potential, degradation, and in vivo testing of HSA-NPs for pulmonary delivery of anti-inflammatory drugs. Despite the extensive research of HSA-NPs for intravenous administration over the years driven by the approval of Abraxane, the inhalation route has a wide range of challenges in terms of formulation, administration and methods for pre-clinical formulation development.

1753 1754

1755 Whilst the manufacture method of RFM-HSA-NPs is widely known and used in the 1756 literature as well as the drug release assay employed to test the kinetic release of RFM 1757 (dialysis bag), the protocol required adaptations to overcome the challenges of RFM itself 1758 and provides a contribution to the field that may be informative for other studies 1759 employing drugs with similar solubility profile. Moreover, the use of trypsin in the in 1760 vitro degradation assay which utilised PDI and derived count rate as parameters is one of 1761 the few presented in the literature investigating the degradation of the HSA-NPs. The 1762 simultaneous quantification of the drug release which may be performed in future studies 1763 would represent a more comprehensive approach to characterising formulation 1764 breakdown and drug release than is currently performed according to the literature.

1765 1766

1767

1768

1769

1770

1771

This work also represents the first attempt at improving the therapeutic window of a PDE4 inhibitor via the use of HSA-NPs as drug delivery system generally, but more specifically for pulmonary delivery. Despite some experimental limitations and the need for key additional studies, the thesis makes several contributions to identifying the challenges and providing tools that can be used to evaluate the potential of RFM for pulmonary delivery and the contribution of HSA-NPs as a formulation platform.

1772

7.4 **Experimental limitations**

1773 1774

1775 In Chapter 4 and in Chapter 6, the main limitation was correlated to the unexpected lack 1776 of RFM activity in the bioassay which hindered the establishment of a baseline effect.

- 1777 This subsequently prevented the investigation of any possible enhancement that the NP
- 1778 formulation may produce compared to not-encapsulated RFM.
- Based on the nanocarrier's EE achieved in **Chapter 2**, the estimated delivered dose of
- 1780 RFM as inhaled RFM-HSA-NPs could be adequate to induce an anti-inflammatory effect
- in vivo in the LPS-challenged guinea pig model designed. However, the lack of
- experimental results in this context did not allow to confirm this hypothesis, hindering
- any further optimisation of the formulation (i.e., albumin drug ratio) which may have
- benefited the achievement of a higher target dose.
- Moreover, in Chapter 2 the discussion of the results of the RFM-HSA-NPs kinetic of
- release may have benefited from the evaluation of the exact distribution of the drug in the
- NPs, if mainly in the matrix or whether on the surface.
- 1788 The main issue in the delivery of the spray dried microparticles which development was
- described in **Chapter 3** may be the excipient burden which could limit the maximum
- deliverable dose and subsequently the viability of the delivery concept.
- 1791 The designed whole-body LPS model (Chapter 5 and 6) was informative for the
- preliminary objectives of this thesis. However, the use of a more advanced nose-only
- aerosol exposure system would have overall benefited the study. Its use would have
- ensured i) exposure mostly to the respiratory tract; ii) use of less material. The possibility
- to acquire the breathing data of the species would have improved the accuracy of the
- estimation of the inhalation doses. In addition, the possibility to have an unbiased sample
- 1797 from the species breathing zone would have been key to determine the sampling
- efficiency of the subject. Besides the typical nose-only exposure system that can also
- allocate multiple species at the same time due to multiple exposure tubes (Phalen et al.,
- 1800 2014), the PreciseInhale® also allows to achieve precise lung deposition of the powder of
- interest to a single animal at a time. The use of the PreciseInhale® combined with the
- nose-only exposure model would allow reducing the variability of exposure between
- species; in addition, the active monitoring of aerosol concentration and individual
- breathing parameters would further ensure high precision of dosing.
- The main limitation of **Chapter 6** was correlated to the lack of a dose-response study for
- 1806 RFM suspension and for the RFM-HSA-NPs. Although preliminary results in this work
- showed that lung inflammation in species exposed to LPS is not reduced by nebulised 50
- 1808 µg/kg RFM, a follow up experiment with two additional higher doses (100 and 200
- 1809 µg/kg) would have been significant in drafting a more accurate conclusion. In the first
- case, the main challenge was the almost complete insolubility of RFM in aqueous medium

which hindered the achievement of the desired dose in a biocompatible vehicle. Indeed, the lack of time also did not allow the investigation of alternative formulation strategies such as the use of a micronized powder coupled with a different inhalation device. Finally, resources and ethical constraints limited the use of larger testing groups *in vivo* which would have improved the understanding of the final results.

7.5 Future work

Extensive further experiments should be performed to elucidate the unclear lack of antiinflammatory activity reported in this thesis for nebulised RFM. We have hypothesised that the lack of pharmacological activity in the *in vivo* lung inflammation model could be due to the unsuitability of the formulation used (RFM suspension in saline/ Tween 80/ DMSO) which may have resulted in crystallised RFM not available for absorption and therefore in undissolved particulate matter due to the poor water solubility of RFM (R. M. Jones & Neef, 2012). An additional hypothesis is that Tween 80 present above the CMC in the vehicle used for in vivo lung delivery of RFM may have entrapped RFM reducing its cells uptake in the lungs. Similarly, the accumulation of paclitaxel in human erythrocytes was severely altered by paclitaxel being trapped in Cremophor micelles when used above the CMC (van Zuylen et al., 2001). Future in vitro and in vivo investigation of the cellular distribution of RFM in inflammatory cells expressing PDE4 and lung tissue would elucidate whether the entrapping of RFM in Tween 80 micelles hindered RFM from binding the PDE4 enzyme and express anti-inflammatory activity. On the other hand, the use of a different formulation as micronised RFM powder rather than RFM in suspension may also help to elucidate whether the lack of anti-inflammatory activity in the model adopted was due to a formulation or pharmacological reason.

An additional hypothesis is that RFM once deposited into the lungs does not undergo sufficient metabolization by CYP 3A4 and 1A2 which cell-specific localisation in the lung is still largely unknown (Hukkanen et al., 2001). The expression of the cytochrome 3A4 and 1A2 in the lungs should therefore be investigated via Western blot or reverse transcription polymerase chain reaction. However, despite the N-oxide metabolite also accounts for the total therapeutic activity, the parent molecule, RFM, can exert a pharmacological effect even if not metabolised. Therefore, the above-mentioned hypothesis does not fully explain the lack of anti-inflammatory activity reported in this thesis.

Despite the target dose adopted (50 µg/kg) was in agreement with other studies in which in vivo anti-inflammatory activity of pulmonary delivered RFM was described (Chapman et al., 2007), further experiments should investigate the effect of a higher target dose (single administration) or multiple administrations in the same LPS model designed in Chapter 5.

Meanwhile, besides the investigation of the reasons for the lack of the effect of RFM itself, it should be highlighted that in this thesis RFM served also as a prototype. Therefore, the investigation of the *in vivo* biodistribution of inhaled blank HSA-NPs may further corroborate the proof of concept for the formulation and its potential for clinical use. The use of the LPS guinea pig model designed in this thesis could be combined to imagining technique. In addition, the encapsulation of a different drug – perhaps with a less complex solubility profile – into the HSA-NPs would expedite the understanding of the potential of pulmonary delivered HSA-NPs, allowing the *in vivo* testing of the NPs.

Finally, the investigation of the exact distribution of RFM in the HSA-NPs would enhance the understanding of the potential of this carrier. This could be conducted with the formulation of fluorescent RFM- HSA-NPs.

Moreover, in view of the optimisation of the respirability of the HSA-NPs, full aerodynamic assessment of the NEMs should be carried out besides the evaluation of their disintegration in a more biorelevant assay. It would also be key to evaluate the simultaneous release kinetic of the drug from the drug delivery system adopting the same assay.

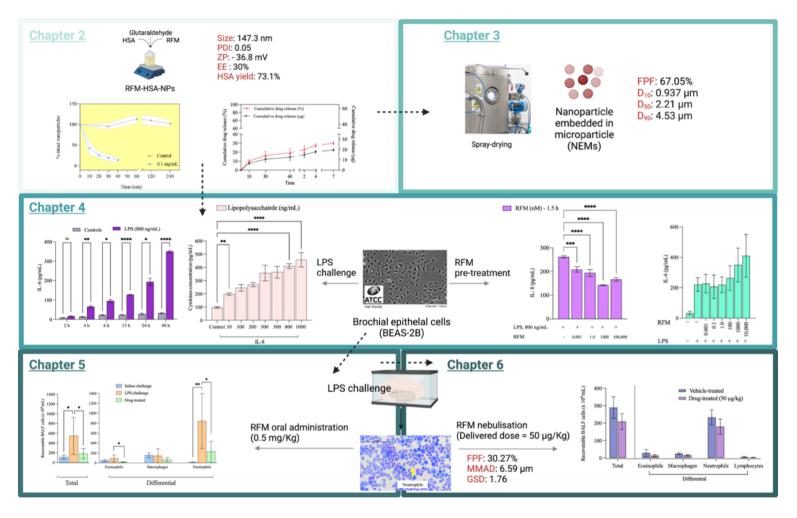
7.6 Conclusion

The data presented in this work demonstrate how the use of HSA-NPs for pulmonary administration of anti-inflammatory drugs should be further pursued. This drug delivery system has been showed to encapsulate a hydrophobic drug and to undergo degradation in a lung simulated environment. The encapsulation of RFM in HSA-NPs resulted in a modified kinetic of release of the drug, providing a mechanism that would prolong drug retention in the lungs.

The RFM-HSA-NPs were successfully processed into NP embedded microparticles

The RFM-HSA-NPs were successfully processed into NP embedded microparticles (NEMs) providing a respirable powder dosage form, which combined with the use of suitable inhalation manoeuvres, has good potential as a product for clinical use.

Additionally, this thesis established an *in vitro* respiratory epithelial model and an *in vivo* LPS model of inflammation, in which the effects of anti-inflammatory positive controls (dexamethasone and orally delivered RFM, respectively) were clearly seen. Unexpectedly, the effect of RFM administered to the cell culture model and delivered as an aerosol to the *in vivo* model, resulted in little or no anti-inflammatory activity. This was a fundamental step upon which plans to proceeding into the optimisation of the formulation strategy foundered. Although results showed that RFM may not be able to exert an anti-inflammatory activity when delivered locally to the lungs, further studies are required to elucidate the mechanisms behind this lack of therapeutic activity. Overall, the work presented in this thesis, provides a solid foundation for future research in the field of pulmonary delivery and in the application of HSA-NPs as PK-modifying inhaled drug delivery system.



2 Figure 7.1General abstract showing main outcomes of each experimental chapter

1 References

2 A. Taheri et al. (2011). Nanoparticles of conjugated methotrexate-human serum albumin:

- 3 Preparation and cytotoxicity evaluations. Journal of Nanomaterials, 2011.
- 4 https://doi.org/10.1155/2011/768201
- 5 Aaron, S. D., Angel, J. B., Lunau, M., Wright, K., Fex, C., le Saux, N., & Dales, R. E.
- 6 (2001). Granulocyte Inflammatory Markers and Airway Infection during Acute
- 7 Exacerbation of Chronic Obstructive Pulmonary Disease. Am J Respir Crit Care
- 8 *Med*, 163, 349–355. www.atsjournals.org
- 9 Abbott-Banner, K. H., & Page, C. P. (2014). Dual PDE3/4 and PDE4 inhibitors: Novel
- treatments for COPD and other inflammatory airway diseases. Basic and Clinical
- 11 Pharmacology and Toxicology, 114(5), 365–376.
- 12 https://doi.org/10.1111/bcpt.12209
- Abboud, R. T., & Vimalanathan, S. (2008). Pathogenesis of COPD. Part I. The role of
- protease-antiprotease imbalance in emphysema. International Journal of
- 15 Tuberculosis and Lung Disease, 12(4), 361–367.
- Abdelaziz, H. M., Gaber, M., Abd-Elwakil, M. M., Mabrouk, M. T., Elgohary, M. M.,
- Kamel, N. M., Kabary, D. M., Freag, M. S., Samaha, M. W., Mortada, S. M.,
- Elkhodairy, K. A., Fang, J. Y., & Elzoghby, A. O. (2018). Inhalable particulate drug
- delivery systems for lung cancer therapy: Nanoparticles, microparticles,
- 20 nanocomposites and nanoaggregates. *Journal of Controlled Release*, 269, 374–392.
- 21 https://doi.org/10.1016/j.jconrel.2017.11.036
- 22 Aerogen ® Pro System Instruction Manual. (n.d.). www.aerogen.com
- Alexander, D. J., Collins, C. J., Coombs, D. W., Gilkison, I. S., Hardy, C. J., Healey, G.,
- Karantabias, G., Johnson, N., Karlsson, A., Kilgour, J. D., & McDonald, P. (2008).
- Association of Inhalation Toxicologists (AIT) Working Party Recommendation for
- 26 Standard Delivered Dose Calculation and Expression in Non-Clinical Aerosol
- 27 Inhalation Toxicology Studies with Pharmaceuticals. *Inhalation Toxicology*, 20(13),
- 28 1179–1189. https://doi.org/10.1080/08958370802207318
- 29 Alexis, N. E., Lay, J. C., Zeman, K. L., Geiser, M., Kapp, N., & Bennett, W. D. (2006).
- In vivo particle uptake by airway macrophages in healthy volunteers. *American*
- 31 Journal of Respiratory Cell and Molecular Biology, 34(3), 305–313.
- 32 https://doi.org/10.1165/rcmb.2005-0373OC
- 33 Alhajj, N., O'Reilly, N. J., & Cathcart, H. (2021). Designing enhanced spray dried
- particles for inhalation: A review of the impact of excipients and processing

- parameters on particle properties. *Powder Technology*, 384, 313–331.
- 36 https://doi.org/10.1016/j.powtec.2021.02.031
- 37 Amighi, F., Emam-Djomeh, Z., & Labbafi-Mazraeh-Shahi, M. (2020). Effect of different
- cross-linking agents on the preparation of bovine serum albumin nanoparticles.
- 39 Journal of the Iranian Chemical Society, 0123456789.
- 40 https://doi.org/10.1007/s13738-019-01850-9
- 41 Anderson, C. F., Grimmett, M. E., Domalewski, C. J., & Cui, H. (2020). Inhalable
- anotherapeutics to improve treatment efficacy for common lung diseases. In Wiley
- 43 Interdisciplinary Reviews: Nanomedicine and Nanobiotechnology (Vol. 12, Issue
- 1). Wiley-Blackwell. https://doi.org/10.1002/wnan.1586
- 45 Anthonisen, N. R., Manfreda, J., W Warren, C. P., Hershfield, E. S., M Harding, G. K.,
- 46 & Nelson, N. A. (1987). Antibiotic Therapy in Exacerbations of Chronic Obstructive
- 47 Pulmonary Disease. *Annals of Internal Medicine*, 106, 196–204. https://annals.org
- 48 Anton, N., Jakhmola, A., & Vandamme, T. F. (2012). Trojan microparticles for drug
- 49 delivery. *Pharmaceutics*, 4(1), 1–25.
- 50 https://doi.org/10.3390/pharmaceutics4010001
- Ari, A. (2014). Jet, Ultrasonic, and Mesh Nebulizers: An Evaluation of Nebulizers for
- 52 Better Clinical Outcomes. Eurasian Journal of Pulmonology, 16(1), 1–7.
- 53 https://doi.org/10.5152/ejp.2014.00087
- Ariga, M., Neitzert, B., Nakae, S., Mottin, G., Bertrand, C., Pruniaux, M. P., Jin, S.-L.
- 55 C., & Conti, M. (2004). Nonredundant Function of Phosphodiesterases 4D and 4B
- in Neutrophil Recruitment to the Site of Inflammation. *The Journal of Immunology*,
- 58 Arikayce liposomal Product Information. (n.d.).
- 59 https://www.ema.europa.eu/en/medicines/human/EPAR/arikayce-liposomal
- Armani, E., Amari, G., Rizzi, A., Fanti, R. de, Ghidini, E., Capaldi, C., Carzaniga, L.,
- Caruso, P., Guala, M., Peretto, I., la Porta, E., Bolzoni, P. T., Facchinetti, F., Carnini,
- 62 C., Moretto, N., Patacchini, R., Bassani, F., Cenacchi, V., Volta, R., ... Villetti, G.
- 63 (2014). Novel class of benzoic acid ester derivatives as potent PDE4 inhibitors for
- inhaled administration in the treatment of respiratory diseases. *Journal of Medicinal*
- 65 *Chemistry*, 57(3), 793–816. https://doi.org/10.1021/jm401549m
- Arnedo, A., Espuelas, S., & Irache, J. M. (2002). Albumin nanoparticles as carriers for a
- phosphodiester oligonucleotide. *International Journal of Pharmaceutics*, 244, 59–
- 68 72. www.elsevier.com/locate/ijpharm

- 69 Arpagaus, C. (2018). Pharmaceutical Particle Engineering via Nano Spray Drying -
- Process Parameters and Application Examples on the Laboratory-Scale.
- 71 International Journal of Medical Nano Research, 5(1).
- 72 https://doi.org/10.23937/2378-3664.1410026
- Asgharian, B., Kelly, J. T., & Tewksbury, E. W. (2003). Respiratory Deposition and
- 74 Inhalability of Monodisperse Aerosols in Long-Evans Rats. *Toxicological Sciences*
- 75 , 71, 104–111. https://academic.oup.com/toxsci/article/71/1/104/1639596
- Baghdan, E., Duse, L., Schüer, J. J., Pinnapireddy, S. R., Pourasghar, M., Schäfer, J.,
- 77 Schneider, M., & Bakowsky, U. (2019). Development of inhalable curcumin loaded
- Nano-in-Microparticles for bronchoscopic photodynamic therapy. European
- 79 Journal of Pharmaceutical Sciences, 132, 63–71.
- 80 https://doi.org/10.1016/j.ejps.2019.02.025
- 81 Bailey, M. M., & Berkland, C. J. (2009). Nanoparticle formulations in pulmonary drug
- 82 delivery. *Medicinal Research Reviews*, 29(1), 196–212.
- https://doi.org/10.1002/med.20140
- 84 Barnes, P. J. (2008). The cytokine network in asthma and chronic obstructive pulmonary
- disease. In *Journal of Clinical Investigation* (Vol. 118, Issue 11, pp. 3546–3556).
- 86 https://doi.org/10.1172/JCI36130
- 87 Barnes, P. J. (2013). Theophylline. American Journal of Respiratory and Critical Care
- 88 *Medicine*, 188(8), 901–906. https://doi.org/10.1164/rccm.201302-0388PP
- 89 Barnes, P. J., Burney, P. G. J., Silverman, E. K., Celli, B. R., Vestbo, J., Wedzicha, J. A.,
- Wouters, E. F. M. (2015). Chronic obstructive pulmonary disease. *Nature Reviews*
- 91 *Disease Primers*, 1. https://doi.org/10.1038/nrdp.2015.76
- Barnes, P. J., Chowdhury, B., Kharitonov, S. A., Magnussen, H., Page, C. P., Postma, D.,
- 8 Saetta, M. (2006). Pulmonary biomarkers in chronic obstructive pulmonary
- 94 disease. American Journal of Respiratory and Critical Care Medicine, 174(1), 6-
- 95 14. https://doi.org/10.1164/rccm.200510-1659PP
- 96 Barreneche, C., Gil, A., Sheth, F., Inés Fernández, A., & Cabeza, L. F. (2013). Effect of
- d-mannitol polymorphism in its thermal energy storage capacity when it is used as
- 98 PCM. Solar Energy, 94, 344–351. https://doi.org/10.1016/j.solener.2013.05.023
- 99 Baye, J. (2012). Roflumilast (Daliresp). *P&T*, *37*(3).
- Beavo, J. H., & Brunton, L. L. (2002). Cyclic nucleotide research still expanding after
- half a century. *Nat Rev Mol Cell Biol*, *3*, 710–718.

- Beck-Broichsitter, M., Stoisiek, K., Bohr, A., Aragão-Santiago, L., Gessler, T., Seeger,
- W., & Kissel, T. (2016). Potential of the isolated lung technique for the examination
- of sildenafil absorption from lung-delivered poly(lactide-co-glycolide)
- microparticles. Journal of Controlled Release, 226, 15–20.
- 106 https://doi.org/10.1016/j.jconrel.2016.01.057
- Benetti, A. A., Bianchera, A., Buttini, F., Bertocchi, L., & Bettini, R. (2021). Mannitol
- polymorphs as carrier in dpis formulations: Isolation characterization and
- performance. *Pharmaceutics*, 13(8).
- https://doi.org/10.3390/pharmaceutics13081113
- Bethke, T. D., Böhmer, G. M., Hermann, R., Hauns, B., Fux, R., Mörike, K., David, M.,
- Knoerzer, D., Wurst, W., & Gleiter, C. H. (2007). Dose-proportional intraindividual
- single- and repeated-dose pharmacokinetics of roflumilast, an oral, once-daily
- phosphodiesterase 4 inhibitor. *Journal of Clinical Pharmacology*, 47(1), 26–36.
- https://doi.org/10.1177/0091270006294529
- Bhowmik, A., Seemungal, T. A. R., Sapsford, R. J., & Wedzicha, J. A. (2000). Relation
- of sputum inflammatory markers to symptoms and lung function changes in COPD
- exacerbations. *Thorax*, 55(2), 114–120. https://doi.org/10.1136/thorax.55.2.114
- Biddiscombe, M. F., & Usmani, O. S. (2018). Is there room for further innovation in
- inhaled therapy for airways disease? *Breathe*, 14(3), 216–224.
- 121 https://doi.org/10.1183/20734735.020318
- Bohr, A., Ruge, C. A., & Beck-Broichsitter, M. (2014). Preparation of Nanoscale
- Pulmonary Drug Delivery Formulations by Spray Drying. In D. G. Capco & Y. Chen
- 124 (Eds.), Nanomaterial: Impact on Cell Biology and Medicine (Vol. 811, pp. 183–
- 125 206). Springer Netherlands . http://www.springer.com/series/5584
- Boswell-Smith, V., Cazzola, M., & Page, C. (2006). Are phosphodiesterase 4 inhibitors
- just more theophylline? *Journal of Allergy and Clinical Immunology*, 117(6), 1237–
- 128 1243. https://doi.org/10.1016/j.jaci.2006.02.045
- Bozinovski, S., Jones, J., Beavitt, S.-J., Cook, A. D., Hamilton, J. A., & Anderson, G. P.
- 130 (2004). Innate immune response to LPS in mouse lung are suppressed and reversed
- by neutralization of GM-CSF via repression of TLR-4. Am J Physiol Lung Cell Mol
- 132 *Physiol*, 286, 877–885. https://doi.org/10.1152/ajplung.00275.2003.-The
- Bucchioni, E., Kharitonov, S. A., Allegra, L., & Barnes, P. J. (2003). High levels of
- interleukin-6 in the exhaled breath condensate of patients with COPD. *Respiratory*
- 135 *Medicine*, 97(12), 1299–1302. https://doi.org/10.1016/j.rmed.2003.07.008

- Buenestado, A., Chaumais, M. C., Grassin-Delyle, S., Risse, P. A., Naline, E.,
- Longchampt, E., Tenor, H., & Devillier, P. (2013). Roflumilast Inhibits
- Lipopolysaccharide-Induced Tumor Necrosis Factor-α and Chemokine Production
- by Human Lung Parenchyma. *PLoS ONE*, 8(9).
- 140 https://doi.org/10.1371/journal.pone.0074640
- Buenestado, A., Grassin-Delyle, S., Guitard, F., Naline, E., Faisy, C., Israël-Biet, D.,
- Sage, E., Bellamy, J. F., Tenor, H., & Devillier, P. (2012). Roflumilast inhibits the
- release of chemokines and TNF-α from human lung macrophages stimulated with
- lipopolysaccharide. British Journal of Pharmacology, 165(6), 1877–1890.
- 145 https://doi.org/10.1111/j.1476-5381.2011.01667.x
- Buhecha, M. D., Lansley, A. B., Somavarapu, S., & Pannala, A. S. (2019). Development
- and characterization of PLA nanoparticles for pulmonary drug delivery: Co-
- encapsulation of theophylline and budesonide, a hydrophilic and lipophilic drug.
- 149 Journal of Drug Delivery Science and Technology, 53.
- https://doi.org/10.1016/j.jddst.2019.101128
- Bundschuh, D. S., Eltze, M., Barsig, J., Wollin, L., Hatzelmann, A., & Beume, R. (2001).
- In vivo efficacy in airway disease models of roflumilast, a novel orally active PDE4
- inhibitor. The Journal of Pharmacology and Experimental Therapeutics, 297(1),
- 154 280–290. http://www.ncbi.nlm.nih.gov/pubmed/11259555
- Bustamante-Marin, X. M., & Ostrowski, L. E. (2016). Cilia and mucociliary clearance.
- 156 Cold Spring Harbor Perspectives in Biology.
- 157 https://doi.org/10.1101/cshperspect.a028241
- 158 Calverley, P. M., Rabe, K. F., Goehring, U. M., Kristiansen, S., Fabbri, L. M., &
- Martinez, F. J. (2009). Roflumilast in symptomatic chronic obstructive pulmonary
- disease: two randomised clinical trials. *The Lancet*, 374(9691), 685–694.
- 161 https://doi.org/10.1016/S0140-6736(09)61255-1
- 162 Canning, B. J., & Chou, Y. (2008). Using guinea pigs in studies relevant to asthma and
- 163 COPD. Pulmonary Pharmacology and Therapeutics, 21(5), 702–720.
- 164 https://doi.org/10.1016/j.pupt.2008.01.004
- 165 Carpenter, R. L., Jiang, Y., Jing, Y., He, J., Rojanasakul, Y., Liu, L. Z., & Jiang, B. H.
- 166 (2011). Arsenite induces cell transformation by reactive oxygen species, AKT,
- 167 ERK1/2, and p70S6K1. Biochemical and Biophysical Research Communications,
- 168 *414*(3), 533–538. https://doi.org/10.1016/j.bbrc.2011.09.102

- 169 Carvalho, T. C., Carvalho, S. R., & McConville, J. T. (2011). Formulations for pulmonary
- administration of anticancer agents to treat lung malignancies. *Journal of Aerosol*
- 171 Medicine and Pulmonary Drug Delivery, 24(2), 61–80.
- 172 https://doi.org/10.1089/jamp.2009.0794
- 173 Carvalho, T. C., Peters, J. I., & Williams III, R. O. (2011). Influence of particle size on
- regional lung deposition What evidence is there? *International Journal of*
- 175 *Pharmaceutics*, 406(1–2), 1–10. https://doi.org/10.1016/j.ijpharm.2010.12.040
- 176 Cayman Chemical. (n.d.). *Roflumilast Product Information*.
- 177 Cazzola, M., Cavalli, F., Usmani, O. S., & Rogliani, P. (2020). Advances in pulmonary
- drug delivery devices for the treatment of chronic obstructive pulmonary disease.
- 179 Expert Opinion on Drug Delivery, 0(0), 1.
- https://doi.org/10.1080/17425247.2020.1739021
- 181 Celli, B. R., & Barnes, P. J. (2007). Exacerbations of chronic obstructive pulmonary
- disease. European Respiratory Journal, 29(6), 1224–1238.
- https://doi.org/10.1183/09031936.00109906
- 184 Celli, B. R., Fabbri, L. M., Aaron, S. D., Agusti, A., Brook, R., Criner, G. J., Franssen, F.
- M. E., Humbert, M., Hurst, J. R., O'Donnell, D., Pantoni, L., Papi, A., Rodriguez-
- Roisin, R., Sethi, S., Torres, A., Vogelmeier, C. F., & Wedzicha, J. A. (2021). An
- updated definition and severity classification of chronic obstructive pulmonary
- disease exacerbations: The rome proposal. American Journal of Respiratory and
- 189 *Critical Care Medicine*, 204(11), 1251–1258. https://doi.org/10.1164/rccm.202108-
- 190 1819PP
- 191 Chang, Q., Pan, J., Wang, X., Zhang, Z., Chen, F., & Shi, X. (2010). Reduced reactive
- oxygen species-generating capacity contributes to the enhanced cell growth of
- arsenic-transformed epithelial cells. Cancer Research, 70(12), 5127–5135.
- 194 https://doi.org/10.1158/0008-5472.CAN-10-0007
- 195 Chapman, R. W., House, A., Jones, H., Richard, J., Celly, C., Prelusky, D., Ting, P.,
- Hunter, J. C., Lamca, J., & Phillips, J. E. (2007). Effect of inhaled roflumilast on the
- prevention and resolution of allergen-induced late phase airflow obstruction in
- Brown Norway rats. European Journal of Pharmacology, 571(2-3), 215-221.
- 199 https://doi.org/10.1016/j.ejphar.2007.05.074
- 200 Chen, L., Xu, J., Deng, M., Liang, Y., Ma, J., Zhang, L., Wang, Y., & Zhang, J. (2021).
- Telmisartan mitigates lipopolysaccharide (LPS)-induced production of mucin 5AC

- 202 (MUC5AC) through increasing suppressor of cytokine signaling 1 (SOCS1).
- 203 Bioengineered, 12(1), 3912–3923. https://doi.org/10.1080/21655979.2021.1943605
- Chen, N., Brachmann, C., Liu, X., Pierce, D. W., Dey, J., Kerwin, W. S., Li, Y., Zhou,
- S., Hou, S., Carleton, M., Klinghoffer, R. A., Palmisano, M., & Chopra, R. (2015).
- Albumin-bound nanoparticle (nab) paclitaxel exhibits enhanced paclitaxel tissue
- distribution and tumor penetration. Cancer Chemotherapy and Pharmacology,
- 208 76(4), 699–712. https://doi.org/10.1007/s00280-015-2833-5
- 209 Cheng, Z., Li, M., Dey, R., & Chen, Y. (2021). Nanomaterials for cancer therapy: current
- progress and perspectives. Journal of Hematology and Oncology, 14(1).
- 211 https://doi.org/10.1186/s13045-021-01096-0
- 212 Chow, M. Y. T., Qiu, Y., Liao, Q., Kwok, P. C. L., Chow, S. F., Chan, H. K., & Lam, J.
- 213 K. W. (2019). High siRNA loading powder for inhalation prepared by co-spray
- drying with human serum albumin. *International Journal of Pharmaceutics*, 572.
- 215 https://doi.org/10.1016/j.ijpharm.2019.118818
- Christensen, P. J., Goodman, R. E., Pastoriza, L., Moore, B., & Toews, G. B. (1999).
- Animal Model Induction of Lung Fibrosis in the Mouse by Intratracheal Instillation
- of Fluorescein Isothiocyanate Is Not T-Cell-Dependent. American Journal of
- 219 *Pathology*, 155(5), 1773–1779.
- 220 Chung, K. F. (2001). Cytokines in chronic obstructive pulmonary disease. European
- 221 Respiratory Journal, Supplement, 18(34).
- 222 https://doi.org/10.1183/09031936.01.00229701
- Conti, M., Richter, W., Mehats, C., Livera, G., Park, J. Y., & Jin, C. (2003). Cyclic AMP-
- specific PDE4 phosphodiesterases as critical components of cyclic AMP signaling.
- 225 Journal of Biological Chemistry, 278(8), 5493–5496.
- 226 https://doi.org/10.1074/jbc.R200029200
- 227 Corlateanu, A., Mendez, Y., Wang, Y., Garnica, R. de J. A., Botnaru, V., & Siafakas, N.
- 228 (2020). "Chronic obstructive pulmonary disease and phenotypes: a state-of-the-art."
- 229 Pulmonology, 26(2), 95–100. https://doi.org/10.1016/j.pulmoe.2019.10.006
- Craparo, E. F., Cabibbo, M., Scialabba, C., Giammona, G., & Cavallaro, G. (2022).
- Inhalable Formulation Based on Lipid-Polymer Hybrid Nanoparticles for the
- Macrophage Targeted Delivery of Roflumilast. *Biomacromolecules*, 23(8), 3439–
- 233 3451. https://doi.org/10.1021/acs.biomac.2c00576

- 234 Crocetti, L., Floresta, G., Cilibrizzi, A., & Giovannoni, M. P. (2022). An Overview of
- PDE4 Inhibitors in Clinical Trials: 2010 to Early 2022. *Molecules*, 27(15), 4964.
- 236 https://doi.org/10.3390/molecules27154964
- Culpitt, S. v., de Matos, C., Russell, R. E., Donnelly, L. E., Rogers, D. F., & Barnes, P.
- J. (2002). Effect of theophylline on induced sputum inflammatory indices and
- 239 neutrophil chemotaxis in chronic obstructive pulmonary disease. *American Journal*
- of Respiratory and Critical Care Medicine, 165(10), 1371–1376.
- 241 https://doi.org/10.1164/rccm.2105106
- 242 Cunningham, S. M., & Tanner, D. A. (2020). A review: The prospect of inhaled insulin
- 243 therapy via vibrating mesh technology to treat diabetes. *International Journal of*
- 244 Environmental Research and Public Health, 17(16), 1–14.
- 245 https://doi.org/10.3390/ijerph17165795
- Dailey, L. A., Schmehl, T., Gessler, T., Wittmar, M., Grimminger, F., Seeger, W., &
- 247 Kissel, T. (2003). Nebulization of biodegradable nanoparticles: impact of nebulizer
- technology and nanoparticle characteristics on aerosol features. Journal of
- 249 *Controlled Release*, 86, 131–144. www.elsevier.com/locate/jconrel
- 250 Darquenne, C. (2012). Aerosol deposition in health and disease. Journal of Aerosol
- 251 Medicine and Pulmonary Drug Delivery, 25(3), 140–147.
- 252 https://doi.org/10.1089/jamp.2011.0916
- Das, S., Banerjee, R., & Bellare, J. (2005). Aspirin loaded albumin nanoparticles by
- coacervation: Implications in drug delivery. Trends in Biomaterials and Artificial
- 255 *Organs*, 18(2), 203–212.
- de Boer, A. H., Gjaltema, D., Hagedoorn, P., & Frijlink, H. W. (2002). Characterization
- of inhalation aerosols: a critical evaluation of cascade impactor analysis and laser
- diffraction technique. *International Journal of Pharmaceutics*, 249, 219–231.
- 259 www.elsevier.com/locate/ijpharm
- de Savi, C., Cox, R. J., Warner, D. J., Cook, A. R., Dickinson, M. R., McDonough, A.,
- Morrill, L. C., Parker, B., Andrews, G., Young, S. S., Gilmour, P. S., Riley, R., &
- Dearman, M. S. (2014). Efficacious inhaled PDE4 inhibitors with low emetic
- potential and long duration of action for the treatment of COPD. Journal of
- 264 *Medicinal Chemistry*, 57(11), 4661–4676. https://doi.org/10.1021/jm5001216
- Degryse, A. L., & Lawson, W. E. (2011). Progress toward improving animal models for
- idiopathic pulmonary fibrosis. American Journal of the Medical Sciences, 341(6),
- 267 444–449. https://doi.org/10.1097/MAJ.0b013e31821aa000

- Degryse, A. L., Tanjore, H., Xu, X. C., Polosukhin, V. v., Jones, B. R., McMahon, F. B.,
- Gleaves, L. A., Blackwell, T. S., & Lawson, W. E. (2010). Repetitive intratracheal
- bleomycin models several features of idiopathic pulmonary fibrosis. *American*
- 271 Journal of Physiology Lung Cellular and Molecular Physiology, 299(4).
- 272 https://doi.org/10.1152/ajplung.00026.2010
- Dent, G., White, S. R., Tenor, H., Bodtke, K., Schudt, C., Leff, A. R., Magnussen, H., &
- Rabe, K. F. (1998). Cyclic Nucleopeptide Phosphodiesterase in Human Bronchial
- 275 Epithelial Cells: Characterization of Isoenzymes and Functional Effects of PDE
- 276 Inhibitors. *Pulmonary Pharmacology & Therapeutics*, 11, 47–56.
- 277 Desai. (1999). *United States Patent*.
- Desai, N. (2011). Albumin drug nanoparticles. In: Kratz F, Senter P, Steinhagen H (eds)
- 279 Drug delivery in oncology: from basic research to cancer therapy. In *Drug Delivery*
- in Oncology: From Basic Research to Cancer Therapy (Vol. 2, pp. 1133–1161).
- 281 https://doi.org/10.1002/9783527634057.ch35
- 282 Desai, N., Trieu, V., Yao, Z., Louie, L., Ci, S., Yang, A., Tao, C., De, T., Beals, B., Dykes,
- D., Noker, P., Yao, R., Labao, E., Hawkins, M., & Soon-Shiong, P. (2006). Increased
- antitumor activity, intratumor paclitaxel concentrations, and endothelial cell
- transport of cremophor-free, albumin-bound paclitaxel, ABI-007, compared with
- cremophor-based paclitaxel. Clinical Cancer Research, 12(4), 1317–1324.
- 287 https://doi.org/10.1158/1078-0432.CCR-05-1634
- Desale, J. P., Swami, R., Kushwah, V., Katiyar, S. S., & Jain, S. (2018). Chemosensitizer
- and docetaxel-loaded albumin nanoparticle: Overcoming drug resistance and
- improving therapeutic efficacy. *Nanomedicine*, 13(21), 2759–2776.
- 291 https://doi.org/10.2217/nnm-2018-0206
- 292 Dinh, P. U. C., Paudel, D., Brochu, H., Popowski, K. D., Gracieux, M. C., Cores, J.,
- Huang, K., Hensley, M. T., Harrell, E., Vandergriff, A. C., George, A. K., Barrio,
- R. T., Hu, S., Allen, T. A., Blackburn, K., Caranasos, T. G., Peng, X., Schnabel, L.
- V., Adler, K. B., ... Cheng, K. (2020). Inhalation of lung spheroid cell secretome
- and exosomes promotes lung repair in pulmonary fibrosis. *Nature Communications*,
- 297 *11*(1). https://doi.org/10.1038/s41467-020-14344-7
- Dockal, M., Carter, D. C., & Rü, F. (1999). The Three Recombinant Domains of Human
- Serum Albumin. The Journal of Biological Chemistry, 274(41), 29303–29310.
- 300 http://www.jbc.org

- 301 Domscheit, H., Hegeman, M. A., Carvalho, N., & Spieth, P. M. (2020a). Molecular
- 302 Dynamics of Lipopolysaccharide-Induced Lung Injury in Rodents. In Frontiers in
- 303 Physiology (Vol. 11). Frontiers Media S.A.
- 304 https://doi.org/10.3389/fphys.2020.00036
- 305 Domscheit, H., Hegeman, M. A., Carvalho, N., & Spieth, P. M. (2020b). Molecular
- 306 Dynamics of Lipopolysaccharide-Induced Lung Injury in Rodents. In Frontiers in
- 307 Physiology (Vol. 11). Frontiers Media S.A.
- 308 https://doi.org/10.3389/fphys.2020.00036
- 309 Edis, Z., Wang, J., Waqas, M. K., Ijaz, M., & Ijaz, M. (2021). Nanocarriers-mediated
- drug delivery systems for anticancer agents: An overview and perspectives.
- 311 International Journal of Nanomedicine, 16, 1313–1330.
- 312 https://doi.org/10.2147/IJN.S289443
- Edwards, D. A., Hanes, J., Caponetti, G., Hrkach, J., Ben-Jebria, A., Eskew, M. L.,
- Mintzes, J., Deaver, D., Lotan, N., & Langer, R. (1997). Large Porous Particles for
- Pulmonary Drug Delivery. Science, 276, 1868–1871.
- Edwards, M. R., Facchinetti, F., Civelli, M., Villetti, G., & Johnston, S. L. (2016). Anti-
- inflammatory effects of the novel inhaled phosphodiesterase type 4 inhibitor
- 318 CHF6001 on virus-inducible cytokines. *Pharmacology Research and Perspectives*,
- 319 4(1). https://doi.org/10.1002/prp2.202
- 320 Elhissi, A. M. A., Faizi, M., Naji, W. F., Gill, H. S., & Taylor, K. M. G. (2007). Physical
- 321 stability and aerosol properties of liposomes delivered using an air-jet nebulizer and
- a novel micropump device with large mesh apertures. *International Journal of*
- 323 *Pharmaceutics*, 334(1–2), 62–70. https://doi.org/10.1016/j.ijpharm.2006.10.022
- Elsharkasy, O. M., Nordin, J. Z., Hagey, D. W., de Jong, O. G., Schiffelers, R. M.,
- Andaloussi, S. EL, & Vader, P. (2020). Extracellular vesicles as drug delivery
- 326 systems: Why and how? Advanced Drug Delivery Reviews, 159, 332–343.
- 327 https://doi.org/10.1016/j.addr.2020.04.004
- 328 El-Sherbiny, I. M., El-Baz, N. M., & Yacoub, M. H. (2015). Inhaled nano -and
- 329 microparticles for drug delivery. In Global Cardiology Science and Practice (Vol.
- 330 2015, Issue 1). HBKU Press. https://doi.org/10.5339/gcsp.2015.2
- Elzoghby, A. O., Elgohary, M. M., & Kamel, N. M. (2015). Implications of Protein- and
- Peptide-Based Nanoparticles as Potential Vehicles for Anticancer Drugs. In
- 333 Advances in Protein Chemistry and Structural Biology (1st ed., Vol. 98). Elsevier
- 334 Inc. https://doi.org/10.1016/bs.apcsb.2014.12.002

- Elzoghby, A. O., Samy, W. M., & Elgindy, N. A. (2012). Albumin-based nanoparticles
- as potential controlled release drug delivery systems. *Journal of Controlled Release*,
- 338 European Medicines Agency. (2010). CHMP assessment report- Daxas.
- 339 www.ema.europa.eu
- 340 Facchinetti, F., Civelli, M., Singh, D., Papi, A., Emirova, A., & Govoni, M. (2021).
- Tanimilast, A Novel Inhaled PDE-4 Inhibitor for the Treatment of Asthma and
- Chronic Obstructive Pulmonary Disease. Frontiers in Pharmacology, 12.
- 343 https://doi.org/10.3389/fphar.2021.740803
- 344 Fang, C. L., Wen, C. J., Aljuffali, I. A., Sung, C. T., Huang, C. L., & Fang, J. Y. (2015).
- Passive targeting of phosphatiosomes increases rolipram delivery to the lungs for
- treatment of acute lung injury: An animal study. Journal of Controlled Release, 213,
- 347 69–78. https://doi.org/10.1016/j.jconrel.2015.06.038
- 348 FDA. (2012). $OPTISON^{TM}$ (Perflutren Protein-Type A Microspheres Injectable
- 349 Suspension, USP).
- 350 Fischer, B. M., Pavlisko, E., & Voynow, J. A. (2011). Pathogenic triad in COPD:
- Oxidative stress, protease-antiprotease imbalance, and inflammation. *International*
- 352 *Journal of COPD*, 6(1), 413–421. https://doi.org/10.2147/COPD.S10770
- Forde, É., Kelly, G., Sweeney, L., Fitzgerald-Hughes, D., Macloughlin, R., & Devocelle,
- M. (2019). Vibrating mesh nebulisation of pro-antimicrobial peptides for use in
- 355 cystic fibrosis. *Pharmaceutics*, 11(5).
- 356 https://doi.org/10.3390/pharmaceutics11050239
- Foster, J. E., Gott, K., Schuyler, M. R., Kozak, W., & Tesfaigzi, Y. (2003). LPS-induced
- neutrophilic inflammation and Bcl-2 expression in metaplastic mucous cells. Am J
- 359 Physiol Lung Cell Mol Physiol, 285, 405–414.
- 360 https://doi.org/10.1152/ajplung.00249.2002.-Our
- Fredenberg, S., Wahlgren, M., Reslow, M., & Axelsson, A. (2011). The mechanisms of
- drug release in poly(lactic-co-glycolic acid)-based drug delivery systems A review.
- 363 International Journal of Pharmaceutics, 415(1-2), 34-52.
- 364 https://doi.org/10.1016/j.ijpharm.2011.05.049
- 365 Fu, Q., Sun, J., Zhang, W., Sui, X., Yan, Z., & He, Z. (2009). Nanoparticle Albumin -
- Bound (NAB) Technology is a Promising Method for Anti-Cancer Drug Delivery.
- Recent Patents on Anti-Cancer Drug Discovery, 4(3), 262–272.
- 368 https://doi.org/10.2174/157489209789206869

- Fuentes-Mattei, E., Rivera, E., Gioda, A., Sanchez-Rivera, D., Roman-Velazquez, F. R.,
- 370 & Jimenez-Velez, B. D. (2010). Use of human bronchial epithelial cells (BEAS-2B)
- 371 to study immunological markers resulting from exposure to PM2.5 organic extract
- from Puerto Rico. Toxicology and Applied Pharmacology, 243(3), 381–389.
- 373 https://doi.org/10.1016/j.taap.2009.12.009
- 374 Fung, S. Y., Oyaizu, T., Yang, H., Yuan, Y., Han, B., Keshavjee, S., & Liu, M. (2011).
- 375 The potential of nanoscale combinations of self-assembling peptides and amino
- acids of the Src tyrosine kinase inhibitor in acute lung injury therapy. *Biomaterials*,
- 32(16), 4000–4008. https://doi.org/10.1016/j.biomaterials.2011.02.005
- 378 Gagliardi, A., Giuliano, E., Venkateswararao, E., Fresta, M., Bulotta, S., Awasthi, V., &
- Cosco, D. (2021). Biodegradable Polymeric Nanoparticles for Drug Delivery to
- 380 Solid Tumors. Frontiers in Pharmacology, 12.
- 381 https://doi.org/10.3389/fphar.2021.601626
- 382 Galisteo-González, F., & Molina-Bolívar, J. A. (2014). Systematic study on the
- preparation of BSA nanoparticles. Colloids and Surfaces B: Biointerfaces, 123, 286–
- 384 292. https://doi.org/10.1016/j.colsurfb.2014.09.028
- Gallo, J. M., Hung, C. T., & Perrier, D. G. (1984). Analysis of albumin microsphere
- preparation. *International Journal of Pharmaceutics*, 22, 63–74.
- 387 Gao, W., Jia, X., Wu, J., Song, Y., Yin, J., Zhang, M., Qiu, N., Li, X., Wu, P., Qi, X., &
- Liu, Z. (2019). Preparation and evaluation of folate-decorated human serum albumin
- nanoparticles for the targeted delivery of sorafenib to enhance antihepatocarcinoma
- 390 efficacy. Journal of Drug Delivery Science and Technology, 54(September),
- 391 101349. https://doi.org/10.1016/j.jddst.2019.101349
- 392 GE Healthcare. (2015). NANOCOLL; Healthcare professional information.
- 393 https://doi.org/10.7810/9780046140205 4
- 394 Geiser, M. (2010). Update on Macrophage Clearance of Inhaled Micro- and
- Nanoparticles. Journal of Aerosol Medicine and Pulmonary Drug Delivery, 23(4),
- 396 207–217. https://doi.org/DOI: 10.1089=jamp.2009.0797
- 397 Geiser, M., Baumann, M., Cruz-Orive, L. M., Im Hof, V., Waber, U., & Gehr, P. (1994).
- The effect of particle inhalation on macrophage number and phagocytic activity in
- 399 the intrapulmonary conducting airways of hamsters. American Journal of
- 400 Respiratory Cell and Molecular Biology, 10(6), 594–603.
- 401 https://doi.org/10.1165/ajrcmb.10.6.8003338

- 402 Geiser, M., Casaulta, M., Kupferschmid, B., Schulz, H., Semmler-Behnke, M., &
- Kreyling, W. (2008). The role of macrophages in the clearance of inhaled ultrafine
- 404 titanium dioxide particles. American Journal of Respiratory Cell and Molecular
- 405 *Biology*, 38(3), 371–376. https://doi.org/10.1165/rcmb.2007-0138OC
- 406 Geiser, M., Cruz-Orive, L. M., Hof, V. I., & Gehr, P. (1990). Assessment of particle
- retention and clearance in the intrapulmonary conducting airways of hamster lungs
- with the fractionator. Journal of Microscopy, 160(3), 75–88.
- 409 https://doi.org/10.1016/0021-8502(90)90059-7
- 410 Geiser, M., Quaile, O., Wenk, A., Wigge, C., Eigeldinger-Berthou, S., Hirn, S., Schäffler,
- 411 M., Schleh, C., Möller, W., Mall, M. A., & Kreyling, W. G. (2013). Cellular uptake
- and localization of inhaled gold nanoparticles in lungs of mice with chronic
- obstructive pulmonary disease. Particle and Fibre Toxicology, 10(1), 1–10.
- 414 https://doi.org/10.1186/1743-8977-10-19
- 415 General Chapters_ 601_ AEROSOLS, NASAL SPRAYS, METERED-DOSE INHALERS,
- 416 AND DRY POWDER INHALERS. (n.d.).
- 417 Ghorani, V., Boskabady, M. H., Khazdair, M. R., & Kianmeher, M. (2017). Experimental
- animal models for COPD: a methodological review. *Tobacco Induced Diseases*,
- 419 *15*(1), 1–13. https://doi.org/10.1186/s12971-017-0130-2
- 420 Gill, K. K., Nazzal, S., & Kaddoumi, A. (2011). Paclitaxel loaded PEG5000-DSPE
- 421 micelles as pulmonary delivery platform: Formulation characterization, tissue
- distribution, plasma pharmacokinetics, and toxicological evaluation. European
- 423 Journal of Pharmaceutics and Biopharmaceutics, 79(2), 276–284.
- 424 https://doi.org/10.1016/j.ejpb.2011.04.017
- 425 Gohy, S., Carlier, F. M., Fregimilicka, C., Detry, B., Lecocq, M., Ladjemi, M. Z.,
- Verleden, S., Hoton, D., Weynand, B., Bouzin, C., & Pilette, C. (2019). Altered
- generation of ciliated cells in chronic obstructive pulmonary disease. *Scientific*
- 428 Reports, 9(1). https://doi.org/10.1038/s41598-019-54292-x
- 429 Gold Initiative for Chronic Obstructive Lung Disease, Global Strategy for the diagnosis,
- 430 managment, and prevention of chronic obstructive pulmonary disease. (2022).
- 431 Gong, J., Huo, M., Zhou, J., Zhang, Y., Peng, X., Yu, D., Zhang, H., & Li, J. (2009).
- Synthesis, characterization, drug-loading capacity and safety of novel octyl modified
- serum albumin micelles. *International Journal of Pharmaceutics*, 376(1–2), 161–
- 434 168. https://doi.org/10.1016/j.ijpharm.2009.04.033

- Greene, C. M., & McElvaney, N. G. (2009). Proteases and antiproteases in chronic
- neutrophilic lung disease Relevance to drug discovery. British Journal of
- 437 *Pharmacology*, 158(4), 1048–1058. https://doi.org/10.1111/j.1476-
- 438 5381.2009.00448.x
- 439 Grootendorst, D. C., Gauw, S. A., Verhoosel, R. M., Sterk, P. J., Hospers, J. J.,
- Bredenbröker, D., Bethke, T. D., Hiemstra, P. S., & Rabe, K. F. (2007). Reduction
- in sputum neutrophil and eosinophil numbers by the PDE4 inhibitor roflumilast in
- 442 patients with COPD. *Thorax*, 62(12), 1081–1087.
- 443 https://doi.org/10.1136/thx.2006.075937
- 444 Guillott, L., Medjane, S., Le-Barillec, K., Balloy, V., Danel, C., Chignard, M., & Si-
- Tahar, M. (2004). Response of human pulmonary epithelial cells to
- lipopolysaccharide involves toll-like receptor 4 (TLR4)-dependent signaling
- pathways: Evidence for an intracellular compartmentalization of TLR4. *Journal of*
- 448 *Biological Chemistry*, 279(4), 2712–2718. https://doi.org/10.1074/jbc.M305790200
- Gulati, N., Chellappan, D. K., MacLoughlin, R., Dua, K., & Dureja, H. (2021). Inhaled
- nano-based therapeutics for inflammatory lung diseases: Recent advances and future
- 451 prospects. *Life Sciences*, 285. https://doi.org/10.1016/j.lfs.2021.119969
- 452 Han, X., Na, T., Wu, T., & Yuan, B. Z. (2020). Human lung epithelial BEAS-2B cells
- exhibit characteristics of mesenchymal stem cells. *PLoS ONE*, 15(1).
- 454 https://doi.org/10.1371/journal.pone.0227174
- 455 Hassanin, I., & Elzoghby, A. (2020). Albumin-based nanoparticles: A promising strategy
- 456 to overcome cancer drug resistance. Cancer Drug Resistance, 3(4), 930–946.
- 457 https://doi.org/10.20517/cdr.2020.68
- 458 Hatzelmann, A., Morcillo, E. J., Lungarella, G., Adnot, S., Sanjar, S., Beume, R., Schudt,
- 459 C., & Tenor, H. (2010). The preclinical pharmacology of roflumilast A selective,
- oral phosphodiesterase 4 inhibitor in development for chronic obstructive pulmonary
- disease. Pulmonary Pharmacology and Therapeutics, 23(4), 235–256.
- 462 https://doi.org/10.1016/j.pupt.2010.03.011
- 463 Hatzelmann, A., & Schudt, C. (2001). Anti-inflammatory and immunomodulatory
- potential of the novel PDE4 inhibitor roflumilast in vitro. J Pharmacol Exp Ther,
- 465 297(1), 267–279. internal-pdf://6.28.148.40/Hatzelmann-2001-J Pharmacol Exp
- Ther.pdf%5Cnhttp://jpet.aspetjournals.org/content/jpet/297/1/267.full.pdf%5Cnhtt
- p://www.ncbi.nlm.nih.gov/pubmed/11259554

- 468 Hawkins, M. J., Soon-Shiong, P., & Desai, N. (2008). Protein nanoparticles as drug
- carriers in clinical medicine. Advanced Drug Delivery Reviews, 60(8), 876–885.
- 470 https://doi.org/10.1016/j.addr.2007.08.044
- 471 Hecker, L., Logsdon, N. J., Kurundkar, D., Kurundkar, A., Bernard, K., Hock, T.,
- Meldrum, E., Sanders, Y. Y., & Thannickal, V. J. (2014). Reversal of persistent
- fibrosis in aging by targeting Nox4-Nrf2 redox imbalance. Science Translational
- 474 *Medicine*, 6(231). https://doi.org/10.1126/scitranslmed.3008182
- 475 Heyder, J. (2004). Deposition of inhaled particles in the human respiratory tract and
- 476 consequences for regional targeting in respiratory drug delivery. *Proceedings of the*
- 477 American Thoracic Society, 1(4), 315–320. https://doi.org/10.1513/pats.200409-
- 478 046TA
- 479 Hofmann, W. (2011). Modelling inhaled particle deposition in the human lung-A review.
- 480 *Journal of Aerosol Science*, 42(10), 693–724.
- 481 https://doi.org/10.1016/j.jaerosci.2011.05.007
- 482 Hohlfeld, J. M., Schoenfeld, K., Lavae-Mokhtari, M., Schaumann, F., Mueller, M.,
- Bredenbroeker, D., Krug, N., & Hermann, R. (2008). Roflumilast attenuates
- pulmonary inflammation upon segmental endotoxin challenge in healthy subjects:
- 485 A randomized placebo-controlled trial. Pulmonary Pharmacology and
- 486 Therapeutics, 21(4), 616–623. https://doi.org/10.1016/j.pupt.2008.02.002
- Hoppentocht, M., Hagedoorn, P., Frijlink, H. W., & de Boer, A. H. (2014). Technological
- and practical challenges of dry powder inhalers and formulations. Advanced Drug
- 489 Delivery Reviews, 75, 18–31. https://doi.org/10.1016/j.addr.2014.04.004
- 490 Hornok, V. (2021). Serum albumin nanoparticles: Problems and prospects. *Polymers*,
- 491 *13*(21). https://doi.org/10.3390/polym13213759
- Hossen, S., Hossain, M. K., Basher, M. K., Mia, M. N. H., Rahman, M. T., & Uddin, M.
- J. (2019). Smart nanocarrier-based drug delivery systems for cancer therapy and
- 494 toxicity studies: A review. Journal of Advanced Research, 15, 1–18.
- 495 https://doi.org/10.1016/j.jare.2018.06.005
- 496 Houslay, M. D., & Adams, D. R. (2003). PDE4 cAMP phosphodiesterases: modular
- 497 enzymes that orchestrate signalling cross-talk, desensitization and
- 498 compartmentalization. *Biochem. J*, 370, 1–18.
- 499 Hudy, M. H., & Proud, D. (2013). Cigarette smoke enhances human rhinovirus-induced
- 500 CXCL8 production via HuR-mediated mRNA stabilization in human airway

- 501 epithelial cells. *Respiratory Research*, *14*(1). https://doi.org/10.1186/1465-9921-14-
- 502 88
- Hudy, M. H., Traves, S. L., Wiehler, S., & Proud, D. (2010). Cigarette smoke modulates
- 504 rhinovirus-induced airway epithelial cell chemokine production. European
- 505 Respiratory Journal, 35(6), 1256–1263.
- 506 https://doi.org/10.1183/09031936.00128809
- Hukkanen, J., Pelkonen, O., & Raunio, H. (2001). Expression of xenobiotic-metabolizing
- enzymes in human pulmonary tissue: possible role in susceptibility for ILD.
- 509 European Respiratory Journal , 18(32), 122–126.
- 510 Hureaux, J., Lagarce, F., Gagnadoux, F., Vecellio, L., Clavreul, A., Roger, E., Kempf,
- M., Racineux, J. L., Diot, P., Benoit, J. P., & Urban, T. (2009). Lipid nanocapsules:
- Ready-to-use nanovectors for the aerosol delivery of paclitaxel. *European Journal*
- of Pharmaceutics and Biopharmaceutics, 73(2), 239–246.
- 514 https://doi.org/10.1016/j.ejpb.2009.06.013
- 515 Ibarra-Sánchez, L. Á., Gámez-Méndez, A., Martínez-Ruiz, M., Nájera-Martínez, E. F.,
- Morales-Flores, B. A., Melchor-Martínez, E. M., Sosa-Hernández, J. E., Parra-
- 517 Saldívar, R., & Iqbal, H. M. N. (2022). Nanostructures for drug delivery in
- respiratory diseases therapeutics: Revision of current trends and its comparative
- analysis. Journal of Drug Delivery Science and Technology, 70.
- 520 https://doi.org/10.1016/j.jddst.2022.103219
- 521 Ibrahim, N. K., Desai, N., Legha, S., Soon-Shiong, P., Theriault, R. L., Rivera, E.,
- Esmaeli, B., Ring, S. E., Bedikian, A., Hortobagyi, G. N., & Ellerhorst, J. A. (2002).
- Phase I and pharmacokinetic study of ABI-007, a Cremophor-free, protein-
- stabilized, nanoparticle formulation of paclitaxel. Clinical Cancer Research: An
- 525 Official Journal of the American Association for Cancer Research, 8(5), 1038–1044.
- 526 Ibrahim, N. K., Samuels, B., Page, R., Doval, D., Patel, K. M., Rao, S. C., Nair, M. K.,
- Bhar, P., Desai, N., & Hortobagyi, G. N. (2005). Multicenter phase II Trial of ABI-
- 528 007, an albumin-bound paclitaxel, in women with metastatic breast cancer. *Journal*
- *of Clinical Oncology*, 23(25), 6019–6026. https://doi.org/10.1200/JCO.2005.11.013
- 530 Ito, E., Takai, A., Kondo, F., Masui, H., Imanishi, S., & Harada, K.-I. (2002). Comparison
- of protein phosphatase inhibitory activity and apparent toxicity of microcystins and
- related compounds. *Toxicon*, 1017–1025. www.elsevier.com/locate/toxicon
- Jahanban-Esfahlan, A., Dastmalchi, S., & Davaran, S. (2016). A simple improved
- desolvation method for the rapid preparation of albumin nanoparticles. *International*

- 535 Journal of Biological Macromolecules, 91, 703–709.
- 536 https://doi.org/10.1016/j.ijbiomac.2016.05.032
- Jakobsson, J. K. F., Aaltonen, H. L., Nicklasson, H., Gudmundsson, A., Rissler, J.,
- Wollmer, P., & Löndahl, J. (2018). Altered deposition of inhaled nanoparticles in
- subjects with chronic obstructive pulmonary disease. BMC Pulmonary Medicine,
- 540 18(1). https://doi.org/10.1186/s12890-018-0697-2
- Jang, B.-K., Lee, J. W., Choi, H., & Yim, S. V. (2020). Aronia melanocarpa fruit bioactive
- fraction attenuates lps-induced inflammatory response in human bronchial epithelial
- 543 cells. *Antioxidants*, 9(9), 1–14. https://doi.org/10.3390/antiox9090816
- 544 Jang, H. H., Cho, S. Y., Kim, M. J., Kim, J. B., Lee, S. H., Lee, M. Y., & Lee, Y. M.
- 545 (2016). Anti-inflammatory effects of Salvia plebeia R. Br extract in vitro and in
- ovalbumin-induced mouse model. Biological Research, 49(1).
- 547 https://doi.org/10.1186/s40659-016-0102-7
- Jenkins, R. G., Moore, B. B., Chambers, R. C., Eickelberg, O., Konigshoff, M., Kolb, M.,
- Laurent, G. J., Nanthakumar, C. B., Olman, M. A., Pardo, A., Selman, M., Sheppard,
- 550 D., Sime, P. J., Tager, A. M., Tatler, A. L., Thannickal, V. J., & White, E. S. (2017).
- An official American Thoracic Society Workshop Report: Use of Animal Models
- for the Preclinical Assessment of Potential Therapies for Pulmonary Fibrosis.
- American Journal of Respiratory Cell and Molecular Biology, 56(5), 667–679.
- 554 https://doi.org/10.1165/rcmb.2017-0096ST
- Jolley, C. J., & Moxham, J. (2009). A physiological model of patient-reported
- breathlessness during daily activities in COPD. European Respiratory Review,
- Jones, B., Donovan, C., Liu, G., Gomez, H. M., Chimankar, V., Harrison, C. L.,
- Wiegman, C. H., Adcock, I. M., Knight, D. A., Hirota, J. A., & Hansbro, P. M.
- 560 (2017). Animal models of COPD: What do they tell us? In Respirology (Vol. 22,
- Issue 1, pp. 21–32). Blackwell Publishing. https://doi.org/10.1111/resp.12908
- Jones, R. M., & Neef, N. (2012). Interpretation and prediction of inhaled drug particle
- accumulation in the lung and its associated toxicity. *Xenobiotica*, 42(1), 86–93.
- 564 https://doi.org/10.3109/00498254.2011.632827
- Joshi, M., Nagarsenkar, M., & Prabhakar, B. (2020). Albumin nanocarriers for pulmonary
- drug delivery: An attractive approach. Journal of Drug Delivery Science and
- 567 Technology, 56(January), 101529. https://doi.org/10.1016/j.jddst.2020.101529

- Joshi, M., & Prabhakar, B. (2021). Development of respirable rifampicin loaded bovine
- serum albumin formulation for the treatment of pulmonary tuberculosis. *Journal of*
- 570 Drug Delivery Science and Technology, 61.
- 571 https://doi.org/10.1016/j.jddst.2020.102197
- Karadag, F., Karul, A. B., Cildag, O., Yilmaz, M., & Ozcan, H. (2008). Biomarkers of
- systemic inflammation in stable and exacerbation phases of COPD. *Lung*, 186(6),
- 574 403–409. https://doi.org/10.1007/s00408-008-9106-6
- 575 Karami, K., Jamshidian, N., Hajiaghasi, A., & Amirghofran, Z. (2020a). BSA
- nanoparticles as controlled release carriers for isophethalaldoxime palladacycle
- 577 complex; synthesis, characterization,: In vitro evaluation, cytotoxicity and release
- kinetics analysis. New Journal of Chemistry, 44(11), 4394–4405.
- 579 https://doi.org/10.1039/c9nj05847h
- 580 Karami, K., Jamshidian, N., Hajiaghasi, A., & Amirghofran, Z. (2020b). BSA
- nanoparticles as controlled release carriers for isophethalaldoxime palladacycle
- complex; Synthesis, characterization,: In vitro evaluation, cytotoxicity and release
- kinetics analysis. New Journal of Chemistry, 44(11), 4394–4405.
- 584 https://doi.org/10.1039/c9nj05847h
- Karimi, M., Bahrami, S., Ravari, S. B., Zangabad, P. S., Mirshekari, H., Bozorgomid, M.,
- Shahreza, S., Sori, M., & Hamblin, M. R. (2016). Albumin nanostructures as
- advanced drug delivery systems. Expert Opinion on Drug Delivery, 13(11), 1609–
- 588 1623. https://doi.org/10.1080/17425247.2016.1193149
- Kaur, J., & Singh, P. K. (2022). Trypsin Detection Strategies: A Review. *Critical Reviews*
- 590 in Analytical Chemistry, 52(5), 949–967.
- 591 https://doi.org/10.1080/10408347.2020.1846490
- Ke, H., Wang, H., & Ye, M. (2011). Structural Insights into the Substrate Specificity of
- 593 Phosphodiesterases. In *Handbook of Experimental Pharmacology* (Vol. 204, pp.
- 594 121–132). https://doi.org/10.1007/978 3 642 13443 2
- Ke', Y., Reddel', R. R., Gerwin', B. I., Miyashita2, M., Mcmenamin', M., Lechner', J.
- F., & Harris, C. C. (1988). Human bronchial epithelial cells with integrated SV40
- *virus T antigen genes retain the ability to undergo squamous differentiation.*
- Keatings, V. M., Collins, P. D., Scott, D. M., & Barnes, P. J. (1996). Differences in
- Interleukin-8 and Tumor Necrosis Factor-a in Induced Sputum from Patients with
- 600 Chronic Obstructive Pulmonary Disease or Asthma. Am J Respir Crit Care Med,
- 601 *153*, 530–534.

- Keravis, T., & Lugnier, C. (2012). Cyclic nucleotide phosphodiesterase (PDE) isozymes
- as targets of the intracellular signalling network: Benefits of PDE inhibitors in
- various diseases and perspectives for future therapeutic developments. British
- 605 Journal of Pharmacology, 165(5), 1288–1305. https://doi.org/10.1111/j.1476-
- 606 5381.2011.01729.x
- Ketrat, S., Japrung, D., & Pongprayoon, P. (2020). Exploring how structural and dynamic
- properties of bovine and canine serum albumins differ from human serum albumin.
- 609 Journal of Molecular Graphics and Modelling, 98.
- https://doi.org/10.1016/j.jmgm.2020.107601
- Khan, O., & Chaudary, N. (2020). The use of amikacin liposome inhalation suspension
- 612 (Arikayce) in the treatment of refractory nontuberculous mycobacterial lung disease
- 613 in adults. Drug Design, Development and Therapy, 14, 2287–2294.
- 614 https://doi.org/10.2147/DDDT.S146111
- Kho, K., Cheow, W. S., Lie, R. H., & Hadinoto, K. (2010). Aqueous re-dispersibility of
- spray-dried antibiotic-loaded polycaprolactone nanoparticle aggregates for inhaled
- anti-biofilm therapy. *Powder Technology*, 203(3), 432–439.
- 618 https://doi.org/10.1016/j.powtec.2010.06.003
- Kho, K., & Hadinoto, K. (2010a). Aqueous re-dispersibility characterization of spray-
- dried hollow spherical silica nano-aggregates. Powder Technology, 198(3), 354
- 621 363. https://doi.org/10.1016/j.powtec.2009.11.031
- Kho, K., & Hadinoto, K. (2010b). Effects of excipient formulation on the morphology
- and aqueous re-dispersibility of dry-powder silica nano-aggregates. Colloids and
- 624 Surfaces A: Physicochemical and Engineering Aspects, 359(1-3), 71-81.
- 625 https://doi.org/10.1016/j.colsurfa.2010.01.066
- Kim, G., Piao, C., Oh, J., & Lee, M. (2018). Self-assembled polymeric micelles for
- combined delivery of anti-inflammatory gene and drug to the lungs by inhalation.
- 628 Nanoscale, 10(18), 8503–8514. https://doi.org/10.1039/c8nr00427g
- Kim, V., & Criner, G. J. (2015). The chronic bronchitis phenotype in chronic obstructive
- pulmonary disease: Features and implications. Current Opinion in Pulmonary
- 631 *Medicine*, 21(2), 133–141. https://doi.org/10.1097/MCP.000000000000145
- 632 Kimbell, J. S., Gross, E. A., Joyner, D. R., Godo, M. N., & Morgan, K. T. (1993).
- Application of Computational Fluid Dynamics to Regional Dosimetry of Inhaled
- 634 Chemicals in the Upper Respiratory Tract of the Rat. *Toxicology and Applied*
- 635 *Pharmacology*, 121, 253–263.

- Kips, J. C., Tavernier, J., & Pauwels, R. A. (1992). Tumor Necrosis Factor Causes
- Bronchial Hyperresponsiveness in Rats. American Review of Respiratory Disease,
- 638 *145*(2), 332–336.
- Koshkina, N. v, Gilbert, B. E., Clifford Waldrep, J., Seryshev, A., & Knight, V. (1999).
- Distribution of camptothecin after delivery as a liposome aerosol or following
- intramuscular injection in mice. Cancer Chemother Pharmacol, 44, 187–192.
- Koshkina, N. v, Waldrep, J. C., Roberts, L. E., Golunski, E., Melton, S., & Knight, V.
- 643 (2001). Paclitaxel Liposome Aerosol Treatment Induces Inhibition of Pulmonary
- Metastases in Murine Renal Carcinoma Model. Clinical Cancer Research, 7, 3258–
- 645 3262. http://aacrjournals.org/clincancerres/article-
- 646 pdf/7/10/3258/2078574/df1001003258.pdf
- Kouchakzadeh, H., Shojaosadati, S. A., & Shokri, F. (2014). Efficient loading and
- entrapment of tamoxifen in human serum albumin based nanoparticulate delivery
- system by a modified desolvation technique. Chemical Engineering Research and
- 650 Design, 92(9), 1681–1692. https://doi.org/10.1016/j.cherd.2013.11.024
- Krimmer, D. I., & Oliver, B. G. G. (2011). What can in vitro models of COPD tell us?
- 652 Pulmonary Pharmacology and Therapeutics, 24(5), 471–477.
- https://doi.org/10.1016/j.pupt.2010.12.002
- Kroll, F., Karlsson, J.-A., Lundberg, J. M., & Persson, C. G. A. (1990). Capsaicin-induced
- bronchoconstriction and neuropeptide release in guinea pig perfused lungs. *Journal*
- 656 of Applied Physiology, 68(4), 1679–1687.
- Kuehl, P. J., Anderson, T. L., Candelaria, G., Gershman, B., Harlin, K., Hesterman, J. Y.,
- Holmes, T., Hoppin, J., Lackas, C., Norenberg, J. P., Yu, H., & McDonald, J. D.
- 659 (2012). Regional particle size dependent deposition of inhaled aerosols in rats and
- 660 mice. *Inhalation Toxicology*, 24(1), 27–35.
- https://doi.org/10.3109/08958378.2011.632787
- Kufleitner, J., Wagner, S., Worek, F., Von Briesen, H., & Kreuter, J. (2010). Adsorption
- of obidoxime onto human serum albumin nanoparticles: Drug loading, particle size
- and drug release. Journal of Microencapsulation, 27(6), 506–513.
- https://doi.org/10.3109/02652041003681406
- Kunde, S. S., & Wairkar, S. (2022). Targeted delivery of albumin nanoparticles for breast
- 667 cancer: A review. Colloids and Surfaces B: Biointerfaces, 213.
- https://doi.org/10.1016/j.colsurfb.2022.112422

- Kuschner, W. G., D'Alessandro, A., Wong, H., & Blanc, P. D. (1996). Dose-dependent
- cigarette smoking-related inflammatory responses in healthy adults. European
- 671 Respiratory Journal, 9(10), 1989–1994.
- https://doi.org/10.1183/09031936.96.09101989
- 673 Laan, M., Bozinovski, S., & Anderson, G. P. (2004). Cigarette Smoke Inhibits
- 674 Lipopolysaccharide-Induced Production of Inflammatory Cytokines by Suppressing
- the Activation of Activator Protein-1 in Bronchial Epithelial Cells. *The Journal of*
- 676 *Immunology*, 173(6), 4164–4170. https://doi.org/10.4049/jimmunol.173.6.4164
- Labiris, N. R., & Dolovich, M. B. (2003). Pulmonary drug delivery. Part I: Physiological
- factors affecting therapeutic effectiveness of aerosolized medications. British
- 679 *Journal of Clinical Pharmacology*, 56(6), 588–599. https://doi.org/10.1046/j.1365-
- 680 2125.2003.01892.x
- Lakatos, H. F., Burgess, H. A., Thatcher, T. H., Redonnet, M. R., Hernady, E., Williams,
- J. P., & Sime, P. J. (2006). Oropharyngeal aspiration of a silica suspension produces
- a superior model of silicosis in the mouse when compared to intratracheal
- instillation. Experimental Lung Research, 32(5), 181–199.
- 685 https://doi.org/10.1080/01902140600817465
- 686 Laliberté, F., Han, Y., Govindarajan, A., Giroux, A., Liu, S., Bobechko, B., Lario, P.,
- Bartlett, A., Gorseth, E., Gresser, M., & Huang, Z. (2000). Conformational
- difference between PDE4 apoenzyme and holoenzyme. *Biochemistry*, 39(21), 6449–
- 689 6458. https://doi.org/10.1021/bi992432w
- Langer, K., Anhorn, M. G., Steinhauser, I., Dreis, S., Celebi, D., Schrickel, N., Faust, S.,
- & Vogel, V. (2008). Human serum albumin (HSA) nanoparticles: Reproducibility
- of preparation process and kinetics of enzymatic degradation. *International Journal*
- 693 of Pharmaceutics, 347(1–2), 109–117.
- 694 https://doi.org/10.1016/j.ijpharm.2007.06.028
- Langer, K., Balthasar, S., Vogel, V., Dinauer, N., von Briesen, H., & Schubert, D. (2003).
- Optimization of the preparation process for human serum albumin (HSA)
- 697 nanoparticles. International Journal of Pharmaceutics, 257(1–2), 169–180.
- 698 https://doi.org/10.1016/S0378-5173(03)00134-0
- 699 Larsson, R., Rocksén, D., Lilliehöök, B., Jonsson, Å., & Bucht, A. (2000). Dose-
- dependent activation of lymphocytes in endotoxin-induced airway inflammation.
- 701 Infection and Immunity, 68(12), 6962–6969.
- 702 https://doi.org/10.1128/IAI.68.12.6962-6969.2000

- 703 Laube, B. L., Links, J. M., Lafrance, N. D., Wagner, H. N., & Rosenstein, B.]. (1989).
- Homogeneity of Bronchopulmonary Distribution of 99mTc Aerosol in Normal
- Subjects and in Cystic Fibrosis Patients*. *Chest*, 95, 822–830.
- Laulicht, F., Brocato, J., Cartularo, L., Vaughan, J., Wu, F., Kluz, T., Sun, H., Oksuz, B.
- A., Shen, S., Paena, M., Medici, S., Zoroddu, M. A., & Costa, M. (2015). Tungsten-
- induced carcinogenesis in human bronchial epithelial cells. *Toxicology and Applied*
- 709 *Pharmacology*, 288(1), 33–39. https://doi.org/10.1016/j.taap.2015.07.003
- 710 Lea, S., Metryka, A., Li, J., Higham, A., Bridgewood, C., Villetti, G., Civelli, M.,
- Facchinetti, F., & Singh, D. (2019). The modulatory effects of the PDE4 inhibitors
- 712 CHF6001 and roflumilast in alveolar macrophages and lung tissue from COPD
- 713 patients. *Cytokine*, *123*. https://doi.org/10.1016/j.cyto.2019.154739
- 714 Lee, S. H., Heng, D., Ng, W. K., Chan, H. K., & Tan, R. B. H. (2011). Nano spray drying:
- A novel method for preparing protein nanoparticles for protein therapy.
- 716 International Journal of Pharmaceutics, 403(1–2), 192–200.
- 717 https://doi.org/10.1016/j.ijpharm.2010.10.012
- 718 Lee, S.-Y., Cho, J.-H., Cho, S. S., Bae, C.-S., Kim, G.-Y., & Park, D.-H. (2018).
- Establishment of a chronic obstructive pulmonary disease mouse model based on
- the elapsed time after LPS intranasal instillation. Laboratory Animal Research,
- 721 34(1), 1. https://doi.org/10.5625/lar.2018.34.1.1
- Leong, E. W. X., & Ge, R. (2022). Lipid Nanoparticles as Delivery Vehicles for Inhaled
- Therapeutics. *Biomedicines*, 10(2179). https://doi.org/10.3390/biomedicines
- Leung, K. K. M., Bridges, P. A., & Taylor, K. M. G. (1996). The stability of liposomes
- to ultrasonic nebulisation. *International Journal of Pharmaceutics*, 145, 102.
- 726 Lin, C. Y., Hsu, C. Y., Elzoghby, A. O., Alalaiwe, A., Hwang, T. L., & Fang, J. Y. (2019).
- Oleic acid as the active agent and lipid matrix in cilomilast-loaded nanocarriers to
- assist PDE4 inhibition of activated neutrophils for mitigating psoriasis-like lesions.
- Acta Biomaterialia, 90, 350–361. https://doi.org/10.1016/j.actbio.2019.04.002
- 730 Lin, W., Garnett, M. C., Davis, S. S., Schacht, E., Ferruti, P., & Illum, L. (2001a).
- Preparation and characterisation of rose Bengal-loaded surface-modified albumin
- nanoparticles. Journal of Controlled Release, 71(1), 117–126.
- 733 https://doi.org/10.1016/S0168-3659(01)00209-7
- Lin, W., Garnett, M. C., Davis, S. S., Schacht, E., Ferruti, P., & Illum, L. (2001b).
- Preparation and characterisation of rose Bengal-loaded surface-modified albumin

- nanoparticles. Journal of Controlled Release: Official Journal of the Controlled
- 737 *Release Society*, 71(1), 117–126.
- 738 Liu, F. C., Yu, H. P., Lin, C. Y., Elzoghby, A. O., Hwang, T. L., & Fang, J. Y. (2018).
- Use of cilomilast-loaded phosphatiosomes to suppress neutrophilic inflammation for
- attenuating acute lung injury: The effect of nanovesicular surface charge. *Journal of*
- 741 *Nanobiotechnology*, 16(1). https://doi.org/10.1186/s12951-018-0364-z
- Liu, F., Li, W., Pauluhn, J., Trübel, H., & Wang, C. (2013). Lipopolysaccharide-induced
- acute lung injury in rats: Comparative assessment of intratracheal instillation and
- 744 aerosol inhalation. *Toxicology*, 304, 158–166.
- 745 https://doi.org/10.1016/j.tox.2012.12.020
- 746 Lohcharoenkal, W., Wang, L., Chen, Y. C., & Rojanasakul, Y. (2014). Protein
- nanoparticles as drug delivery carriers for cancer therapy. BioMed Research
- 748 *International*, 2014. https://doi.org/10.1155/2014/180549
- Lomis, N., Westfall, S., Farahdel, L., Malhotra, M., Shum-Tim, D., & Prakash, S.
- 750 (2016a). Human Serum Albumin Nanoparticles for Use in Cancer Drug Delivery:
- Process Optimization and In Vitro Characterization. *Nanomaterials*, 6(6), 116.
- 752 https://doi.org/10.3390/nano6060116
- Lomis, N., Westfall, S., Farahdel, L., Malhotra, M., Shum-Tim, D., & Prakash, S.
- 754 (2016b). Human serum albumin nanoparticles for use in cancer drug delivery:
- Process optimization and in vitro characterization. *Nanomaterials*, 6(6).
- 756 https://doi.org/10.3390/nano6060116
- Lu, Y. C., Yeh, W. C., & Ohashi, P. S. (2008). LPS/TLR4 signal transduction pathway.
- 758 In *Cytokine* (Vol. 42, Issue 2, pp. 145–151).
- 759 https://doi.org/10.1016/j.cyto.2008.01.006
- 760 Mahmoud, A. A., Elkasabgy, N. A., & Abdelkhalek, A. A. (2018). Design and
- characterization of emulsified spray dried alginate microparticles as a carrier for the
- dually acting drug roflumilast. European Journal of Pharmaceutical Sciences, 122,
- 763 64–76. https://doi.org/10.1016/j.ejps.2018.06.015
- Malm, S. W., Amouzougan, E. A., & Klimecki, W. T. (2018). Fetal bovine serum induces
- sustained, but reversible, epithelial-mesenchymal transition in the BEAS-2B cell
- 766 line. *Toxicology in Vitro*, 50, 383–390. https://doi.org/10.1016/j.tiv.2018.04.008
- 767 Mannino, D. M. (2003). Chronic Obstructive Pulmonary Disease: Definition and
- 768 Epidemiology. *Respiratory Care*, 48(12), 1185–1191.

- 769 Mariotti, F., Govoni, M., Lucci, G., Santoro, D., & Nandeuil, M. A. (2018). Safety,
- tolerability, and pharmacokinetics of single and repeat ascending doses of CHF6001,
- a novel inhaled phosphodiesterase-4 inhibitor: Two randomized trials in healthy
- volunteers. International Journal of COPD, 13, 3399–3410.
- 773 https://doi.org/10.2147/COPD.S174156
- Marple, V. A., Olson, B. A., Santhanakrishnan, K., Roberts, D. L., Mitchell, J. P., &
- Hudson-curtis, B. L. (2004). Next Generation Pharmaceutical Impactor: A New
- 776 Impactor for Pharmaceutical Inhaler Testing. Part III. Extension of Archival
- 777 Calibration to 15 L/min. JOURNAL OF AEROSOL MEDICINE, 17(4).
- 778 Marple Virgil A., Ph. D. (2003). Next Generation Pharmaceutical Impactor (A New
- 779 Impactor for Pharmaceutical Inhaler Testing). Part I: Design. Journal of Aerosol
- 780 *Medicine*, 16(3), 283–299.
- Marsh, S. E., Travers, J., Weatherall, M., Williams, M. V., Aldington, S., Shirtcliffe, P.
- 782 M., Hansell, A. L., Nowitz, M. R., McNaughton, A. A., Soriano, J. B., & Beasley,
- R. W. (2008). Proportional classifications of COPD phenotypes. *Thorax*, 63(9),
- 784 761–767. https://doi.org/10.1136/thx.2007.089193
- Martorana, P. A., Beume, R., Lucattelli, M., Wollin, L., & Lungarella, G. (2005).
- Roflumilast fully prevents emphysema in mice chronically exposed to cigarette
- smoke. American Journal of Respiratory and Critical Care Medicine, 172(7), 848–
- 788 853. https://doi.org/10.1164/rccm.200411-1549OC
- Matthews, A. A., Ee, P. L. R., & Ge, R. (2020). Developing inhaled protein therapeutics
- for lung diseases. *Molecular Biomedicine*, 1(1). https://doi.org/10.1186/s43556-
- 791 020-00014-z
- Matute-Bello, G., Downey, G., Moore, B. B., Groshong, S. D., Matthay, M. A., Slutsky,
- 793 A. S., & Kuebler, W. M. (2011). An official american thoracic society workshop
- report: Features and measurements of experimental acute lung injury in animals. In
- 795 American Journal of Respiratory Cell and Molecular Biology (Vol. 44, Issue 5).
- 796 https://doi.org/10.1165/rcmb.2009-0210ST
- 797 Mazdaei, M., & Asare-Addo, K. (2022). A mini-review of Nanocarriers in drug delivery
- systems. British Journal of Pharmacy, 7(1). https://doi.org/10.5920/bjpharm.780
- 799 MeiLan K., H., Agusti, A., Calverley, P. M., Celli, B. R., Criner, G., Curtis, J. L., Fabbri,
- L. M., Goldin, J. G., Jones, P. W., MacNee, W., Make, B. J., Rabe, K. F., Rennard,
- S. I., Sciurba, F. C., Silverman, E. K., Vestbo, J., Washko, G. R., Wouters, E. F. M.,
- & Martinez, F. J. (2010). Chronic obstructive pulmonary disease phenotypes.

- 803 American Journal of Respiratory and Critical Care Medicine, 182(5), 598–604.
- 804 https://doi.org/10.1164/rccm.200912-1843CC
- Merodio, M., Arnedo, A., Renedo, M. J., & Irache, J. M. (2000). Ganciclovir-loaded
- albumin nanoparticles: Characterization and in vitro release properties. *European*
- 807 Journal of Pharmaceutical Sciences, 12(3), 251–259.
- 808 https://doi.org/10.1016/S0928-0987(00)00169-X
- Mitchell, J., Newman, S., & Chan, H.-K. (2007). In Vitro and In Vivo Aspects of Cascade
- Impactor Tests and Inhaler Performance: A Review. AAPS PharmSci Tech 2007.
- http://www.aapspharmscitech.org
- Moazeni, E., Gilani, K., Najafabadi, A. R., Reza Rouini, M., Mohajel, N., Amini, M., &
- Barghi, M. A. (2012). Preparation and evaluation of inhalable itraconazole chitosan
- based polymeric micelles. DARU, Journal of Pharmaceutical Sciences, 20(1).
- 815 https://doi.org/10.1186/2008-2231-20-85
- Moeller, A., Ask, K., Warburton, D., Jack, G. #, & Kolb, M. (2008). The bleomycin
- animal model: a useful tool to investigate treatment options for idiopathic pulmonary
- fibrosis? *International Journal of Biochemistry Cell Biology*, 40(3), 362–382.
- 819 Mohanraj, V. J., & Chen, Y. (2006). Nanoparticles A Review. Tropical Journal of
- 820 Pharmaceutical Research, 561–573.
- 821 https://doi.org/10.15621/ijphy/2015/v2i1/60039
- Moinard-Checot, D., Chevalier, Y., Briançon, S., Fessi, H., & Guinebretière, S. (2006).
- Nanoparticles for drug delivery: Review of the formulation and process difficulties
- 824 illustrated by the emulsion-diffusion process. Journal of Nanoscience and
- 825 Nanotechnology, 6(9–10), 2664–2681. https://doi.org/10.1166/jnn.2006.479
- Mokry, J., Giembycz, M., & Mokra, D. (2021). Editorial: Phosphodiesterases as Drug
- Targets in Airway and Inflammatory Diseases. Frontiers in Pharmacology, 12.
- 828 https://doi.org/10.3389/fphar.2021.657596
- Moore, B. B., & Hogaboam, C. M. (2008). Murine models of pulmonary fibrosis. Am J
- 830 Physiol Lung Cell Mol Physiol, 294, 152–160.
- https://doi.org/10.1152/ajplung.00313.2007.-Human
- Moore, B. B., Lawson, W. E., Oury, T. D., Sisson, T. H., Raghavendran, K., &
- Hogaboam, C. M. (2013). Animal models of fibrotic lung disease. In *American*
- *Journal of Respiratory Cell and Molecular Biology* (Vol. 49, Issue 2, pp. 167–179).
- https://doi.org/10.1165/rcmb.2013-0094TR

- Mora-Huertas, C. E., Fessi, H., & Elaissari, A. (2010). Polymer-based nanocapsules for
- drug delivery. International Journal of Pharmaceutics, 385(1–2), 113–142.
- https://doi.org/10.1016/j.ijpharm.2009.10.018
- Moretto, N., Caruso, P., Bosco, R., Marchini, G., Pastore, F., Armani, E., Amari, G.,
- Rizzi, A., Ghidini, E., de Fanti, R., Capaldi, C., Carzaniga, L., Hirsch, E., Buccellati,
- 841 C., Sala, A., Carnini, C., Patacchini, R., Decanale, M., Civelli, M., ... Facchinetti,
- F. (2015). CHF6001 II: A novel highly potent phosphodiesterase 4 inhibitor with
- robust anti-inflammatory activity and suitable for topical pulmonary delivery.
- Journal of Pharmacology and Experimental Therapeutics, 352(3), 559–567.
- 845 https://doi.org/10.1124/jpet.114.220558
- Müller, B. G., Leuenberger, H., & Kissel, T. (1996). Albumin nanospheres as carriers for
- passive drug targeting: An optimized manufacturing technique. *Pharmaceutical*
- 848 Research, 13(1), 32–37. https://doi.org/10.1023/A:1016064930502
- 849 Munkholm, M., & Mortensen, J. (2014a). Mucociliary clearance: Pathophysiological
- aspects. Clinical Physiology and Functional Imaging, 34(3), 171–177.
- https://doi.org/10.1111/cpf.12085
- Munkholm, M., & Mortensen, J. (2014b). Mucociliary clearance: Pathophysiological
- 853 aspects. Clinical Physiology and Functional Imaging, 34(3), 171–177.
- 854 https://doi.org/10.1111/cpf.12085
- 855 Murad, H. A., Habib, H. S., Rafeeq, M. M., Sulaiman, M. I., Abdulrahman, A. S., &
- Khabaz, M. N. (2017). Co-inhalation of roflumilast, rather than formoterol, with
- 857 fluticasone more effectively improves asthma in asthmatic mice. Experimental
- 858 *Biology* and *Medicine*, 242(5), 516–526.
- 859 https://doi.org/10.1177/1535370216685006
- 860 Muthumalage, T., & Rahman, I. (2019). Cannabidiol differentially regulates basal and
- LPS-induced inflammatory responses in macrophages, lung epithelial cells, and
- 862 fibroblasts. Toxicology and Applied Pharmacology, 382.
- 863 https://doi.org/10.1016/j.taap.2019.114713
- Najlah, M., Parveen, I., Alhnan, M. A., Ahmed, W., Faheem, A., Phoenix, D. A., Taylor,
- K. M. G., & Elhissi, A. (2014). The effects of suspension particle size on the
- performance of air-jet, ultrasonic and vibrating-mesh nebulisers. *International*
- 867 *Journal of Pharmaceutics*, 461(1–2), 234–241.
- 868 https://doi.org/10.1016/j.ijpharm.2013.11.022

- Nan, Y. (2019). Lung carcinoma therapy using epidermal growth factor receptor-targeted
- lipid polymeric nanoparticles co-loaded with cisplatin and doxorubicin. *Oncology*
- 871 Reports, 42(5), 2087–2096. https://doi.org/10.3892/or.2019.7323
- Nasr, M., Najlah, M., D'Emanuele, A., & Elhissi, A. (2014). PAMAM dendrimers as
- aerosol drug nanocarriers for pulmonary delivery via nebulization. *International*
- 874 *Journal of Pharmaceutics*, 461(1–2), 242–250.
- 875 https://doi.org/10.1016/j.ijpharm.2013.11.023
- Nassimi, M., Schleh, C., Lauenstein, H. D., Hussein, R., Hoymann, H. G., Koch, W.,
- Pohlmann, G., Krug, N., Sewald, K., Rittinghausen, S., Braun, A., & Müller-
- Goymann, C. (2010). A toxicological evaluation of inhaled solid lipid nanoparticles
- used as a potential drug delivery system for the lung. European Journal of
- 880 Pharmaceutics and Biopharmaceutics, 75(2), 107–116.
- https://doi.org/10.1016/j.ejpb.2010.02.014
- Newman, S. P. (2022). Fine Particle Fraction: The Good and the Bad. *Journal of Aerosol*
- 883 Medicine and Pulmonary Drug Delivery, 35(1), 2–10.
- https://doi.org/10.1089/jamp.2021.29056.spn
- Nials, A. T., Tralau-Stewart, C. J., Gascoigne, M. H., Ball, D. I., Ranshaw, L. E., &
- Knowles, R. G. (2011). In Vivo Characterization of GSK256066, a High-Affinity
- Inhaled Phosphodiesterase 4 Inhibitor. *Journal of Pharmacology and Experimental*
- 888 Therapeutics, 337(1), 137–144. https://doi.org/10.1124/jpet.110.173641
- 889 Nie, H., Xie, X., Zhang, D., Zhou, Y., Li, B., Li, F., Li, F., Cheng, Y., Mei, H., Meng, H.,
- 890 & Jia, L. (2020). Use of lung-specific exosomes for miRNA-126 delivery in non-
- 891 small cell lung cancer. Nanoscale, 12(2), 877–887.
- https://doi.org/10.1039/c9nr09011h
- 893 Niknejad, H., & Mahmoudzadeh, R. (2015). Comparison of different crosslinking
- methods for preparation of docetaxel-loaded albumin nanoparticles. *Iranian Journal*
- 895 *of Pharmaceutical Research*, *14*(2), 385–394.
- 896 Oberdörster, G. (1993). Lung dosimetry: Pulmonary clearance of inhaled particles.
- 897 Aerosol Science and Technology, 18(3), 279–289.
- 898 https://doi.org/10.1080/02786829308959605
- 899 O'Donnell, R., Breen, D., Wilson, S., & Djukanovic, R. (2006). Inflammatory cells in the
- 900 airways in COPD. *Thorax*, 61(5), 448–454.
- 901 https://doi.org/10.1136/thx.2004.024463

- 902 Osman, N., Kaneko, K., Carini, V., & Saleem, I. (2018). Carriers for the targeted delivery
- of aerosolized macromolecules for pulmonary pathologies. Expert Opinion on Drug
- 904 Delivery, 15(8), 821–834. https://doi.org/10.1080/17425247.2018.1502267
- 905 Osman, N. M., Sexton, D. W., & Saleem, I. Y. (2020). Toxicological assessment of
- nanoparticle interactions with the pulmonary system. *Nanotoxicology*, 14(1), 21–58.
- 907 https://doi.org/10.1080/17435390.2019.1661043
- Pandey, K. C., De, S., & Mishra, P. K. (2017). Role of proteases in chronic obstructive
- 909 pulmonary disease. Frontiers in Pharmacology, 8(AUG), 1–9.
- 910 https://doi.org/10.3389/fphar.2017.00512
- 911 Pápay, Z. E., Kósa, A., Böddi, B., Merchant, Z., Saleem, I. Y., Zariwala, M. G.,
- Klebovich, I., Somavarapu, S., & Antal, I. (2017). Study on the Pulmonary Delivery
- 913 System of Apigenin-Loaded Albumin Nanocarriers with Antioxidant Activity.
- Journal of Aerosol Medicine and Pulmonary Drug Delivery, 30(4), 274–288.
- 915 https://doi.org/10.1089/jamp.2016.1316
- Paranjpe, M., & Müller-Goymann, C. C. (2014). Nanoparticle-mediated pulmonary drug
- 917 delivery: A review. *International Journal of Molecular Sciences*, 15(4), 5852–5873.
- 918 https://doi.org/10.3390/ijms15045852
- 919 Park, Y. hee, Kim, D., Dai, J., & Zhang, Z. (2015). Human bronchial epithelial BEAS-
- 920 2B cells, an appropriate in vitro model to study heavy metals induced carcinogenesis.
- 921 Toxicology and Applied Pharmacology, 287(3), 240–245.
- 922 https://doi.org/10.1016/j.taap.2015.06.008
- 923 Patel. (2018). Microencapsulated human albumin nanoparticles for drug delivery to the
- 924 *lungs*. King's College London.
- Patel, A. R., Patel, A. R., Singh, S., Singh, S., & Khawaja, I. (2019). Global Initiative for
- 926 Chronic Obstructive Lung Disease: The Changes Made. Cureus.
- 927 https://doi.org/10.7759/cureus.4985
- 928 Patel, A., Redinger, N., Richter, A., Woods, A., Neumann, P. R., Keegan, G.,
- Childerhouse, N., Imming, P., Schaible, U. E., Forbes, B., & Dailey, L. A. (2020).
- In vitro and in vivo antitubercular activity of benzothiazinone-loaded human serum
- albumin nanocarriers designed for inhalation. Journal of Controlled Release, 328,
- 932 339–349. https://doi.org/10.1016/j.jconrel.2020.08.022
- 933 Pathak, Y., & Thassu, D. (2016). Drug Delivery Nanoparticles Formulation and
- 934 Characterization. In Drug Delivery Nanoparticles Formulation and
- 935 *Characterization* (Vol. 191). https://doi.org/10.3109/9781420078053

- 936 Patil, G. v. (2003). Biopolymer albumin for diagnosis and in drug delivery. Drug
- 937 Development Research, 58(3), 219–247. https://doi.org/10.1002/ddr.10157
- Patton, J. S., & Byron, P. R. (2007). Inhaling medicines: Delivering drugs to the body
- 939 through the lungs. *Nature Reviews Drug Discovery*, 6(1), 67–74.
- 940 https://doi.org/10.1038/nrd2153
- Peters, T. (1996). All about albumin: biochemistry, genetics, and medical applications.
- 942 Academic Press.
- 943 Phalen, R. F., Mendez, L. B., & Oldham, M. J. (2014). Nose-only aerosol exposure
- systems: Design, operation, and performance. In *Inhalation Toxicology* (pp. 43–56).
- 945 CRC Press. https://doi.org/10.1201/b16781
- Phillips, J. E. (2020a). Inhaled Phosphodiesterase 4 (PDE4) Inhibitors for Inflammatory
- 947 Respiratory Diseases. Frontiers in Pharmacology, 11(March), 1–7.
- 948 https://doi.org/10.3389/fphar.2020.00259
- Phillips, J. E. (2020b). Inhaled Phosphodiesterase 4 (PDE4) Inhibitors for Inflammatory
- 950 Respiratory Diseases. Frontiers in Pharmacology, 11.
- 951 https://doi.org/10.3389/fphar.2020.00259
- 952 Pilcer, G., Vanderbist, F., & Amighi, K. (2009). Preparation and characterization of
- spray-dried tobramycin powders containing nanoparticles for pulmonary delivery.
- 954 International Journal of Pharmaceutics, 365(1-2), 162–169.
- 955 https://doi.org/10.1016/j.ijpharm.2008.08.014
- 956 Pinto Reis, C., Neufeld, R. J., Ribeiro, A. J., & Veiga, F. (2006). Nanoencapsulation I.
- Methods for preparation of drug-loaded polymeric nanoparticles. *Nanomedicine*:
- 958 Nanotechnology, Biology, and Medicine, 2(1), 8–21.
- 959 https://doi.org/10.1016/j.nano.2005.12.003
- 960 Pleasants, R. A., & Hess, D. R. (2018). Aerosol delivery devices for obstructive lung
- 961 diseases. *Respiratory Care*, 63(6), 708–733. https://doi.org/10.4187/respcare.06290
- Praphawatvet, T., Peters, J. I., & Williams, R. O. (2020). Inhaled nanoparticles—An
- 963 updated review. International Journal of Pharmaceutics, 587.
- 964 https://doi.org/10.1016/j.ijpharm.2020.119671
- Pugin, J., Schurer-Malyt, C.-C., Leturcqt, D., Moriartyt, A., Ulevitch, R. J., & Tobias, P.
- 966 S. (1993). Lipopolysaccharide activation of human endothelial and epithelial cells is
- mediated by lipopolysaccharide-binding protein and soluble CD14. In *Proc. Natl.*
- 968 Acad. Sci. USA (Vol. 90).

- 969 Qu, N., Sun, Y., Li, Y., Hao, F., Qiu, P., Teng, L., Xie, J., & Gao, Y. (2019). Docetaxel-
- loaded human serum albumin (HSA) nanoparticles: Synthesis, characterization, and
- 971 evaluation. *BioMedical Engineering Online*, 18(1), 1–14.
- 972 https://doi.org/10.1186/s12938-019-0624-7
- Raabe, O. G., Al-Bayati, M. A., Teague, S. v., & Rasolt, A. (1988). Regional Deposition
- of Inhaled Monodisperse Coarse and Fine Aerosol Particles In Small Laboratory
- 975 Animals. *Ann. Occup. Hyg.* , *32*(Supplement 1), 53–63.
- 976 https://academic.oup.com/annweh/article/32/inhaled_particles_VI/53/152800
- Rabe, K. F., Bateman, E. D., O'Donnell, D., Witte, S., Bredenbroker, D., & Bethke, T.
- D. (2005). Roflumilast an oral anti-inflammatory treatment of chronic obstructive
- pulmonary disease: a randomised controlled trial. *The Lancet*, 366, 563–571.
- 980 Respaud, R., March, D., Parent, C., Pelat, T., Thullier, P., Tournamille, J. F., Viaud-
- 981 Massuard, M. C., Diot, P., Si-Tahar, M., Vecellio, L., & Heuzé-VourC'H, N. (2014).
- 982 Effect of formulation on the stability and aerosol performance of a nebulized
- 983 antibody. *MAbs*, 6(5), 1347–1355. https://doi.org/10.4161/mabs.29938
- Rietschel, E. T., Kirikae, T., Schade, F. U., Mamat, U., Schmidt, G., Loppnow, H., Ulmer,
- A. J., Zähringer, U., Seydel, U., & di Padova, F. (1994). Bacterial endotoxin:
- 986 molecular relationships of structure to activity and function. *The FASEB Journal*,
- 987 8(2), 217–225. https://doi.org/10.1096/fasebj.8.2.8119492
- 988 Robichaud, A., Stamatiou, P. B., Jin, S.-L. C., Lachance, N., MacDonald, D., Laliberté,
- 989 F., Liu, S., Huang, Z., Conti, M., & Chan, C.-C. (2002). Deletion of
- phosphodiesterase 4D in mice shortens α2-adrenoceptor–mediated anesthesia, a
- behavioral correlate of emesis. Journal of Clinical Investigation, 110(7), 1045-
- 992 1052. https://doi.org/10.1172/jci15506
- 993 Roca, M., Verduri, A., Corbetta, L., Clini, E., Fabbri, L. M., & Beghé, B. (2013).
- Mechanisms of acute exacerbation of respiratory symptoms in chronic obstructive
- 995 pulmonary disease. European Journal of Clinical Investigation, 43(5), 510–521.
- 996 https://doi.org/10.1111/eci.12064
- 997 Rodriguez-Roisin, R. (2000). Toward a Consensus Definition for COPD Exacerbations*.
- 998 *Chest*, 17 (5 Suppl 2), 398S-401S.
- 999 Rojas, M., Xu, J., Woods, C. R., Mora, A. L., Spears, W., Roman, J., & Brigham, K. L.
- 1000 (2005). Bone marrow-derived mesenchymal stem cells in repair of the injured lung.
- 1001 American Journal of Respiratory Cell and Molecular Biology, 33(2), 145–152.
- 1002 https://doi.org/10.1165/rcmb.2004-0330OC

- 1003 Ruan, C., Liu, L., Lu, Y., Zhang, Y., He, X., Chen, X., Zhang, Y., Chen, Q., Guo, Q.,
- Sun, T., & Jiang, C. (2018). Substance P-modified human serum albumin
- nanoparticles loaded with paclitaxel for targeted therapy of glioma. Acta
- 1006 Pharmaceutica Sinica B, 8(1), 85–96. https://doi.org/10.1016/j.apsb.2017.09.008
- Rubin, L. F. (1975). Toxicity of dimethyl sulfoxide alone and in combination. *Annals of*
- the New York Academy of Sciences, 243(1), 98–103. https://doi.org/10.1111/j.1749-
- 1009 6632.1975.tb25348.x
- 1010 Rudokas, M., Najlah, M., Alhnan, M. A., & Elhissi, A. (2016). Liposome Delivery
- 1011 Systems for Inhalation: A Critical Review Highlighting Formulation Issues and
- 1012 Anticancer Applications. *Medical Principles and Practice*, 25(2), 60–72.
- 1013 https://doi.org/10.1159/000445116
- Ruge, C. A., Bohr, A., Beck-Broichsitter, M., Nicolas, V., Tsapis, N., & Fattal, E. (2016).
- Disintegration of nano-embedded microparticles after deposition on mucus: A
- mechanistic study. Colloids and Surfaces B: Biointerfaces, 139, 219-227.
- 1017 https://doi.org/10.1016/j.colsurfb.2015.12.017
- 1018 Sadeghi, R., Moosavi-Movahedi, A. A., Emam-Jomeh, Z., Kalbasi, A., Razavi, S. H.,
- Karimi, M., & Kokini, J. (2014). The effect of different desolvating agents on BSA
- nanoparticle properties and encapsulation of curcumin. Journal of Nanoparticle
- 1021 Research, 16(9). https://doi.org/10.1007/s11051-014-2565-1
- Salvator, H., Buenestado, A., Brollo, M., Naline, E., Victoni, T., Longchamp, E., Tenor,
- H., Grassin-Delyle, S., & Devillier, P. (2020). Clinical Relevance of the Anti-
- inflammatory Effects of Roflumilast on Human Bronchus: Potentiation by a Long-
- 1025 Acting Beta-2-Agonist. Frontiers in Pharmacology, 11.
- 1026 https://doi.org/10.3389/fphar.2020.598702
- 1027 Schioppa, T., Nguyen, H. O., Salvi, V., Maugeri, N., Facchinetti, F., Villetti, G., Civelli,
- M., Gaudenzi, C., Passari, M., Sozio, F., Barbazza, I., Tamassia, N., Cassatella, M.
- A., del Prete, A., Bosisio, D., & Tiberio, L. (2022). The PDE4 Inhibitor Tanimilast
- 1030 Restrains the Tissue-Damaging Properties of Human Neutrophils. *International*
- Journal of Molecular Sciences, 23(9). https://doi.org/10.3390/ijms23094982
- Schulz, C., Farkas, L., Wolf, K., Kra È Tzel, K., Eissneryz, G., & Pfeifer, M. (2002).
- 1033 Differences in LPS-Induced Activation of Bronchial Epithelial Cells (BEAS-2B) and
- 1034 Type II-Like Pneumocytes (A-549).
- 1035 Scutera, S., Argenziano, M., Sparti, R., Bessone, F., Bianco, G., Bastiancich, C.,
- 1036 Castagnoli, C., Stella, M., Musso, T., & Cavalli, R. (2021). Enhanced antimicrobial

- and antibiofilm effect of new colistin-loaded human albumin nanoparticles.
- 1038 *Antibiotics*, 10(1), 1–13. https://doi.org/10.3390/antibiotics10010057
- 1039 Sebak, S., Mirzaei, M., Malhotra, M., Kulamarva, A., & Prakash, S. (2010). Human
- serum albumin nanoparticles as an efficient noscapine drug delivery system for
- potential use in breast cancer: Preparation and in vitro analysis. *International*
- Journal of Nanomedicine, 5(1), 525–532. https://doi.org/10.2147/IJN.S10443
- Segal, L. N., Weiden, M. D., & Horowitz, H. W. (2015). Acute Exacerbations of Chronic
- Obstructive Pulmonary Disease. In Mandell, Douglas, and Bennett's Principles and
- 1045 *Practice of Infectious Diseases* (pp. 810–817).
- Shah, S., Cristopher, D., Sharma, S., Soniwala, M., & Chavda, J. (2020). Inhalable
- linezolid loaded PLGA nanoparticles for treatment of tuberculosis: Design,
- development and in vitro evaluation. Journal of Drug Delivery Science and
- 1049 *Technology*, 60. https://doi.org/10.1016/j.jddst.2020.102013
- Shan, X., Gong, X., Li, J., Wen, J., Li, Y., & Zhang, Z. (2022). Current approaches of
- nanomedicines in the market and various stage of clinical translation. Acta
- 1052 *Pharmaceutica Sinica B*, 12(7), 3028–3048.
- 1053 https://doi.org/10.1016/j.apsb.2022.02.025
- Sherje, A. P., Jadhav, M., Dravyakar, B. R., & Kadam, D. (2018). Dendrimers: A versatile
- nanocarrier for drug delivery and targeting. *International Journal of Pharmaceutics*,
- 548(1), 707–720. https://doi.org/10.1016/j.ijpharm.2018.07.030
- Shi, D., He, Z., & Qi, W. (2005). Lumping kinetic study on the process of tryptic
- hydrolysis of bovine serum albumin. *Process Biochemistry*, 40(5), 1943–1949.
- 1059 https://doi.org/10.1016/j.procbio.2004.07.009
- Siegel, A., & Walton, R. M. (2020). Hematology and Biochemistry of Small Mammals.
- In Ferrets, Rabbits and Rodent (pp. 569–582).
- Siepmann, J., & Siepmann, F. (2020). Sink conditions do not guarantee the absence of
- saturation effects. International Journal of Pharmaceutics, 577.
- 1064 https://doi.org/10.1016/j.ijpharm.2019.119009
- 1065 Silva, A. S., Tavares, M. T., & Aguiar-Ricardo, A. (2014). Sustainable strategies for
- nano-in-micro particle engineering for pulmonary delivery. *Journal of Nanoparticle*
- 1067 Research, 16(11). https://doi.org/10.1007/s11051-014-2602-0
- Singh, D., Lea, S., & Mathioudakis, A. G. (2021). Inhaled Phosphodiesterase Inhibitors
- for the Treatment of Chronic Obstructive Pulmonary Disease. *Drugs*, 81(16), 1821–
- 1070 1830. https://doi.org/10.1007/s40265-021-01616-9

- 1071 Sleep, D. (2015). Albumin and its application in drug delivery. Expert Opinion on Drug
- 1072 Delivery, 12(5), 793–812. https://doi.org/10.1517/17425247.2015.993313
- Sleijfer, S. (2001). Bleomycin-Induced Pneumonitis*. *Chest*, 120(2), 617–624.
- Smith, K. R., Leonard, D., McDonald, J. D., & Tesfaigzi, Y. (2011). Inflammation,
- mucous cell metaplasia, and Bcl-2 expression in response to inhaled
- lipopolysaccharide aerosol and effect of rolipram. Toxicology and Applied
- 1077 *Pharmacology*, 253(3), 253–260. https://doi.org/10.1016/j.taap.2011.04.001
- 1078 Snider. (1989). Chronic Obstructive Pulmonary Disease: A Definition and Implications
- of Structural Determinants of Airflow Obstruction for Epidemiology [Article]. Am
- 1080 Rev Respir Dis, 140, S3–S8. https://doi.org/10.1164/ajrccm/140.3_pt_2.s3
- 1081 Souness, J. E., & Rao, S. (1997). Proposal for Pharmacologically Distinct Conformers of
- 1082 PDE4 Cyclic AMP Phosphodiesterases. *Cell. Signal*, 9(4), 227–236.
- Spada, A., Emami, J., Tuszynski, J. A., & Lavasanifar, A. (2021). The Uniqueness of
- 1084 Albumin as a Carrier in Nanodrug Delivery. Molecular Pharmaceutics,
- acs.molpharmaceut.1c00046. https://doi.org/10.1021/acs.molpharmaceut.1c00046
- 1086 Stecenko, A. A., King, G., Torii, K., Breyer, R. M., Dworski, R., Blackwell, T. S.,
- 1087 Christman, J. W., & Brigham, K. L. (2001). Dysregulated Cytokine Production in
- Human Cystic Fibrosis Bronchial Epithelial Cells. *Inflammation*, 25(3).
- 1089 Stockley, R. A. (1999). Neutrophils and protease/antiprotease imbalance. American
- 1090 *Journal of Respiratory and Critical Care Medicine*, 160(5 II).
- Sundar, S., Kundu, J., & Kundu, S. C. (2010). Biopolymeric nanoparticles. Science and
- 1092 Technology of Advanced Materials, 11(1), 014104. https://doi.org/10.1088/1468-
- 1093 6996/11/1/014104
- Sung, J. C., Pulliam, B. L., & Edwards, D. A. (2007). Nanoparticles for drug delivery to
- the lungs. Trends in Biotechnology, 25(12), 563–570.
- 1096 https://doi.org/10.1016/j.tibtech.2007.09.005
- Takenaka, S., Möller, W., Semmler-Behnke, M., Karg, E., Wenk, A., Schmid, O.,
- Stoeger, T., Jennen, L., Aichler, M., Walch, A., Pokhrel, S., Mädler, L., Eickelberg,
- O., & Kreyling, W. G. (2012). Efficient internalization and intracellular
- translocation of inhaled gold nanoparticles in rat alveolar macrophages.
- Nanomedicine, 7(6), 855–865. https://doi.org/10.2217/nnm.11.152
- 1102 Tanner, L., & Single, A. B. (2019). Animal Models Reflecting Chronic Obstructive
- Pulmonary Disease and Related Respiratory Disorders: Translating Pre-Clinical

- Data into Clinical Relevance. Journal of Innate Immunity.
- 1105 https://doi.org/10.1159/000502489
- 1106 Tantra, R., Schulze, P., & Quincey, P. (2010). Effect of nanoparticle concentration on
- zeta-potential measurement results and reproducibility. Particuology, 8(3), 279-
- 1108 285. https://doi.org/10.1016/j.partic.2010.01.003
- 1109 Tarhini, M., Benlyamani, I., Hamdani, S., Agusti, G., Fessi, H., Greige-Gerges, H.,
- Bentaher, A., & Elaissari, A. (2018). Protein-based nanoparticle preparation via
- 1111 nanoprecipitation method. *Materials*, 11(3), 1–18.
- 1112 https://doi.org/10.3390/ma11030394
- 1113 Tarhini, M., Greige-Gerges, H., & Elaissari, A. (2017). Protein-based nanoparticles:
- From preparation to encapsulation of active molecules. *International Journal of*
- 1115 *Pharmaceutics*, 522(1–2), 172–197. https://doi.org/10.1016/j.ijpharm.2017.01.067
- 1116 Tashiro, J., Rubio, G. A., Limper, A. H., Williams, K., Elliot, S. J., Ninou, I., Aidinis, V.,
- 1117 Tzouvelekis, A., & Glassberg, M. K. (2017). Exploring Animal Models That
- 1118 Resemble Idiopathic Pulmonary Fibrosis. Frontiers in Medicine, 4(JUL).
- 1119 https://doi.org/10.3389/fmed.2017.00118
- Thakor, A. S., Jokerst, J. v., Ghanouni, P., Campbell, J. L., Mittra, E., & Gambhir, S. S.
- 1121 (2016). Clinically Approved Nanoparticle Imaging Agents. Journal of Nuclear
- 1122 *Medicine*, 57(12), 1833–1837. https://doi.org/10.2967/jnumed.116.181362
- Thanh, N. T. K., Maclean, N., & Mahiddine, S. (2014). Mechanisms of nucleation and
- growth of nanoparticles in solution. *Chemical Reviews*, 114(15), 7610–7630.
- 1125 https://doi.org/10.1021/cr400544s
- 1126 Thao, L. Q., Byeon, H. J., Lee, C., Lee, S., Lee, E. S., Choi, H. G., Park, E. S., & Youn,
- Y. S. (2016). Pharmaceutical potential of tacrolimus-loaded albumin nanoparticles
- having targetability to rheumatoid arthritis tissues. *International Journal of*
- 1129 *Pharmaceutics*, 497(1–2), 268–276. https://doi.org/10.1016/j.ijpharm.2015.12.004
- Torge, A., Grützmacher, P., Mücklich, F., & Schneider, M. (2017). The influence of
- mannitol on morphology and disintegration of spray-dried nano-embedded
- microparticles. European Journal of Pharmaceutical Sciences, 104, 171-179.
- https://doi.org/10.1016/j.ejps.2017.04.003
- 1134 Toward, T. J., & Broadley, K. J. (2000). Airway reactivity, inflammatory cell in influx
- and nitric oxide in guinea-pig airways after lipopolysaccharide inhalation. *British*
- Journal of Pharmacology, 131(2), 271–281. www.nature.com/bjp

- 1137 Tralau-Stewart, C. J., Williamson, R. A., Nials, A. T., Gascoigne, M., Dawson, J., Hart,
- G. J., Angell, A. D. R., Solanke, Y. E., Lucas, F. S., Wiseman, J., Ward, P., Ranshaw,
- L. E., & Knowles, R. G. (2011). GSK256066, an exceptionally high-affinity and
- selective inhibitor of phosphodiesterase 4 suitable for administration by inhalation:
- In vitro, kinetic, and in vivo characterization. Journal of Pharmacology and
- 1142 Experimental Therapeutics, 337(1), 145–154.
- 1143 https://doi.org/10.1124/jpet.110.173690
- 1144 Trucillo, P. (2021). Drug carriers: Classification, administration, release profiles, and
- industrial approach. *Processes*, 9(3). https://doi.org/10.3390/pr9030470
- 1146 Tsapis, N., Bennett, D., Jackson, B., Weitz, D. A., & Edwards, D. A. (2002). Trojan
- particles: Large porous carriers of nanoparticles for drug delivery. *PNAS September*,
- 1148 17, 12001–12005. www.pnas.orgcgidoi10.1073pnas.182233999
- 1149 Ungaro, F., D'Angelo, I., Miro, A., La Rotonda, M. I., & Quaglia, F. (2012). Engineered
- 1150 PLGA nano- and micro-carriers for pulmonary delivery: Challenges and promises.
- 1151 Journal of Pharmacy and Pharmacology, 64(9), 1217–1235.
- 1152 https://doi.org/10.1111/j.2042-7158.2012.01486.x
- United Stated Pharmacopeia (USP) 35. (2012). US Pharmacopoeia.: Vol. 36(2) (p. 534).
- van Zuylen, L., Karlsson, M. O., Verweij, J., Brouwer, E., de Bruijn, P., Nooter, K.,
- Stoter, G., & Sparreboom, A. (2001). Pharmacokinetic modeling of paclitaxel
- encapsulation in Cremophor EL micelles. Cancer Chemotherapy and
- 1157 *Pharmacology*, 47(4), 309–318. https://doi.org/10.1007/s002800000215
- 1158 Varshosaz, J., Hassanzadeh, F., Mardani, A., & Rostami, M. (2015). Feasibility of
- haloperidol-anchored albumin nanoparticles loaded with doxorubicin as dry powder
- inhaler for pulmonary delivery. *Pharmaceutical Development and Technology*,
- 20(2), 183–196. https://doi.org/10.3109/10837450.2013.852576
- 1162 Vecellio, L. (2006). The mesh nebuliser. *Breathe*, 2(3), 252–260.
- 1163 Veranth, J. M., Cutler, N. S., Kaser, E. G., Reilly, C. A., & Yost, G. S. (2008). Effects of
- cell type and culture media on Interleukin-6 secretion in response to environmental
- particles. Toxicology in Vitro, 22(2), 498–509.
- 1166 https://doi.org/10.1016/j.tiv.2007.10.011
- 1167 Veranth, J. M., Kaser, E. G., Veranth, M. M., Koch, M., & Yost, G. S. (2007). Cytokine
- responses of human lung cells (BEAS-2B) treated with micron-sized and
- nanoparticles of metal oxides compared to soil dusts. *Particle and Fibre Toxicology*,
- 4. https://doi.org/10.1186/1743-8977-4-2

- 1171 Veranth, J. M., Reilly, C. A., Veranth, M. M., Moss, T. A., Langelier, C. R., Lanza, D.
- L., & Yost, G. S. (2004). Inflammatory cytokines and cell death in BEAS-2B lung
- cells treated with soil dust, lipopolysaccharide, and surface-modified particles.
- 1174 Toxicological Sciences, 82(1), 88–96. https://doi.org/10.1093/toxsci/kfh248
- 1175 Verma, D., Gulati, N., Kaul, S., Mukherjee, S., & Nagaich, U. (2018). Protein Based
- Nanostructures for Drug Delivery. Journal of Pharmaceutics, 2018, 1–18.
- 1177 https://doi.org/10.1155/2018/9285854
- 1178 Vestbo, J., Hurd, S. S., Agustí, A. G., Jones, P. W., Vogelmeier, C., Anzueto, A., Barnes,
- P. J., Fabbri, L. M., Martinez, F. J., Nishimura, M., Stockley, R. A., Sin, D. D., &
- 1180 Rodriguez-Roisin, R. (2013). Global strategy for the diagnosis, management, and
- prevention of chronic obstructive pulmonary disease GOLD executive summary.
- American Journal of Respiratory and Critical Care Medicine, 187(4), 347–365.
- 1183 https://doi.org/10.1164/rccm.201204-0596PP
- 1184 Viertelhaus, M., Holst, H. C., Volz, J., & Hummel, R. P. (2013). Roflumilast A
- reversible single-crystal to single-crystal phase transition at 50 °c. Journal of
- 1186 *Molecular Structure*, 1031, 254–262.
- 1187 https://doi.org/10.1016/j.molstruc.2012.10.005
- Villandre, J., White, V., Lear, T. B., Chen, Y., Tuncer, F., Vaiz, E., Tuncer, B.,
- Lockwood, K., Camarco, D., Liu, Y., Chen, B. B., & Evankovich, J. (2022). A
- Repurposed Drug Screen for Compounds Regulating Aquaporin 5 Stability in Lung
- 1191 Epithelial Cells. Frontiers in Pharmacology, 13.
- https://doi.org/10.3389/fphar.2022.828643
- Villetti, G., Carnini, C., Battipaglia, L., Preynat, L., Bolzoni, P. T., Bassani, F., Caruso,
- P., Bergamaschi, M., Pisano, A. R., Puviani, V., Stellari, F. F., Cenacchi, V., Volta,
- 1195 R., Bertacche, V., Mileo, V., Bagnacani, V., Moretti, E., Puccini, P., Catinella, S.,
- 1196 ... Civelli, M. (2015). CHF6001 II: A novel phosphodiesterase 4 inhibitor, suitable
- for topical pulmonary administration In vivo preclinical pharmacology profile
- defines a potent anti-inflammatory compound with a wide therapeutic window.
- Journal of Pharmacology and Experimental Therapeutics, 352(3), 568–578.
- 1200 https://doi.org/10.1124/jpet.114.220558
- 1201 Vogelmeier, C. F., Román-Rodríguez, M., Singh, D., Han, M. L. K., Rodríguez-Roisin,
- 1202 R., & Ferguson, G. T. (2020). Goals of COPD treatment: Focus on symptoms and
- 1203 exacerbations. Respiratory Medicine, 166.
- 1204 https://doi.org/10.1016/j.rmed.2020.105938

- von Storp, B., Engel, A., Boeker, A., Ploeger, M., & Langer, K. (2012). Albumin
- nanoparticles with predictable size by desolvation procedure. Journal of
- 1207 *Microencapsulation*, 29(2), 138–146.
- 1208 https://doi.org/10.3109/02652048.2011.635218
- 1209 Wang, M., Zhang, Y., Xu, M., Zhang, H., Chen, Y., Chung, K. F., Adcock, I. M., & Li,
- F. (2019). Roles of TRPA1 and TRPV1 in cigarette smoke -induced airway
- epithelial cell injury model. Free Radical Biology and Medicine, 134, 229–238.
- 1212 https://doi.org/10.1016/j.freeradbiomed.2019.01.004
- Wang, X., Mychajlowycz, M., Lau, C., Gutierrez, C., Scott, J. A., & Chow, C. W. (2012).
- Spleen tyrosine kinase mediates BEAS-2B cell migration and proliferation and
- human rhinovirus-induced expression of vascular endothelial growth factor and
- interleukin-8. Journal of Pharmacology and Experimental Therapeutics, 340(2),
- 1217 277–285. https://doi.org/10.1124/jpet.111.186429
- 1218 Wang, Y., Mao, G., Lv, Y., Huang, Q., & Wang, G. (2015). MicroRNA-181b stimulates
- inflammation via the nuclear factor-κB signaling pathway in vitro. Experimental and
- 1220 Therapeutic Medicine, 10(4), 1584–1590. https://doi.org/10.3892/etm.2015.2702
- Warheit, D. B., & Hartsky, M. A. (1993). Role of alveolar macrophage chemotaxis and
- phagocytosis in pulmonary clearance responses to inhaled particles: Comparisons
- among rodent species. *Microscopy Research and Technique*, 26(5), 412–422.
- 1224 https://doi.org/10.1002/jemt.1070260509
- Wartlick, H., Spänkuch-Schmitt, B., Strebhardt, K., Kreuter, J., & Langer, K. (2004).
- Tumour cell delivery of antisense oligonucleeotides by human serum albumin
- nanoparticles. Journal of Controlled Release, 96(3), 483–495.
- 1228 https://doi.org/10.1016/j.jconrel.2004.01.029
- Weber, C., Coester, C., Kreuter, J., & Langer, K. (2000). Desolvation process and surface
- characterisation of protein nanoparticles. *International Journal of Pharmaceutics*,
- 1231 194(1), 91–102. https://doi.org/10.1016/S0378-5173(99)00370-1
- Wedzicha, J. A., Calverley, P. M. A., Albert, R. K., Anzueto, A., Criner, G. J., Hurst, J.
- 1233 R., Miravitlles, M., Papi, A., Rabe, K. F., Rigau, D., Sliwinski, P., Tonia, T., Vestbo,
- J., Wilson, K. C., & Krishnan, J. A. (2017). Prevention of COPD exacerbations: A
- 1235 European Respiratory Society/ American Thoracic Society guideline. European
- 1236 Respiratory Journal, 50(3). https://doi.org/10.1183/13993003.02265-2016
- Wilson, B., Lavanya, Y., Priyadarshini, S. R. B., Ramasamy, M., & Jenita, J. L. (2014).
- Albumin nanoparticles for the delivery of gabapentin: Preparation, characterization

- and pharmacodynamic studies. *International Journal of Pharmaceutics*, 473(1–2),
- 1240 73–79. https://doi.org/10.1016/j.ijpharm.2014.05.056
- Wong, B. A., Ross, P. W., & Arden, J. (2008). Development and use of a single-animal
- whole-body system for inhalation exposure. *Lab Animal*, 37(1).
- Woods, A., Andrian, T., Sharp, G., Bicer, E. M., Vandera, K. K. A., Patel, A., Mudway,
- 1244 I., Dailey, L. A., & Forbes, B. (2020). Development of new in vitro models of lung
- protease activity for investigating stability of inhaled biological therapies and drug
- delivery systems. European Journal of Pharmaceutics and Biopharmaceutics,
- Woods, A., Patel, A., Spina, D., Riffo-Vasquez, Y., Babin-Morgan, A., de Rosales, R. T.
- M., Sunassee, K., Clark, S., Collins, H., Bruce, K., Dailey, L. A., & Forbes, B.
- 1250 (2015). In vivo biocompatibility, clearance, and biodistribution of albumin vehicles
- for pulmonary drug delivery. Journal of Controlled Release, 210, 1–9.
- 1252 https://doi.org/10.1016/j.jconrel.2015.05.269
- 1253 Wright, J. L., Cosio, M., & Churg, A. (2008). Animal models of chronic obstructive
- pulmonary disease. Am J Physiol Lung Cell Mol Physiol, 295, 1–15.
- 1255 https://doi.org/10.1152/ajplung.90200.2008.-The
- 1256 Wright, S. D., Ramos, R. A., Tobias, P. S., Ulevitch, R. J., & Mathison, J. C. (1990).
- 1257 CD14, a Receptor for Complexes of Lipopolysaccharide (LPS) and LPS Binding
- Protein. Infect. Immun, 107, 1431–1433. https://doi.org/DOI:
- 1259 10.1126/science.1698311
- 1260 Yang, L., Cui, F., Cun, D., Tao, A., Shi, K., & Lin, W. (2007). Preparation,
- characterization and biodistribution of the lactone form of 10-hydroxycamptothecin
- 1262 (HCPT)-loaded bovine serum albumin (BSA) nanoparticles. *International Journal*
- 1263 of Pharmaceutics, 340(1-2), 163-172.
- 1264 https://doi.org/10.1016/j.ijpharm.2007.03.028
- 1265 Yang, Y., Di, T., Zhang, Z., Liu, J., Fu, C., Wu, Y., & Bian, T. (2021). Dynamic evolution
- of emphysema and airway remodeling in two mouse models of COPD. BMC
- 1267 Pulmonary Medicine, 21(1). https://doi.org/10.1186/s12890-021-01456-z
- 1268 Yang, Y., Liu, J., Hu, A., Nie, T., Cheng, Z., & Liu, W. (2022). A Critical Review on
- Engineering of d-Mannitol Crystals: Properties, Applications, and Polymorphic
- 1270 Control. Crystals, 12(8), 1080. https://doi.org/10.3390/cryst12081080

- 1271 Yaqub, N., Wayne, G., Birchall, M., & Song, W. (2022). Recent advances in human
- respiratory epithelium models for drug discovery. In *Biotechnology Advances* (Vol.
- 1273 54). Elsevier Inc. https://doi.org/10.1016/j.biotechadv.2021.107832
- Ye, R., & Liu, Z. (2020). ACE2 exhibits protective effects against LPS-induced acute
- lung injury in mice by inhibiting the LPS-TLR4 pathway. Experimental and
- 1276 *Molecular Pathology*, 113. https://doi.org/10.1016/j.yexmp.2019.104350
- 1277 Yin, T., Dong, L., Cui, B., Wang, L., Yin, L., Zhou, J., & Huo, M. (2015). A toxic organic
- solvent-free technology for the preparation of PEGylated paclitaxel nanosuspension
- based on human serum albumin for effective cancer therapy. *International Journal*
- 1280 of Nanomedicine, 10, 7397–7412. https://doi.org/10.2147/IJN.S92697
- Yoon, J. S., Kim, H. H., Lee, Y., & Lee, J. S. (2007). Cytokine induction by respiratory
- syncytial virus and adenovirus in bronchial epithelial cells. *Pediatric Pulmonology*,
- 1283 42(3), 277–282. https://doi.org/10.1002/ppul.20574
- 1284 Yoshimura, T., Kurita, C., Nagao, T., Usami, E., Nakao, T., Watanabe, S., Kobayashi, J.,
- 1285 Yamazaki, F., Tanaka, H., & Nagai, H. (1997). Effects of cAMP-Phosphodiesterase
- 1286 Isozyme Inhibitor on Cytokine Production by Lipopolysaccharide-Stimulated
- Human Peripheral Blood Mononuclear Cells. In *Gen. Pharmac* (Vol. 29, Issue 4).
- 1288 Yu, S., Pu, X., Ahmed, M. U., Yu, H. H., Mutukuri, T. T., Li, J., & Zhou, Q. T. (2021).
- Spray-freeze-dried inhalable composite microparticles containing nanoparticles of
- 1290 combinational drugs for potential treatment of lung infections caused by
- 1291 Pseudomonas aeruginosa. International Journal of Pharmaceutics, 610.
- 1292 https://doi.org/10.1016/j.ijpharm.2021.121160
- 1293 Yu Shaoyong, Yao Ping, Jiang Ming, Z. G. (2006). Nanogels Prepared by Self-assembly
- of Oppositely Chrged Globular Proteins. *Biopolymers*, 83, 148–158.
- 1295 https://doi.org/10.1002/bip
- Zhang, J., Leifer, F., Rose, S., Chun, D. Y., Thaisz, J., Herr, T., Nashed, M., Joseph, J.,
- Perkins, W. R., & DiPetrillo, K. (2018). Amikacin liposome inhalation suspension
- 1298 (ALIS) penetrates non-tuberculous mycobacterial biofilms and enhances amikacin
- 1299 uptake into macrophages. Frontiers in Microbiology, 9(MAY).
- https://doi.org/10.3389/fmicb.2018.00915
- 1301 Zhang, M., Jiang, H., Wu, L., Lu, H., Bera, H., Zhao, X., Guo, X., Liu, X., Cun, D., &
- Yang, M. (2022). Airway epithelial cell-specific delivery of lipid nanoparticles
- loading siRNA for asthma treatment. *Journal of Controlled Release*, 352, 422–437.
- 1304 https://doi.org/10.1016/j.jconrel.2022.10.020

| 1305 | Zhang, P., Mak, J. C., Man, R. Y., & Leung, S. W. (2019). Flavonoids reduces |
|------|--|
| 1306 | lipopolysaccharide-induced release of inflammatory mediators in human bronchial |
| 1307 | epithelial cells: Structure-activity relationship. European Journal of Pharmacology, |
| 1308 | 865. https://doi.org/10.1016/j.ejphar.2019.172731 |
| 1309 | Zhao, D., Zhao, X., Zu, Y., Li, J., Zhang, Y., Jiang, R., & Zhang, Z. (2010). Preparation, |
| 1310 | characterization, and in vitro targeted delivery of folate-decorated paclitaxel-loaded |
| 1311 | bovine serum albumin nanoparticles. International Journal of Nanomedicine, 5(1), |
| 1312 | 669–677. https://doi.org/10.2147/IJN.S12918 |
| 1313 | Zhao, F., & Klimecki, W. T. (2015). Culture conditions profoundly impact phenotype in |
| 1314 | BEAS-2B, a human pulmonary epithelial model. Journal of Applied Toxicology, |
| 1315 | 35(8), 945–951. https://doi.org/10.1002/jat.3094 |
| 1316 | Zhong, Q., Bielski, E. R., Rodrigues, L. S., Brown, M. R., Reineke, J. J., & Da Rocha, S. |
| 1317 | R. P. (2016). Conjugation to poly(amidoamine) dendrimers and pulmonary delivery |
| 1318 | reduce cardiac accumulation and enhance antitumor activity of doxorubicin in lung |
| 1319 | metastasis. <i>Molecular Pharmaceutics</i> , 13(7), 2363–2375. |
| 1320 | https://doi.org/10.1021/acs.molpharmaceut.6b00126 |
| 1321 | |
| 1322 | |
| 1323 | |
| 1324 | |
| 1325 | |
| 1326 | |
| 1327 | |
| 1328 | |
| 1329 | |
| 1330 | |
| 1331 | |
| 1332 | |
| 1333 | |
| 1334 | |
| 1335 | |
| 1336 | |
| 1337 | |
| 1338 | |

1339 Appendix

Supplementary data

Figure 0.1 Schematic representation of the method (method 1) adopted for the direct quantification of the roflumilast encapsulated in HSA-NPs.

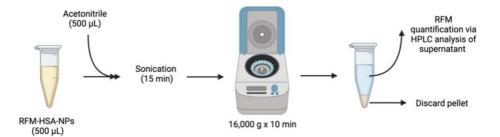


Figure 0.2 Schematic representation of the method (method 2) adopted for the direct quantification of the roflumilast encapsulated in HSA-NPs.

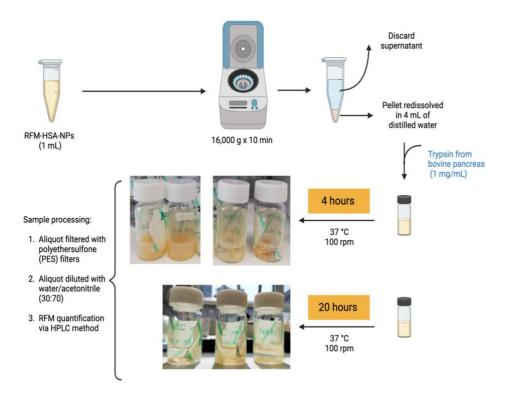


Figure 0.3 Representative HPLC chromatograms of RFM in water:acetonitrile (30:70)

1352 (samples obtained via method 1 and method 2).

